NANYANG TECHNOLOGICAL UNIVERSITY

DEVELOPMENT OF PHENYLPROPANOID SUCROSE ESTERS AS LEAD DRUG CANDIDATES FOR ALPHA GLUCOSIDASE INHIBITION

SURABHI DEVARAJ

SCHOOL OF CHEMICAL AND BIOMEDICAL ENGINEERING

2016

DEVELOPMENT OF PHENYLPROPANOID SUCROSE ESTERS AS LEAD DRUG CANDIDATES FOR ALPHA GLUCOSIDASE INHIBITION

SURABHI DEVARAJ

SCHOOL OF CHEMICAL AND BIOMEDICAL ENGINEERING

A thesis submitted to the Nanyang Technological University in partial fulfillment of the requirement for the degree of

Doctor of Philosophy

2016

ACKNOWLEDGEMENTS

I would like to express my heartfelt gratitude to my supervisor, Associate Professor Zaher Judeh, for his constant encouragement and guidance. Without his enthusiasm and valuable guidance, this thesis wouldn't materialize. I am indebted to him for providing an excellent working environment and for the countless fruitful discussions over the course of my PhD years.

I would like to thank the other members in the lab group past and present, Dr. Parthasarathi Panda, Dr. Khong Duc Thinh, Dr. Sudipta Chatterjee, Ong Li Lin, Varsha Siri Pamarthy and Kathy Wong for their help in reviewing and proofreading my thesis. A big thanks to Dr. Ong Teng Teng, Dr. Wang Xiu Juan, and Jessica Gan for technical support.

Many thanks to Dr. Zhang Dawei and Yip Yew Mun (School of Physical and Mathematical Sciences), for teaching me the necessary skills to conduct research in computational biology.

I would like to thank Dr. Yusuf Ali (Lee Kong Chian School of Medicine) for allowing me access to his lab and guiding me with the *in vivo* animal studies that are part of this thesis. Many thanks to Dr. Manesh Chittezhath and Vanessa Tay for their great patience in familiarizing me with animal handling techniques.

I am grateful to the School of Chemical and Biomedical Engineering and Nanyang Technological University for the generous scholarship support

Last but not the least, I owe the deepest gratitude to my family, especially my parents, and my husband who have always encouraged me to aim for the stars and are a constant source of joy and motivation.

ABSTRACT

This research work focuses on the development of Phenylpropanoid Sucrose Esters (PSEs) as lead antidiabetic Alpha Glucosidase Inhibitors (AGIs) with the ultimate aim of eliminating the side effects associated with the current commercial drugs (Acarbose, Miglitol and Voglibose). Structure Activity Relationship (SAR) studies (*in vitro, in silico* and *in vivo*) have been used to guide this aim.

In vitro inhibition studies indicate that most of our PSEs (feruloyl, coumaroyl and cinnamoyl) are much better than the standard drug Acarbose in inhibiting α-glucosidase. The IC_{50} values for the most active PSEs range from 4 to 9μM as compared to 328μM for Acarbose. Most of the PSEs examined show less inhibition of α-amylase in comparison to Acarbose and the most active PSEs have IC_{50} values comparable to Acarbose (0.7-2μM for the PSEs and 5μM for Acarbose). This indicates a greater selectivity of the PSEs towards α-glucosidase than α-amylase. This selectivity is thought to play important role in reducing the GI side effects that accompany the AGIs. From the *in vitro* studies, we can conclude that the type, position and number of phenylpropanoid substituents on the sucrose core, the aromatic 'OH' group, and the diisopropylidene rings greatly affect the anti-diabetic activity of the PSEs. Molecular docking studies of the PSEs show excellent correlation with the experimental data. From the binding mode pictures, we can conclude that the presence of free 'OH' groups on the aromatic substituents and the substitution at position 3 on sucrose core are critical for inhibition. PSEs dock close to the active site of α-glucosidase. Docking with α-amylase indicate multiple binding sites. PSEs where all four substituent groups interact with the amino acid residues at the catalytic site show a higher inhibition. Inhibition kinetic studies of all PSEs show mixed inhibition of the enzyme, α-glucosidase. All of the PSEs show a mixed partial type of inhibition of α-amylase except PSE **4FI** (uncompetitive).

One lead drug, PSE **4FI** was selected to test its ability to mitigate post prandial hyperglycemia *in vivo*. Administration of the drug orally with starch is seen to reduce the increase in blood glucose levels following an oral starch tolerance test in STZ treated mice. PSE **4FI** is as effective as Acarbose in reducing the surge in blood glucose after a starch load in the test mice. Further SAR studies were conducted with newly synthesized PSEs to identify the characteristics of the ideal PSE AGI. We conclude that the structural features

essential to the anti-diabetic activity of the PSEs are found to be: four substituents on the sucrose core, alkenyl C=C, phenyl ring, diisopropylidene ring and the aromatic ‘OH’ groups. The most effective hydroxycinnamic acid substituents are the feruloyl and the caffeoyl moieties.

LIST OF ABBREVIATIONS

^{13}C NMR	Carbon Nuclear Magnetic Resonance
^{1}H NMR	Proton Nuclear Magnetic Resonance
Å	Angstrom
Ac	Acetyl
Ac_2O	Acetic anhydride
CAN	Acetonitrile
AcOH	Acetic acid
AGE	Advanced Glycation End-products
AGIs	Alpha Glucosidase Inhibitors
ARG	Arginine
ASN	Asparagine
ASP	Aspartic acid
Caff	Caffeoyl
$CDCl_3$	Deuterated chloroform
Cinn	Cinnamoyl
CinnCl	Cinnamoyl chloride
cm^{-1}	Wavenumber
Coum	Coumaroyl
CoumAc	4-Acetylcoumaroyl
CVD	Cardiovascular diseases
d	Day; doublet (in NMR spectroscopy)
dd	Doublet of doublet
DI	De-ionised
DM	Diabetes Mellitus
DMAP	N,N-Dimethylaminopyridine
DMF	N,N-Dimethylformamide
DMSO	Dimethyl sulfoxide
DNSA	3,5-Dinitrosalicylic acid
equiv.	equivalent

EtOAc	Ethyl acetate
EtOH	Ethanol
Fig	Figure
FT-IR	Fourier Transformed Infrared Spectroscopy
g	Gram
GI	Gastro-intestinal
GLU	Glutamic acid
h	Hour
HbA1C	Glycosylated haemoglobin
HIS	Histidine
HP55	Hypromellose Phthalate
HPLC	High Performance Liquid Chromatography
HR-ESI-MS	High Resolution Electrospray Ionization Mass Spectroscopy
Hz	Hertz
IC_{50}	Half maximal Inhibitory Concentration
IGT	Impaired Glucose Tolerance
J	Coupling constant (in NMR spectroscopy)
K_i	Inhibitor Constant
LID	Ligand Interaction Diagram
LYS	Lysine
m	Multiplet (in NMR spectroscopy)
m/z	Mass/ charge
MD	Molecular Dynamics
MeOH	Methanol
min	Minute
mmol	Milimole
Mp	Melting point
MW	Molecular weight
^oC	Degree Celsius
PDB	Protein Data Bank
PHE	Phenylalanine

PNPG	p-Nitrophenol-α-D-Glucopyranoside
PPHG	Post-prandial Hyperglycemia
ppm	parts per million
PSEs	Phenylpropanoid Sucrose Esters
p-TsOH	p-Toluenesulfonic acid
R_f	Retention factor
rt	Room temperature
SAR	Structure-Activity Relationship
SGF	Simulated Gastric fluid
SIF	Simulated Intestinal Fluid
STZ	Streptozotocin
t	Triplet (in NMR spectroscopy)
T1D	Type 1 diabetes
T2D	Type 2 diabetes
TLC	Thin layer chromatography
TYR	Tyrosine
δ	Chemical shift in parts per million downfield from tetramethylsilane

Table of Contents

Chapter 1. Introduction

1.1 Diabetes

Diabetes mellitus (or simply diabetes) is an epidemic that plagues nearly 415 million people across the globe.[1] According to the International Diabetes Federation, worldwide, 5.0 million diabetes-related deaths are reported annually, a number far greater than that of HIV/AIDS-related deaths (1.5 million). One in every 20 deaths is attributed to diabetes equating to 8,700 deaths per day, or 6 deaths every minute.[1] Diabetes mellitus is a chronic metabolic disease in which a person has high blood sugar, either because the pancreas does not produce enough insulin or because the pancreatic beta cells do not respond to the insulin that is produced or both.[2]

There are three types of diabetes, namely:

1. Type 1 diabetes (T1D): It is also called "juvenile diabetes" or "Insulin Dependent Diabetes Mellitus" (IDDM). This kind of diabetes is seen to develop in the early years, teenage or early adulthood. It is not very common and accounts for only 10% of all cases of diabetes. The only treatment option for those suffering from this is to take injections of insulin, life-long.[3]
2. Type 2 diabetes (T2D): This is also known as "Non-Insulin Dependent Diabetes Mellitus" (NIDDM). Type 2 diabetes is the more commonly occurring type and accounts for 90% of the worldwide cases of diabetes.[4,5] The risk factors for diabetes type 2 are obesity, lifestyle (diet and exercise) choices and genetic factors. In a healthy body, fat is stored in muscles. However, excessive fat starts accumulating in the pancreas. As the amount of fat increases further, the pancreas eliminates the existing fat by non-oxidative metabolism. This causes damage to the pancreatic beta cells and it leads to decreased production of insulin. Failure to diagnose diabetes in the early stages, and improper management puts the individual at risk for blindness, kidney malfunction and cardiovascular diseases. Diabetes can cause heart diseases, it is the major contributor towards kidney failure worldwide and is also responsible for amputation of fingers and toes due to nerve damage.[6, 7]

3. Gestational diabetes: This type of diabetes affects women during pregnancy. This is caused due to an insufficient production of insulin during pregnancy. As a result, the glucose produced is not transported into cells and blood glucose levels become high. In most cases, this can be controlled using exercise and careful diet. In a few cases, some drugs may be required to control the blood glucose levels. A diet that is very high in animal fat and cholesterol, prior to pregnancy, is thought to be a risk factor for gestational diabetes. If undiagnosed, gestational diabetes can cause complications during childbirth.[3]

Some of the main symptoms associated with diabetes are shown in figure 1 below. Although, some symptoms are common between the two types of diabetes, the characteristic ones for T2D are Polydipsia (increased thirst), Polyphagia (excessive hunger), Polyuria (increased urination) and Glycosuria (excess glucose in urine) along with weight gain. In contrast, T1D is characterized by weight loss, gastric and other respiratory symptoms.

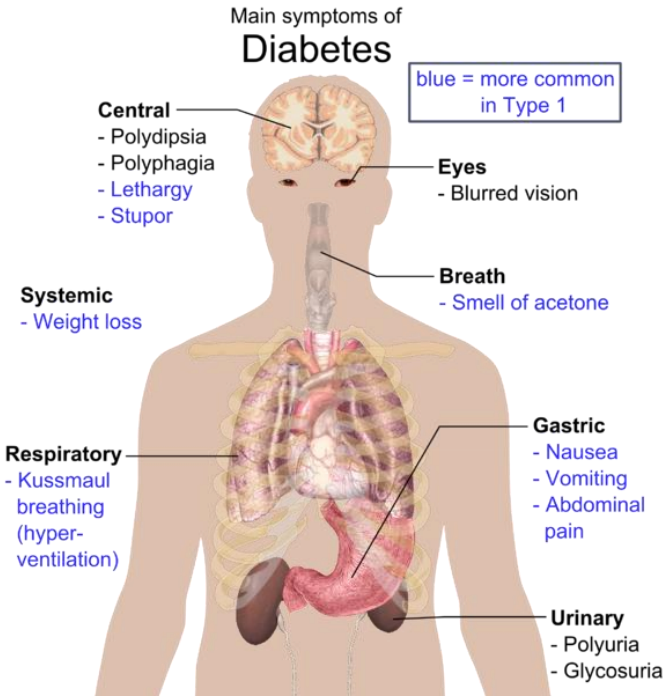

Figure 1: Symptoms associated with diabetes.[3]

There are three main tests to diagnose diabetes:

1. A1C test: This is a test for blood glucose levels. It is also sometimes called HbA1C test or test for glycosylated haemoglobin. This test measures the amount of glucose carried by haemoglobin. A1C level less than 5.7% is the normal blood glucose level while A1C level between 5.7% and 5.99%, it is indicative of the pre-diabetic stage. A1C level of 6.5% or higher is indicative of diabetes.[3,8]
2. FPG or Fasting Plasma Glucose test: This test measures the amount of glucose in the blood in the fasting state. FPG level less than 100mg/dl is normal, while that between 100mg/dl and 125.99 mg/dl is indicative of the pre-diabetic stage and greater than 126mg/dl is indicative of diabetes. [3,8]
3. Oral Glucose Tolerance Test (OGTT): In this test, the patient is given a solution of glucose to drink in order to measure how the body breaks it down. After this, the blood glucose level is tested. If the blood glucose level is below 140mg/dl it is normal, if it is between 140 and 199.9 mg/dl the patient is pre-diabetic and if it is above 200mg/dl then the patient is diagnosed to be diabetic.[3,8]

This research work focuses on the development of new treatments for T2D and therefore, the treatments for T2D will be discussed in the following sections. The aetiology of T1D and its corresponding treatment regime is very different from the former and involves, mainly, life-long injections of insulin. This is beyond the scope of the current project and thus further discussions will be limited to T2D.

1.2 Current Treatments for diabetes type 2

The most common treatment for type 2 diabetes is a long acting formulation of insulin with increasing dosage. There are however, many side effects linked to insulin, some of the primary ones being weight gain, lipodystrophy, hypoglycemia and insulin shock.[4] Over time, many patients may develop insulin resistance and allergies at the injection site, not to mention they have to undergo painful injections. There are oral drugs that are available for the treatment of type 2 diabetes, mainly Sulphonylureas, Biguanides and

Thiazolidinediones. Once again, these are accompanied by many side effects like weight gain, gastrointestinal disturbances, cardiac failure, upper respiratory tract infections etc.[4,5,9] Monotherapy is usually ineffective over long periods, and therefore, combination therapy becomes essential for diabetic patients. Although for most patients, ultimately insulin becomes necessary, by using anti-hyperglycemic drugs, the amount of insulin required can be minimized.[6,10] Diabetes Mellitus is a growing problem. As most patients develop resistance to the drugs over time and there are a lot of associated side effects with the current drugs, there is an ever increasing need to screen for more potential drug candidates to treat diabetes mellitus.

The following sections give a brief account of the current oral treatments for Type 2 diabetes, the mode of action and disadvantages of each of these treatments. Of the several classes of oral drugs available for treatment, all except Alpha Glucosidase Inhibitors (AGIs) are systemic in nature and they work by means of affecting one or the other pathways involving glucose metabolism while AGIs work non-systemically by reducing postprandial blood glucose levels and will be dealt with in more detail as the current research work pertains to this.

1.3 Oral anti-diabetics

1.3.1 Sulfonylureas

Sulfonylureas are a class of drugs characterized by the presence of S-arylsulfonylurea group (highlighted in bold in Fig. 2 ($-SO_2(NH)_2CO$)). These drugs act by stimulating the secretion of insulin by binding to the sulfonyl receptors in the beta pancreatic cells. They help to reduce excessive glucose in the fasting stage. The reduction in glycosylated hemoglobin (HbAlC) level achieved with these drugs is about 1-2%. Some of the side effects of this class of drugs includes weight gain, allergic reactions and sometimes severe hypoglycemia.[7,11]Another limitation of sulfonylureas is that they are only effective when

used with insulin.[5] Examples of drugs of this class are Glibenclamide and Glipizide (Fig. 2).[12]

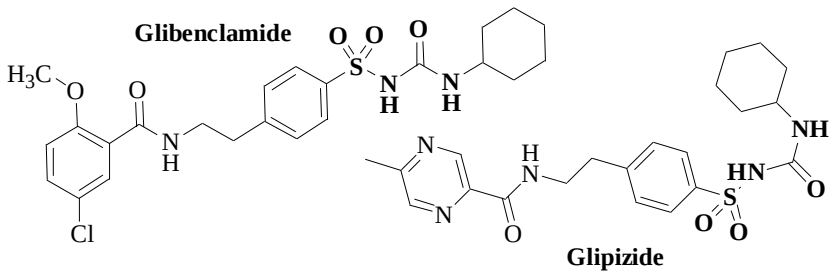

Figure 2: Sulfonlyureas- Glibenclamide and Glipizide.

1.3.2 Meglitinides

Drugs that work as secretagogues by inducing secretion of insulin by binding to beta cells in the pancreas are classed as Meglitinides. The three currently marketed drugs were synthetically prepared. They are associated with the risk of causing hypoglycemia especially in the elderly age group.[5] The weight gain linked to their use is lesser than that for other oral drugs. These drugs when used in stand-alone therapy are known to reduce HbAlC by 1.57%.[7] Examples of dugs belonging to this class are Nateglinides and Repaglinides (Fig. 3).

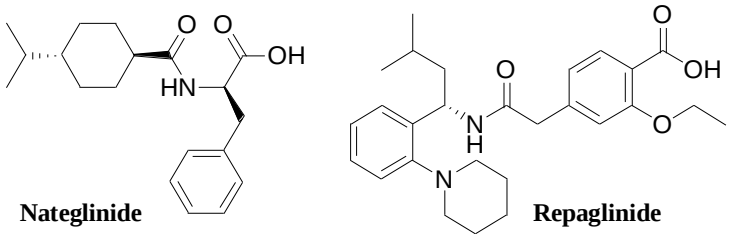

Figure 3: Meglitinides- Nateglinide and Repaglinide.

1.3.3 Biguanides

Biguanide is an organic compound that has the formula $HN(C(NH)NH_2)_2$. Derivatives of Biguanide that work as anti-hyperglycemic agents are classed under Biguanides. This class of drugs works by reducing the amount of glucose produced by the liver. It helps to control the fasting blood glucose level. Of the drugs of this type, the one that is mostly in use is metformin (Fig.4). Although metformin reduces the glycosylated hemoglobin by 1-2%,

there are a number of side effects associated with this drug. It is known to cause nausea, abdominal discomfort, diarrhea and has a high risk for lactic acidosis which can be fatal.[7,11] Like the sulfonylureas, these drugs also need to be used in combination with insulin for them to be effective.[5]

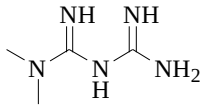

Metformin

Figure 4: Biguanide – Metformin.

1.3.4 Thiazolidinediones

Thiazolidinediones (TZDs) are drugs that contain the Thiazolidine functional groups which is converted to a dione (highlighted in Fig. 5). TZDs do not affect the production of insulin but they increase the sensitivity of muscle, liver and fat cells to insulin.[6,7] These can lead to a 1-1.5% reduction in glycosylated hemoglobin. Some of the side effects include weight gain, edema and possibly liver damage. The first drug of this class, that was sold, Troglitazone (Fig. 5), had to be recalled because it caused idiopathic hepatotoxicity and was fatal in several cases. Therefore, these drugs are not recommended for patients with liver disorders.

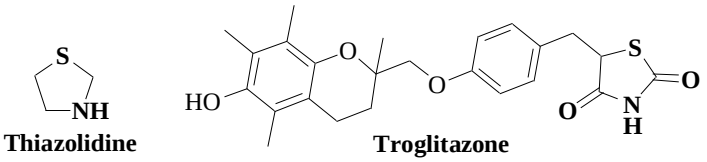

Thiazolidine **Troglitazone**

Figure 5: TZD-Troglitazone.

1.3.5 DPP-4 Inhibitors

DPP-4 inhibitors are a class of drugs that work by inhibiting the Dipeptidyl peptidase-4 (DPP4) enzyme that degrades the GLP-1 hormone. The function of this hormone is to promote insulin secretion by the beta pancreatic cells and to decrease the production of glucose in the liver. There is a reduction of about 0.5-0.9% HbAlC with the use of these drugs. There is no significant risk of hypoglycemia associated with this class of drugs.

However, since these drugs are eliminated in the unchanged form in the urine, they are contra indicatory to patients already suffering from kidney damage.[7] The drugs of this category have not been extensively studied and there is not yet complete information regarding their toxicity.[11] The first drug of this class to be approved by FDA was Sitagliptin (Fig. 6) which was released by Merck and Co. in 2006.

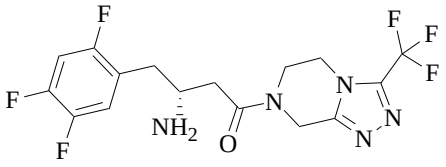

Sitagliptin

Figure 6: DPP4 inhibitor-Sitagliptin.

1.3.6 α-Glucosidase Inhibitors (AGIs)

Of all the available oral drugs for the treatment of diabetes mellitus, AGIs have been researched upon the least.[13] However, this class has seen increased attention in the recent years with active research on isolation and screening of both natural and synthetic lead compounds.[14–17] AGIs are a class of compounds that inhibit the α-glucosidase enzyme (Fig.7) located in the brush border cells of the small intestine. α-glucosidases are a class of enzymes that catalyze the final step in the digestion of carbohydrates. α-Glucosidases break down and absorb oligo- and disaccharides in the intestine. Inhibition of this enzyme can lead to decreased postprandial hyperglycemia and help combat Type 2 diabetes.[7] Postprandial Hyperglycemia can lead to cardiovascular disorders, cause strokes and even make muscles resistant to insulin.[9,18] As diabetes is linked to postprandial hyperglycemia, a better way to treat this would be to inhibit the α-glucosidase enzyme in the brush border cells in the intestine.

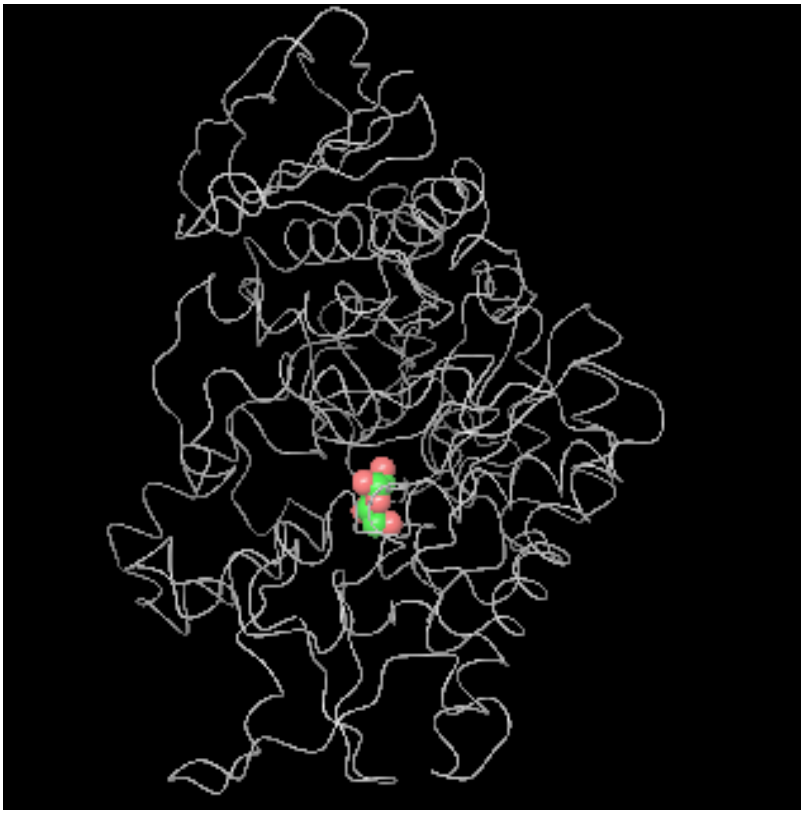

Figure 7: α-Glucosidase enzyme from *Saccharomyces cerevisiae* homology modelled using yeast isomaltase (PDB ID: 3A4A), visualized using Maestro software. The figure shows a glucose molecule docked at the active site.

The major advantage of these compounds lies in the fact that they are non-systemic drugs as their site of action is in the lumen of the intestine and hence need not reach systemic circulation. In addition, these drugs do not interact with other drugs and hence can be used in combination therapy. They can thus act as second or third line therapies in patients diagnosed with Type 2 diabetes.[13] In the case of patients suffering from Impaired Glucose Tolerance (IGT), AGIs can be used to control progression of IGT to Type 2 diabetes.[9] It is now known that strict control of postprandial glucose level is imperative to check diabetes. α-Glucosidase inhibitors have been shown to be the most effective of the available drugs in terms of controlling postprandial hyperglycemia.[18] α-Glucosidase inhibitors actually delay the absorption of glucose by blocking the enzyme. Thus, the breakdown takes place a long time after meals are consumed and this is precisely why they are effective in controlling postprandial hyperglycemia (Fig. 8). The AGIs lower the plasma insulin level indirectly

through a reduction in the absorbed glucose and they also help in reducing the risk for cardiovascular diseases in diabetic patients.[4,5,9] AGIs are also known to modulate the insulin response of the body to match the glucose level in the serum.[13] These drugs improve the sensitivity of cells to insulin and also have a protective effect on pancreatic beta cells.[9] They also decrease the amount of glycosylated haemoglobin (HbAlC). According to the American Diabetes Association, an HbAlC level of <7% is recommended for a healthy individual.[18] A reduction in 1% HbAlC level reduces the risk of other complications (cardiovascular, renal etc.) by 21%.[6] AGIs can reduce HbAlC levels by 0.5-1% when used with other drugs.[7,9] AGIs have very few contraindications as compared to the other drugs and are deemed to be very safe as their mode of action is non systemic. Also, with them, there is no risk of hypoglycemia. They are the only drugs that are capable of reducing post-prandial hyperglycemia. The problems associated with the current drugs of this class are the extremely poor solubility and their rapid excretion. As a consequence, the dosage is quite high and the drugs need to be taken with every meal.[18] The primary concern with AGIs is the Gastrointestinal (GI) side effects like abdominal bloating, flatulence and diarrhea. These side effects can be reduced by increasing the dosage in a stepwise manner. This can reduce the side effects from 70% to 31%. On continued usage, it is seen that the gastrointestinal side effects reduce to less than 20%. These side effects can also be reduced by modifying the diet.[9,18]

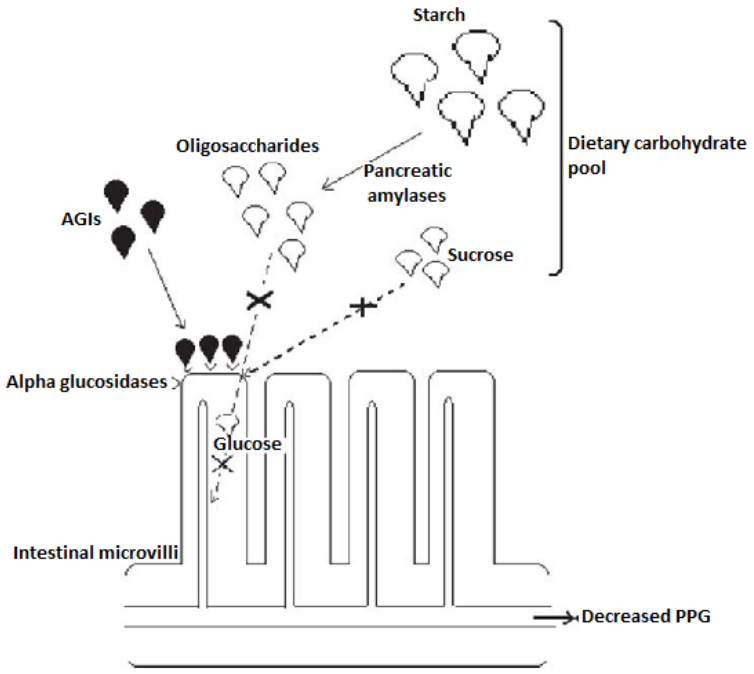

Figure 8: Mechanism of action of AGIs.[5]

1.3.7 General Structure of AGIs

Currently, there are three AGIs commercially available which are used to treat diabetes, namely Acarbose, Miglitol and Voglibose (Fig. 9). Of the three drugs, Acarbose is prescribed more in Asia as it is suitable for the starch rich Asian diet as it specifically inhibits glucoamylase. However, in the USA especially, Miglitol is more commonly used as it is suitable for the western diet.[9] Voglibose is marketed in certain Asian countries like Japan, Phillipines and Thailand. These AGIs have a common pharmacophore comprising a cyclohexane ring and a 4,6-dideoxy-4-amino-D-Glucose unit.[5] The secondary amino group present in these structures is thought to be responsible for the inhibitory effect on α-glucosidase due to its binding with the carbonyl group at the binding site.[5,9] This amino group reacts with the carboxyl group in the α-glucosidase by forming an amide bond and prevents oxidation of glycosidic oxygen bonds in the substrate (the starch or carbohydrates) thus leading to enzyme inhibition.[5] The AGIs act as competitive inhibitors of the enzyme

and consequently, they must be at the site of the enzymes at the same time as the carbohydrates to prevent their breakdown into glucose.[9]

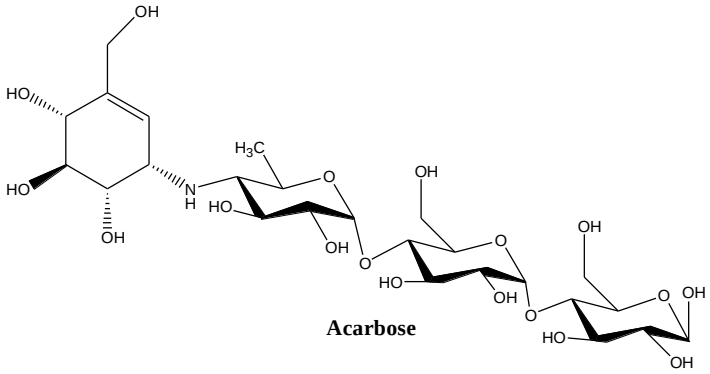

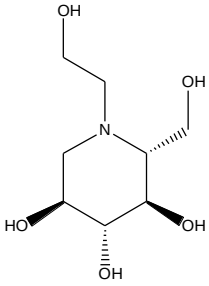

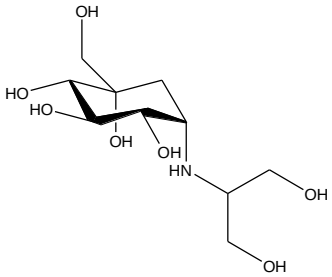

Figure 9: AGIs currently in the market.

1.3.8 Acarbose

Acarbose is the first AGI approved by the FDA for treating diabetes mellitus and is the most widely used drug. This pseudo tetrasaccharide is of microbial origin and was first introduced into the market in 1990. It shows the highest inhibition against glucoamylase followed by sucrase, maltase and dextranase (various classes of α-glucosidase). In its native form, only 0.5-1.7% of the drug is absorbed while the rest is degraded by bacterial enzymes. Acarbose improves the sensitivity to insulin in elderly patients with Diabetes Type 2. So far, it is the only anti-diabetic drug which reduces the risk for cardiovascular diseases by lowering the blood pressure in patients.[9] Acarbose has proved to be a safe drug to be used either on its own or in combination with insulin therapy.[10,19] It also has a significant effect on the reduction of postprandial hyperglycemia and reduces the HbAlC level by 0.69% when used in combination with insulin. It also reduces instances of hypoglycemia.

However, there are still the gastrointestinal side effects (flatulence and diarrhea) that are commonly observed with the use of Acarbose.[5,10]

These gastrointestinal side effects are caused by the breakdown of the unabsorbed carbohydrates that remain behind in the intestine by the intestinal microflora. This produces gas and causes flatulence and other gastric discomforts. The recommended doses of Acarbose vary from 25mg to 100mg during the start of every meal, three times a day.[5,18] The mechanism by which Acarbose delays carbohydrate absorption is illustrated in the following diagram (Fig 10). Here, Acarbose competitively inhibits α-glucosidase by binding to the enzyme instead of the substrate (oligosaccharide from starch) thus preventing the breakdown of it and decreasing glucose production.

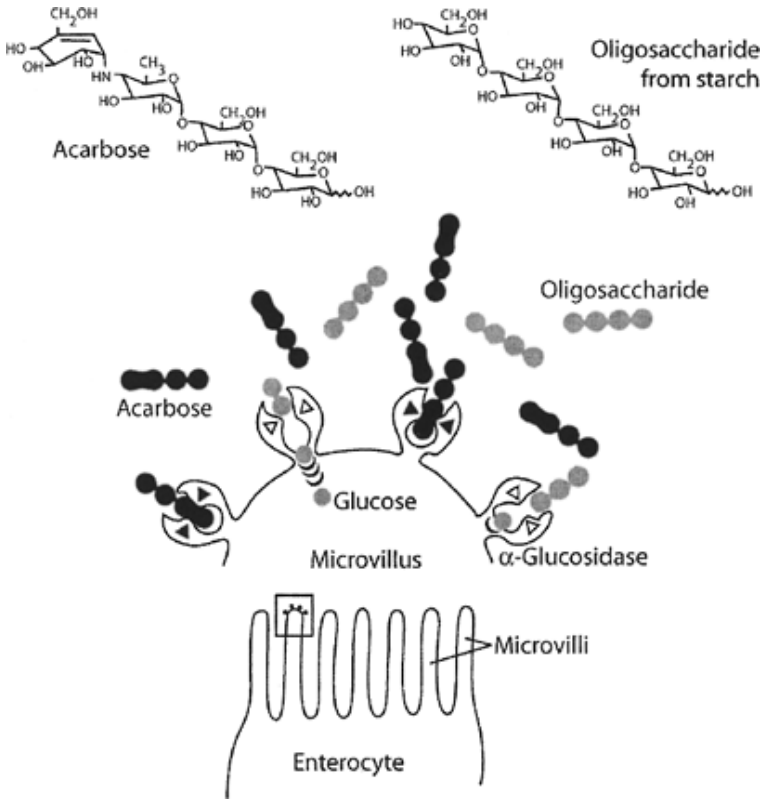

Figure 10: Mechanism of action of Acarbose.[20]

1.3.9 Miglitol

Miglitol was released in 1998 by Bayer, the same company that released Acarbose.[5] It is derived from the parent compound 1-deoxynojirimycin. It mainly inhibits disaccharide digesting enzymes. Its mechanism of action is the same as that of Acarbose. Miglitol is absorbed almost in entirety in the small intestine and has a longer circulating time.[9] As a result, in addition to GI side-effects, Miglitol causes stress to the kidneys.[21,22]

1.3.10 Voglibose

Voglibose is made by the reductive alkylation of valiolamine. Voglibose was developed by the Japanese company, Takeda. Currently, it is marketed in Japan, Philippines, Thailand and South Korea.[5] Voglibose, like Acarbose, is poorly absorbed (only 3-5%) and mostly excreted out in feces.[18] Voglibose's efficacy is far less than that of Acarbose requiring higher doses and resulting in even more of the side effects (seen in up to 25% of the patients).[23,24] As a result, Acarbose remains the preferred treatment option as compared to Voglibose.

1.4 Phenylpropanoid sucrose esters (PSEs)

Phenylpropanoid sucrose esters (PSEs) are a naturally occurring class of compounds mainly isolated from plant families like Arecaceae, Liliaceae, Polygonaceae, Rosaceae, Brassicaceae and Smilaceae. PSEs have one or more *trans*-Ar-CH=CH-CO- ester-forming moieties connected to a sucrose core through the OH group(s), primarily at the C-6, C-1', C-3', and C-6' (Fig. 11).[25] The ester-forming moieties are mainly cinnamic, coumaric, ferulic, caffeic and sinapic acids.[25]

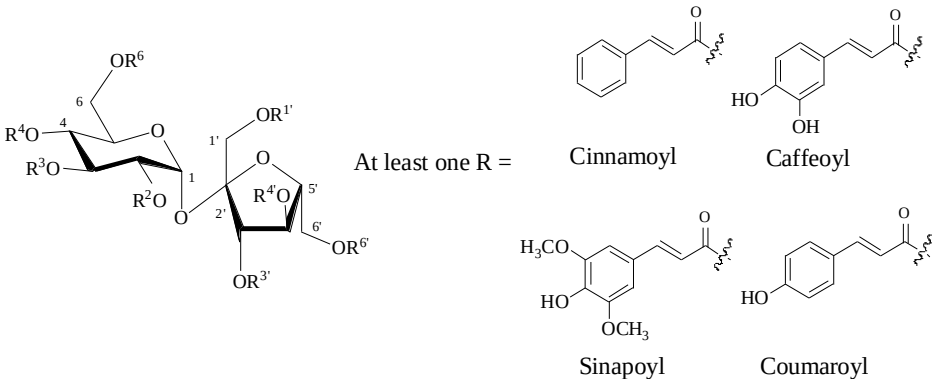

Figure 11: The core structure of PSEs.

1.4.1 Biological activities of PSEs

PSE extracts have been used in various traditional or folk medicines.[26] PSEs are known to have a vast array of biological activities including anti-cancer, antibacterial, antiplasmodial, antioxidant, acetylcholine esterase, α and β-glucosidase inhibitory activities[25,27,28–31]. Panda *et al.* reported the antiproliferative activity of analogs of Helonioside A and Lapathoside D (Fig. 12) against HeLa cell. Helonioside A and Lapathoaside D showed antiproliferative activity at concentration greater than 100μM[32,33]. They reported the IC_{50} values of 3′,6′-di-*o*-acetoxycinnamoyl-2,1:4,6-di-*O*-diisopropylidene sucrose (Fig. 12) and 3',4',6'-Tri-*O*-cinnamoylsucrose (Fig. 12) to be 2.46 and 4.10μM after 48 hours of exposure.[32] Suo *et al* reported the antioxidant activities of phenylpropanoid glycosides from *Tabebuia* avellanedae. The PSE with the best IC_{50} from their study was found to be 1′-*O*-β-(3,4-dihydroxyphenyl)-ethyl-[4″-*O*-caffeoyl-(α-L-fucopyranosyl)]-(l-3′)-D-galactopyranoside (Fig.12) with an IC_{50} value of 0.24 ± 0.01μM[34]. Vanicosides A and B (Fig.12) were reported to have antimicrobial activity against the fish pathogen *Photobacterium damselae* with MIC values being 32μg/ml and 64μg/ml respectively.[35] Vanicosides A and B (Fig. 12) are also known to exhibit β-glucosidase with IC_{50} values of 598.8 and 48.3μg/ml respectively.[36] Phenylpropanoid glycosides were also reported to have better inhibition of the α-glucosidase enzyme as compared to the standard drug Acarbose.[31] Phenolic glycosides derived from red maple bark showed excellent α-Glucosidase inhibition (IC_{50} values ranging from 7-16μM) when compared to the standard drug Acarbose (IC_{50} of 161μM).[37] A caffeoyl glycoside, Dolichandroside A (Fig. 12**)** was reported to have an IC_{50} value of 139.78μg/ml in the inhibition of yeast α-glucosidase.[38] Diboside A (Fig. 12) or 1,3,6'-tri-p-coumaroyl-6-feruloyl sucrose is a phenylpropanoid glycoside with three coumaroyl and one feruloyl substituent on sucrose which was reported to be an excellent inhibitor of α-Glucosidase, sucrase with an IC_{50} value of 72.4 ± 7.0 μM..[39]

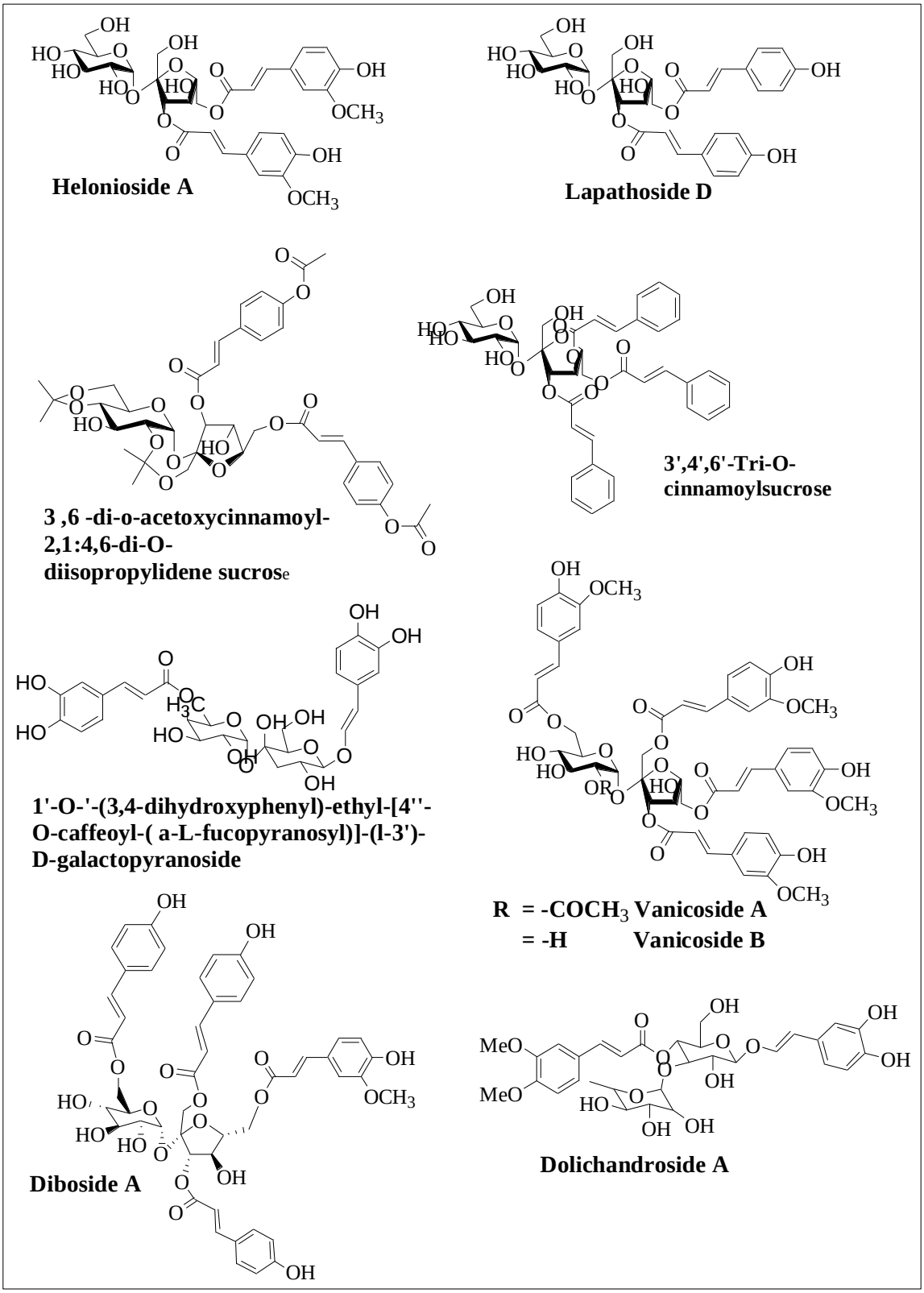

Figure 12: Examples of biologically active PSEs.

1.4.2 PSEs and Phenylpropanoid glycosides as anti-diabetics

Although there is limited reported work on PSEs as anti-diabetics, there are several examples in literature of plant extracts containing phenylpropanoid glycosides that are used to treat diabetes. These natural compounds are structurally and functionally similar to PSEs but differ in terms of the type of sugar in their core structure. One such example is the genus *Marrubium*. These plants produce several important classes of compounds, one of which is the phenylpropanoids. *Marrubium deserti* is a plant that grows in Algeria and is reported to be used in the treatment of Diabetes. *Marrubium vulgare* is another plant of this genus used in the treatment of diabetes in Mexico. The compositional analysis of this plant revealed the presence of phenylpropanoid glycosides among other compounds.[40] The plant extract of *Marrubium vulgare* was studied for its anti-diabetic properties by Boudjelal and coworkers. They isolated a mixed derivative, caffeoyl phenylpropanoid and phenylethanoid sucrose ester (verbacoside - Fig. 13) among other flavonoids and polyphenols from the plant extract. The aqueous extract was administered to Alloxan induced diabetic Wistar rats. A 100mg/kg dose of the extract was seen to decrease the blood glucose levels by 50% while doses of 200mg/kg and 300mg/kg reduced the blood glucose level by more than 60%.[41] In another example, the extract of the flower *Spiraea cantoniensis* was observed to inhibit α-glucosidase.[42] The extract on analysis was found to contain flavonol caffeoyl glycosides as the active ingredients. Similarly, the extract of *Hippophae rhamnoides* which contained a coumaroyl and feruloyl glucoside was found to inhibit yeast α-glucosidase with an IC_{50} value of 2.1 µg/ml.[43] A review by Mncwangi et al., [44] details the phytochemistry and biological activities of the plant *Harpagophytum procumbens* (Devil's claw). The secondary tuber of this plant is reported to have good anti-diabetic activity whose compositional analysis showed the presence of multiple phenylpropanoid glycosides. Andrade Cetto[45] and coworkers tested the hypoglycemic effect of the extract of aerial parts of *Equisetum myriochaetum* on diabetic rats and found that it considerably lowers the plasma glucose level. The compositional analysis of the extract revealed one of the four compounds to be a caffeoyl glucoside. Vinholes and colleagues[46] studied the effect of hydromethanolic extract of *Spergularia rubra* on yeast α-glucosidase inhibition and found the IC_{50} value to be 2.55 mg/ml which contained several feruloyl, dihydroferuloyl and sinapoyl glucoside substituted flavonoids.

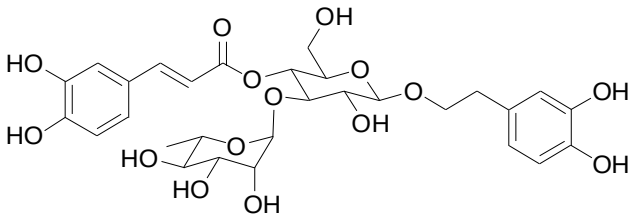

1 Verbacoside

Figure 13: Verbacoside.

It can thus be observed that the phenylpropanoid group contributes to the biological activities of the various plant extracts mentioned above. The following section gives a brief account of some of the phenylpropanoid glycoside derivatives and PSEs that have been reported to show anti-diabetic activity along with their structures. The classification is done based on the type and number of the hydroxycinnamic acid substituent(s) in these compounds.

1.4.3 Coumaric acid substituted phenylpropanoid glycoside derivatives

1.4.3.1 Mono coumaroyl substituted

Phytochemicals from highbush blueberry flowers (*Vaccinium corymbosum*) were isolated by Wan and colleagues and tested for their alpha glucosidase inhibitory activities. Among the phytochemicals isolated, there were phenylpropanoid glycoside derivatives. [47] Three of these compounds were derivatives of mono coumaroyl glycosides, compounds **2**, **3** and **4** (Fig. 14). All three compounds showed significant IC_{50} values for alpha glucosidase inhibition, 67.70 ± 0.95, 31.02 ± 2.11 and 84.97 ± 6.18µM respectively which was much better than the standard drug Acarbose which has an IC_{50} value of 200.68 ± 19.63 µM. Of all the compounds tested by the authors, the phenylpropanoid glycoside derivatives showed superior IC_{50} values indicating that this class of compounds show superior anti-diabetic activity.

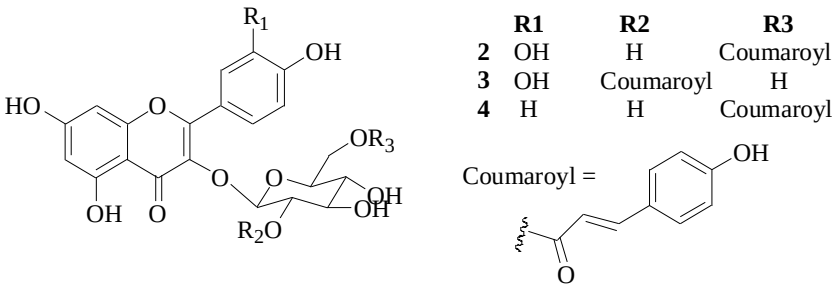

	R1	R2	R3
2	OH	H	Coumaroyl
3	OH	Coumaroyl	H
4	H	H	Coumaroyl

Figure 14: Mono coumaroyl glycoside derivatives.

1.4.3.2 Di coumaroyl substituted

Shoei-Sheng and coworkers isolated certain active constituents from the leaves of *Machilus philippinense*.[48] These were glycosides substituted with coumaric acid and other flavonoids. They isolated two compounds, both of which had two coumaric acid substituents. The structures of these compounds **5** and **6** are detailed below (Fig. 15).

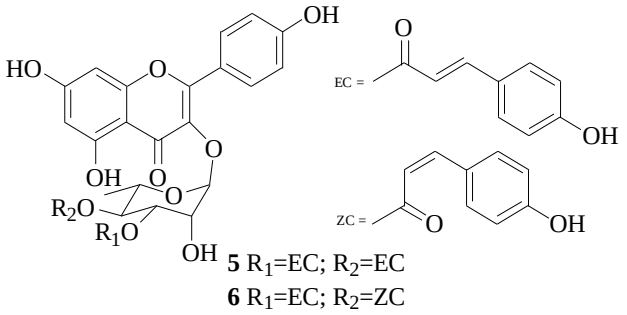

5 R_1=EC; R_2=EC

6 R_1=EC; R_2=ZC

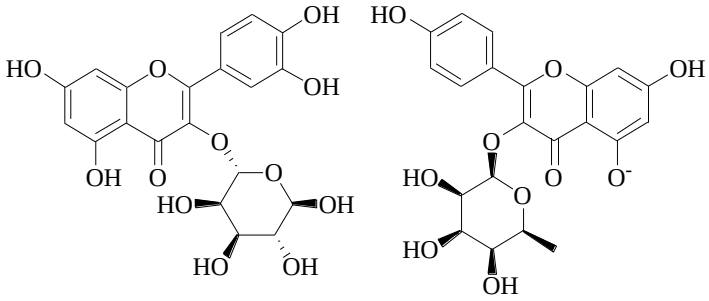

7 Quercetin 3-O-rhamnopyranoside **8 kaempferol-3-rhamnoside**

Figure 15: Dicoumaroyl glycoside derivatives; and flavonoids.

The IC_{50} value for α-glucosidase inhibition (α-glucosidase type IV from *Bacillus stearothermophilus)* of the compound **5** was 6.10 ± 0.28 µM while that of compound **6** was 1.00 ± 0.01 µM as compared to 0.046 ± 0.01 µM for Acarbose. They compared the values against those of Quercitin-3-O-rhamnopyranoside **7** (IC_{50} 33.05 ± 2.68 µM) and Kaempferol-3-O-rhamnopyranoside **8** (IC_{50} 228.11 ± 9.50 µM). From these studies the authors concluded that the coumaroyl substituent plays an important role in α-glucosidase inhibition and greatly enhances the activity of the compound. Also, the presence of an acylated moiety was thought be important as evidenced by the better IC_{50} values for **5** and **6** as compared to Quercitin-3-O-rhamnopyranoside **7** or Kaempferol-3-O-rhamnopyranoside **8**. The authors further concluded that the geometric orientation of the coumaroyl groups also played an important role in determining the activity as it can be seen that compound **6** had better activity than compound **5**.

In another study by Fan and coworkers, the dicoumaroyl PSE, Lapathoside D (Fig. 12) was isolated from Polygonum sachalinensis and the compound was tested for yeast α-glucosidase inhibition at a concentration of 225µg/ml.[49] At this concentration Lapathoside D showed an inhibition of 76.7±4.03% which was much greater than the standard drug Acarbose with an inhibition of 42.1±3.17%. Lapathoside D was found to have an IC_{50} value of 0.113mM for alpha glucosidase inhibition. They also compared the activity to the aglycone, Quercitin which did not have the same level of activity. Hence, the authors concluded that the sugar moiety is important for activity.

1.4.3.3 Tri coumaroyl substituted

Fan et.al also isolated a tricoumaroyl PSE, Hydropiperoside **9** (Fig. 16) from Polygonum sachalinensis.[49] This compound was seen to have an alpha glucosidase inhibitory value of 38.3±4.33% at a concentration of 225µg/ml. There is a drop in the activity as compared to Lapathoside D (section 1.4.3.2) indicating that the position at which the hydroxycinnamic acids are substituted on the sugar moiety plays a role in determining the activity as well.

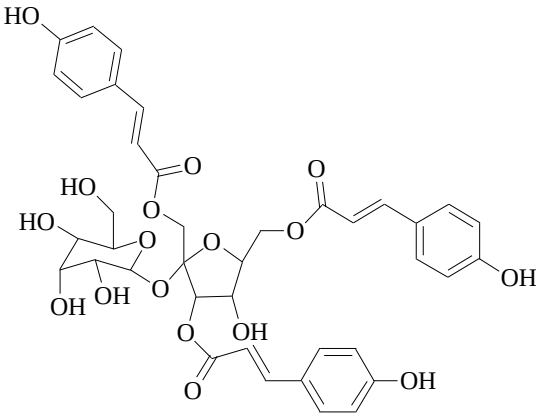

9 Hydropiperoside

Figure 16: Tricoumaroyl glycoside-Hydropiperoside.

1.4.4 Caffeic acid based phenylpropanoid glycoside derivatives

1.4.4.1 Mono caffeoyl substituted

The analysis of the extract of the leaves of *Dodecadenia grandiflora* was found to have considerable antihyperglycemic activity. One of the isolates from the extract was found to be a derivative of a caffeoyl glycoside, 2-[(6-O-(E)-caffeoyl)-b-D-glucopyranosyl]-oxyphenol, named dodegranoside A, **10**. This compound was tested for its percentage anti-hyperglycemic activity in Sprague Dawley rats and it was found to be 24.2% and 23.9% after 5 and 24 hours respectively. Here, percentage hyperglycemic activity was a measure of the blood glucose level after administration of the test compound.[50]

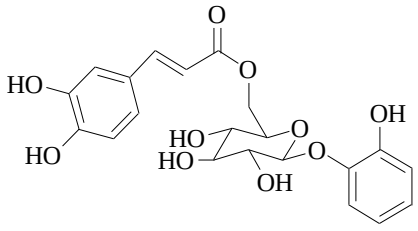

10

Figure 17: Mono caffeoyl glycoside derivative.

A caffeoyl ester of dihydrochalcone glucosides, **11** was isolated along with other compounds from *Balanophora tobiracola* by Tanaka et al (Fig. 18). The IC_{50} value of this compound **11** for yeast α-glucosidase inhibition was 1.1 µg/ml.[51] On comparison with coumaroyl glycosides, it can be seen that the caffeoyl glycoside **11** has a higher inhibitory activity. This indicates that the type of hydroxycinnamic acid substituent also influences the activity.

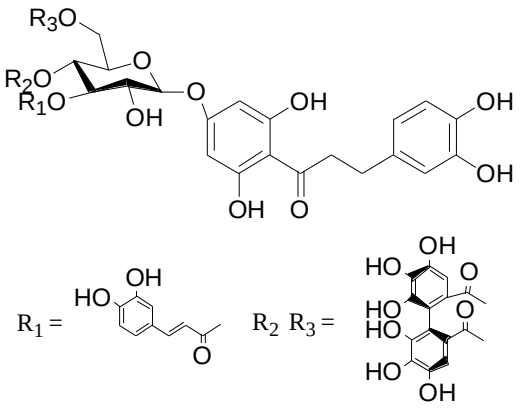

11

Figure 18: Mono caffeoyl dihydrochalcone glucoside.

1.4.5 Cinnamic acid based phenylpropanoid glycoside derivatives

Wan and coworkers studied the α-glucosidase inhibition (from yeast) of two cinnamic acid derives phenylpropanoid glycosides amongst various other compounds from highbush blueberry flowers. The two compounds **12** and **13** were found to have no detectable inhibition of the α-glucosidase enzyme.[47] Once again this lends to the hypothesis that type of hydroxycinnamic substituents affects the activity. Here, cinnamic acid shows lesser activity as compared to caffeic or coumaric acid. However, the number of substituents or substitution pattern may also play a significant role in enzyme inhibition.

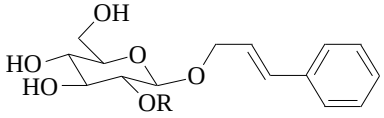

12 R = H
13 R = b-D-glucopyranose

Figure 19: Mono cinnamoyl glucoside.

1.4.6 Mixed hydroxycinnamic acid based phenylpropanoid glycoside derivatives

Matsuura et al. reported the rat intestinal glucosidase inhibition of a cinnamoyl glucoside substituted compound **14** (Fig. 20) extracted from *Hyssopus officinalis*. It was found to have an inhibition of 54% at a concentration of 3mM. [52]

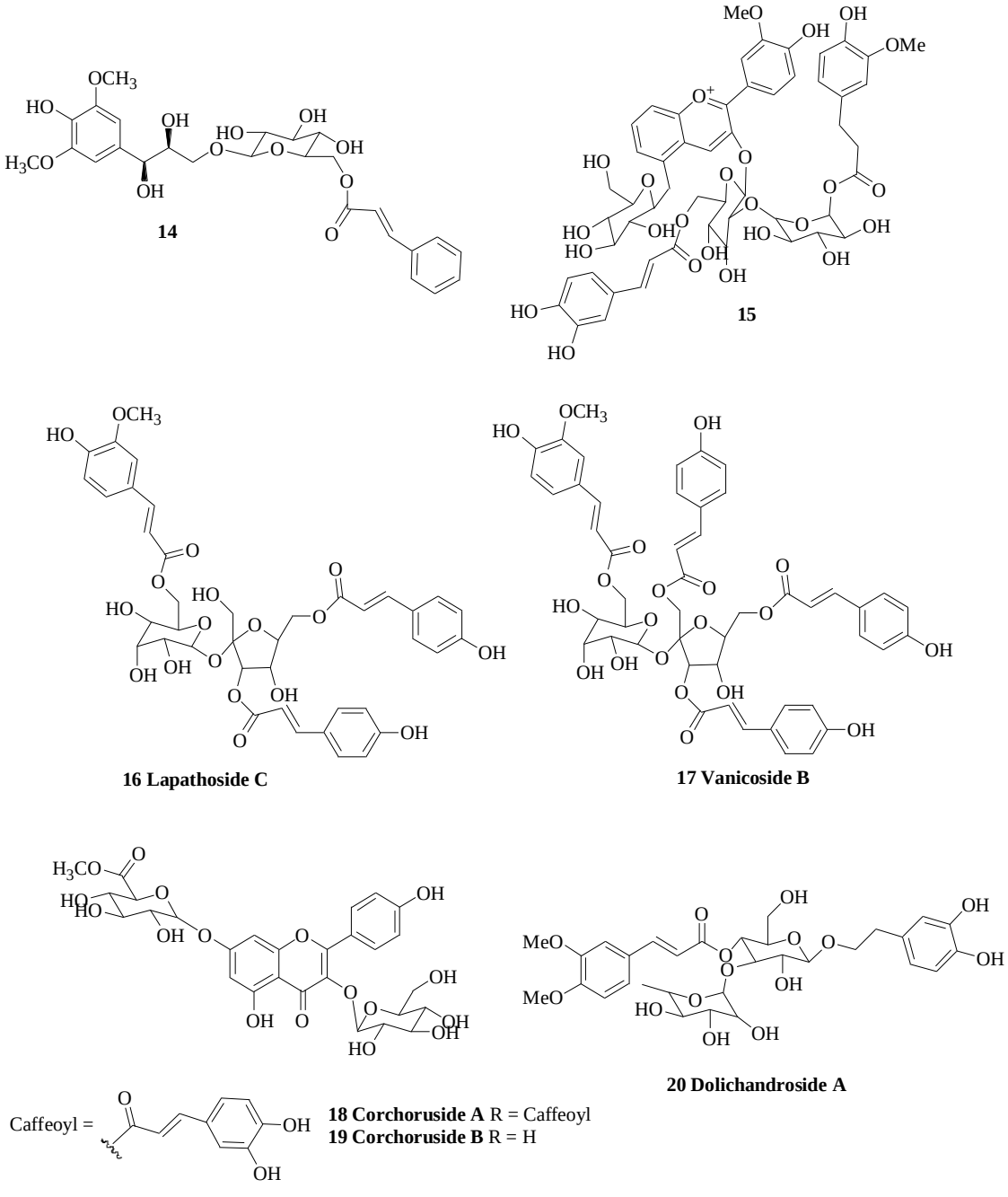

Figure 20: Mixed phenylpropanoid derivatives-1.

In another study, Matsui and coworkers isolated peonidin 3-O-[2-O-(6-O-Eferuloyl-*â*-D-glucopyranosyl)-6-O-E-caffeoyl-*â*-D-glucopyranoside]-5-O-*â*-D-glucopyranoside **15** (Fig. 20) from purple sweet potato and tested its anti-diabetic activity in Sprague-Dawley rats after a single dose (100mg/kg) following maltose (2g/kg) given by the oral route. The blood glucose level, after 30 minutes of administration of the compound, decreased by 16.5%.[53] The authors thus concluded that administration of the plant extract containing this compound caused a significant decrease in post-prandial hyperglycemia. They also found that its administration reduced the secretion of insulin indicating a lower blood glucose level.

Two mixed substituted (Feruloyl and Coumaroyl) PSEs were isolated from *Polygonum sachalinensis* by Fan and coworkers, namely, Lapathoside C **16** and Vanicoside B **17** (Fig. 20). Both of these showed considerable yeast α-glucosidase inhibitory values of 24.8±1.92% and 23.8±5.53% respectively at 225µg/ml concentration.[49] The authors compared the activities to Acarbose (42.1 $\pm$ 3.17) and Quercitin **7** (36.1 $\pm$ 6.91) (Fig. 15) and found the activities comparable.

Two new flavanol glycosides Corchorusides A **18** and B **19** (Fig. 20) were isolated from a vegetable, *Corchorus olitorius* by Phuwapraisirisan et al. Of the two, **18** had a phenylpropanoid glycoside moiety apart from the flavonol group. They observed that the IC_{50} for α-glucosidase inhibition was found to be 0.18±0.01 mM and 0.72±0.03 mM for **18** and **19** respectively when compared with 0.62±0.03 mM for Acarbose. The authors observed that the caffeoyl residue played an important role in enhancing the inhibition as the IC_{50} was much higher for **19** which lacked the caffeoyl moiety while that of **18** was three times lower than that of Acarbose.[54]

A mixed derivative of phenylpropanoid glycoside containing a caffeoyl group, Dolichandroside A **20** (Fig. 20), was isolated from *Dolichandrone falcate* stem by Aparna et al. It was reported to have an IC_{50} value 18.73µg/ml in the inhibition of intestinal α-glucosidase as compared to 8.74µg/ml for Acarbose.[38]

Liu et al reported a phenylpropanoid sucrose ester, Diboside A **21** (Fig. 21) to be an excellent inhibitor of α-Glucosidase, sucrase with an IC_{50} value of 72.4 ± 7.0μM. Diboside A or 1,3,6'-tri-p-coumaroyl-6-feruloyl sucrose is a Phenylpropanoid glycoside with three coumaroyl and one feruloyl substituent on sucrose. [55]

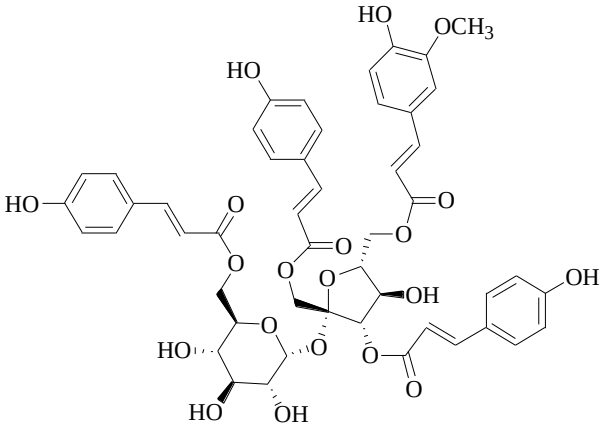

21 Diboside A

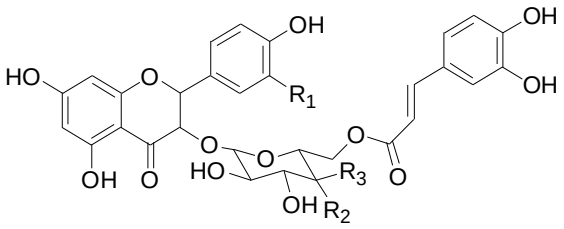

22 $R_1 = R_2 = OH, R_3 = H$
23 $R_1 = H, R_2 = OH, R_3 = H$
24 $R_1 = R_2 = H, R_3 = OH$

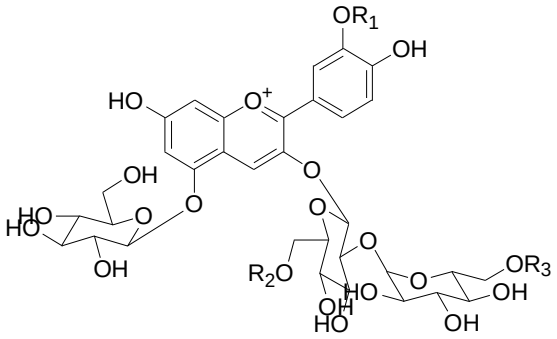

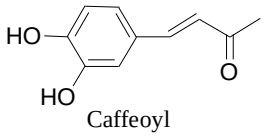

Caffeoyl

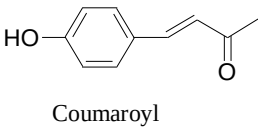

Coumaroyl

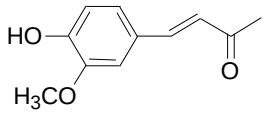

Feruloyl

31 R_1 = methyl, R_2 = caffeoyl, R_3 = H
33 R_1 = methyl, R_2 = caffeoyl, R_3 = caffeoyl
34 R_1 = methyl, R_2 = caffeoyl, R_3 = caffeoyl

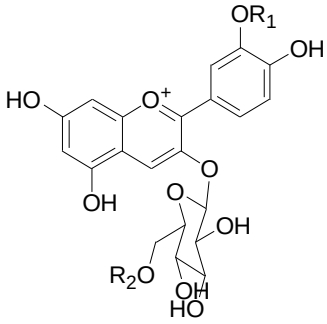

32 R_1 = H, R_2 = Coumaroyl

Figure 21: Mixed phenylpropanoid derivatives-2.

Yoshida and colleagues extracted three major compounds from the dried flowers of *Spiraea cantoniensis*.[56] The compounds isolated had caffeoyl glucoside as the substructure in the compound and were evaluated for their rat intestinal glucosidase inhibitory activities. The authors also compared the activities of other caffeoyl glycosides reported in literature. The three compounds isolated **22, 23** and **24** (Fig. 21) were found to have IC_{50} values for inhibition of rat intestinal glucosidase as 0.085mM, 0.35mM and 0.47mM respectively. From the results of their study, and by comparing the data for compounds in literature the authors concluded that substitution of the sugar by caffeic acid or presence of a caffeoyl substructure in flavonol glycosides enhances the glucosidase inhibition activity. Also, the caffeoyl moiety leads to better inhibition than the presence of a p-coumaroyl moiety.

Hua et al., isolated several phenylpropanoid glycosides from *Scrophularia ningpoensis* and tested their inhibition of yeast α-glucosidase.[57] They found that many of the compounds displayed a moderate inhibition of the enzyme as compared to Acarbose (IC_{50} = 0.37±0.01). The structures and the activities of the compounds showing activity are summarized below. From the activities of the compounds in table 1, it can be seen that the presence of an additional phenylpropanoid moiety on the sugar enhances the activity as evidenced by the lower IC_{50} values (**26**, **28-30**).

Table 1: Phenylpropanoid glycosides from *Scrophularia ningpoensis* and their IC_{50} values for yeast α-glucosidase inhibition.

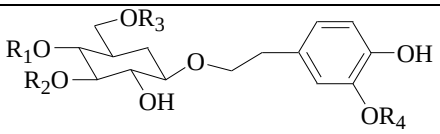

Compound	R_1	R_2	R_3	R_4	IC_{50} (mM)
25	H	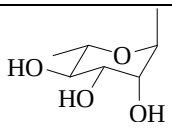	H	CH_3	5.51±1.12
26	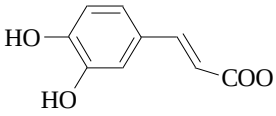	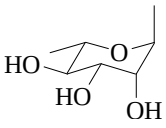	H	H	1.62±0.29
27	H	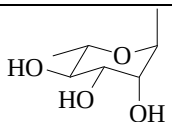	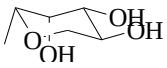	CH_3	12.01±0.663

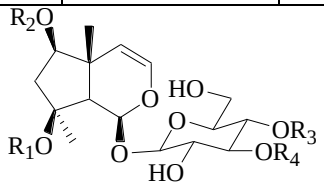

Compound	R_1	R_2	R_3	R_4	IC_{50} (mM)
28	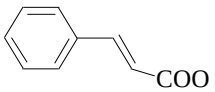	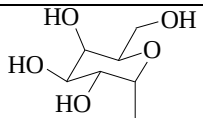	H	H	2.16±0.13
29	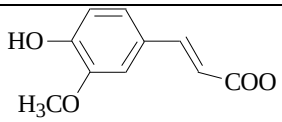	H	H	H	3.02±0.16
30	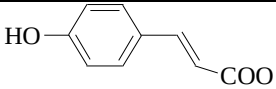	H	H	H	3.09±0.16

Qiu et al. isolated phenylpropanoid glucoside substituted anthocyanins from purple sweet potato and tested their effects on inhibition of α-glucosidase and found that the compounds showed good to moderate inhibition as compared to Acarbose.[58] From their experiments they concluded that acylation of the anthocyanin with caffeic or ferulic acid is important for maltase inhibition. The percentage inhibition of the compounds, **31, 32, 33**, **34** (Fig. 21) and standard Acarbose at 0.4mg/ml concentration is 95%, 85%, 54%, 54.8% and 80% respectively.

All the above compounds that are reported to have significant α-glucosidase inhibitory activities are structurally similar to the compounds in our study. From the literature review the following conclusions can be drawn in relation to the anti-diabetic activity of phenylpropanoid glycoside derivatives.

- The sugar moiety plays a significant role in inhibition.
- Presence of acylated phenylpropanoid substituents along with sugar is essential to activity.
- The type, number and position of substituents controls the amount of inhibition with caffeoyl being the best and the others (feruloyl, cinnamoyl and coumaroyl) displaying various levels of activity.

The PSEs in this project will be developed along these lines by extensive SAR studies using a compound library with PSEs that are substituted differently. Using this data, lead drug candidates will be synthesized, tested and developed as oral AGI drugs. The in vitro activity of the PSEs will be tested foremost followed by molecular modeling of the PSEs with the target enzymes and finally testing in animal models. The following sections give a brief introduction of the importance of molecular modeling and animal models in drug development.

1.5 Molecular modeling in drug design

Drug development began in earnest in the early 20th century where it consisted of a repeated cycle of modification, synthesis and testing of a series of compounds for the desired biological activity experimentally.[59] This approach is tedious, expensive, time consuming and does not really account for the toxicity of the analogs. The concept of structure based drug design was first postulated by Emil Fischer with his "lock and key" hypothesis.[60] Molecular modeling is applied in a variety of scenarios today. It is used to predict ligands that can bind to specific drug receptors, targets for enzymes, build homology models for proteins where the 3D structure is not available and also to visualize ligand complexes with the binding site of a protein.[60,61] The interactions between drugs and their active sites can lead to the design of biologically active molecules. Using a series of structurally similar compounds for docking and analyzing their docking modes can provide valuable information regarding the factors responsible for the potency of the compound(s). Interaction of drugs with the target site is governed by many factors that include conformational flexibility, steric fit and electrostatic charges among others.[59] Docking methods can predict to a high degree of accuracy the steric fit of ligands at the docking site. However, factors such as charge distribution and solvation effects are more difficult to predict computationally. Docking can also help predict the factors that contribute to the binding free energy of the docked complexes such as van der Waals forces and internal strain of the ligand.[60] Molecular modeling when combined with other aspects of drug design like chemical synthesis, in vitro and in vivo testing form the basis of rational drug design. It can help elucidate the 3D interactions between drugs and their receptors which will eventually lead to the design of novel drugs with high potency.[62] It combines the advantages of being cost effective, less time-consuming and helps design drugs that are more selective and have lesser side effects.

In this thesis, molecular modeling is used to study the interactions of the PSEs with the enzymes α-glucosidase and α-amylase. The results from the analysis of the binding modes will help determine the possible site(s) of binding and the structural features essential to binding of the PSEs which contribute to the biological activity of the PSEs.

1.6 Animal models in drug testing

Although most scientific research does not involve the use of animal models, they are used in certain areas of research and medicine to study disease pathways and then to develop safe treatments. Animal models are employed to test the effects of novel drugs, to monitor the efficacy as well as safety of the drugs. However, the use of animals in experimentation poses an ethical dilemma. Due to a lack of suitable alternatives, the use of animal models is indispensable in some areas of research. To ensure ethical treatment of experimental animals and responsible care and handling, research work involving animals is regulated by various governing bodies.[63,64] In Singapore, the 'Agri-Food & Veterinary Authority of Singapore' (AVA) has stipulated the National Advisory Committee for Laboratory Animal Research (NACLAR) guidelines for the use of animals in scientific research. The Institutional Animal Care and Use Committee (IACUC) reviews and approves all research protocols and ensures compliance with NACLAR guidelines.[1] Use of animal models in research is governed by the principle of the three Rs: Replacement, Refinement and Reduction. Replacement refers to the use of cell cultures, computation models, use of invertebrates or human volunteers to replace the use of animals wherever possible. Refinement refers to the use of methods that ensure the least discomfort and pain to animals used in experimentation. This ensures not only humane handling of animals but also improves the quality of the results from experiments. The quality of housing and treatment of experimental animals affects their behavior, physiology and immunological responses. The principle of reduction calls for the use of as few animals as possible without compromising the quality of the research data.[63,64]

As this research work focuses on the development and testing of new oral anti-diabetic drugs, it involves the use of an animal model for diabetes, specifically, a mouse model. Diabetes can develop in animals spontaneously just as in humans. Monkeys, cats, dogs, farm animals and rodents have all been documented to have spontaneously developed diabetes. Study of diabetes in human populations is difficult and genetic manipulation not

[1] Institutional Animal Care and Use Committee (IACUC). (n.d.). Retrieved from https://www.brc.a-star.edu.sg/index.php?sectionID=11

permitted for obvious ethical considerations. However, by using animal models, especially rodents, it is easier to study and observe the etiology of diabetes for successive generations and also test the safety and efficacy of new treatments. Although the disease pathway is not identical to humans, various animal models of diabetes have been used to gain insight and knowledge of certain aspects of the disease. Rodents are the most commonly used model due to the ease of manipulation and relatively lower cost as compared to higher mammals.[65]

In this research work, diabetic mice model was used to test the in vivo effect of one lead PSE oral-antidiabetic and is dealt with in detail in chapter 5.

1.7 Motivation behind this research project

Diabetes mellitus (DM) is a chronic metabolic disease where a person suffers from high blood sugar levels over a prolonged period, either because the pancreas does not produce enough insulin (Type 1 DM) and/or because the pancreatic beta cells do not respond to the insulin that is produced (Type 2 DM).[4,5] Failure to diagnose diabetes in the early stages and improper management puts the individual at risk for complications such as blindness, kidney malfunction, cardiovascular diseases, amputation of fingers and toes due to nerve damage.[6,7]

Diabetes is an epidemic that plagues 415 million people across the globe.[1] Type 2 diabetes is more common than Type 1 and accounts for 90% of the worldwide cases of diabetes. According to the World Health Organisation, worldwide 5.0 million diabetes-related deaths are reported annually, a number far greater than that of HIV/AIDS-related deaths (1.5 million). One in every 20 deaths is attributed to diabetes equating to 8,700 deaths per day, or 6 deaths every minute. WHO predicts that by 2030, diabetes will be the seventh leading cause of death in the world.[2] In Singapore, the prevalence rate for diabetes is 12.28%. Apart from this,13.65% of the population has Impaired Glucose Tolerance which is the pre-diabetic stage.[2] The economic burden of diabetes is huge and increasing. Worldwide, the economic cost of health expenditure due to diabetes in 2015 is estimated at US$ 673 billion.[1] Sugar is the new fat, and a high carbohydrate diet (sugar-rich) is more damaging compared to a high fat diet. Existing antidiabetic medications are either being phased out

completely due to serious liver injuries or cause severe side effects that some patients can't endure. Moreover, diabetic patients develop resistance to insulin therapy and a combination of insulin-medication therapy is used. Such a combination has even greater side effects.

There has to be a safe strategy to manage the absorption of sugars. Hence, this project aims to develop PSEs as potent, non-systemic and very selective lead antidiabetic drug candidates that eliminate the side effects experienced with existing therapies. Since PSEs are analogs of natural products present in plant extracts extensively used in traditional medicines they should little to no toxicity. In addition, this project envisions to study the Structure-Activity Relationship (SAR) of various natural and unnatural PSEs and test them for antidiabetic activity in vitro, in silico and in vivo. Using the feedback from the SAR, we can synthesize better drug candidates that can eventually be used for clinical studies.

1.8 Objectives

The overall objective of this thesis was to develop PSEs as potent inhibitors of α-glucosidase and oral anti-diabetic drugs. Some of the specific aims were:

1. Studying the activity of PSEs as inhibitors of the enzyme α-glucosidase (from *Saccharomyces cerevisiae*) and porcine pancreatic α-amylase.
2. Determination of the binding modes using molecular modelling for both the enzymes and SAR studies to correlate structure with activity and selectivity between the two enzymes.
3. Evaluation of inhibition kinetics for PSEs in relation to both the aforementioned enzymes.
4. Synthesis and testing of new PSEs with varied functional groups based on the data from the enzyme studies and molecular modeling to enhance anti-diabetic potential.
5. Evaluation of the lead PSE as anti-diabetic drug in diabetic mouse model.

Chapter 2. In Vitro Studies: α-Glucosidase and α-Amylase Inhibition by PSEs

2.1 Introduction

The sudden surge in blood glucose levels after a meal in pre-diabetic and diabetic patients is termed as postprandial hyperglycemia (PPHG). There are several studies that link PPHG with high risks of cardiovascular diseases (CVD). PPHG plays a particularly greater role in the etiology of CVDs rather than fasting hyperglycemia.[18,66] An acute increase in blood glucose levels after a meal can damage various parts of the body by means of Advanced Glycation End product (AGE) formation, which occurs due to glucose mediated cellular and tissue damage and an increase in oxidative stress. Thus, of late, there is a lot of emphasis on the need to address the problem of PPHG with several organizations like the WHO promoting the adoption of successful treatments for this disorder. This continues to be a problem in the treatment of diabetes and thus far, alpha glucosidase inhibitors (AGIs) are the most effective drugs in tackling this particular problem linked to diabetes. AGIs are a class of compounds that are extremely useful as they work mainly to reduce PPHG. They have an advantage over other diabetic treatments by providing an excellent control of PPHG apart from having no risks of hypoglycemia.[5]

AGIs act by inhibiting the carbohydrate digesting enzymes, α-glucosidase and α-amylase. Inhibition of these enzymes reduces the production of glucose in the lumen of the intestine and therefore its rapid absorption. AGIs work in the lumen of the proximal small intestine and inhibit the α-glucosidase enzymes (maltase, isomaltase, glucoamylase and sucrase). Apart from this, they also inhibit salivary and pancreatic α-amylase.[5]

α-Glucosidase enzymes are present in the brush border cells of the small intestine and they reduce the terminal, non-reducing 1-4 linked α-D-glucose residues to release single α-D glucose units (exohydrolysis). On the other hand, α-amylases catalyze endohydrolysis of 1-4 linked α-D glucosidic linkages in polysaccharide chains.[2] Thus, they are the two key enzymes that are involved in carbohydrate digestion and are targeted by AGIs.

2 retrieved from Swissprot database.

Consequently, in vitro tests for anti-diabetic activity that involve delaying glucose absorption are inhibition studies for these two enzymes.

This chapter focuses on the inhibition of the enzymes, α-glucosidase and α-amylase by a library of PSEs synthesized in our lab. There were several examples of phenylpropanoid glucosides and its derivatives that act as inhibitors of α-glucosidase in the literature review presented in chapter 1. Building on this rationale, PSEs are investigated in their capacity as AGIs in this thesis. Using the data obtained from various studies, Structure-Activity Relationship (SAR) is established to link the various functional groups on the PSE with the enzyme inhibition.

2.2 Methods

2.2.1 PSE compound library

The PSE compound library examined for their anti-diabetic activity in this work were obtained from Dr. Parthasarathi Panda, a former research student in our research group. PSEs having between one to four ferulic, coumaric and cinnamic acid substituents were chosen in order to establish SAR between the type and number of substituent and the anti-diabetic activity. The complete details of the synthesis of these compounds can be found in the publications of the researchers.[32,33] The synthetic route used sucrose as cheap starting material and allows for good control of the chemo-and regio-selectivities. It used protection/deprotection and acylation methodologies as detailed in Scheme 1. For this work, the compounds obtained were subjected to purification by column chromatography and the purity assessed by Nuclear Magnetic Resonance (NMR) prior to testing.

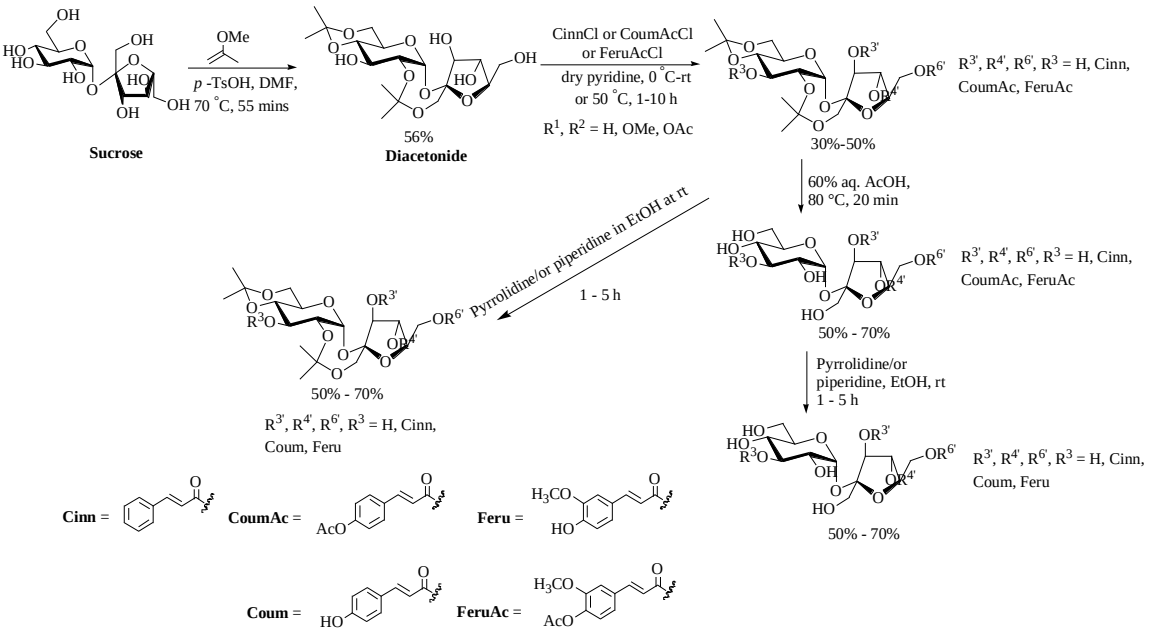

Scheme 1: General synthesis of selected PSEs.

2.2.2 Solubility of PSEs

The solubility of PSEs was assessed by dissolving 1000, 500, 100 and 50µg/ml in two separate tests: a) in plain 0.1M sodium phosphate buffer pH 7.0 and b) with DMSO as a co-solvent in the range 0-10% v/v and observing for turbidity in the solution due to precipitation of the PSEs. This was further verified by testing a sample PSE, **4CiI** (**54**) (Fig. 24; the numbering system will be explained in section 2.3.1) by HPLC using a C18 column (Kromasil 100-3.5C18). The mobile phase used was 100% ACN at a flowrate of 0.6ml/min and with an injection volume of 5µl. A calibration curve was constructed by using different concentrations of **4CiI** (5, 10, 25, 50, 100 and 250µg/ml). The calibration curve was a plot of the concentration of the test compound in ACN vs. area under the curve for the peak represented by **4CiI.** Then, test solutions of concentrations 25, 50 and 100µg/ml of **4CiI** (4%DMSO in buffer) were analyzed by HPLC to estimate the exact amount of compound soluble in the DMSO buffer solution.

2.2.3 α-Glucosidase inhibition

The procedure used for testing α-Glucosidase inhibitory activity was a modified version of that used by Kang and coworkers.[67] 8µl of DMSO corresponding to 50µg/ml final concentration in the net test solution was added to 115µl of 0.1M sodium phosphate buffer

pH 7.0 in a 96 well microtitre plate. To this solution, 50µl of α-glucosidase enzyme solution (0.5U/ml yeast α-glucosidase in phosphate buffer) was added. 'Blank' did not have the α-glucosidase enzyme, but buffer was added instead. 'Positive control' had no PSE inhibitor, and buffer was added to equalize the volume. Acarbose was used as a standard in this procedure. The plate was shaken at 37°C for 15 min. Next, 25µl of 2.5mM PSE substrate (in the same buffer) was added to the wells. The microplate was incubated at 37°C while shaking for another 15 minutes. Finally, the absorbance was then measured at 405 nm using a microplate reader. The percentage inhibition was then calculated using the following formula:

$$(OD_{positive\ control}-OD_{test})/OD_{positive\ control} *100\%.$$

The IC_{50} values for selected compounds were calculated by plotting a dose response curve using Graphpad Prism software. All measurements were performed in triplicates and the values are represented as mean ± std. deviation.

2.2.4 α-Amylase inhibition

The procedure for testing α-amylase inhibition was a slightly modified version of that already reported in literature by Phan and colleagues.[27] 50µl of the PSE in DMSO corresponding to a final concentration of 50µg/ml in the net test solution was taken in a test tube. To this, 100µl of porcine pancreatic α-amylase (5U/ml) and 460µl of sodium phosphate buffer pH6.8, 0.05M was added. The tubes were incubated at 37°C for 10min. Following this, 450µl of 0.5% starch solution was added and the tubes were incubated at 37°C for 20min. After this, 500µl of Dinitro Salicylic Acid (DNSA) reagent was added and the tubes were placed in a boiling water bath for 15 mins. The absorbance of the tubes was recorded at 540nm and the % inhibition calculated using the same formula as in case of α-glucosidase,

$$(OD_{positive\ control}-OD_{test})/OD_{positive\ control} *100\%.$$

The IC_{50} values for selected compounds were calculated by plotting a dose response curve using Graphpad Prism software. All measurements were performed in triplicates and the values are represented as mean ± std. deviation.

2.3 Results and discussion

2.3.1 PSE compound library

The type and structures along with the numbering system of the various compounds selected for this investigation are shown below (Fig. 22, 23 and 24). These compounds were selected because they show differences that can help correlate structure with the activity, in this case, inhibition of α-glucosidase and α-amylase. The compounds chosen differ in terms of: presence or absence of diisopropylidene ring on sucrose; type and number of substituent group(s) on sucrose; protection of the aromatic or sucrose 'OH' groups by the acyl moiety. To easily remember these compounds, the numbering has been developed as follows:

- There are four fields in each compound name.
- The first field is a number representing the number of substituent groups, for example, **1** for mono-substituted, **2** for di-substituted, so on and so forth.
- The second field represents the type of substituent: **F** for Feruloyl; **Ci** for Cinnamoyl acid and **Co** for Coumaroyl acid.
- The third field refers to the presence or absence of diisopropylidene ring on sucrose: if present then '**I'**-denotes "Diisopropylidene" and if absent then '**S**'-denotes "Sucrose".
- The fourth field is only added if the 'OH' groups on the aromatic ring are protected by the acyl moiety. The letter '**P**' is added if there is "Protection". In case of cinnamoyl compounds it refers to protection of sucrose 'OH' groups. If there is no protection, then there is no fourth field in the compound name.

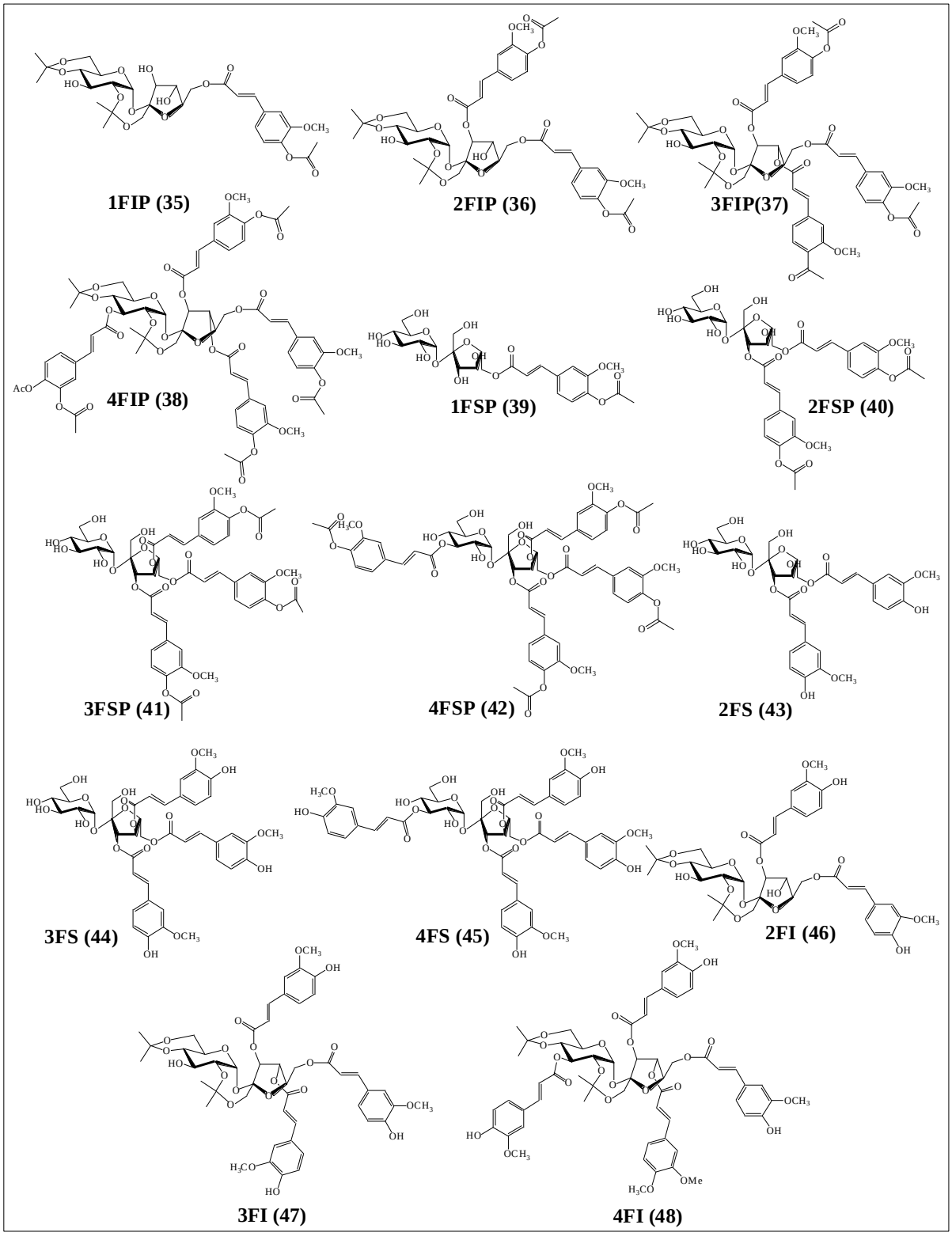

Figure 22: Feruloyl PSEs.

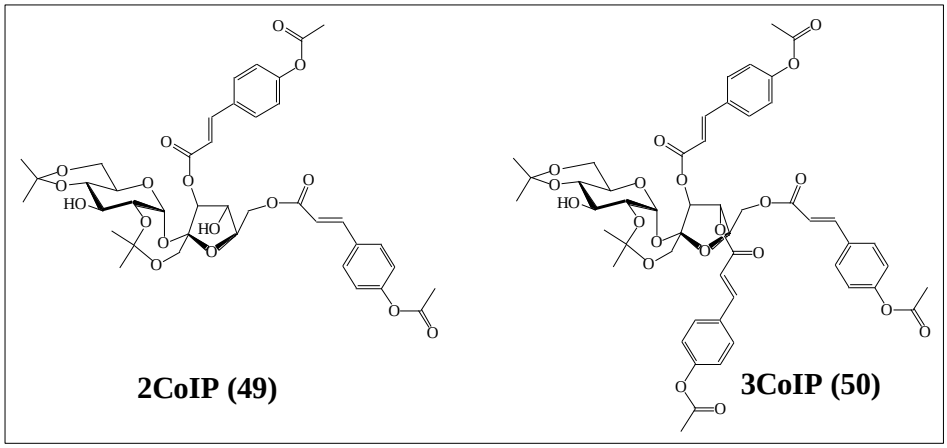

Figure 23: Coumaroyl PSEs.

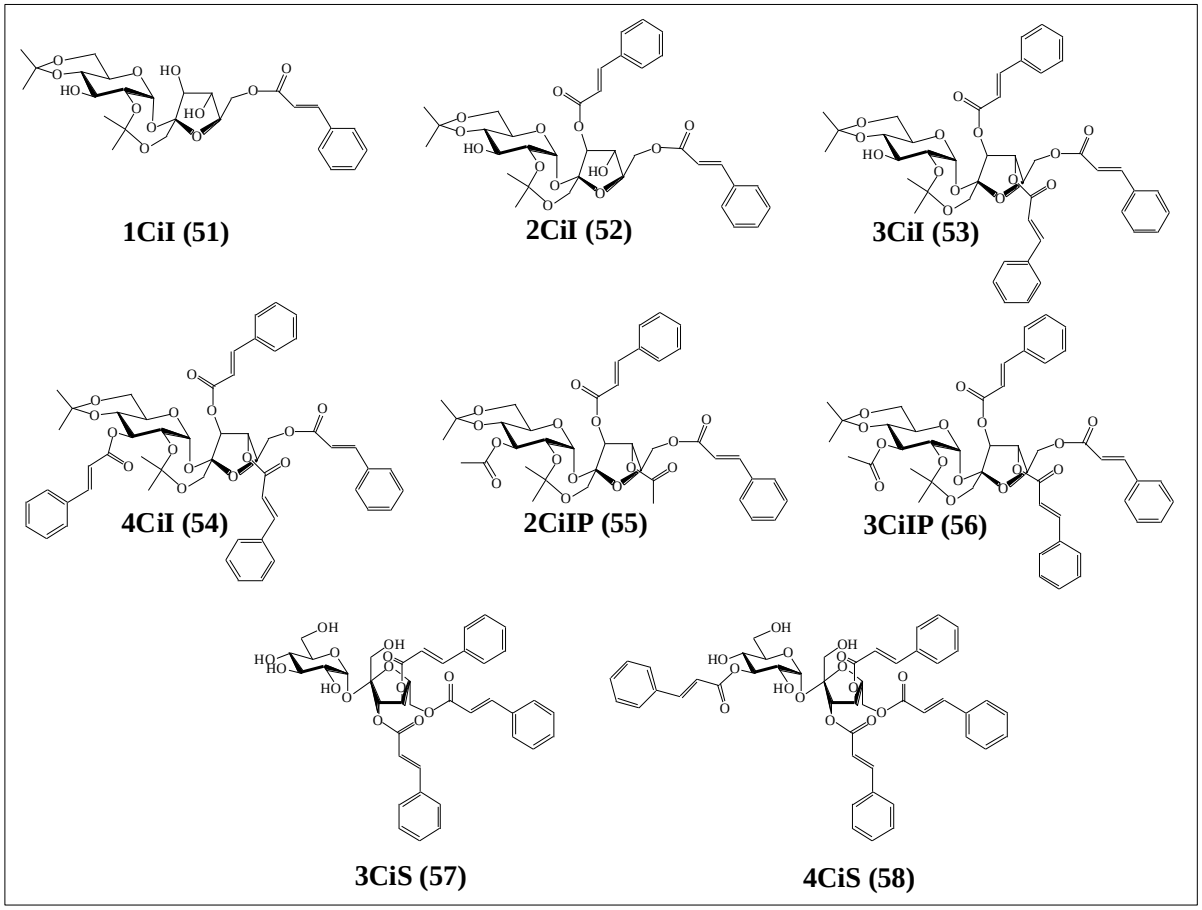

Figure 24: Cinnamoyl PSEs.

2.3.2 Solubility of PSEs

PSEs exhibit low aqueous solubility due to the presence of multiple hydrophobic phenyl moieties. Prior to their use in the enzyme studies, their solubility was tested to ensure that at the concentration used, the PSE was entirely soluble. The solubility of the PSEs was tested at concentrations of 1000, 500 and 250µg/ml following the procedure mentioned earlier (Section 2.2.2). It was found that the PSEs were insoluble in pure 0.1M sodium phosphate buffer, pH 7.0 at all concentrations. Therefore, DMSO was used as a co-solvent to enhance their solubility. It was observed that the maximum amount of DMSO that we can safely use is 4% v/v in 0.1M sodium phosphate buffer, pH 7.0. Higher DMSO concentration leads to loss in the α-glucosidase enzyme activity. At 4% v/v concentration of DMSO, we found that the maximum concentration achievable for the feruloyl and coumaroyl PSEs was 50µg/ml while that for the cinnamoyl PSEs was 25µg/ml. Therefore, these compounds were tested for α-glucosidase and α-amylase inhibition at these initial concentrations. The solubility was further verified using HPLC. The experiment was done using one test compound, **4CiI** (Fig. 24) in a 4% DMSO in DI water solvent. Based on the HPLC spectrum, the retention time for 4CiI in a 100% ACN mobile phase at a flowrate of 0.6ml/min was found to be 14.65 minutes. The calibration curve is represented in the figure below:

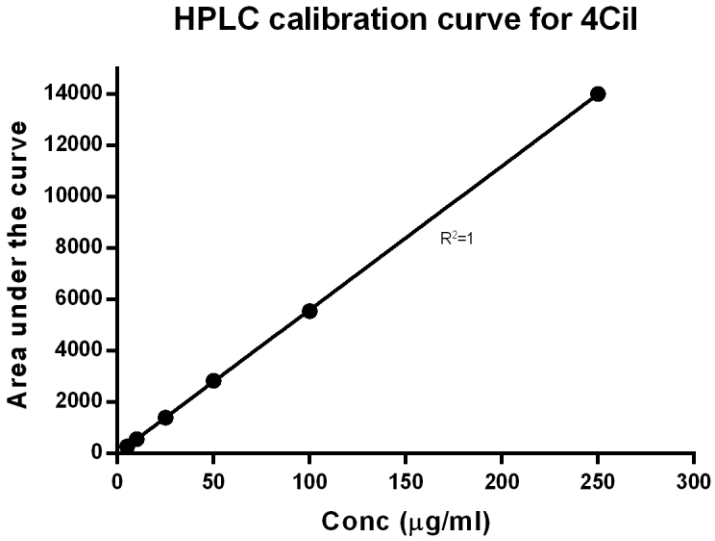

Figure 25: HPLC calibration curve for **4CiI**.

The exact concentrations present in the test solutions was estimated from the calibration curve (Y = 55.99*X + 5.619). The results are given in the table 2, below. From Table 2, it can be seen that up to 50µg/ml, PSEs are soluble in 4% DMSO in buffer as evidenced by entries 1 and 2, where the expected and estimated concentrations are the same for **4CiI** dissolved in 4% DMSO in water. However, in case of 100µg/ml, there is a huge difference between the expected and calculated values indicating that **4CiI** is not entirely soluble with a loss of 25% of the compound due to precipitation (Table 2, entry 3). Therefore, during the in vitro tests, we used 50µg/ml concentration of DMSO and the test compounds. However, as the cinnamoyl PSEs are more hydrophobic than ferulic and visual observation indicated a very mild cloudiness, an even lower concentration of 25µg/ml was used for initial testing of cinnamoyl PSEs.

Table 2: Estimation of concentration of PSE in 4%DMSO solution in DI water by HPLC

Entry	**Conc. of standard solution (µg/ml)**		**Area under the curve (AUC)**		**Conc. of test sample (calculated through HPLC) (µg/ml)**	
	Trial 1	Trial 2	Trial 1	Trial 2	Trial 1	Trial 2
1	25	25	1452.3	1448.8	25.8	25.7
2	50	50	2807.2	2778.4	50.1	49.5
3	100	100	4076.4	3590.1	72.7	64.0

2.3.3 α-Glucosidase inhibition

Once the solubility was addressed, the PSEs were then tested for their α-glucosidase inhibition as a first step towards estimating their anti-diabetic activity in vitro.

2.3.3.1 α-Glucosidase inhibition using feruloyl and coumaroyl PSEs

The feruloyl and coumaroyl PSEs were screened for α-glucosidase inhibition at a concentration of 50µg/ml. The values obtained are summarized in table 3 with a graphical representation shown in figure 26.

Table 3: % α-Glucosidase inhibition using feruloyl and coumaroyl PSEs at 50µg/ml

Entry	Compound (50µg/ml)	% α-Glucosidase Inhibition
1	**4FIP**	46±4
2	**4FSP**	35±10
3	**2FS**	35±3
4	**3FS**	50±5
5	**4FS**	98±4
6	**2FI**	30±6
7	**3FI**	39±4
8	**4FI**	90±8
9	**1FIP**	NSA*
10	**1FSP**	NSA*
11	**2CoIP**	29±7
12	**3CoIP**	30±6
13	**Acarbose**	31±2

**Compounds with less than 5% enzyme inhibition are considered to have No Significant Activity (NSA).*

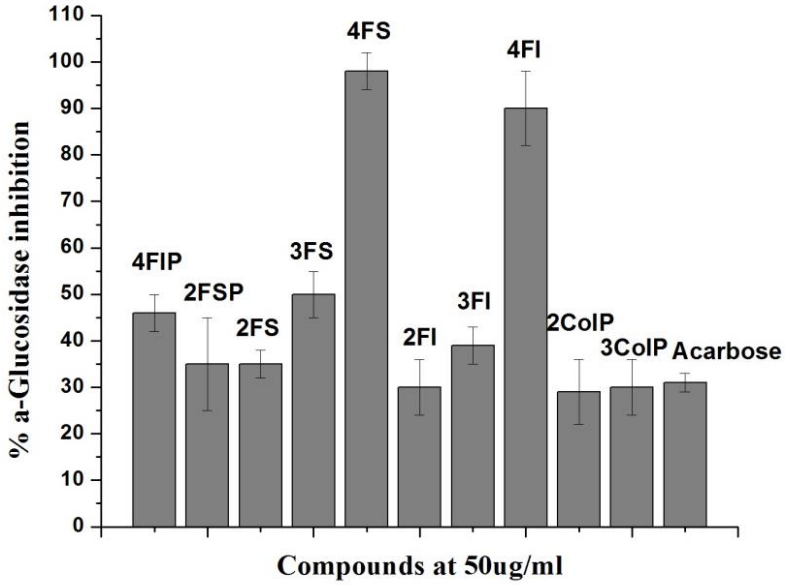

Figure 26: % α-Glucosidase inhibition using feruloyl and coumaroyl PSEs at 50µg/ml.

We can conclude the following based on the data presented in table 3 and figure 26:

1. All of the feruloyl PSEs (except **2FI**, Table 3, entry 6) exhibited higher % α-glucosidase inhibition values (Table 3, entries 1-8) compared to Acarbose as a standard (Table 3, entry 13). Amongst all, compounds **4FS** and **4FI** showed maximum inhibition of 98±4 and 90±8, respectively (Table 3, entries 5 and 8).

2. The coumaroyl PSEs, **2CoIP** and **3CoIP** exhibited % α-glucosidase inhibition values comparable to that of Acarbose.
3. Based on the experimental data, it can be concluded that, as the number of ferulic acid substituent groups increases, so does the % α-glucosidase inhibition. For example, the % α-glucosidase inhibition of **4FS** and **4FI** is 98±4 and 90±8, respectively (Table 3, entries 5 and 8), while for **3FS** and **3FI** is 50±5 and 39±4, respectively (Table 3, entries 4 and 7), and that for **2FS** and **2FI** is 35±3 and 30±6, respectively (Table 3, entries 3 and 6), while **1FSP** and **1FIP** showed inhibition value of less than 5 % and were therefore considered to have no significant activity (Table 3, entries 9 and 10). Therefore, the trend in the % α-glucosidase inhibition is: tetra-substituted > tri-substituted > di-substituted > mono-substituted PSEs.
4. In addition, feruloyl substituents with free OH groups show much better % α-glucosidase inhibition compared to the same ones protected by acyl moiety. For example, the % α-glucosidase inhibition of the tetra substituted compounds **4FS** and **4FI** with free OH is 98±4 and 90±8, respectively (Table 3, entries 5 and 8), while the corresponding **4FIP, 4FSP** with acyl protection is 46±4 and 35±10, respectively (Table 3, entries 1 and 2)**.** The values obtained indicate that acyl protected feruloyl **4FIP** and **4FSP** showed only half the % α-glucosidase inhibition of the free feruloyl **4FS** and **4FI**.
5. The diisopropylidene protecting group has limited effect on the % α-glucosidase inhibition activity. Consider the % α-glucosidase inhibition values of the pairs **4FIP** and **4FSP** with 46±4 and 35±10 (Table 3, entries 1 and 2), **3FS** and **3FI**, 50±5 and 39±4 (Table 3, entries 4 and 7) and **2FS** and **2FI** 35±3 and 30±6 (Table 3, entries 2 and 6).
6. At 50µg/ml concentration, both coumaroyl PSEs **3CoIP** and **2CoIP** showed comparable (29±7and 30±6, respectively, Table 3 entries 11 and 12) % α-glucosidase inhibition values to Acarbose (31±2, Table 3, entry 13). **3CoIP** and **2CoIP s**howed no noticeable difference in the % α-glucosidase inhibition values although **3CoIP** is tri-substituted PSE while **2CoIP** is a di-substituted PSE. This could be perhaps attributed to the fact that there are no free 'OH' groups on the aromatic ring in both these compounds. From point 4, we have already seen that for

feruloyl PSEs, the ones with free OH groups show much better % α-glucosidase inhibition compared to the same ones protected by acyl moiety

2.3.3.2 α-Glucosidase inhibition using cinnamoyl PSEs

The cinnamoyl PSEs were screened for α-glucosidase inhibition at a concentration of 25µg/ml. The values obtained are summarized in table 4 with a graphical representation shown in figure 27.

Table 4: % α-Glucosidase inhibition using cinnamoyl PSEs at 25µg/ml

Entry	Compound (25µg/ml)	% α-Glucosidase Inhibition
1	**1CiI**	NSA*
2	**2CiI**	35±5
3	**3CiI**	32±3
4	**2CiIP**	46±3
5	**3CiIP**	46±2
6	**4CiI**	77±5
7	**3CiS**	34±4
8	**4CiS**	74±9
9	**Acarbose**	27±4

**Compounds with less than 5% enzyme inhibition are considered to have No Significant Activity (NSA).*

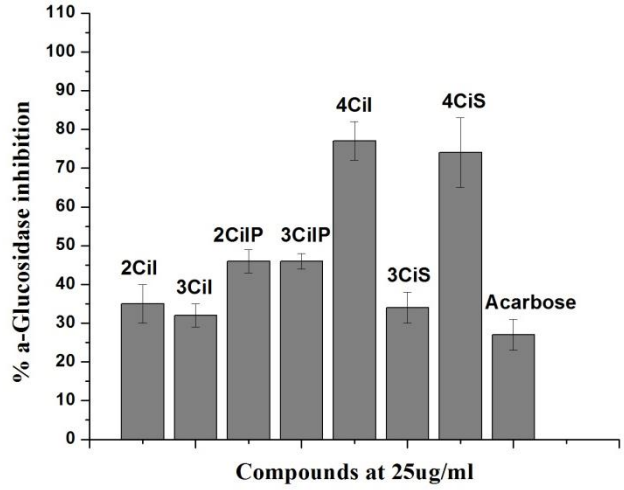

Figure 27: % α-Glucosidase inhibition using cinnamoyl PSEs at 25µg/ml.

We can conclude the following based on the data presented in table 4 and figure 27:

1. All of the cinnamoyl PSEs (except **1CiI**, Table 4, entry 1) exhibited higher % α-glucosidase inhibition values (Table 4, entries 2-8) compared to Acarbose, which was used as a standard (Table 4, entry 9). Compounds **4CiI** and **4CiS** showed maximum inhibition of 77±5 and 74±9, respectively (Table 4, entries 4 and 8).
2. Here, unlike the case with feruloyl PSEs, an increase in the number of cinnamic acid substituent groups was not proportional to an increase in the % α-glucosidase inhibition. For example, the % α-glucosidase inhibition of **4CiI** and **4CiS** is 77±5 and 74±9, respectively (Table 4, entries 4 and 8) while for **3CiI**, **3CiS** and **3CiIP** is 32±3, 34±4 and, 46±2 respectively (Table 4, entries 3, 7 and 6), while for **2CiI** and **2CiIP** is 35±5 and 46±3 respectively (Table 4, entries 2 and 5). **1CiI** showed inhibition value of less than 5 % and was therefore considered to have no significant activity (Table 4, entry 1). Based on the experimental data, there is no appreciable difference between the tri-substituted (**3CiI**, **3CiS** and **3CiIP**) and di-substituted PSEs (**2CiI** and **2CiIP**) but there is a significant jump in activity for the tetra-substituted cinnamoyl PSEs (**4CiI** and **4CiS**). For the former two, the % α-glucosidase inhibition is almost comparable. Therefore, the trend in the % α-glucosidase inhibition is: tetra-substituted > tri-substituted ~= di-substituted > mono-substituted PSEs. The reason for this comparable activity between tri-substituted and di-substituted PSEs could be due to the lack of aromatic OH groups on the cinnamic acid substituents. However, in case of the tetra-substituted PSEs, there is some other interaction between the PSEs and α-glucosidase other than due to 'OH' groups that enhances the activity.
3. Cinnamoyl PSEs with free 'OH' groups on sucrose show comparable % α-glucosidase inhibition compared to the ones where sucrose 'OH' is protected by acyl moiety. For example, the % α-glucosidase inhibition of the di and tri- substituted compounds **2CiI** and **3CiI** with free sucrose 'OH' is 35±5 and 32±3, respectively (Table 4, entries 2 and 3), while the corresponding **2CiIP, 3CiIP** with acyl protection is 46±3 and 46±2, respectively (Table 4, entries 5 and 6**).**
4. The diisopropylidene protecting group has limited effect on the % inhibition activity. This is evident by comparing the % α-glucosidase inhibition values of the pairs **4CiI**

and **4CiS** with 77±5 and 74±9 (Table 4, entries 4 and 8), **3CiI** and **3CiS**, 32±3, 34±4 (Table 4, entries 3 and 7), respectively.

In order to calculate the IC_{50} values, only the compounds showing close to 100% inhibition or high solubility (**2FS**) were chosen. This is because in order to obtain accurate values the entire range of inhibition values from 0 to 100% is necessary. Therefore, five compounds, the feruloyl compounds, **2FS, 4FS** and **4FI,** and the cinnamoyl compounds **4CiI** and **4CiS** were tested for their IC_{50} values and were found to be much more potent than the standard Acarbose. The data is represented in the table 5.

Table 5: IC_{50} values of PSEs screened for α-glucosidase inhibition

Entry	Compound	IC_{50} (µg/ml)	IC_{50} (µM)
1	**2FS**	143±7	205±10
2	**4FS**	5±2	5±2
3	**4FI**	4±2	4±2
4	**4CiI**	8±3	9±3
5	**4CiS**	8±3	9±3
6	**Acarbose**	212±5	328±7

From Table 5, it is observed that:

1. All compounds tested shower lower IC_{50} value in comparison to Acarbose.
2. The di-substituted feruloyl PSE, **2FS** was found to have an IC_{50} value of 205±10µM (Table 5, entry 1) which was lower than Acarbose with IC_{50} of 328±7µM (Table 5, entry 6).
3. The tetraferuloyl compounds **4FS**, **4FI** and the tetracinnamoyl compounds **4CiI** and **4CiS** were found to have the lowest IC_{50} values of 5±2, 4±2, 9±3 and 9±3µM respectively (Table 5, entries 2,3,4 and 5). The IC_{50} values for these PSEs were almost 30 times lower than that of Acarbose which was 328±7µM (Table 5, entry 6) indicating that these PSEs were much more potent inhibitors of α-glucosidase than Acarbose.

2.3.4 α-Amylase inhibition

As with the α-glucosidase inhibition, the PSEs were tested at an initial concentration of 50µg/ml for the feruloyl and coumaroyl PSEs and 25µg/ml for cinnamoyl PSEs. Once again Acarbose was used as a standard.

2.3.4.1 α-Amylase inhibition using feruloyl and coumaroyl PSEs

The feruloyl and coumaroyl PSEs were screened for α-amylase inhibition at a concentration of 50µg/ml. The values obtained are summarized in table 6 with a graphical representation shown in figure 28.

Table 6: % α-Amylase inhibition using feruloyl and coumaroyl PSEs at 50µg/ml

Entry	Compound (50µg/ml)	% α-Amylase Inhibition
1	**1FIP**	NSA*
2	**2FIP**	10±5
3	**3FIP**	5±1
4	**4FIP**	13±3
5	**1FSP**	NSA*
6	**2FSP**	8±6
7	**3FSP**	10±2
8	**4FSP**	13±4
9	**2FS**	23±9
10	**3FS**	53±3
12	**4FS**	98±1
13	**2FI**	13±10
14	**3FI**	12±10
15	**4FI**	54±4
16	**2CoIP**	12±10
17	**3CoIP**	7±5
18	**Acarbose**	95±1

**Compounds with less than 5% enzyme inhibition are considered to have No Significant Activity (NSA).*

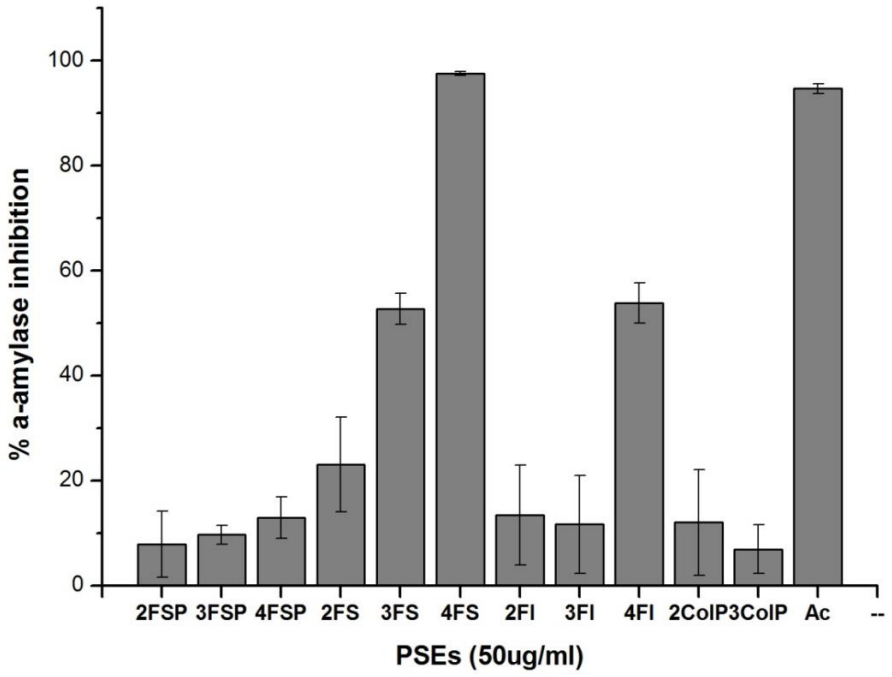

Figure 28: % α-Amylase inhibition using feruloyl and coumaroyl PSEs at 50µg/ml.

We can conclude the following based on the data presented in table 6 and figure 28:

1. Only half of the feruloyl PSEs (**4FIP,4FSP, 2FS-4FS, 2FI-4FI**, Table 6) exhibited % α-amylase inhibition values greater than 10% when compared to 95±1% of Acarbose as a standard (Table 6, entry 18). Compound **4FS** showed the highest inhibition of 98±1 (Table 6, entry 12).
2. The coumaroyl PSEs, **2CoIP** and **3CoIP** exhibited % α-amylase inhibition values of 12±10 and 7±5 respectively (Table 6, entries 16 and 17) which is far lesser than that of Acarbose.
3. In general, as the number of ferulic acid substituent groups increased, so did the % α-amylase inhibition. For example, the % α-amylase inhibition of **4FS** and **4FI** is 98±1 and 54±4, respectively (Table 6, entries 12 and 15), while for **3FS** and **3FI** is 53±3 and 12±9, respectively (Table 6, entries 10 and 14), while for **2FS** and **2FI** is 23±9 and 13±10, respectively (Table 6, entries 9 and 13), while **1FIP** and **1FSP** showed inhibition value of less than 10% and were therefore considered to have no significant activity (Table 6, entries 1 and 5). In some cases, the difference between the di and tri substituted feruloyl PSEs was not great or the trend was reversed but

the difference in % inhibition was small as with the pairs **2FIP** and **3FIP** or **2FI** and **3FI.** Therefore, the trend in the % α-amylase inhibition is: tetra-substituted > tri-substituted ≥ di-substituted > mono-substituted PSEs.

4. Feruloyl substituents with free 'OH' groups show much better % α-amylase inhibition compared to the same ones protected by acyl moiety, just as it was the case with the α-glucosidase inhibition. For example, the % α-amylase inhibition of the tetra substituted compounds **4FS** and **4FI** with free OH is 98±1 and 54±4, respectively (Table 6, entries 12 and 15), while the corresponding **4FIP** and **4FSP** with acyl protection is 13±3 and 13±4, respectively (Table 6, entries 4 and 8)**.** Acyl protected feruloyl **4FIP** and **4FSP** showed almost half the % α-amylase inhibition of the free feruloyl **4FS** and **4FI**.
5. The diisopropylidene protecting group has a great effect on the % α-amylase inhibition activity in case of the feruloyl PSEs with free aromatic OH groups which is in contrast with the case of α-glucosidase inhibition. Consider the % α-amylase inhibition values of the pairs **4FS** and **4FI** with 98±1 and 54±4 (Table 6, entries 12 and 15), **3FS** and **3FI**, 53±3 and 12±10 (Table 6, entries 10 and 14) and **2FS** and **2FI** 23±10 and 13±10 (Table 6, entries 9 and 13).
6. At 50µg/ml concentration, both coumaroyl PSEs **2CoIP** and **3CoIP** showed very low (12±10 and 7±5, respectively, Table 6 entries 16 and 17) % α-amylase inhibition values compared to Acarbose (95±1, Table 6, entry 18).

2.3.4.2 α-Amylase inhibition using cinnamoyl PSEs

The cinnamoyl PSEs were screened for α-amylase inhibition at a concentration of 25µg/ml. The values obtained are summarized in table 7 with a graphical representation shown in figure 29.

Table 7: % α-Amylase inhibition using cinnamoyl PSEs at 25µg/ml

Entry	PSE (25µg/ml)	% α-Amylase Inhibition
1	**1CiI**	NSA*
2	**2CiI**	9±5
3	**3CiI**	8±4
4	**4CiI**	98±2
5	**2CiIP**	14±4
6	**3CiIP**	13±7
7	**3CiS**	16±2
8	**4CiS**	99±1
9	**Acarbose**	93±2

**Compounds with less than 5% enzyme inhibition are considered to have No Significant Activity (NSA).*

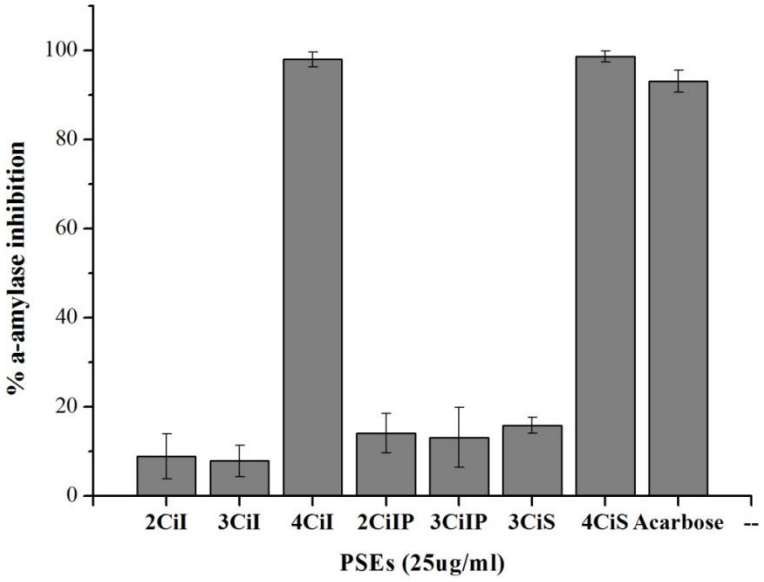

.

Figure 29: % α-amylase inhibition using cinnamoyl PSEs at 25µg/ml.

We can conclude the following based on the data presented in table 7 and figure 29:

1. All except three of the cinnamoyl PSEs (**1CiI**, **2CiI** and **3CiI** Table 7, entries 1-3) exhibited higher than 10% α-amylase inhibition values (Table 7, entries 4-8) compared to Acarbose as a standard (Table 7, entry 9). Compounds **4CiI** and **4CiS** showed maximum inhibition of 98±2 and 99±1%, respectively (Table 7, entries 4 and 8).
2. Here, as with α-glucosidase inhibition, unlike the case with feruloyl PSEs, an increase in the number of cinnamic acid substituent groups was not proportional to

an increase in the % α-amylase inhibition. For example, the % α-amylase inhibition of **4CiI** and **4CiS** is 98±2 and 99±1, respectively (Table 7, entries 4 and 8) while for **3CiI**, **3CiS** and **3CiIP** is 8±4, 16±2 and 13±7 respectively (Table 7, entries 3, 7 and 6), while for **2CiI** and **2CiIP** is 9±5 and 14±4 (Table 7, entries 2 and 5). **1CiI** showed inhibition value of less than 5 % and was therefore considered to have no significant activity (Table 7, entry 1). Here, there is not an appreciable difference between the tri-substituted (**3CiI**, **3CiS** and**3CiIP**) and di-substituted PSEs (**2CiI** and **2CiIP**) but there is a huge jump in activity in case of the tetra-substituted cinnamoyl PSEs (**4CiI** and **4CiS**). Therefore, the trend in the % α-amylase inhibition is: tetra-substituted > tri-substituted ~= di-substituted > mono-substituted PSEs. In this case, the presence or absence of the diisopropylidene ring does not influence the activity very much, there is some other interaction between the PSEs and α-amylase that enhances the activity for the tetra-substituted PSEs.

3. Cinnamoyl PSEs with free OH groups on sucrose show comparable % α-amylase inhibition compared to the same ones where sucrose 'OH' is protected by acyl moiety. For example, the % α-amylase inhibition of the di and tri- substituted compounds **2CiI** and **3CiI** with free sucrose OH is 9±5 and 8±4, respectively (Table 7, entries 2 and 3), while the corresponding **2CiIP, 3CiIP** with acyl protection is 14±4 and 13±7, respectively (Table 7, entries 5 and 6)**.**
4. The diisopropylidene protecting group has limited effect on the % inhibition activity. Consider the % α-amylase inhibition values of the pairs **4CiI** and **4CiS** with 98±2 and 99±1, respectively (Table 7, entries 4 and 8), **3CiI** and **3CiS**, 8±4 and 16±2 (Table 7, entries 3 and 7).

Similar to the case of α-glucosidase, in this case, three PSEs, **4FS, 4CiI** and **4CiS** were tested for their IC_{50} values and were found to be comparable to the standard, Acarbose. The data is represented in the table 8.

Table 8: IC_{50} values of PSEs screened for α-amylase inhibition

Entry	Compound	IC_{50} (µM)
1	**4FS**	2 ±1
2	**4CiI**	1±0.2
3	**4CiS**	0.8±0.1
4	**Acarbose**	5±0.1

From Table 8, it is observed that the tetraferuloyl PSE, **4FS** and the tetracinnamoyl compounds **4CiI** and **4CiS** were found to have IC_{50} values comparable to that of Acarbose and were just as potent as Acarbose.

A comparison of the α-glucosidase inhibition and the α-amylase inhibition of the PSEs is summarized in figure 30 below.

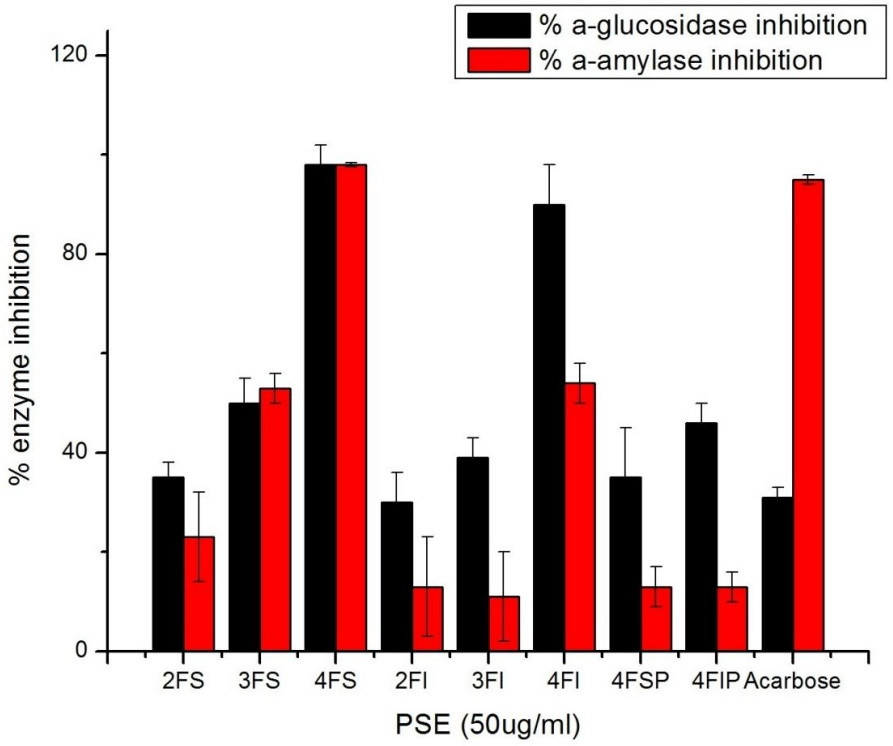

Figure 30: Comparison of the α-glucosidase and the α-amylase inhibition of PSEs.

From figure 30, it can be seen that for most of the PSEs except **3FS** and **4FS**, the PSE has a higher inhibition of α-glucosidase than that of α-amylase. Selective inhibition of α-glucosidase is critical to dampen formation of sugars. α-Amylase is responsible for the

breakdown of starch into oligo and disaccharides and therefore its inhibition would give rise to an intestinal environment rich in long chain carbohydrates which are ideal for fermentation by gut microbiota. The fermentation products cause flatulence, diarrhea, bloating, abdominal pain or discomfort.[18] Remarkably, in case of Miglitol, the severity of these side effects is lower as compared to Acarbose. That's because Miglitol shows lower inhibition of α-amylase in comparison to Acarbose.[9] We hypothesize that potent, non-systemic drugs with greater selectivity towards α-glucosidase and minimum inhibition of α-amylase should exhibit lesser side effects. Towards this end, we aim to develop Phenylpropanoid Sucrose Esters (PSEs) as lead antidiabetic drug candidates that fulfill the above criteria to overcome the side effects (as seen from the in vitro results).

2.4 Summary

In vitro inhibition studies for PSEs indicated that most of the PSEs (feruloyl, coumaroyl and cinnamoyl) were much better than the standard drug Acarbose at a concentration of 50µg/ml towards the inhibition of α-glucosidase. Among the feruloyl PSEs, two of them, **4FI** and **4FS** showed almost complete inhibition of α-glucosidase (90 and 98% respectively) and in case of the cinnamoyl PSEs, the highest inhibition was recorded for the tetracinnamoyl PSEs, **4CiI** and **4CiS** which was 77% and 74% respectively. The IC_{50} values for these four compounds ranged from 4 to 9µM as compared to 328µM for Acarbose. This indicates that the PSEs are much more potent than Acarbose. For the feruloyl group of compounds, the trend in the % α-glucosidase inhibition is: tetra-substituted > tri-substituted > di-substituted > mono-substituted PSEs while that for cinnamoyl is tetra-substituted > tri-substituted ~= di-substituted > mono-substituted PSEs. As regards α-amylase, the trend in enzyme inhibition for both feruloyl and cinnamoyl PSEs is tetra-substituted > tri-substituted ≥ di-substituted > mono-substituted PSEs. Most of the PSEs were not as active as Acarbose in their inhibition, with only three PSEs, **4FS**, **4CiI** and **4CiS** having a percentage inhibition similar to that of Acarbose, (between 97 to 98%) and their IC_{50} values were comparable to Acarbose (0.7-2µM for the former three and 5µM for Acarbose). This result is desirable to us because, as discussed in chapter one, a greater selectivity towards α-glucosidase than α-amylase would reduce the GI side effects that come with the AGIs. Therefore, PSEs may be better situated in terms of reduction of these side-effects.

This study has provided the following information regarding the SAR for PSEs:

1. The type, position and number of phenylpropanoid substituents on the sucrose core greatly influence the inhibition for both the enzymes, α-glucosidase and α-amylase.
2. In general, the greater the number of phenylpropanoid substituents, the greater is the inhibition for both the enzymes.
3. The presence of a free 'OH' group on the phenyl ring is important to the potency and the protection of this 'OH' by acyl moiety impedes the potency.
4. In case of the cinnamoyl compounds, the absence of free phenyl 'OH' for the tetra substituted compounds does not diminish the activity indicating that in this case, there could be a different binding mechanism to the enzymes.
5. The diisopropylidene group does not seem to play a great role in the inhibition of α-glucosidase, however, the presence of the diisopropylidene group reduces the activity by half the value in case of α-amylase inhibition.

Based on these results, PSEs prove to be useful candidates as new lead AGI drugs and their potential needs to be investigated further. The succeeding chapters will deal with in silico and in vivo studies of PSEs along with further SAR studies.

Chapter 3. In silico studies: Docking of PSEs with α-glucosidase and α-amylase

3.1 Introduction

In the previous chapter, the anti-diabetic activities of PSEs were tested by measuring the inhibition of the enzymes, α-glucosidase and α-amylase. From the results, it was evident that most of the PSEs are good candidates as AGIs. Another important study in the drug discovery process is to study the binding of the drug/ligand (PSE) with the afore-mentioned enzymes. Through the docking simulations, one can identify the various modes by which the ligand binds to the enzymes, which would give us an idea of the various functional groups and the 3D orientations that contribute to better binding with the enzyme active site(s). Docking study usually involves the calculation of ligand binding affinities in order to rank and determine the most likely conformations that the ligand adopts at the binding site. The following sections give a very brief introduction to calculation of binding affinities (employed in docking) and on docking as well as Molecular Dynamics (MD) simulations.

Accurate calculations of ligand binding affinities computationally are very difficult as a lot of factors play a role in determining the binding energy. One not only has to consider interactions between the ligand and the protein but also the myriads of interactions between the surrounding water molecules and counter ions in the environment of the protein. Also, in vivo the protein and ligand are not rigid but are flexible in three dimensions. Therefore, flexibility also plays a big role in determining the binding energy. Even so, there have been several advances in the use of computational methods to determine binding affinity which can greatly help in the drug design process. There are several factors that affect the binding energy like potential energy, pH, environment surrounding the enzyme and other ligand-enzyme interactions. It is possible to calculate the potential energy of ligand, protein or the complex using quantum molecular techniques. Either ‘ab-initio’ methods (quantum chemistry) or ‘semi-empirical’ methods (quantum chemistry methods with several approximations) can be used, with the latter being faster and less expensive computationally. Bond stretching, angle bending, bond torsions, van der Waals interactions and Coulombic forces all contribute to potential energy. As stated earlier, protein-ligand binding is greatly influenced by the surrounding media which consists mainly of salts and

water. Therefore, the dielectric environment created by water, solvation energy and hydrophobic interactions also need to be considered for calculation of binding affinities. Charge interactions between atoms are screened when water molecules form a hydration shell around the atoms. Dissolved salts also cause electrostatic screening. The pH also greatly affects binding affinity. Each of the factors affecting the binding energy is calculated separately by various mathematical models. The various docking programs use the 'Poisson Boltzmann' equation to solve for the electrostatic part of the solvation energy due to such molecular interactions. This model is called the PB (Poisson Boltzmann model). A faster, more generalized model called the GB (Generalized Born) equation can also be used. Hydrophobic interactions are calculated by a separate solvation energy term which is proportional to molecular surface area (SA). Thus together this gives either PBSA or GBSA methods, one of the two methods routinely used in docking. Methods such as MD (Molecular Dynamics) or MC (Monte Carlo) simulations use simulations with explicit water molecules to calculate the effect of solvent in binding of ligands to protein. These approaches include effects of dielectric screening, hydrophobicity, solvation energy due to polar groups etc. [68,69]

Entropy of ligand as well as the protein also contribute significantly to free energy. If one or both of them have a strained configuration during binding, that will contribute positively to binding energy in the sense that it will make the binding energy less negative or oppose binding. The free energy of binding is calculated using the equation,

$$\Delta G = \mu_{PL} - \mu_P - \mu_L$$

where ΔG stands for free energy of binding, μ = free energy, PL= protein ligand complex, P = protein and L = ligand.

Docking is one of the approaches to study binding modes of the ligand as well as to calculate the free energy of binding. Docking helps to identify the best or most stable conformation for binding. A docking algorithm gives the best docked poses for a ligand bound with the protein and each docked pose is assigned a score. It ranks the conformations generated according to the score, i.e. from the most stable (most negative binding energy) to the least stable. [68,70] These docked scores are not very efficient predictors of binding affinities. In

certain cases, where a known 3D structure for the protein does not exist, homology modeling is used to generate a 3D model of the protein for the purpose of docking.[70] Some programs include ligand charges and solvent effects thus making the docking score better. PBSA and GBSA models include solvation models into docking. Flexibility of the ligand and protein are also important factors in docking. Traditional methods use rigid ligand and protein which may not be very accurate as, in biological systems, that is never the case. However, docking processes can be made to include sidechain flexibility where certain residues present in the active site of the enzyme can be made flexible which improves the fit of the ligand.[70,71,72]

Another approach to calculate binding affinity is the use of free energy methods, an example of which is the MM-PBSA (Molecular Mechanics-Poisson Boltzmann Surface Area) or MM-GBSA method. In this method, MD simulations of ligand, protein and their complex are run to calculate the binding energy. This method takes into account explicit water (solvent) molecules as well as empirical force field. MD takes into account the dynamic nature of the complex as opposed to a rigid or static model used in docking. Although MD simulations are time consuming they give a more accurate value for binding energy.[70]

A combination of docking and MD simulations is an effective technique to screen and identify potential drug candidates. Docking does not take into account explicit solvent molecules or the flexibility of the ligand and protein and the scoring functions used in docking have imperfections.[69] Although docking is not very accurate, is a fast and computationally inexpensive method to screen huge compound libraries. MD simulations are computationally more expensive and thus can be used at later stages to refine the docking or scoring process. However, MD simulations take the flexibility of both ligand and protein into account and also use explicit water molecules in the simulation and MD simulations generally return accurate values of binding energies. As such, a combination of the two can be very useful in drug discovery or design process. [70]

3.2 Methods

3.2.1 Molecular docking of PSEs with α-glucosidase

The feruloyl and cinnamoyl PSEs docked were selected according to differences in structures. The binding modes for each of the PSEs docked into homology-modeled yeast α-glucosidase using the Maestro suite of applications are given in this section. The X-ray crystal structure for α-glucosidase from *Saccharomyces cerevisiae* has thus far not been reported. In order to find a suitable template to build a homology model of this enzyme, proteins with similar sequences were found using the 'BLAST' algorithm. Yeast isomaltase (PDB ID: 3A4A) which shared 72% sequence identity and 85% similarity with yeast α-glucosidase was used as a template to construct the homology model (Fig. 7).[73] AutoDock was used for docking simulations and visualizations of the binding modes were done with Maestro. The receptor was prepared by first removing water molecules before adding Gasteiger charges and hydrogen atoms. In order to increase the flexibility of the docked ligands, the maximum number of rotatable bonds was chosen. The gridded binding site was chosen to be the site that houses the glucose molecule in the yeast isomaltase. The Lamarckian Genetic algorithm was chosen for the docking and a total of 100 binding modes were chosen.

3.2.2 Molecular docking of PSEs with α-amylase

Schrödinger's Maestro software was used to study the molecular interaction of the PSEs with porcine pancreatic α-amylase. For these studies, only 6 PSEs (2FS, 3FS, 4FS, 4FI, 4CiS and 4CiI) having % α-amylase inhibition higher than 20% were used. The aim of the study was to discover the probable binding modes of the PSEs at the primary and also secondary binding sites, if any, and finally to calculate binding affinity using the molecular dynamics (MD) approach. The enzyme, porcine pancreatic α-amylase (PDB ID: 1OSE)[74] was imported and the structure was processed using the Protein Preparation Wizard module. Following this, the receptor grid was generated based on the coordinates of the bound Acarbose in the crystal structure, which was known as the primary binding site. Liu et al. had characterized two other binding sites within the enzyme[74], which are known as secondary binding sites and they will be annotated as SS1 and SS2. The Glide suite was

used to perform the docking of the PSEs with the Extra Precision (XP) option. Water molecules that are 5 Å away from the primary binding site were retained during the docking. In addition, residues that possess bonds containing hydroxyl and thiol groups were considered to be flexible. On the other hand, single bonds not having a specific chirality in the ligands are considered to be flexible as well. After the docking, the lowest-energy docked pose was chosen for each PSE and analyzed for the interactions between the ligand and the enzyme to account for its experimental activity.

3.2.3 Molecular dynamics (MD) simulations

MD simulations were only carried out for docking with α-amylase because structural information for it is available whereas a homology model was built for α-glucosidase. The lowest-energy docked poses for each PSE were used as initial structures for MD simulations. Structure preparation was done using LEaP module, while molecular dynamics production with ff99SB force field[75] was done using 'pmemd' module, both modules are part of AMBER 9.0 suite,[76] TIP3P water molecules were added with the minimal distance between the complex and the edge of water box set as 5 Å. Counterions were added to maintain neutrality of the system. Non-bonded cutoff was set to 12.0 Å. SHAKE algorithm[77] was applied with all bonds involving hydrogen atoms restrained. After minimisation and heating up from 10 to 300 K in 100 ps, production MD was carried out at 300 K, with timestep of 2.0 fs for 5 ns period, with complex conformation collected every 1 ps. For post-processing analysis and binding free energy calculation, all water molecules, counterions, and periodic boundary information were removed from the trajectory. Single-trajectory approach was used for all binding free energy calculations. Five hundred regular snapshots were used for solvated interaction energy (SIE) using sietraj[78,79] to calculate binding free energy.

3.3 Results and Discussion

3.3.1. Docking of PSEs with α-glucosidase

The colouring scheme in the binding mode pictures for docking with α-glucosidase inhibition is as follows:

- The sucrose core of the ligand (PSE) is coloured in green.
- The substituents at various positions on the ligand (PSE) are coloured as; Substituent at the 6' position is coloured in pink; Substituent at the 4' position is coloured in purple; Substituent at the 3' position is coloured in blue; Substituent at the 3 position is coloured in yellow.
- The enzyme is represented in 'ribbon style' and the active site shows a molecule of glucose docked in it in ball representation.

3.3.1.1 Docking of feruloyl PSEs with α-glucosidase

3.3.1.1.1 Feruloyl diisopropylidene PSEs

The first category of compounds under the feruloyl PSEs are the group of compounds having the diisopropylidene ring in the sucrose moiety. These compounds also do not have the acetoxy protection on the 'OH' group of ferulic acid. Table 9 shows the % α-glucosidase inhibition of the PSEs. The binding mode pictures for these PSEs are given in figure 31.

Table 9: % α-glucosidase inhibition values for feruloyl diisopropylidene PSEs

Entry	PSE	% α-glucosidase Inhibition
1	**2FI**	30±6
2	**3FI**	39±4
3	**4FI**	90±8

From the in vitro experimental data presented in Table 9, entries1-3, it is seen that the compound **4FI** has the highest enzyme inhibition in this category, namely 90±8 (Table 9, entry 3). On correlating the activity or enzyme inhibition with the binding modes, one can

see the differences that could possibly explain the variation in the activities of the compounds.

- First let us consider the diferuloyl compound, **2FI** (Fig. 31). In this case it is seen that the sucrose core projects into the binding pocket while the other feruloyl substituents at 3' position (blue) and that at 6' position (pink) are spread out at the periphery of the enzyme.
- From looking at the binding mode picture for compound **3FI** (Fig. 31), one can see a similar trend but now there is a third feruloyl group at the periphery (at 4' position- purple).
- Finally, in case of the tetra feruloyl compound, **4FI** (Fig. 31), by means of a reorientation, the fourth feruloyl group at position 3 (yellow) is seen to project towards the active site where the glucose molecule is docked. From our analysis it was seen that all of the above compounds did not dock into the active site but rather at a different site close to the active site and seem to block the entry of the substrate into the active site, thus inhibiting the enzyme. This is similar to the inhibition of α-glucosidase by a similar means reported by Yan and colleagues.[73] The substituent at position 3 (yellow) is seen to form a hydrogen bond (refer Ligand Interaction Diagram or LID- Fig. 32) with one of the residues, ARG442. There is another hydrogen bond between the substituent at 3' position with ASN242. There are four π-π stacking bonds between the aromatic rings of the PSE with the residues PHE178, PHE158, PHE314 and ARG442. Although the di and tri-feruloyl compounds also show significant enzyme inhibition30±6 and 39±4% respectively (Table 9, entries 1 and 2), we believe that in those cases the interaction with the enzyme is not as strong as in case of **4FI**. In case of **4FI**, the substituents at positions other than at position 3 on the sucrose core, are thought to orient the molecule in order to facilitate stronger interactions which in this case indicates the interaction of the fourth substituent at position 3 with amino acid residues close to the active site. The tetrasubstituted feruloyl compound **4FI** has therefore the highest activity of 90±8 (Table 9, entry 3). The ligand interaction diagram below (Fig. 32) gives a 2D picture of the PSE **4FI** bound to the enzyme and the various interactions holding it in place.

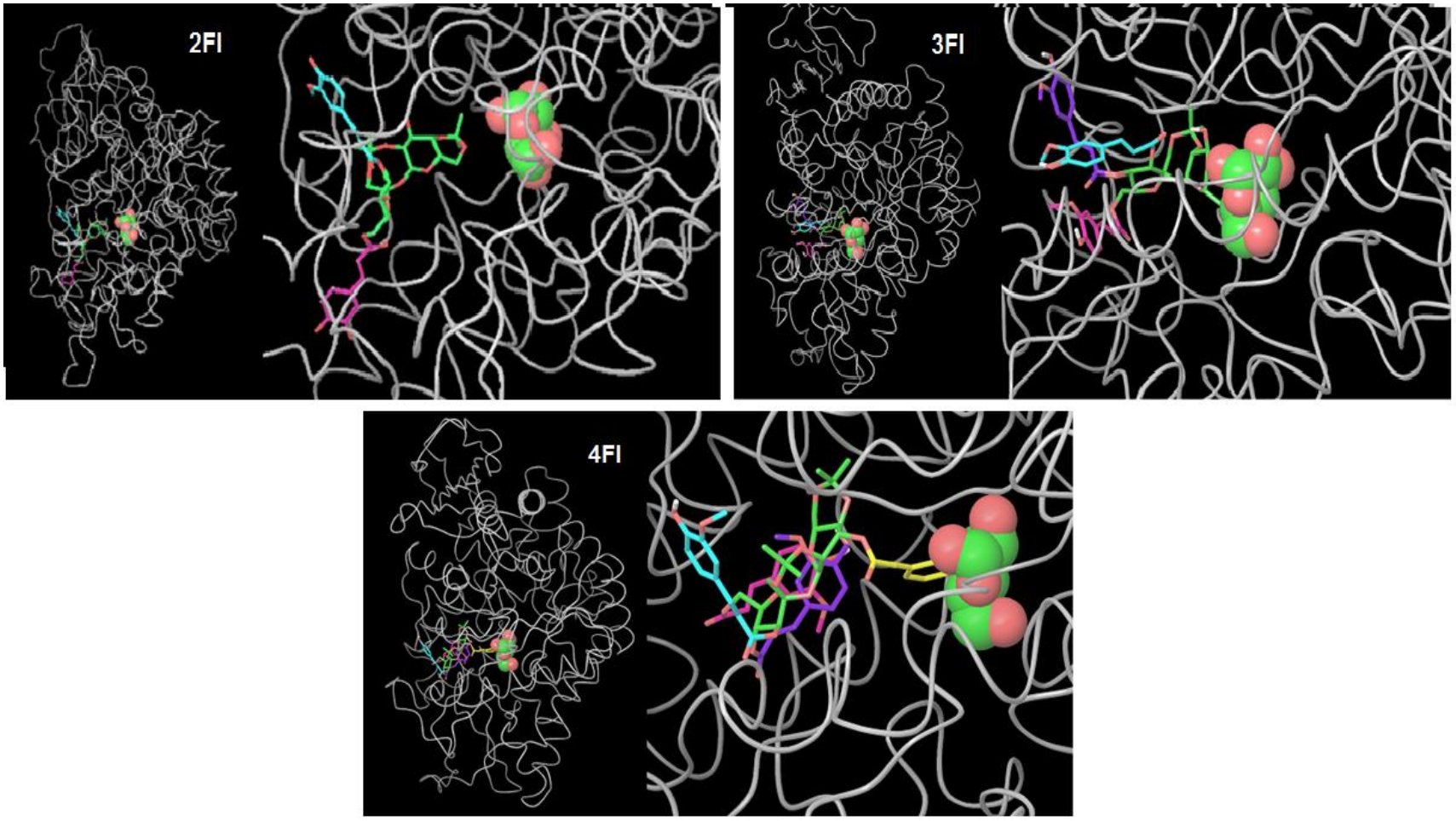

Figure 31: Binding mode pictures for feruloyl diisopropylidene PSEs.

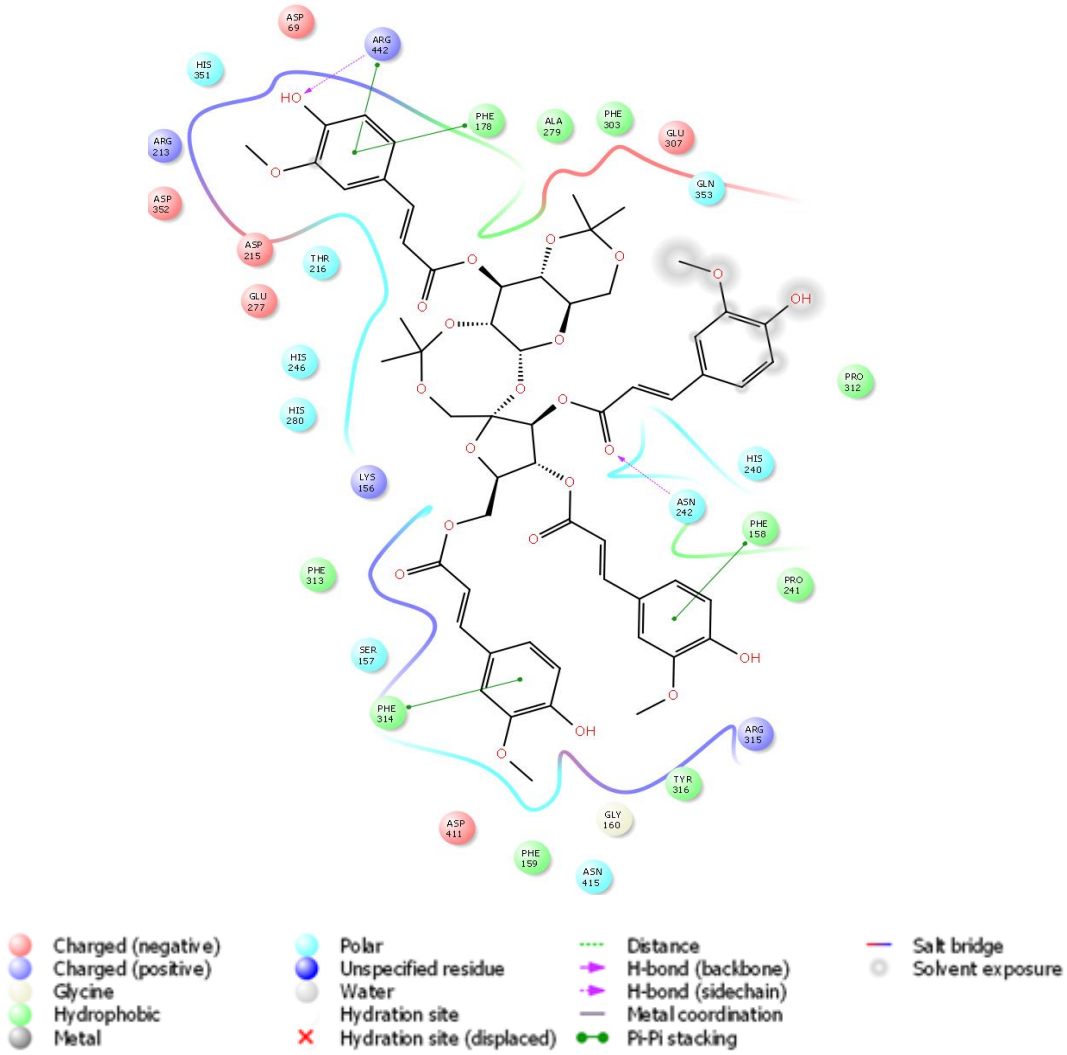

Figure 32: Ligand Interaction Diagram for **4FI.**

3.3.1.1.2 Feruloyl sucrose PSEs

The compounds under this category are feruloyl PSEs that have a sucrose core without the diisopropylidene ring. There is no acetoxy protection on the 'OH' groups of the feruloyl substituents. Table 10 recapitulates the % α-glucosidase inhibition values obtained experimentally and the binding mode pictures (Fig. 33) follow.

Table 10: % α-glucosidase inhibition values for feruloyl sucrose PSEs

Entry	PSE	% α-glucosidase Inhibition
1	**2FS**	35±3
2	**3FS**	50±5
3	**4FS**	98±4

Once again the binding modes for the compounds in this category show a similar trend as with the earlier ones. The following conclusions are made based on Table 10 and Figure 33:

- The di and triferuloyl compounds **2FS** and **3FS** have moderate inhibition activity of 35±3 and 50±5 (Table 10, entry 1 and 2). They each have the sucrose core projecting slightly into the binding pocket while the rest of the substituents are spread along the surface of the enzyme close to the active site with the glucose molecule.
- Here, in case of the tetra substituted compound, **4FS,** once again, the substituent at the position 3 on sucrose (yellow) is projecting into the binding pocket and is positioned almost at the active site and seems to be overlapping with the site where the glucose molecule is docked. Here once again the substituent at position 3 (yellow) interacts withthe acidic regions in the enzyme. Compound **4FS** is seen experimentally to have the highest inhibition value of 98±4% (Table 10, entry 3) all the feruloyl compounds tested. The substituent at position 3 is seen to form a

hydrogen bond with ASP215 while the one at 3’ position forms a hydrogen bond with GLU277 (refer LID Fig 34). The aromatic rings of the PSE show π-π stacking interactions with the residues HIS240, HIS246, HIS280, PHE158 and PHE303. Here, it can be seen that unlike the previous tetra subsitutued compound, **4FI**, the compound is not solvent exposed. **4FS** does not have the diisopropylidene ring on the sucrose core. Therefore, as the core becomes more flexible or is less restricted there is more freedom for **4FS** in the steric sense. Hence, the molecule assumes the best possible conformation.

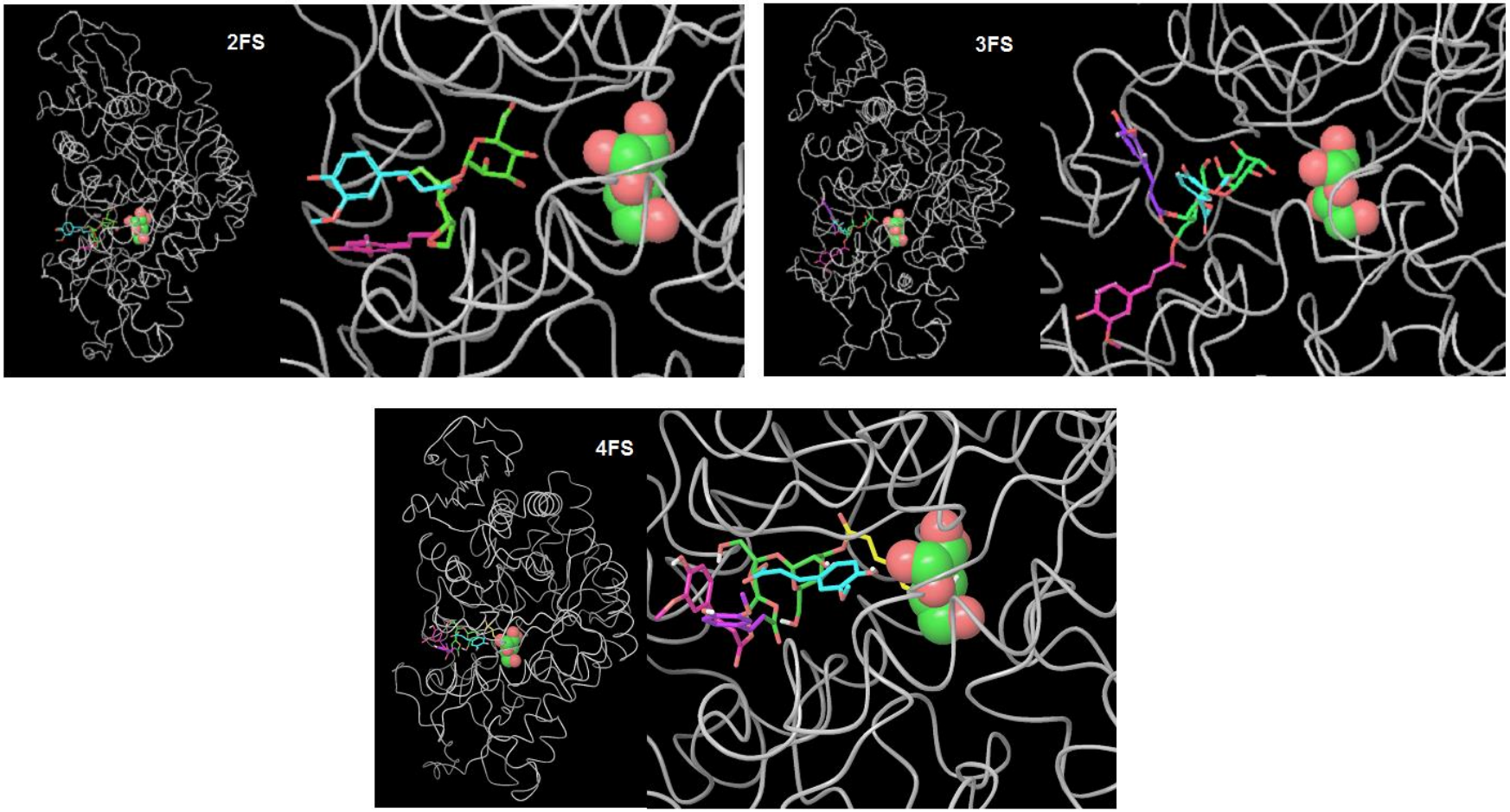

Figure 33: Binding mode pictures for feruloyl sucrose PSEs.

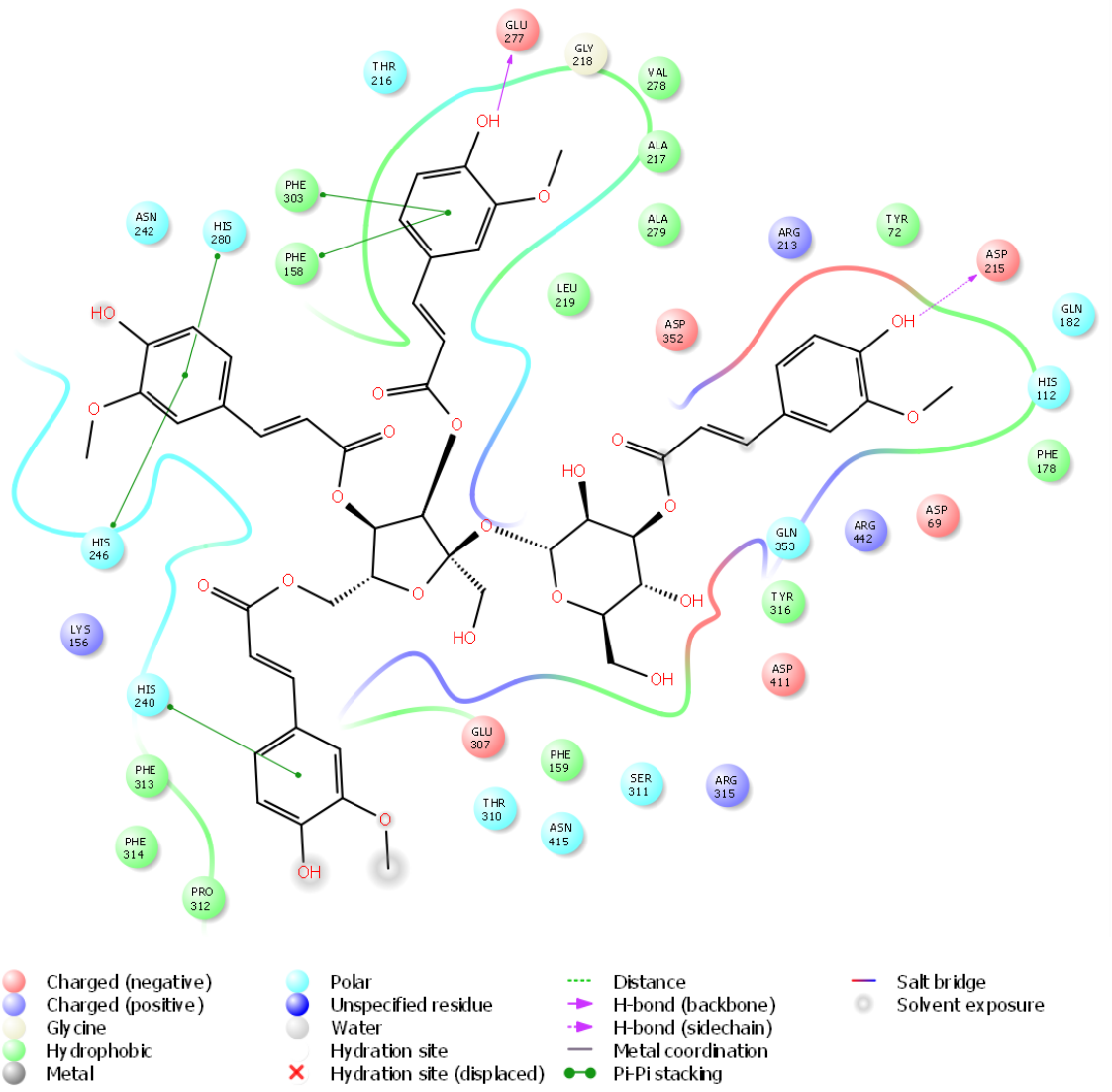

Figure 34: Ligand Interaction Diagram for **4FS**.

3.3.1.2 Docking of cinnamoyl PSEs with α-glucosidase

3.3.1.2.1 Cinnamoyl diisopropylidene PSEs

The compounds under this group have the diisopropylidene ring on the sucrose core. A summary of the experimentally obtained % α-glucosidase inhibition values for these PSEs is given in table 11 followed by the binding mode pictures (Fig 35).

Table 11: % α-glucosidase inhibition values for cinnamoyl diisopropylidene PSEs

Entry	PSE	% α-glucosidase Inhibition
1	**3CiI**	32±3
2	**2CiI**	35±5

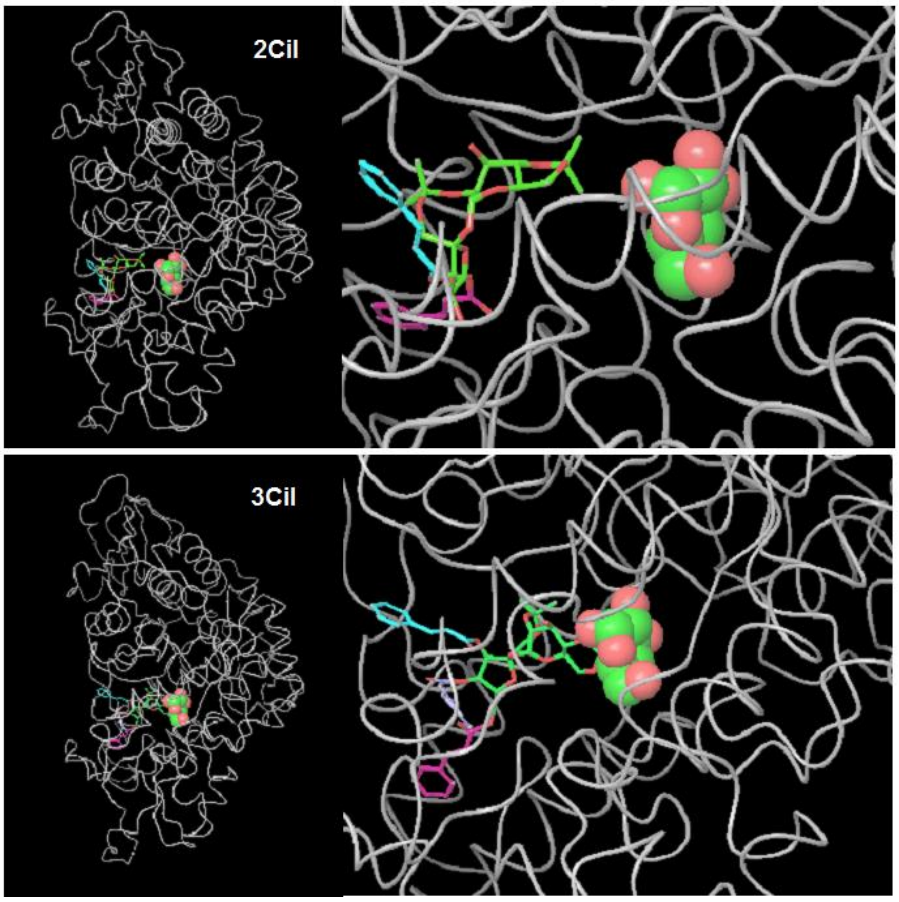

Figure 35: Binding mode pictures for cinnamoyl diisopropylidene PSEs.

- This group of compounds is similar to the first group under the feruloyl series. The sucrose core in these PSEs has the diisopropylidene ring. Once again, here the di and tri cinnamoyl PSEs, **2CiI** and **3CiI** with inhibition values of 35±5 and 32±3% (Table 11, entries 1 and 2) have their sucrose core projecting into the binding pocket while the other substituents are oriented along the surface. There were no major differences in the inhibition values and no major differences in docking orientations.

3.3.1.2.2 Cinnamoyl acetoxy diisopropylidene PSEs

The compounds in this category have the diisopropylidene group and in addition, the OH groups on the sucrose core have acetoxy protection groups**.** A summary of the experimentally obtained % α-glucosidase inhibition values for these PSEs is given in table 12 followed by the binding mode pictures (Fig. 36).

Table 12: % α-glucosidase inhibition values for cinnamoyl acetoxy diisopropylidene PSEs

Entry	PSE	% α-glucosidase Inhibition
1	**3CiIP**	46±2
2	**2CiIP**	46±3

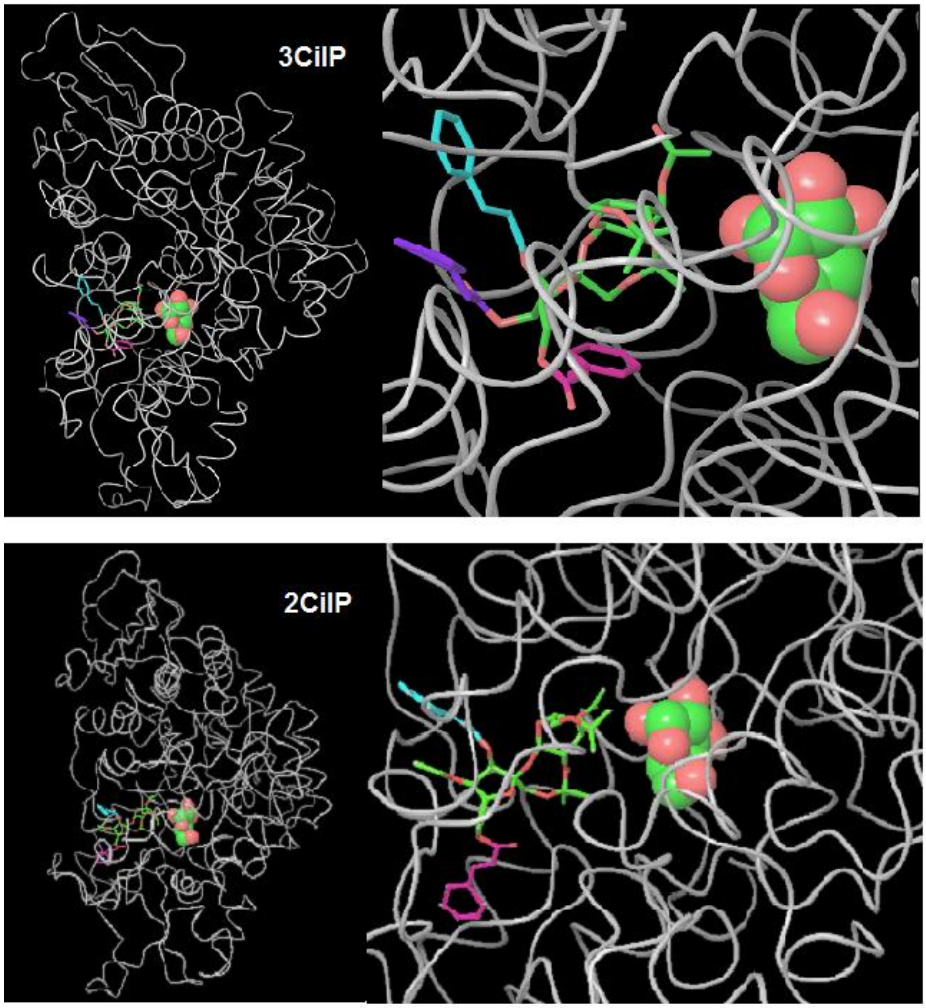

Figure 36: Binding mode pictures for cinnamoyl acetoxy diisopropylidene PSEs.

Almost same values of α-Glucosidase inhibition were observed for both tri and di cinnamoyl PSEs, **3CiIP** and **2CiIP** of 46±2 and 46±3% respectively (Table 12, entries 1 and 2). In this group of compounds, the OH groups on the sucrose core are protected by the acetoxy group. It can be seen that the protection of the sucrose OH does not seem to vary the inhibition values between the two PSEs much and they bind to the enzyme in a similar way as **2CiI** and **3CiI** (Fig. 35).

3.3.1.2.3 Cinnamoyl sucrose PSEs

This is the last category of PSEs tested. These PSEs have the greatest conformational flexibility amongst the cinnamoyl PSEs due to the lack of diisopropylidene ring on sucrose. The % α-glucosidase inhibition is summarized in table 13 and the binding mode pictures for both these PSEs is seen in figure 37.

Table 13: % α-glucosidase inhibition values for cinnamoyl sucrose PSEs

Entry	PSE	% α-glucosidase Inhibition
1	**4CiS**	77±5
2	**3CiS**	34±4

- From looking at the binding mode pictures for the tri and tetra cinnamoyl PSEs (Fig. 37), **3CiS** and **4CiS**, we can once again see that in both cases here, the trend is similar. For the tri substituted cinnamoyl PSE, **3CiS**, the sucrose core (green) projects into the binding pocket while in case of the tetra cinnamoyl PSE, **4CiS**, the PSE reorients itself so that the substituent at position 3 (yellow) is able to project into the binding pocket almost coinciding with the active site containing the glucose molecule. This difference is thought to be due to the increased conformational flexibility.
- **4CiS** shows multiple π-π interactions with the enzyme. The substituent at position 3 has three π-π stacking interactions with three different amino acid residues,

PHE178, ARG442, TYR72. The residue at 3' position interacts with HIS280 and that at 6' position with PHE314 by means of π-π stacking interactions. The latter also forms a salt bridge with LYS156 (Fig 38). **4CiS** has a % inhibition value of 77±5% (Table 13) the highest amongst all the cinnamoyl PSEs. Also, all the other substituents other than that at position 3 (yellow) help to stabilize the geometry of **4CiS** so that they may facilitate stable interactions causing the tetra cinnamoyl PSE to have higher % inhibition. Another interesting thing to note here is that the cinnamoyl PSEs do not have an 'OH' group on the aromatic ring. This limits the number of hydrogen bonds that the PSEs can form with α-glucosidase. In the case of the cinnamoyl PSEs, the interaction is mainly by means of π-π interaction and other hydrophobic interactions.

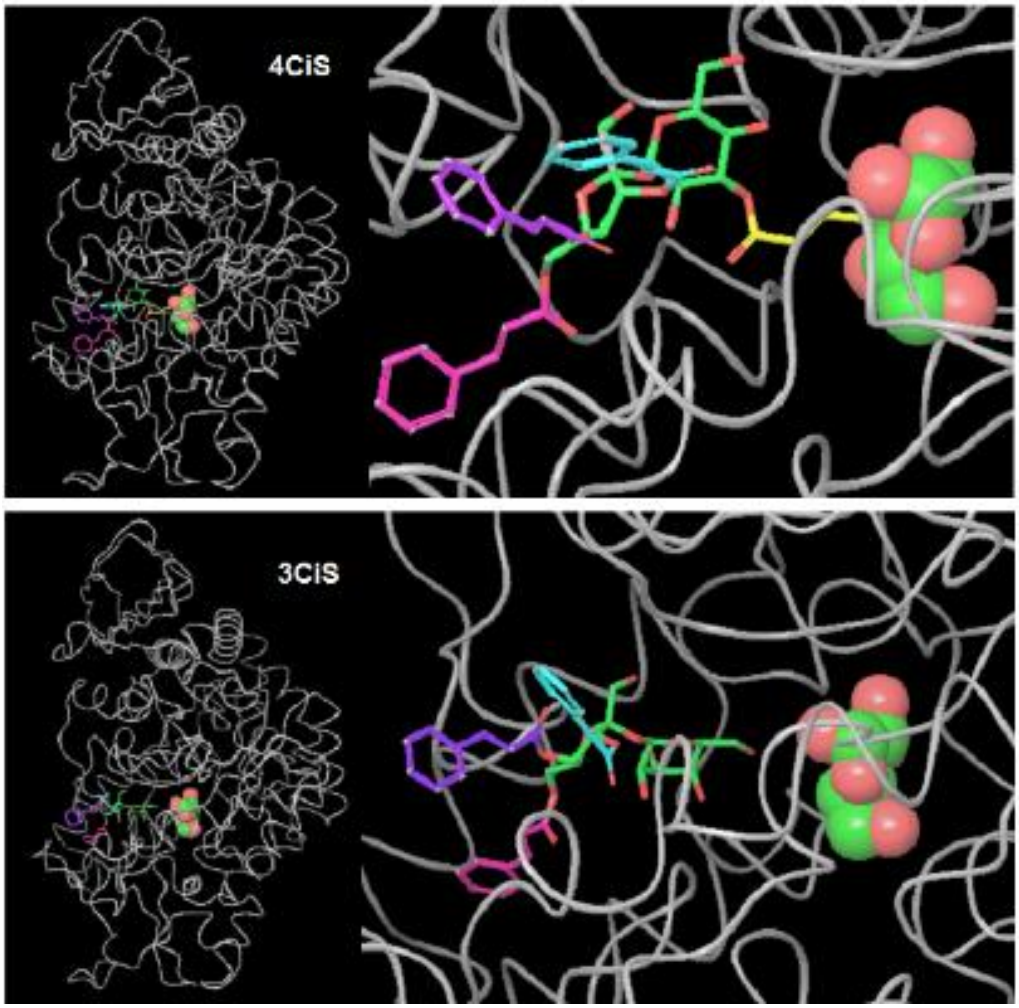

Figure 37: Binding mode pictures for cinnamoyl sucrose.

- Also, it is interesting to note that the tetra cinnamoyl PSE, **4CiS** has inhibition value of 77±5% (Table 13, entry 1) which is less than its feruloyl counterpart, **4FI** which has an inhibition value of 90±8% (Table 13, entry 2). This can be attributed to the fact that there is no free 'OH' group on the aromatic rings that facilitate hydrogen bonding which is thought to increase the strength of the interaction.

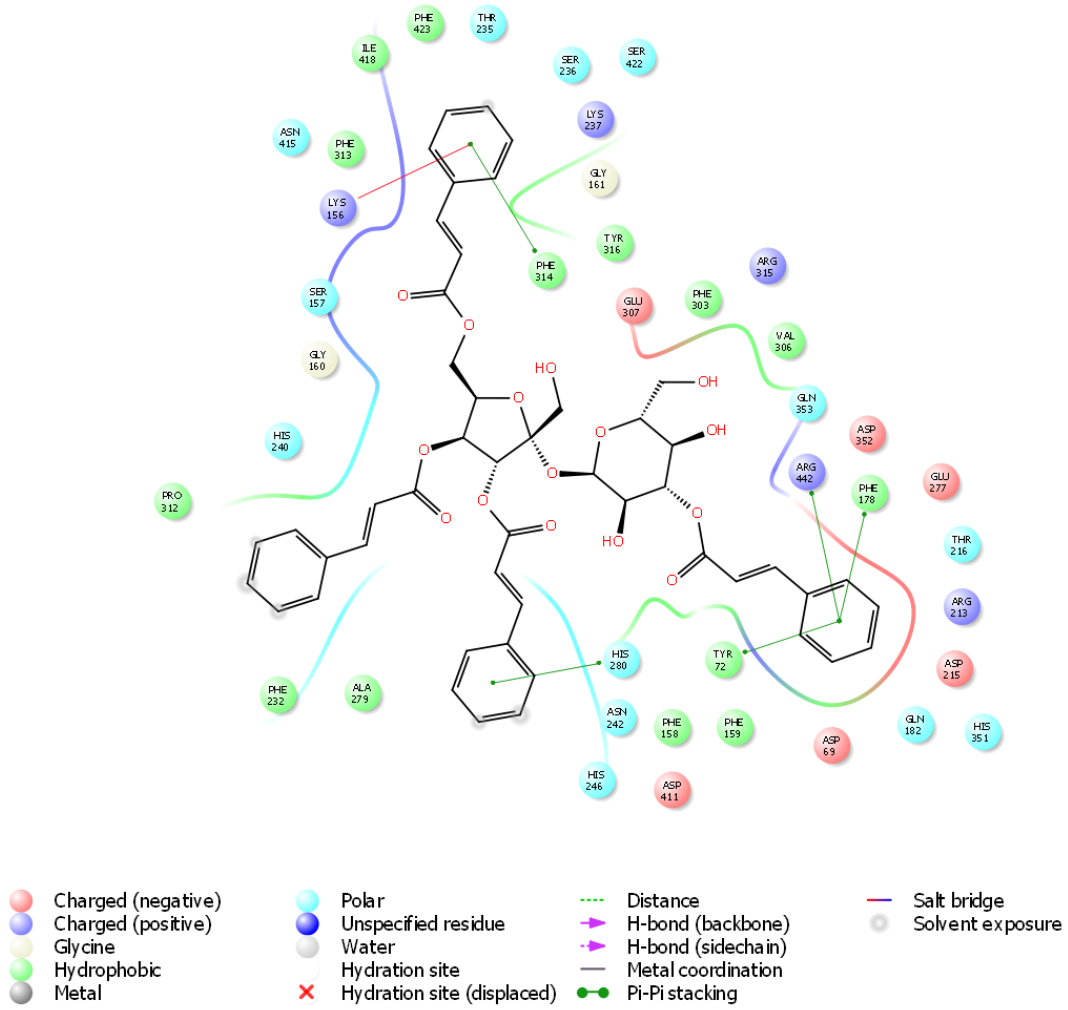

Figure 38: Ligand Interaction Diagram for **4CiS**.

3.3.2 Molecular docking of PSEs with α-amylase

As mentioned in the methods, only 6 PSEs (**2FS, 3FS, 4FS, 4FI, 4CiS** and **4CiI)** having % α-amylase inhibition higher than 20% were used. From the docking studies, it was hypothesized that there were five regions (depicted in red in binding mode pictures) comprising of key residues which form the catalytic site in α-amylase. Interaction of the substituent groups and(or) the core with these residues enhances activity. The greater the interactions, the higher is the inhibition. The following figure (Fig. 39) highlights the catalytic regions in the enzyme.

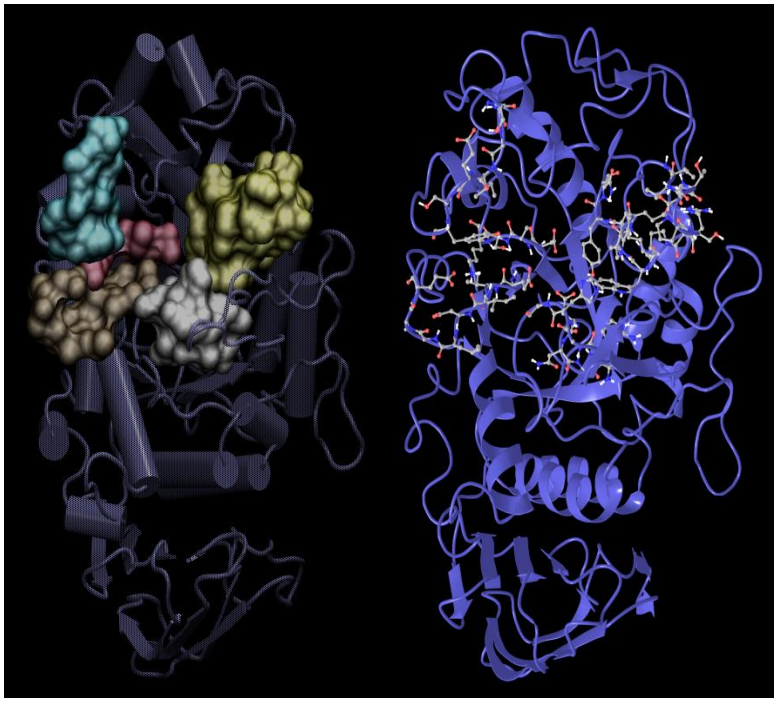

Figure 39: Depiction of catalytic residues in α-amylase (PDB Id: 1OSE).

The binding modes for each of the PSEs docked into the primary binding site of porcine pancreatic α-amylase using the Maestro program are given in this section.

The colouring scheme in all binding mode pictures for α-amylase is as follows:

- The PSEs are depicted in grey.
- From the docking studies, it was hypothesized that there were five regions (depicted in red in binding mode pictures) comprising of key residues which form the catalytic site in α-amylase. Interaction of the substituent groups and(or) the core with these

residues enhances activity. The greater the interactions, the higher is the inhibition. The five regions containing key residues that are thought to be in catalytic site are residues 50-63; 145-151; 197-200; 233-240; 300-306.

- The rest of the enzyme is depicted in blue.

3.3.2.1 Docking of feruloyl PSEs with α-amylase

3.3.2.1.1 Feruloyl sucrose PSEs

The compounds under this category are feruloyl PSEs that have a sucrose core without the diisopropylidene ring. There is no acetoxy protection on the 'OH' groups of the feruloyl substituents. Table 14 recapitulates the % α-amylase inhibition values obtained experimentally and the binding mode pictures (Fig. 40) and LIDs (Fig. 41,42,43) follow.

Table 14: % α-amylase inhibition values for feruloyl sucrose PSEs

Entry	PSE	% α-amylase Inhibition
1	**2FS**	23±9
2	**3FS**	53±3
3	**4FS**	98±1

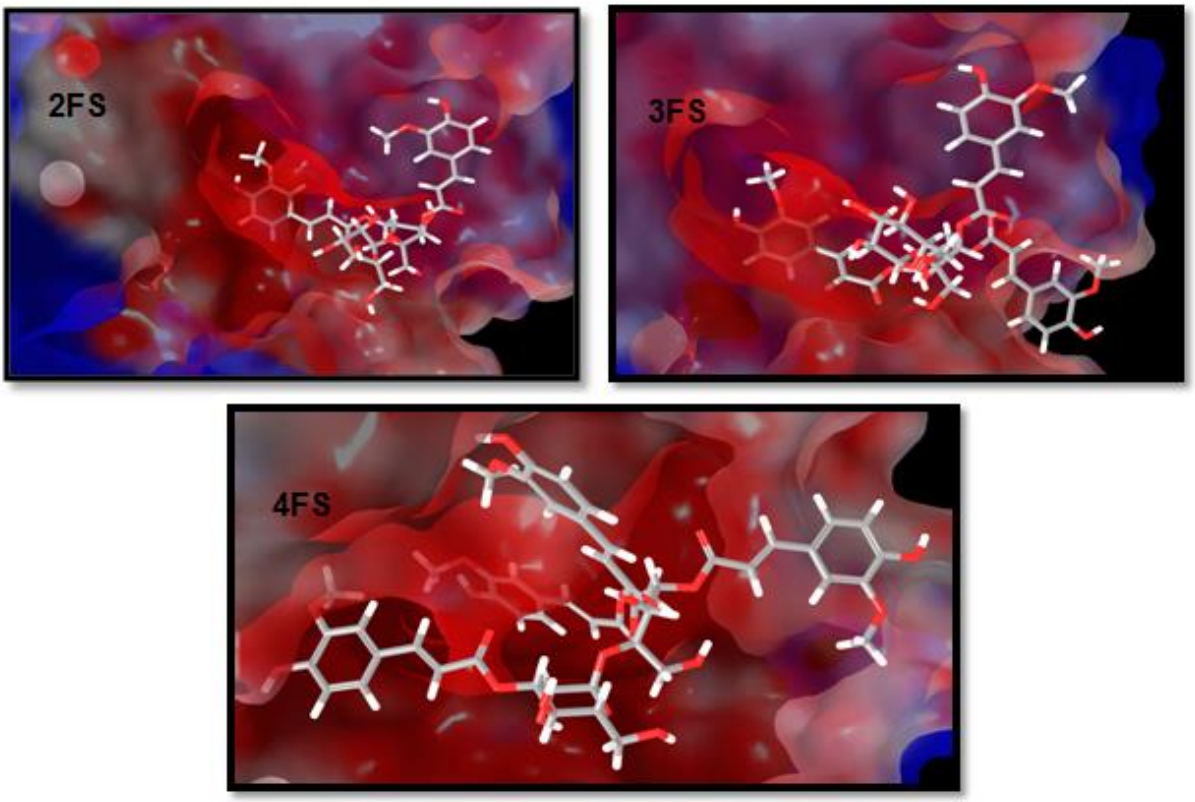

Figure 40: Binding modes for feruloyl sucrose PSEs.

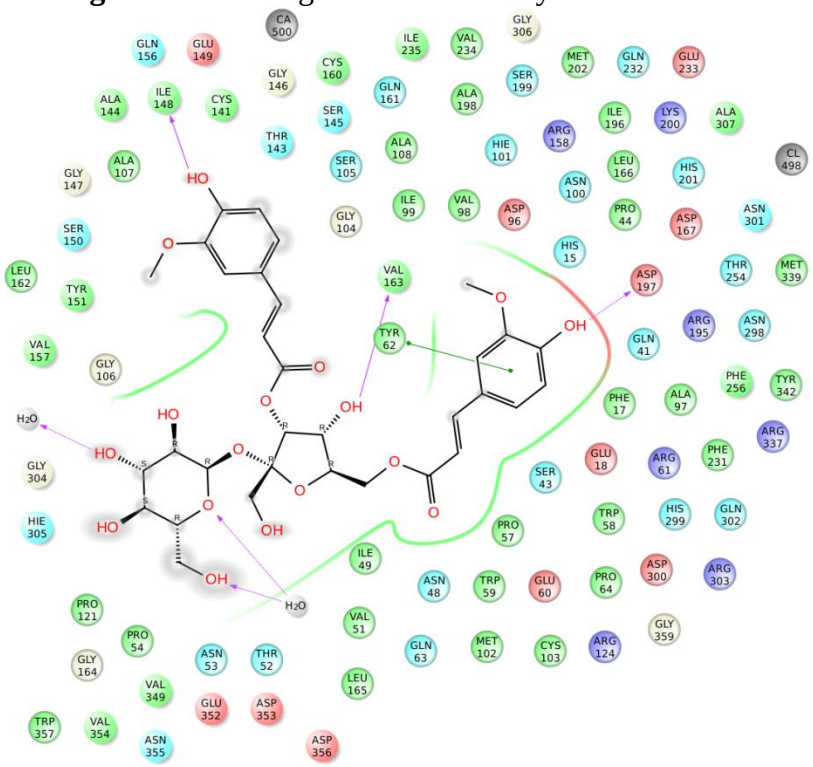

Figure 41: LID for **2FS**.

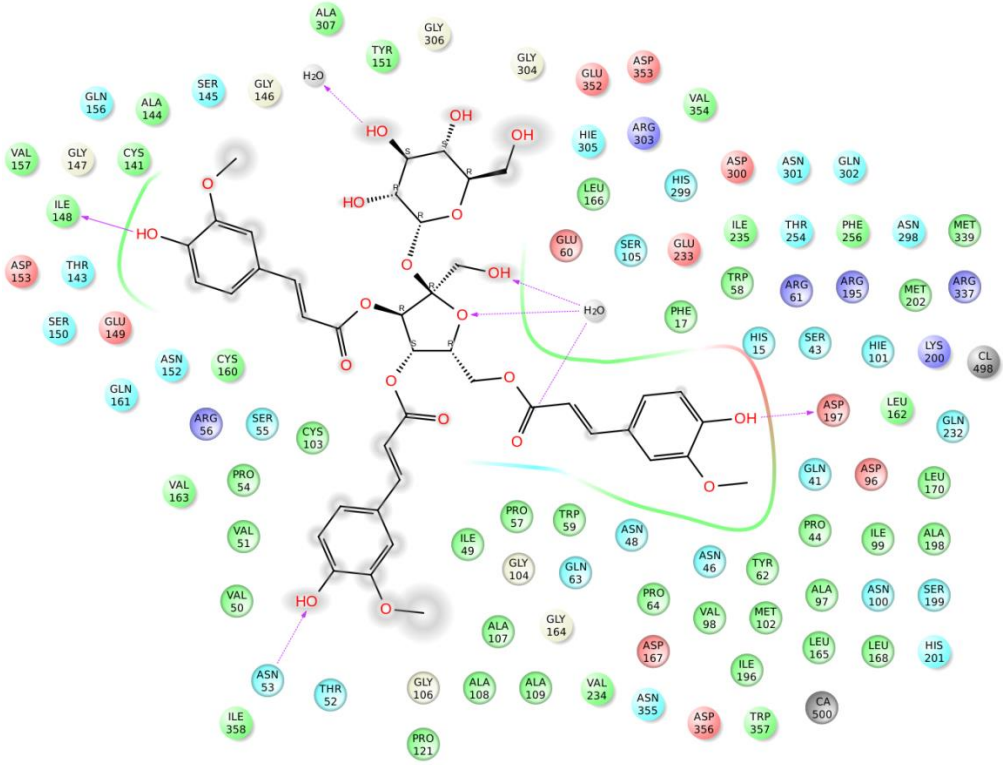

Figure 42: LID for **3FS**.

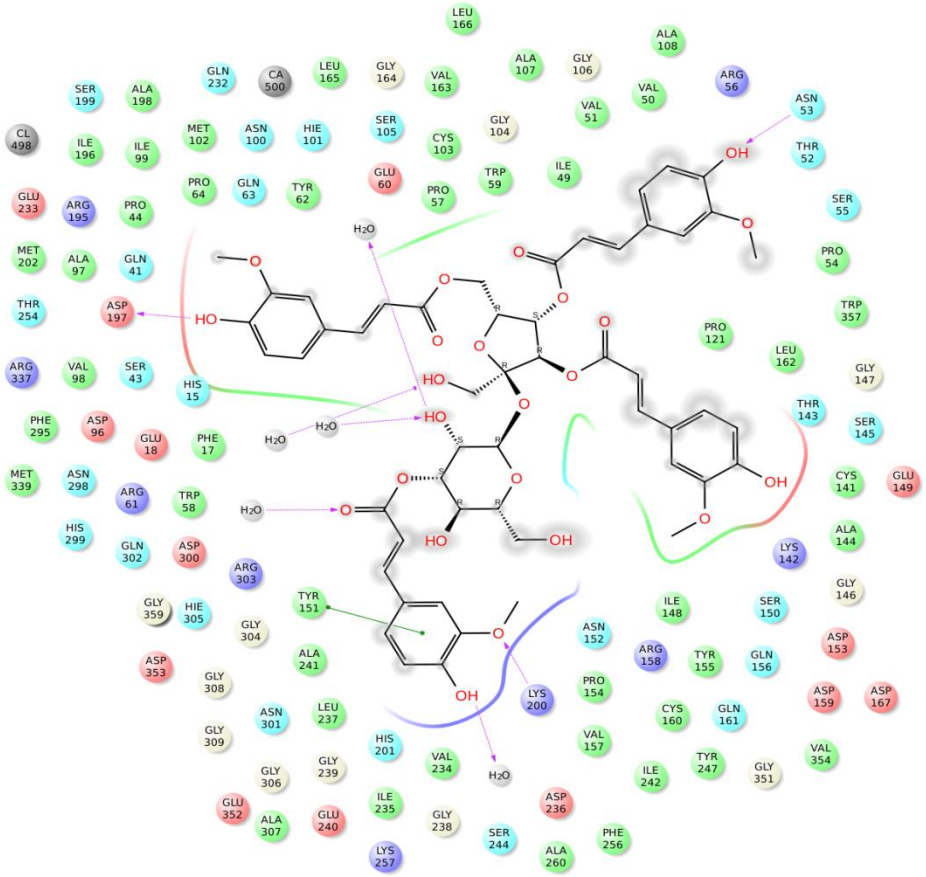

Figure 43: LID for **4FS**.

Looking at the binding modes and LIDs for the compounds in this category, the following conclusions are made based on table 14 and Figures 40-43:

- The di and triferuloyl compounds **2FS** and **3FS** have moderate inhibition activity of 23±9% and 53±3% respectively (Table 14, entry 1 and 2). They each interact with some of the regions in the catalytic site but not all the substituent arms of the PSEs interact with the catalytic region. **3FS** has a higher percentage inhibition than **2FS** due to greater interaction or hydrogen bonds with the catalytic regions as can be seen from the ligand interaction diagrams for the two (Fig. 41,42).
- In case of the tetra substituted compound, **4FS**, the sucrose core as well as all four substituents are seen to interact with the catalytic region. Due to a greater interaction with the said region, the % inhibition rises to 98±1%. As **4FS** has four feruloyl substituents on the sucrose core, the number of possible interactions by means of hydrogen bonds is also greater than the di and tri substituted feruloyl PSEs. Also, the absence of the diisopropylidene ring on the sucrose core gives **4FS** greater steric flexibility enabling it to adapt a better docked conformation.

3.3.2.1.2 Feruloyl diisopropylidene PSEs

Under this category only one PSE, namely **4FI** was chosen for the docking study as the % inhibition of the others was quite low. This compound also does not have the acetoxy protection on the 'OH' group of ferulic acid but it has the diisopropylidene ring on the sucrose core. Table 15 shows the % α-amylase inhibition of the PSE. The binding mode picture and the LID are given in figure 44 and 45.

Table 15: % α-amylase inhibition values for feruloyl diisopropylidene PSEs

Entry	PSE	% α-amylase Inhibition
1	**4FI**	54±4

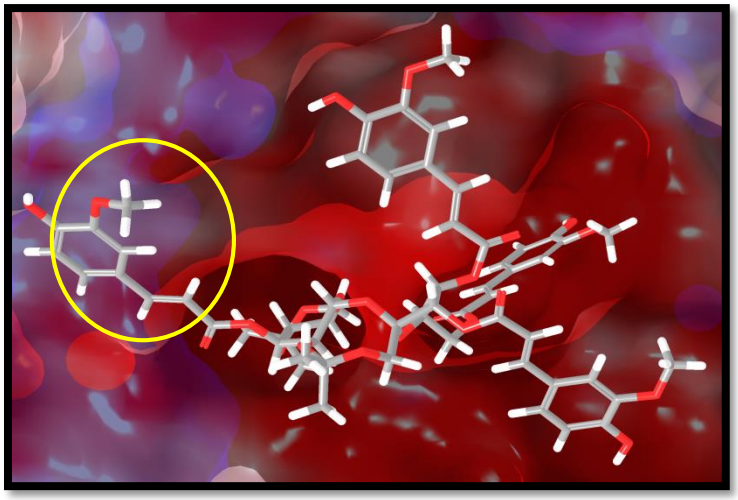

Figure 44: Binding mode picture for **4FI**.

From the experimental data presented in Table 15, it is seen that the compound **4FI** has an α-amylase inhibition of 54±4% (Table 15, entry 1). On correlating the activity or enzyme inhibition with the binding modes, one can see that the main difference between **4FI** and **4FS** is that one of the substituents in **4FI** does not interact with the catalytic region (highlighted in Fig. 44). This is thought to reduce the activity of **4FI.** The % inhibition of **4FI** at 54±4% is almost half of that of **4FS** at 98±1% (table 14, entry 3). Therefore, it is seen that loss of interaction with the catalytic residues is seen to decrease the % inhibition dramatically. The reason for this difference could be due to the presence of the diisopropylidene ring on the sucrose core in **4FI.** The presence of this ring makes the structure more rigid and therefore restricts the steric freedom of **4FI.** Consequently, it is unable to attain a better docked pose at the binding site. Therefore, it can be concluded that the diisopropylidene ring plays an important role in the activity of the PSEs as already seen by the experimental results.

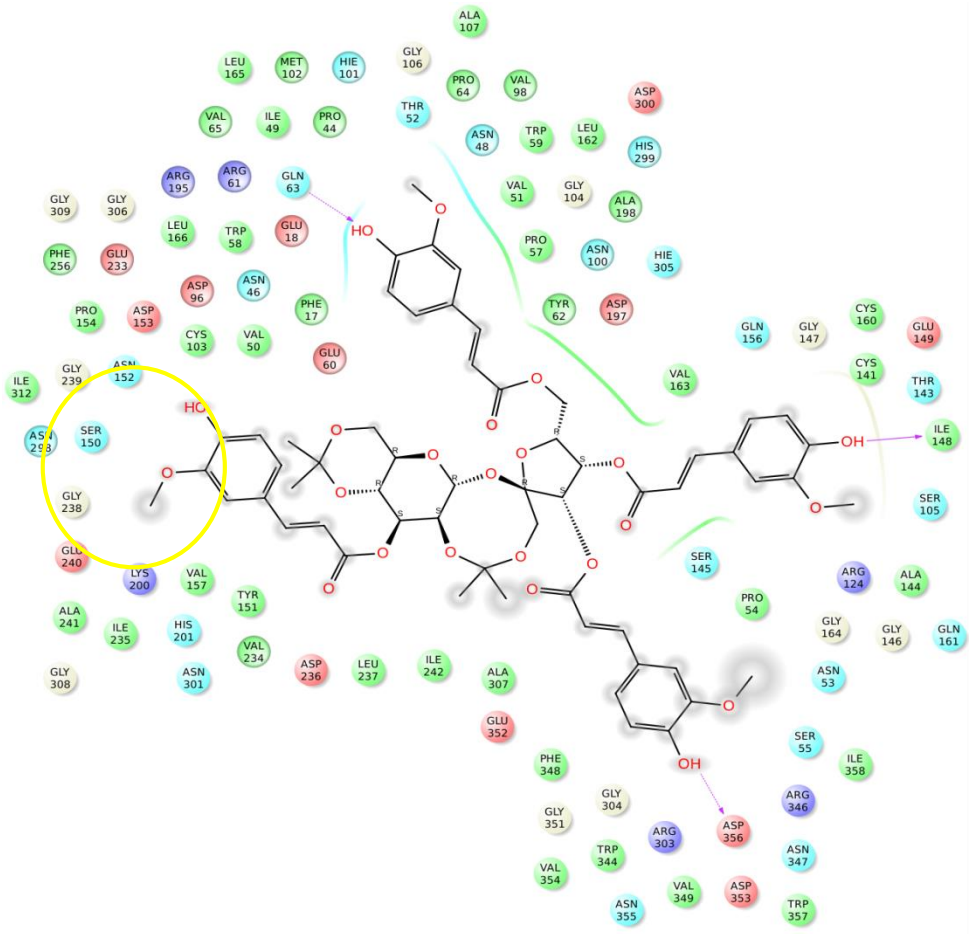

Figure 45: LID for **4FI**.

3.3.2.2 Docking of cinnamoyl PSEs with α-amylase

One of the compounds under this group, **4CiI** has the diisopropylidene ring on the sucrose core while the other, **4CiS** doesn't. A summary of the experimentally obtained % α-amylase inhibition values for these PSEs is given in table 16 followed by the binding mode pictures (Fig 46).

Table 16: % α-amylase inhibition values for cinnamoyl diisopropylidene PSEs

Entry	PSE	% α-amylase Inhibition
1	**4CiI**	98±2
2	**4CiS**	99±1

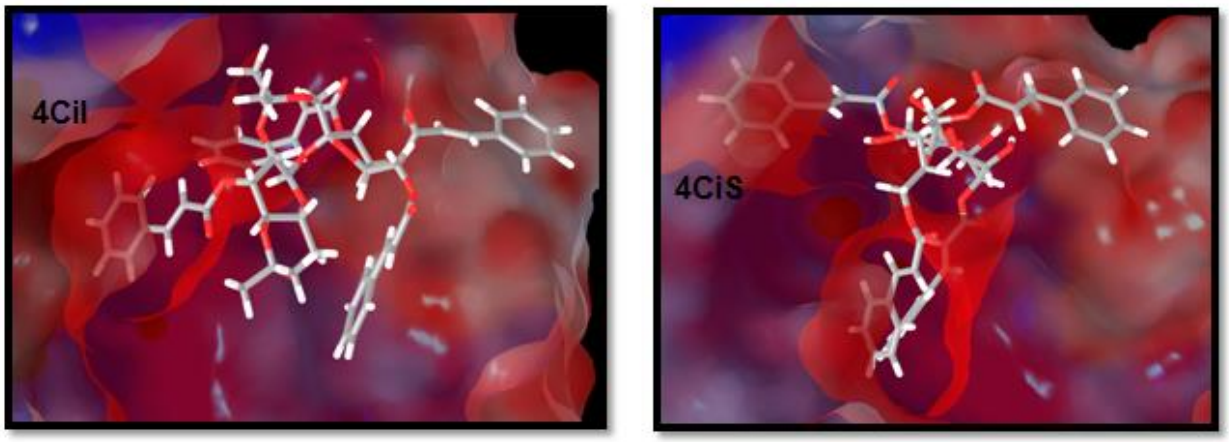

Figure 46: Binding mode pictures for **4CiI** and **4CiS**.

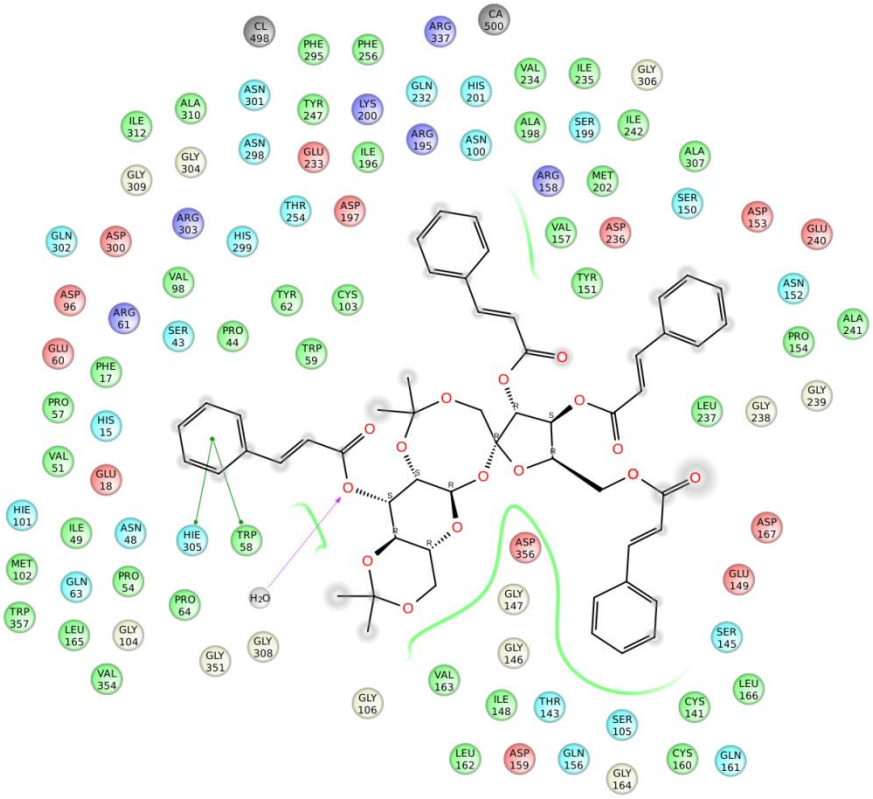

Figure 47: LID for **4CII**.

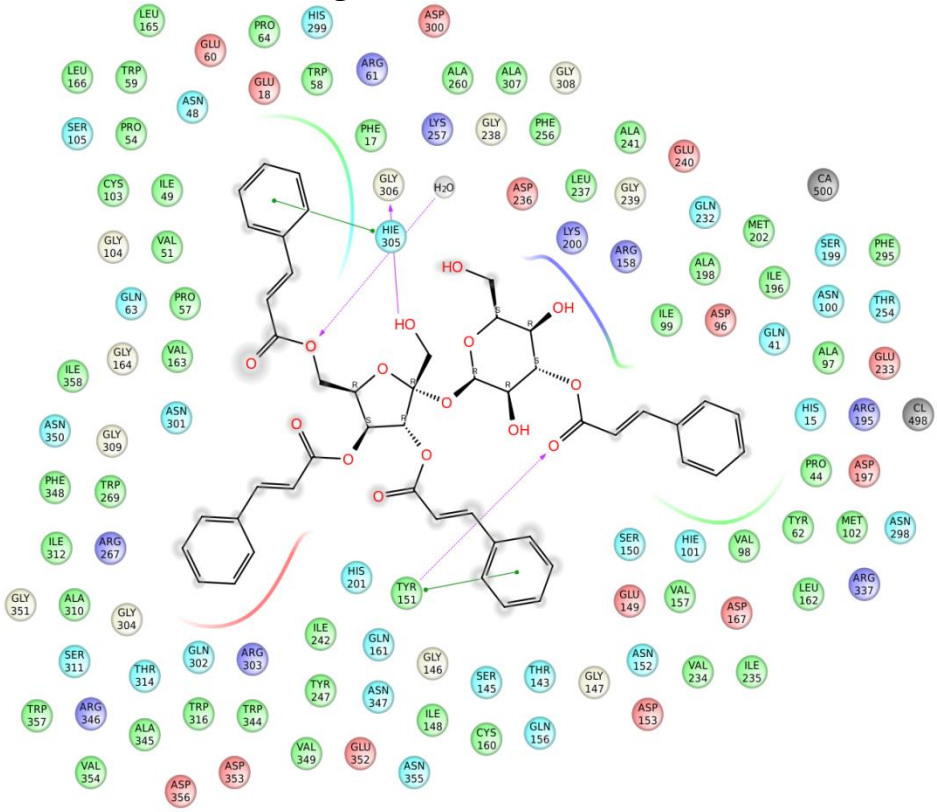

Figure 48: LID for **4CiS**.

While the cinnamoyl group has no hydroxyl groups to form hydrogen bonds in the binding site, it is able to form π-π interactions which leads to relatively high activity. Although the sucrose core in the former PSE, **4CiI** has the diisopropylidene ring while the latter, **4CiS** does not, both of them have considerably high activity of 98±2% and 99±1% respectively (table 16, entries 1 and 2). Therefore, in case of the cinnamoyl PSEs, the means of interaction with the enzyme is different from the feruloyl PSEs, the interaction is mainly by means of π-π interaction and other hydrophobic interactions. Another possible reason for this anomaly could be due to the fact that cinnamoyl PSEs are sterically less bulky than the feruloyl PSEs due to the lack of any substituent groups on the aromatic rings. This could result in greater conformational flexibility making these PSEs reorient themselves in order to maximize interaction with the catalytic residues.

3.3.3 Molecular Dynamics

The lowest energy docked pose for five selected PSEs for docking with α-amylase were used for the MD calculations. MMPBSA method was used to calculate the free energy of binding of the PSEs using the 'sietraj' algorithm. The free energy of binding for each ligand was calculated at the primary as well as the two secondary sites (table 17). This was done in order to compare the affinity of binding of the ligands between the primary and secondary sites. The following section summarizes the results of the MD studies.

Table 17: Free energy of binding of PSEs at the primary and two secondary sites

PSE	Avg. B.E at primary site (kcal/mol)	Avg. B.E at SS1 (kcal/mol)	Avg. B.E at SS2 (kcal/mol)
2FS	-7.41	-5.16	-5.73
3FS	-8.44	-4.89	-5.27
4FS	-9.02	-6.64	-6.43
4FI	-7.96	-5.34	-6.51
4CiI	-6.62	-4.43	-5.66

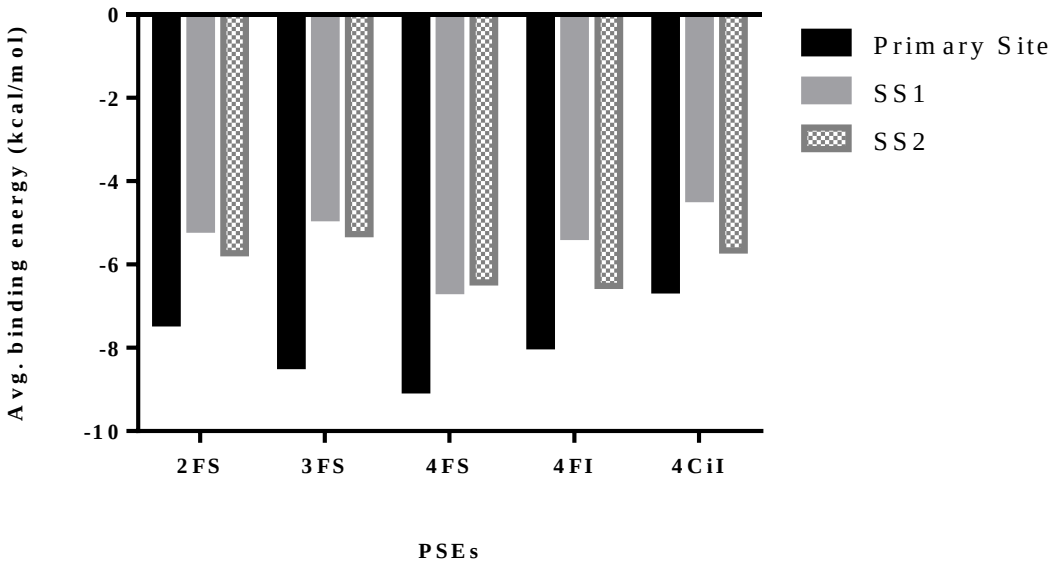

Figure 49: Binding energies of PSEs.

From table 17 and Fig. 49, it can be seen that:

- The free energy of binding is the lowest (most negative) for the primary binding sites for all the PSEs indicating that the primary site is the most preferred for binding.
- The feruloyl PSEs follows the same trend as the experimental results. The free energy of binding decreases (becomes more negative) from **2FS** to **3FS** to **4FS** with values being -7.41, -8.44 and -9.02 kcal/mol respectively (table 17).
- As with the experimental results, the binding energy of **4FI** is lower than **4F**S with the former having a binding energy of -7.96 kcal/mol which is in between that of the di and tri substituted PSEs, **2FS** and **3FS.** This again indicates that the presence of the diisopropylidene ring decreases the binding affinity of **4FI**.
- In case of the tetra cinnamoyl PSE, **4CiI** although experimentally it shows a similar inhibition of the enzyme as **4FS**, there is an anomaly. The binding energy is the lowest at -6.62kcal/mol. MD simulations are very sensitive to initial conformation of the complex, therefore a difference in a single bond rotation may result in a very varied result and in a totally different binding energy. However, the binding free energies of the rest of the PSEs correlate with the % enzyme inhibition, making them suitable models to study the interactions between the PSEs and α-amylase.

- In case of SS1, the binding energies are higher than the primary site (table 17) but follow a similar trend as that of the primary site except for **3FS** whose binding energy is slightly higher than the di substituted PSE, with the values being -4.89 and -5.16 kcal/mol respectively.
- The binding energies at SS2 are lower than that at SS1 (table 17) for all the PSEs indicating that among the two secondary sites, SS2 is preferred more. The trend here in terms of increasing binding energy is **4FI<4FS<2FS<4CiI<3FS.** Here the tetra feruloyl diisopropylidene PSE, **4FI** shows the highest binding affinity with a binding energy of -6.51 kcal/mol.

3.4 Summary

In this chapter, the *in silico* binding mode studies were carried out for selected PSEs with the enzymes, α-glucosidase and α-amylase. Six feruloyl and six cinnamoyl PSEs were selected to study the binding with α-glucosidase. These were selected based on the number and position of the substituents as well as those with and without the diisopropylidene group in order to give a comprehensive idea of the effect of the structural features on the binding. In the first case, feruloyl PSEs, **2FS, 3FS** and **4FS** were docked in the homology modelled α-glucosidase. It was observed that the di and tri substituted PSEs do not project into the active site but rather orient themselves along the surface and bond with the enzyme. However, in case of **4FI**, the presence of the diisopropylidene group and the fourth substituent at position 3 on sucrose reorients the molecule so that the fourth substituent projects into the binding pocket whereas the rest of the molecule is spread along the surface. The ligand interaction diagram shows the binding of the PSEs is achieved by means of hydrogen bonds as well as π-π stacking for feruloyl PSEs. The same results were observed for the feruloyl PSEs without the diisopropylidene group as well. In case of the cinnamoyl PSEs, once again the presence of the fourth substituent is seen to reorient the PSE so that it projects into the binding pocket. But this time, the binding is facilitated by means of π-π stacking interactions between the phenyl ring of the PSEs and the amino acids in the enzyme. The prominent difference between the feruloyl and cinnamoyl PSEs is the hydrogen bonding of the aromatic 'OH' groups with the amino acid residues in the enzyme

(α-glucosidase). As for docking with α-amylase, only six PSEs that displayed an inhibition of greater than 20% were selected which comprised of **2FS, 3FS, 4FS, 4FI, 4CiS** and **4CiI**. These represent both the feruloyl and cinnamoyl groups, di, tri and tetrasubstituted PSEs as well as PSEs with and without the diisopropylidene group. The structure of α-amylase was retrieved from Swissprot database and the binding site was mapped according to available literature. From a study of all the docked poses returned by the software, five regions containing key residues that are thought to be the catalytic site were mapped, namely, residues 50-63; 145-151; 197-200; 233-240; 300-306. It was observed that with the exception of **4FI**, all of the PSEs interacted with the catalytic region making the binding stronger. However, in case of **4FI,** the presence of the diisopropylidene group restricts conformational flexibility making the fourth substituent inaccessible to binding at the catalytic site thus reducing the activity of the compound. α-amylase is already shown to have multiple binding sites that have been mapped out by various previous works. Therefore, the binding energy of the PSEs at the primary as well as two secondary sites were assessed by molecular dynamics study. The results indicated that the free energy of binding is the lowest (most negative) for the primary binding sites for all the PSEs, indicating that the primary site is the most preferred for binding. The feruloyl PSEs follows the same trend as the experimental results. The free energy of binding decreases (becomes more negative) from **2FS** to **3FS** to **4FS.** However, for **4FI** the binding energy is lower than 4FS indicating that the diisopropylidene group reduces the affinity of binding to α-amylase.

Chapter 4. α-Glucosidase and α-Amylase Inhibition Kinetics

In chapter 2 and 3, the in vitro enzyme inhibition and in silico docking results for PSEs were detailed. Since PSEs are enzyme inhibitors, an important next step is to identify the type of inhibition with regard to both the enzymes, α-glucosidase and α-amylase. A brief introduction of steady state enzyme kinetics and inhibition kinetics is given below.

4.1 Introduction

4.1.1Steady state kinetics

The general enzyme reaction, where the enzyme converts a single substrate to a single product can be represented as

$$E + S \underset{K_{-1}}{\overset{K_1}{\rightleftharpoons}} ES \xrightarrow{K_p} P \qquad \text{.....Equation 1}$$

Here, K_1 and K_{-1} represent the rates of forward and back reactions between the enzyme, E and the substrate, S. The rate of product (P) formation from the enzyme substrate complex (ES)

is given by K_p. It is also called the 'turnover number' which is equal to the number of moles of substrate converted to the product per minute per mole of the enzyme. In most cases of steady state reactions, the rate of product formation is directly proportional to the concentration of the enzyme substrate complex.[80] The kinetic theory of enzyme reactions suggests the formation of an equilibrium intermediate between the enzyme and the substrate. This state of equilibrium is represented by means of the dissociation constant expressed as:

$$K_a = \frac{[E][S]}{[ES]} \qquad \text{.....Equation 2}$$

where, K_a is the dissociation constant, [E] is the concentration of free enzyme, [S] is the concentration of the free substrate and [ES] is the concentration of the enzyme-substrate complex. In case of a homogeneous enzyme reaction, the initial reaction velocity is given by the Michaelis Menten equation,

$$v = \frac{V_{max}[S]}{(K_m + [S])} \qquad \text{……Equation 3}$$

where, V_{max} is the maximum reaction velocity obtained when the all of the enzyme is in the form ES or complexed with the substrate and K_m (Michaelis-Menten constant) which denotes the substrate concentration at which the enzyme functions at half-maximal velocity.[80,81] In simpler terms, K_m denotes the affinity between enzyme and substrate. A high K_m indicates a low affinity of the enzyme towards the substrate whereas a lower K_m value is vice-versa. Therefore, a substrate with low K_m and high V_{max} is considered a better substrate than the converse case.

Kinetic constants, K_m and V_{max} are determined graphically. A simple plot of *v* vs. [S] is a hyperbola (Fig. 50 (A)), hence, it is extremely difficult to determine the constants from this plot. Therefore, alternative plots can be made so that a series of straight lines are obtained facilitating the determination of the kinetic constants.[80] Lineweaver and Burk suggested a new method of evaluating enzyme inhibition mechanisms by means of using an equation to represent the enzyme reaction that is linear. Graphical representations of these involve constant slopes and straight line extrapolations and can be used to test the kinetic data as well as to determine dissociation constants for both enzyme-substrate and enzyme-inhibitor complexes. Lineweaver and Burk derived a plot of reciprocal velocity versus reciprocal substrate concentrations which in the simplest of cases would yield a straight line whose intercept is $1/V_{max}$ and slope is K_s/V_{max}.[81] Some of the other alternate plots are, the Hanes-Woolf plot ([S]/v vs. [S]) or the Hofstee plot (v vs. v/[S]) (Fig. 50).

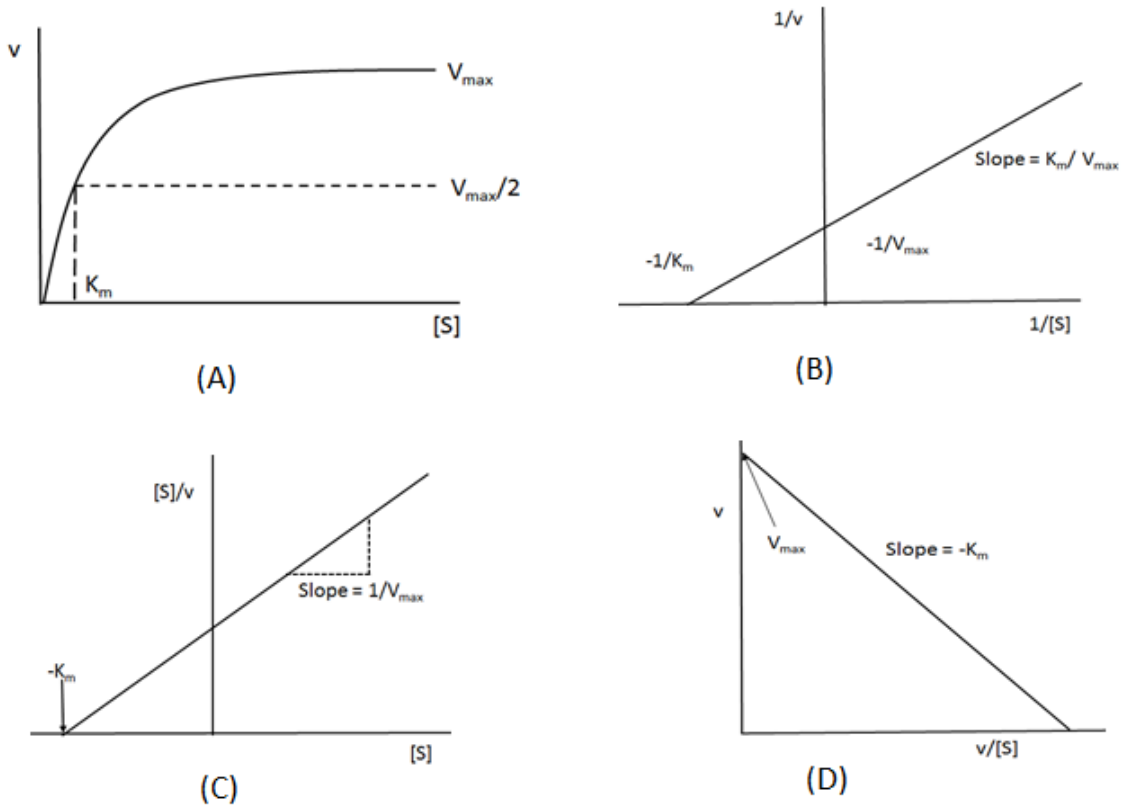

Figure 50: (A) Michaelis Menten plot (B) Lineweaver-Burk double reciprocal plot (C) Hanes-Woolf plot and (D) Hofstee plot.

4.1.2 Enzyme inhibition kinetics

Enzyme inhibitors work by inhibiting the enzyme thus preventing the substrate turnover. They achieve this by slowing down the rate of the reaction or by completely preventing enzyme action. Inhibition of enzymes can have therapeutic action when blocking the enzyme activity can kill a pathogen or correct a dysfunctional metabolic pathway. Enzyme inhibitors can be mainly classified as reversible or irreversible inhibitors. As the name suggests, the latter causes the enzyme to permanently cease to function. Most of the enzyme inhibitors are reversible. In case of reversible inhibition, the inhibitors bind to the enzyme by non-covalent means. In vitro, the enzyme activity can be recovered by separating the reversible inhibitor from the enzyme by dialysis, gel filtration or dilution. Reversible inhibitors achieve an equilibrium state rapidly with the enzyme and are free to associate and dissociate from it. The establishing of the equilibrium state is independent of time. The

equilibrium constant or inhibitor constant (K_i) of a reversible inhibitor gives the potency of the inhibitor. It is given by K_{-1}/K_1 (eq^n 1).[80] K_i and IC_{50} values are the two most commonly used parameters to evaluate the potency of enzyme inhibitors. K_i is the equilibrium constant for the dissociation of the enzyme inhibitor complex whereas the IC_{50} for an inhibitor is the concentration at which the enzyme activity is halved under specified assay conditions. The K_i value for an inhibitor is constant for the given enzyme, whereas the IC_{50} value is relative depending on the substrate concentration.[82]

In case of irreversible inhibition however, the inhibitor binds tightly by means of covalent binding and enzyme activity cannot be recovered. Also, irreversible inhibitors are more often than not time dependent and there does not exist any equilibrium between the enzyme and inhibitor. Therefore, the potency of an irreversible inhibitor cannot be established by means of an inhibitor constant and is instead expressed by other means, for example, velocity constant.

Since the compounds of interest in our study are reversible inhibitors of the carbohydrate digesting enzymes, α-glucosidase and α-amylase, the following sections will focus on the kinetics of reversible inhibitors.

4.1.3 Kinetics of reversible enzyme inhibition

The mechanism of inhibition is often determined qualitatively and quantitatively by collecting data for velocity of enzyme reactions at a series of substrate and inhibitor concentrations. This data is then plotted using one of the various plots, Lineweaver Burk (1/v vs. 1/[S]), Dixon plot (1/v vs [I]) where [I] refers to the inhibitor concentration and the modified Dixon plot ([S]/v vs. [I]). Each of these plots have their own advantages and disadvantages which will be elucidated in the following sections.

4.1.3.1 Complete and Partial inhibition

Enzyme inhibition can be of two types. Complete and partial inhibition. In the former, a plot of reciprocal velocity versus inhibitor concentration gives a straight line while in the latter case, it gives a hyperbola. As the concentration of the inhibitor increases, the velocity becomes close to zero in complete inhibition. However, in case of partial inhibition, the

enzyme is modified to form an enzyme-substrate-inhibitor complex that retains part of its function. The graphical methods of estimation of kinetic parameters like Dixon plot, Cornish-Bowden and Lineweaver Burke plots are useful only for complete or linear inhibition and are not an accurate estimation in case of partial inhibition. Amongst these, the Lineweaver Burke plot provides the least accurate estimation of kinetic constants as it has the disadvantage of having high substrate concentration data points crowding near the ordinate axis. In case of partial inhibition, secondary plots are often needed in order to estimate the kinetic parameters. A secondary plot of fractional velocity (v/V_0-v) versus reciprocal of inhibitor concentration (1/I) is often used to estimate kinetic constants in case of partial inhibition. This plot gives a straight line that intersects the x-axis at the origin for both complete noncompetitive and competitive inhibition (sections 4.1.3.2.1 and 4.1.3.2.2) and away from the origin for both partial noncompetitive inhibition and competitive inhibition.[83,84].

4.1.3.2 Inhibition mechanisms of reversible inhibitors

The equation 1 that was earlier used to represent enzyme reaction can be modified to include action of inhibitors and represented as follows:

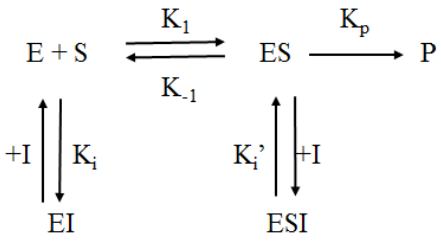

……..Equation 4

Here, 'I' represents the inhibitor which can either bind to the free enzyme or the enzyme substrate complex. For competitive inhibition, only K_i is defined while for noncompetitive inhibition $K_i = K_i'$. In case of uncompetitive inhibition only K_i' is defined. This is based on the binding of the inhibitor either to free enzyme or the ES complex or to both as detailed in the following sections. Depending on whether the inhibitor has an affinity for one or the other or even both, different mechanisms of inhibition are described.

4.1.3.2.1 Competitive inhibition

A competitive inhibitor competes with the substrate to bind to the enzyme active site and prevents the binding of the substrate. In certain cases, it can bind to an allosteric site changing the conformation of the active site and once again prevents the binding of the substrate. At any given time, only one of the two, either the inhibitor or the substrate can bind to the enzyme. This type of inhibition can be overcome by increasing the concentration of the substrate. In competitive inhibition, the V_{max} of the enzyme remains unaltered but the K_m value increases which means that the maximum velocity at which the enzyme operates remain the same but due to the presence of the inhibitor, a higher concentration of the substrate is needed thus increasing the K_m.[80]

The Michaelis Menten equation for competitive inhibition changes to

$$v = \frac{V_{max}[S]}{(K_m^{app}+[S])} \qquad \text{……Equation 5}$$

$$\text{where, } K_m^{app} = K_m\left(1 + \frac{[I]}{K_i}\right)$$

In Lineweaver-Burk plot of competitive inhibition, the intercept remains unchanged but the slope changes.[81] The effect of a competitive inhibitor is illustrated in the Lineweaver-Burk and Dixon plots below (Fig. 51). Fig 51 A shows the effect of competitive inhibitor using Lineweaver-Burk plot. Here, the dashed line represents the change in K_m after the addition of the inhibitor. It can be seen that although the V_{max} remains unaltered, the K_m value increases. In the Dixon plot in figure 51 B, concentration lines are shown for different substrate concentrations. Here, the substrate concentration is decreasing from S_1 to S_3. The Dixon plot can be used to estimate the K_i value as shown in the figure.[85]

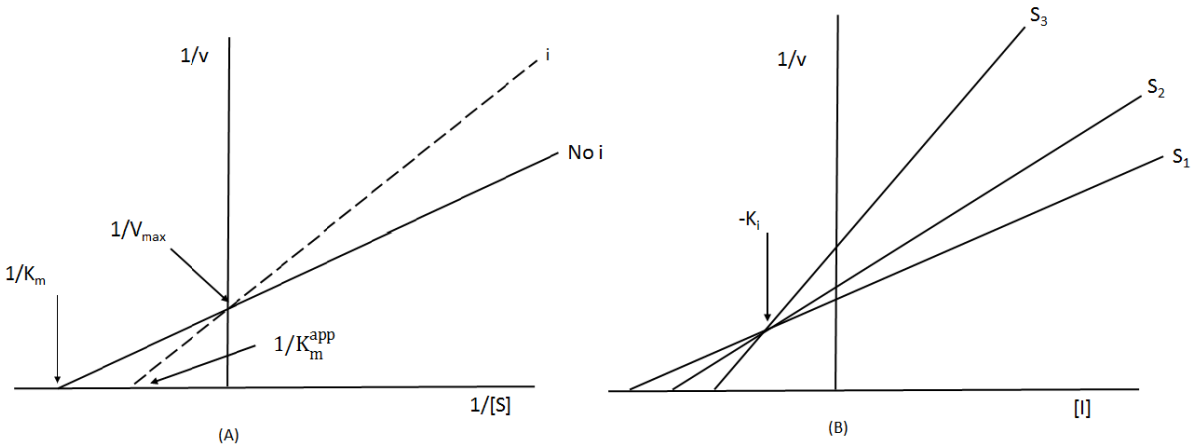

Figure 51: Competitive Inhibition. (A) Lineweaver-Burk plot (B) Dixon plot.

4.1.3.2.2 Noncompetitive inhibition

A noncompetitive inhibitor binds to the enzyme at a site other than the active site. It does not affect the affinity of the substrate to the enzyme, thus, the substrate and the inhibitor bind to the enzyme independent of each other. The inhibitor can bind to both the free enzyme as well as the ES complex at the allosteric site. However, binding of the inhibitor leads to the formation of the enzyme-substrate-inhibitor (ESI) or EI complex which does not yield a product. The enzyme can break down the substrate into the product only when the ESI complex dissociates to give either EI or ES complex; then only the ES complex can give rise to the product. Therefore, a noncompetitive inhibitor functions by reducing the velocity of product formation or reduces the V_{max} but the K_m remains unaltered.[80] The rate equation is given by:

$$v = \frac{V_{max}^{app}[S]}{(K_m+[S])} \qquad \text{.....Equation 6}$$

$$\text{where, } V_{max}^{app} = \frac{V_{max}}{1+\frac{[I]}{K_i}}$$

In the Lineweaver-Burk plot for non-competitive inhibitors, both the slope and intercept change.[81] The Lineweaver-Burk and Dixon plots for competitive inhibition are shown below:

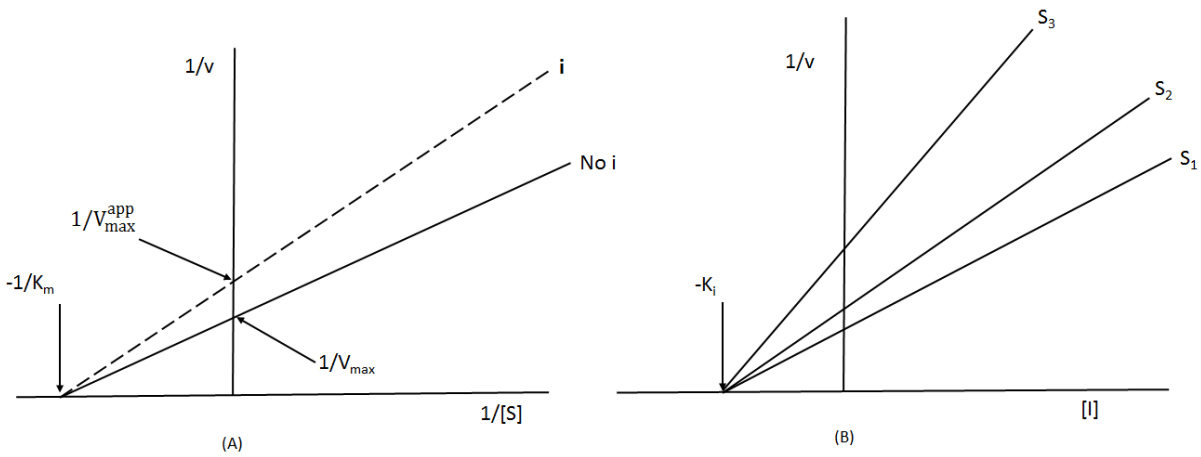

Figure 52: Noncompetitive Inhibition. (A) Lineweaver-Burk plot (B) Dixon plot.

Figure 52 (A) shows the effect of noncompetitive inhibitor using Lineweaver-Burk plot. Here, the dashed line represents the change in V_{max} after the addition of the inhibitor. It can be seen that although the K_m remains unaltered, the V_{max} value decreases. In the Dixon plot in Fig. 52 (B), concentration lines are shown for different substrate concentrations. Here, the substrate concentration is decreasing from S_1 to S_3. The Dixon plot can be used to estimate the K_i value as shown in the figure.[85]

4.1.3.2.3 Uncompetitive inhibition

An uncompetitive inhibitor can bind only to the ES complex and cannot bind to the free enzyme. Thus, it can act only in the presence of the substrate. The formation of the ESI complex prevents the product turnover. An uncompetitive inhibitor decreases both the K_m and V_{max} values. Lineweaver-Burk plots for uncompetitive inhibition gives parallel lines.[80] Uncompetitive inhibition is shown in the Lineweaver-Burk and modified Dixon (Cornish-Bowden) plots below:

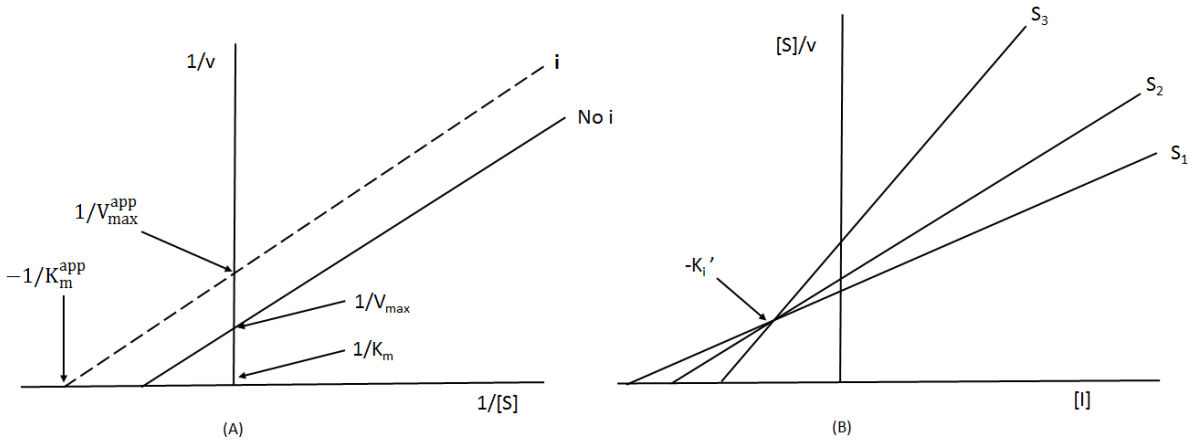

Figure 53: Uncompetitive Inhibition. (A) Lineweaver-Burk plot (B) Dixon plot.

Fig. 53 (A) shows the effect of uncompetitive inhibitor using Lineweaver-Burk plot. Here, the dashed line represents the change in both V_{max} and K_m after the addition of the inhibitor. In the modified Dixon (Cornish Bowden) plot in Fig. 53 (B), concentration lines are shown for different substrate concentrations. Here, the substrate concentration is decreasing from S_1 to S_3. The modified Dixon plot can be used to estimate the K_i' value, characteristic of the uncompetitive inhibitor as shown in the figure.[85]

4.1.3.2.4 Mixed inhibition

In a mixed inhibition, the inhibitor is able to bind to both the free enzyme (active site) as well as the enzyme substrate complex but it has a higher affinity for one of the two. The inhibitor shows a mixed type behavior which could be a combination of competitive, noncompetitive and uncompetitive. If the inhibitor binds more favorably to the free enzyme, then it increases the K_m or reduces the affinity of the substrate to the enzyme. Conversely, if the inhibitor binds to the enzyme substrate complex better, then it increases the affinity of the substrate thus decreasing the K_m value. In both cases, the inhibitor reduces the reaction velocity therefore there is decreased turn-over of the product. [85,86]. In mixed inhibition, affinity ratio, α which is equal to E/ES affinity can be calculated. α is the ratio of uncompetitive inhibition constant to competitive inhibition constant ($\alpha = K_i' / K_i$).[73] If the α value is '1', the inhibitor binds with equal affinity to both free enzyme and the enzyme substrate complex, if it is greater than 1, the inhibitor binds with greater affinity to the free enzyme whereas in case it is lesser than 1, the inhibitor has a greater preference to the ES complex.[87]

Linear mixed inhibition is described by the rate equation:

$$v = \frac{V_{max}[S]}{K_m\left(1+\frac{[I]}{K_i}\right)+[S]\left(1+\frac{[I]}{K_i'}\right)} \qquad \text{.....Equation 7}$$

The Lineweaver-Burk plot for a mixed type inhibitor is illustrated below (Fig. 54). In Lineweaver-Burk plot, the concentration lines intersect in the fourth quadrant in the case of mixed inhibition.[88]

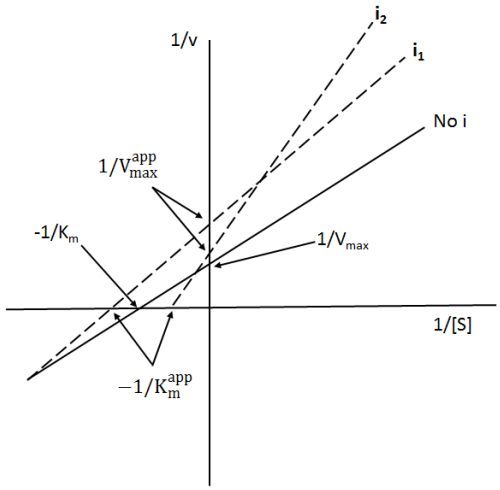

Figure 54: Lineweaver-Burk plot for mixed inhibition.

The Dixon and Cornish Bowden plots for mixed inhibition are as follows:

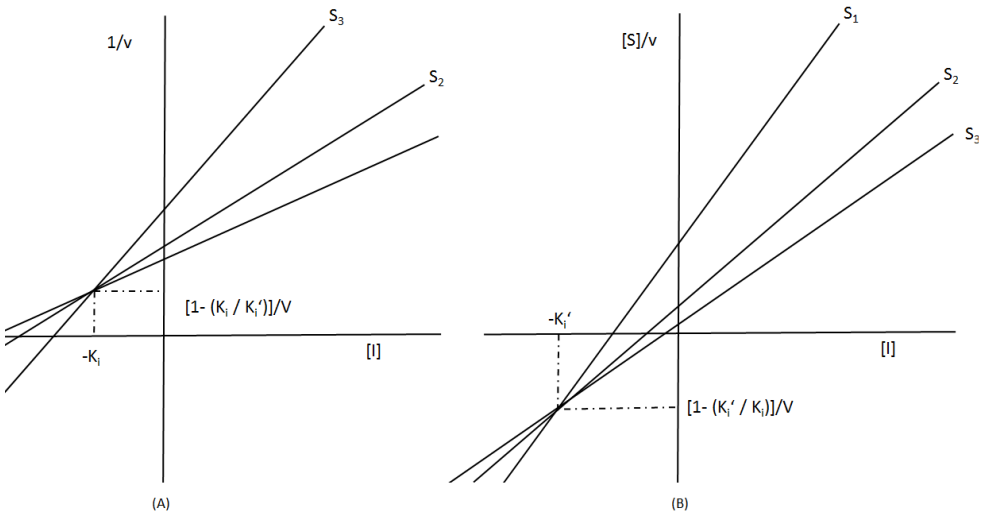

Figure 55: Dixon and modified Dixon (Cornish Bowden) plots for mixed inhibition.

Dixon plot is a plot of reciprocal velocity versus inhibitor concentration. As seen from Fig. 55. Dixon plot does not distinguish between mixed and competitive inhibitors whereas the Cornish Bowden plot does not distinguish between uncompetitive and mixed inhibition. In case of mixed and uncompetitive inhibitors, the Dixon plot does not give the dissociation constant for the EIS complex. Dixon plot provides the value only for dissociation constant of the EI complex or K_i with accuracy. Therefore, Athel Cornish-Bowden provided a new plot for ascertaining the EIS dissociation constant or K_i' for linear mixed inhibition. The Cornish-Bowden plot is a plot of s/v (substrate over velocity) versus the inhibitor concentration, [I]. These two plots complement one another to ascertain the dissociation constants for the EI and the EIS complexes (Ki and Ki' respectively)[85]. In case of mixed linear type of inhibition, the inhibition curves intersect in the fourth quadrant in the Dixon plot and the third quadrant in the Cornish-Bowden plot. In the Dixon plot, intersection of the inhibition curves in the fourth quadrant could mean either competitive or mixed type unlike uncompetitive or noncompetitive where the lines intersect on the negative x axis in the former and run parallel to each other in the latter. Modified Dixon plot or the Cornish Bowden plot can then be used to distinguish between competitive or mixed inhibition. In case of competitive inhibition, the lines run parallel to each other in the modified Dixon plot whereas in case of mixed inhibition they intersect in the third quadrant. [89].

In this chapter, the kinetics of inhibition of α-glucosidase and α-amylase by PSEs was studied. The aim of this study was to correlate the molecular modeling with actual experimental data regarding the type of inhibition. For example, if the PSEs are competitive inhibitors, it would indicate that they compete with the substrate to dock into the active site. However, in case of noncompetitive or uncompetitive inhibition the docking takes places at an allosteric site. From molecular modeling of PSEs docked with the two enzymes α-glucosidase and α-amylase (chapter 3), it was found that the PSEs dock at a site different from the active site although a part of the PSE interacts with the catalytic residues on the active site. Therefore, a study of the kinetics of inhibition will shed light on the likely site of docking (at or away from the active site), whether the presence of the substrate is necessary to docking as well as the affinity of the substrate to either the free enzyme or the enzyme-substrate complex. All of this data when combined with the SAR will help design the PSEs as more potent AGIs.

4.2 Methods

The mode of inhibition of selected PSEs on α-glucosidase and α-amylase was tested by determining the velocity at different concentration of inhibitors and substrates. For each concentration of the inhibitor, the velocity was measured for a series of substrate concentrations.

4.2.1 Kinetics of inhibition of α-glucosidase by PSEs

The kinetics of inhibition of selected PSEs was tested by measuring the reaction velocity at different concentrations of substrate and inhibitor (PSEs). The same procedure used earlier to test the inhibitory activity of PSEs towards α-glucosidase was used with a few modifications. Briefly, different concentrations of PSEs and Acarbose was prepared in DMSO to correspond to 50, 25, 12.5 and 6.25 µg/ml final concentration in the solution. 8µl of the inhibitor of desired concentration was added to a microtitre plate followed by 115µl of sodium phosphate buffer (0.01M, pH 7.0). To this, 50µl of 0.5U/ml yeast α-glucosidase solution in the same buffer was added. The plates were then incubated for 15 minutes at 37ºC while shaking. Then, 25µl of various concentrations of the substrate PNPG (10, 5, 2.5, 1.25, 0.625, 0.3125mM) in buffer was added followed once again by incubation for 15 minutes at 37ºC while shaking. The absorbance was measured using a spectrophotometer at 405nm wavelength. The procedure was repeated for different concentrations of the inhibitor as specified above. A standard curve was constructed using PNPG from which the amount of product was calculated. The initial reaction velocity was calculated as the amount of product formed (calculated from the standard curve) over the time period for the enzyme reaction (15 minutes). Using the data for initial reaction velocity for different substrate and inhibitor concentrations, the mode of inhibition and the inhibitor constants along with other kinetic parameters were calculated by Sigmaplot software by Systat Software Inc.

4.2.2 Kinetics of inhibition of α-amylase by PSEs

Once again, the same procedure used earlier to test the inhibitory activity of PSEs towards α-amylase was used with a few modifications. Various concentrations of PSEs and Acarbose was prepared in DMSO to correspond to 50, 25, 12.5 and 6.25 µg/ml final concentration in the solution. 50µl of the inhibitor of desired concentration was added to

test tubes followed by 100µl 5U/ml of porcine pancreatic α-amylase and 460µl of sodium phosphate buffer (0.05M, pH 6.8). The tubes were then incubated for 10 minutes at 37ºC. Then, 450µl of various concentrations of the substrate, starch solution in DI water, (0.1, 0.3, 0.5, 0.7, 0.9%) was added followed once again by incubation for 20 minutes at 37ºC. Next, 500µl of DNSA solution was added to each tube and then the tubes were placed in boiling water bath for 15 minutes. The solution was then diluted with 5ml of DI water and the absorbance measured at 540nm. The procedure was repeated for different concentrations of the inhibitor as specified above. A standard curve was constructed using maltose from which the amount of product was calculated. The initial reaction velocity was calculated as the amount of product formed (determined from the standard curve) over the time period for the enzyme reaction (20 minutes). Using the data for initial reaction velocity for different substrate and inhibitor concentrations, the mode of inhibition and the inhibitor constants were calculated using Sigmaplot software by Systat Software Inc.

4.3 Results and discussion

4.3.1 α-glucosidase kinetics

The following section details the velocity calculations for selected PSEs towards the inhibition of the enzyme, α-glucosidase. The first section gives the standard curve for the substrate, PNPG which is used in the calculation of the amount of product for all of the PSEs.

4.3.1.1 PNPG standard curve

A standard curve was constructed using different concentrations of the substrate, PNPG for the enzyme α-glucosidase. This curve was used to estimate the amount of product formed in the subsequent kinetic experiments for this enzyme. Table 18 and Figure 56 show the standard curve for PNPG.

Table 18: Absorbance at 540nm for different concentrations of PNPG

PNPG conc. (mM)	Absorbance at 540nm	
	OD	Std. Dev
5.000	2.240	0.089
2.500	1.113	0.162
1.250	0.620	0.084
0.625	0.333	0.032
0.312	0.171	0.011
0.000	0.000	0.000

Figure 56: Standard curve for PNPG.

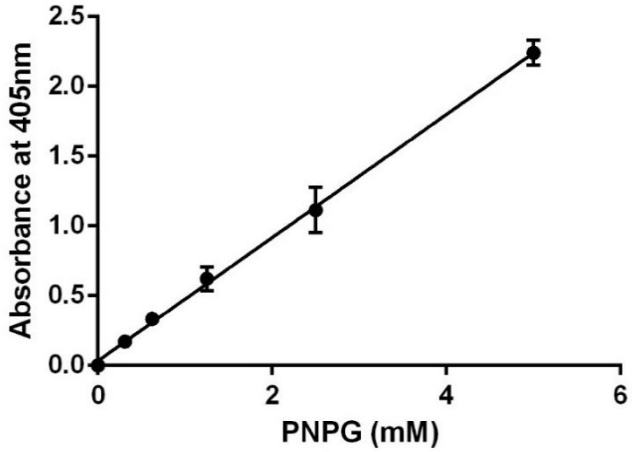

4.3.1.2 Inhibition kinetics of α-glucosidase by PSEs

Four PSEs, **4FI, 4FS, 2FS** and **4CiI** were chosen for the inhibition kinetics study. These PSEs were chosen because at the maximum solubility limit they have a high percentage inhibition for both the enzymes. Also, they represent structural differences that would enhance the SAR by studying whether the type of inhibition is affected by these structural changes. Among the test group there is difference in the number of phenylpropanoid substituents (tetra and di), PSEs with and without the diisopropylidene group as well as PSEs with difference in the hydroxycinnamic acid substituent group. The data for the velocity calculations for PSEs **4FI, 4FS, 2FS, 4CiI,** and Acarbose at different concentrations of the inhibitor (PSE) and the substrate (PNPG) is depicted in tables 19-22 (section 4.5). Table 23 represents the data for Acarbose while table 24 for the enzyme without the inhibitor. The data in the tables has been plotted into inhibition curves. Sigmaplot software was used to construct the kinetics curves for each of the above inhibitors and Acarbose and these curves are represented in figure 57 and 58. The type of inhibition, K_i values and other parameters, where applicable, are detailed in table 24 for each of the inhibitors. For the PSEs, Dixon plots were constructed while Lineweaver-Burk plot is used for Acarbose in this instance.

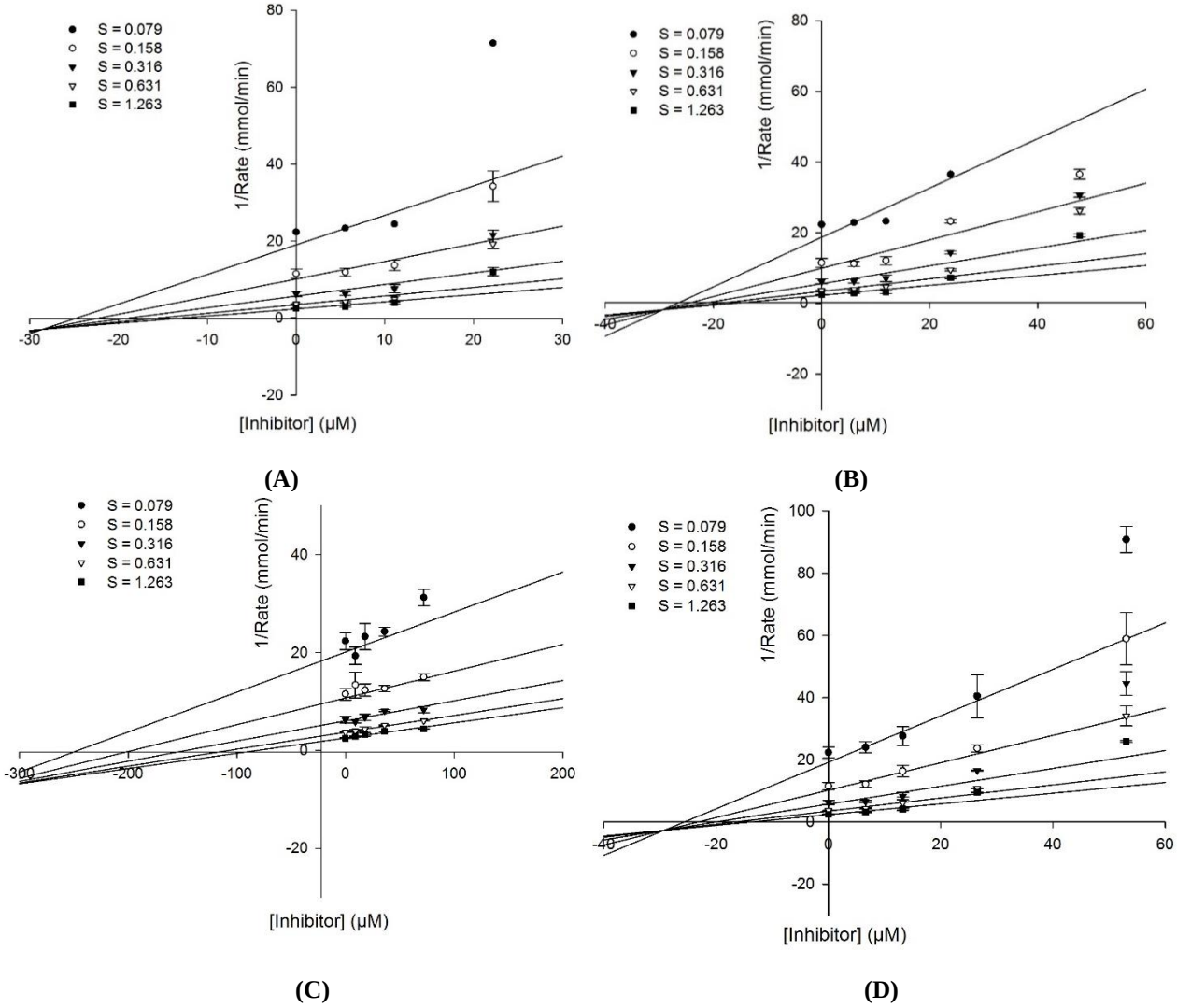

Figure 57: Dixon plots for α-glucosidase inhibition for PSEs (A) **4FI** (B) **4FS** (C) **2FS** (D) **4CiI**.

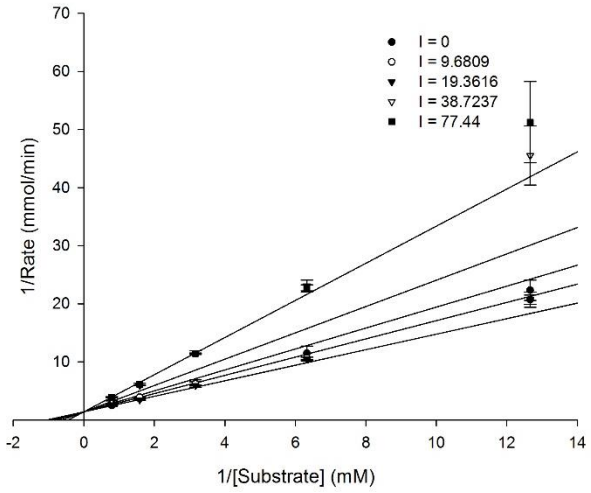

Figure 58: Lineweaver-Burk plot for α-glucosidase inhibition of Acarbose.

Table 24: Kinetic parameters for α-glucosidase inhibition by PSEs

Compound	Type of inhibition	K_i (μM)	α
4FI	Fully mixed	28.5	0.296
4FS	Fully mixed	29.3	0.406
2FS	Fully mixed	347.8	0.138
4CiI	Fully mixed	29.2	0.315
Acarbose	Competitive	55.6	N/A

Figure 57 shows the kinetic curves for the inhibition of α-glucosidase by the PSEs **4FI, 4FS, 2FS** and **4CiI**. From all of the four curves it is evident that the type of inhibition is mixed. For mixed inhibitors, the inhibition lines intersect in the fourth quadrant in the Dixon plot. This means that the PSEs bind to both the free enzyme as well as the enzyme substrate complex but has higher affinity for one of them. The affinity ratio, α, for all four of the PSEs is less than 1 indicating that the PSEs show a greater preference to the enzyme substrate complex rather than the free enzyme. This is in agreement with the in silico results from chapter 3 where it was seen that the PSEs bind to α-glucosidase enzyme at a site other than the active site. In case of Acarbose, the inhibition is competitive as seen from Fig. 58 which is in accordance with literature.[90] The K_i values from table 24 indicate that the PSEs have strong potency towards the inhibition of α-glucosidase as evidenced by the low values which were comparable to that of Acarbose (except for **2FS**). The K_i value for Acarbose is 55.6μM which is similar to that reported in literature (77.9μM).[90] From the above data, it is

evident that the type of inhibition is same between tetra and disubstituted PSEs (**4FS** and **2FS**), between PSEs with or without the diisopropylidene group (**4FS** and **4FI**), and finally also between different types of phenylpropanoid substituents (**4FI** and **4CiI**). Another interesting observation is that the K_i values are similar for all of the tetra substituted compounds (table 24) which was lower than that of Acarbose.

4.3.2 α-amylase kinetics

The following section details the velocity calculations for selected PSEs towards the inhibition of the enzyme, α-amylase. The first section gives the standard curve for the substrate, Maltose (breakdown product of starch) which is used in the calculation of the amount of product for all of the PSEs.

4.3.2.1 Maltose standard curve

A standard curve was constructed using different concentrations of the substrate, Maltose (breakdown product of starch) for the enzyme α-amylase. This curve was used to estimate the amount of product formed in the subsequent kinetic experiments for this enzyme. Table 25 and Figure 59 show the standard curve for Maltose.

Table 25: Absorbance at 540nm for different concentrations of PNPG

Maltose (mg/ml)	Absorbance at 540 nm	
	OD	Std. Dev
0.000	0.113000	0.001528
0.045	0.127667	0.001453
0.090	0.159000	0.009609
0.180	0.254333	0.005925
0.360	0.416000	0.011358
0.721	0.768000	0.008505
1.442	1.392667	0.019751
2.885	2.480667	0.022512

Figure 59: Standard curve for Maltose.

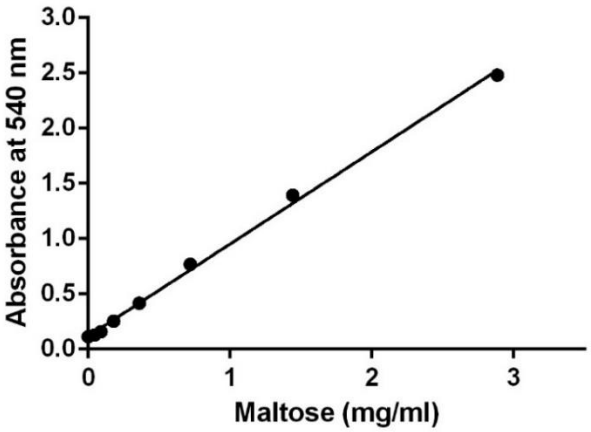

4.3.2.2 Inhibition kinetics of α-amylase by PSEs

The same four PSEs that were chosen earlier for α-glucosidase, **4FI, 4FS, 2FS** and **4CiI** were chosen for the inhibition kinetics study using the same rationale already mentioned. The data for the velocity calculations for PSEs **4FI, 4FS, 2FS, 4CiI,** and Acarbose at different concentrations of the inhibitor (PSE) and the substrate (starch) is depicted in tables 26-30 (section 4.5). Table 31 (section) represents the data for enzyme without the inhibitor. Sigmaplot software was used to construct the kinetics curves for each of the above inhibitors and Acarbose and these curves are represented in figure 60 and 61. The type of inhibition, K_i values and other parameters, where applicable, are detailed in table 32 for each of the inhibitors.

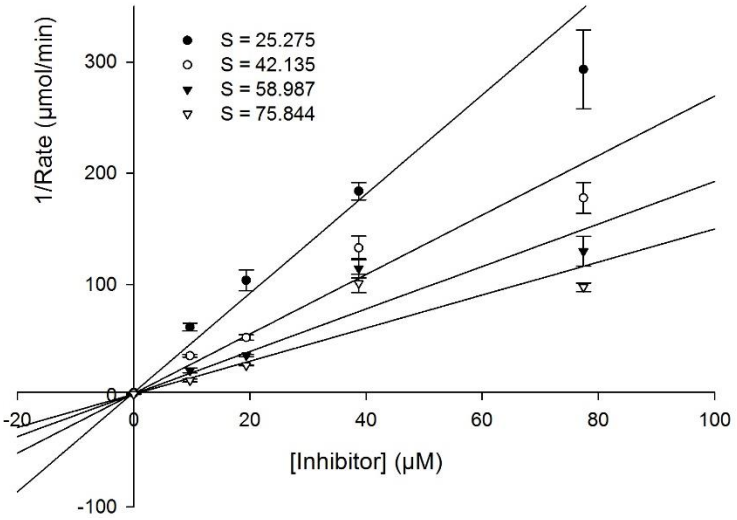

Figure 60: Dixon plot for α-glucosidase inhibition of Acarbose.

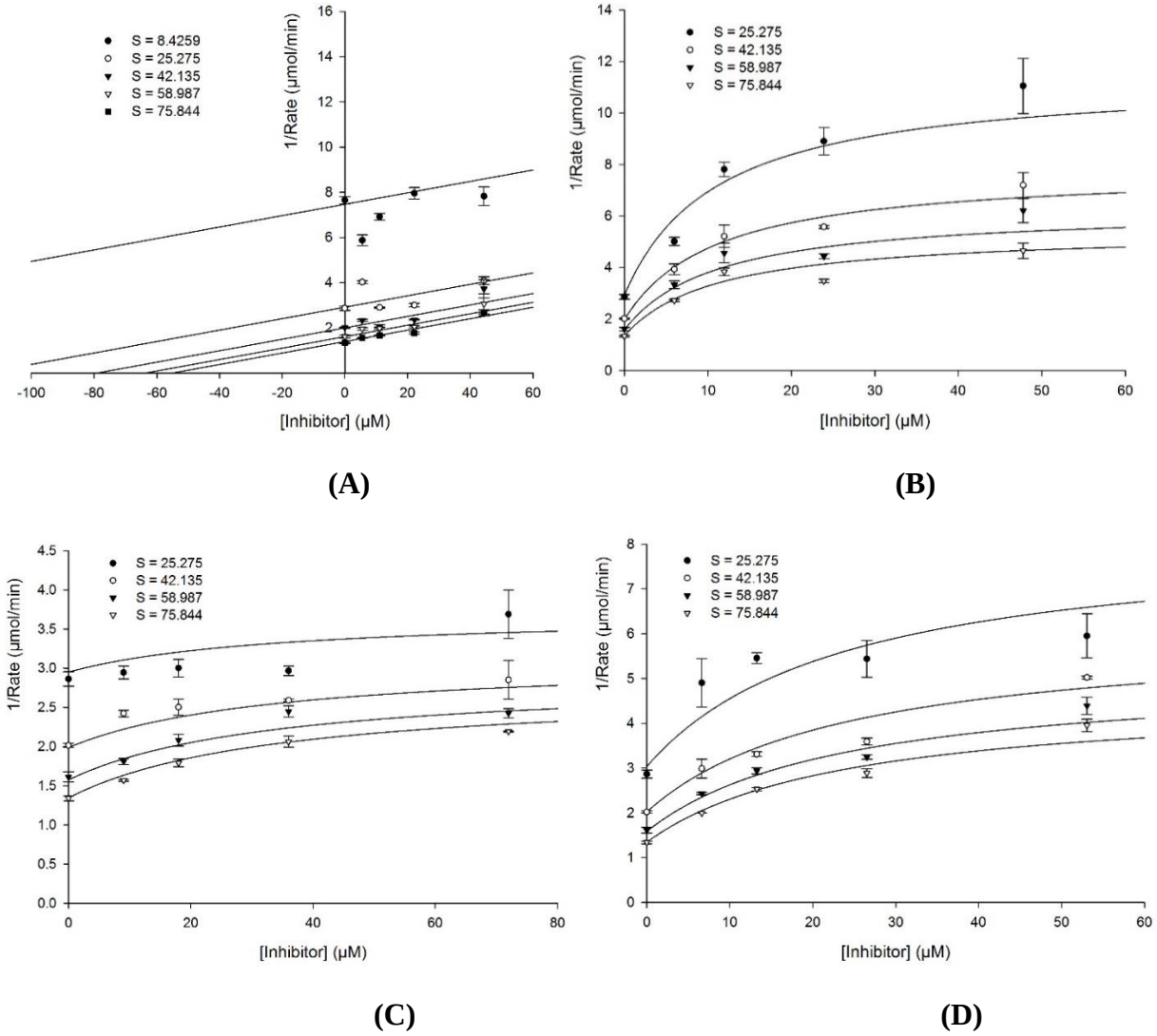

Figure 61: Dixon plots for α-amylase inhibition for PSEs (A) **4FI** (B) **4FS** (C) **2FS** (D) **4CiI**.

Table 32: Kinetic parameters for α-amylase inhibition by PSEs

Compound	Type of inhibition	K_i (μM)
4FI	Uncompetitive	24.9
4FS	Mixed Partial	2.9
2FS	Mixed Partial	58.4
4CiI	Mixed Partial	11.3
Acarbose	Fully mixed	0.537

Figure 61 shows the kinetic curves for the inhibition of α-amylase by the PSEs **4FI, 4FS, 2FS** and **4CiI**. **4FI** is seen to be an uncompetitive inhibitor as can be seen from Fig. 61 (A). This means that **4FI** can bind only to the enzyme substrate complex and not to the free enzyme. It can be seen from a comparison of the K_i values of **4FI** and Acarbose that the former has a lower affinity to α-amylase. The other three PSEs, **4FS, 2FS** and **4CiI** show a mixed partial inhibition towards α-amylase. A mixed partial inhibitor can bind to both the free enzyme as well as the enzyme substrate complex, however, a partial inhibitor works by slowing down the substrate turn-over rather than completely inhibiting the enzyme when bound to it. Once again, it can be seen that the tetra substituted PSEs have a greater affinity to α-amylase as compared to disubstituted. The only exception to the inhibition type among the compounds tested is the PSE **4FI** which as can be seen from both in vitro (chapter 2) and in silico studies (chapter 3), shows a lesser affinity to α-amylase thought to be due to the presence of the diisopropylidene group leading to a less favorable binding to the enzyme. Acarbose was found to be a mixed inhibitor with a K_i value of 0.537μM which was comparable to that found in literature (0.64μM).[90] The PSE, **4FS,** had a K_i value of 2.9μM (table 32), comparable to that of Acarbose showing a high affinity to the enzyme. The affinity ratio, α, and other parameters have not been computed in this case as the various plots used here are not suitable for calculation of kinetic parameters for a partial inhibitor due to the presence of non-linear curves. Therefore, further studies with a wider range of concentrations and secondary plots are necessary. However, it can be concluded that the PSEs are mainly mixed partial inhibitors and bind at a site or multiple sites other than the active site as also evidenced by the in silico studies in chapter 3.

4.4 Summary

The inhibition kinetics study for the PSEs was done in order to confirm the type of inhibition towards the enzymes, α-glucosidase and α-amylase. The kinetics study not only tells us the type of inhibition, but also provides information regarding the affinity of an inhibitor towards the enzyme, the possible site(s) it binds to as well as whether it requires the presence of substrate to function. For all four PSEs tested, **4FI, 4FS, 2FS** and **4CiI**, the inhibition of α-glucosidase was of mixed type. The following conclusions were drawn regarding the kinetics of α-glucosidase inhibition by PSEs.

- Mixed inhibition indicates that the PSEs bind to both the free enzyme as well as the enzyme substrate complex but has higher affinity for one of them.
- The affinity ratio, α, for all four of the PSEs is less than 1 indicating that the PSEs show a greater preference to the enzyme substrate complex rather than the free enzyme. This shows that the PSEs work better in the presence of the substrate.
- Since the inhibition of α-glucosidase is not competitive, it can be concluded that the PSEs do not bind at the active site (also the site for binding of Acarbose). This is in agreement with the in silico results from chapter 3 where it was seen that the PSEs bind to α-glucosidase enzyme at a site other than the active site. In case of Acarbose, the inhibition is competitive which is in accordance with literature.[90] The K_i values indicate that the PSEs have strong potency towards the inhibition of α-glucosidase as evidenced by the low values (~28μM; except for **2FS**) which were comparable to that of Acarbose (55.6μM). From the studies, it can be concluded that the type of inhibition is same between tetra and disubstituted PSEs (**4FS** and **2FS**), between PSEs with or without the diisopropylidene group (**4FS** and **4FI**), and finally also between different types of phenylpropanoid substituents (**4FI** and **4CiI**). Also, K_i values are similar for all of the tetra substituted compounds (table 24) which was lower than that of Acarbose.

The inhibition of α-amylase by the PSEs **4FI, 4FS, 2FS** and **4CiI** was seen to be more diverse. The following conclusions were drawn regarding the kinetics of α-amylase inhibition by PSEs.

- **4FI** was found to be an uncompetitive inhibitor with a K_i value of 24.9μM, much higher than Acarbose (0.537μM), which shows a much lesser affinity for α-amylase. This in accordance with the conclusion from in vitro (chapter 2) and in silico studies (chapter 3). The reduction in the affinity to α-amylase is due to the presence of the diisopropylidene group leading to a less favorable binding to the enzyme due to the 3D conformation being hindered sterically. **4FI** can bind only to the enzyme substrate complex and not to the free enzyme, indicating that it can function only in the presence of the substrate.
- The other three PSEs, **4FS, 2FS** and **4CiI** show a mixed partial inhibition towards α-amylase indicating that they bind to both the free enzyme as well as the enzyme substrate complex, however, they work by slowing down the substrate turn-over rather than completely inhibiting the enzyme when bound to it.
- Once again, it can be seen that the tetra substituted PSEs have a greater affinity to α-amylase as compared to disubstituted.
- Acarbose was found to be a mixed inhibitor similar to that reported in literature (0.64μM).[90] Among the PSEs tested, **4FS,** had the lowest K_i value (2.9μM) and thus the highest affinity to α-amylase.
- The affinity ratio, α, and other parameters were not calculated for α-amylase as the various linear plots used here are not suitable for calculation of kinetic parameters for a partial inhibitor on account of the inhibition lines being hyperbolic. Further studies with a wider range of concentrations and secondary plots are necessary. However, it can be concluded that the PSEs are mainly mixed partial inhibitors and bind at a site or multiple sites other than the active site.

4.5 Supplementary data

4.5.1 α-glucosidase kinetcs

Table 19: Velocity calculations for 4FI

Conc of substrate (mM)	Conc: 25µg/ml											
	Trial 1				Trial 2				Trial 3			
	Absorbance at 405nm	Amt of Product (mmol)	Velocity (mmol/min)	Velocity (µmol/min)	Absorbance at 405nm	Amt of Product (mmol)	Velocity (mmol/min)	Velocity (µmol/min)	Absorbance at 405nm	Amt of Product (mmol)	Velocity (mmol/min)	Velocity (µmol/min)
1.263	0.146	0.251	0.016	16.737	0.165	0.300	0.020	20.043	0.161	0.291	0.019	19.453
0.631	0.055	0.010	0.000	0.000	0.082	0.080	0.005	5.343	0.200	0.394	0.026	26.321
0.316	0.045	0.000	0.001	0.000	0.065	0.036	0.002	2.450	0.057	0.015	0.001	1.013
0.158	0.055	0.011	0.000	0.000	0.052	0.002	0.000	0.000	0.054	0.007	0.000	0.501
0.079	0.037	0.000	0.000	0.000	0.005	0.000	0.000	0.000	0.017	0.000	0.000	0.000
Conc of substrate(mM)	**Conc: 25µg/ml**											
	Trial 1				**Trial2**				**Trial 3**			
	Absorbance at 405nm	**Amt of Product (mmol)**	**Velocity (mmol/min)**	**Velocity (µmol/min)**	**Absorbance at 405nm**	**Amt of Product (mmol)**	**Velocity (mmol/min)**	**Velocity (µmol/min)**	**Absorbance at 405nm**	**Amt of Product (mmol)**	**Velocity (mmol/min)**	**Velocity (µmol/min)**
1.263	0.502	1.198	0.079	79.909	0.649	1.588	0.105	105.886	0.625	1.524	0.101	101.635
0.631	0.378	0.868	0.057	57.887	0.345	0.779	0.051	51.983	0.421	0.980	0.065	65.385
0.316	0.331	0.743	0.049	49.563	0.319	0.710	0.047	47.378	0.375	0.859	0.057	57.297
0.158	0.191	0.370	0.024	24.707	0.256	0.543	0.036	36.220	0.25	0.526	0.035	35.098
0.079	0.084	0.088	0.005	5.874	0.255	0.540	0.036	36.043	0.16	0.287	0.019	19.158
	Conc: 12.5µg/ml											
	Trial 1				**Trial 2**				**Trial 3**			
	Absorbance at 405nm	**Amt of Product (mmol)**	**Velocity (mmol/min)**	**Velocity (µmol/min)**	**Absorbance at 405nm**	**Amt of Product (mmol)**	**Velocity (mmol/min)**	**Velocity (µmol/min)**	**Absorbance at 405nm**	**Amt of Product (mmol)**	**Velocity (mmol/min)**	**Velocity (µmol/min)**
1.263	1.516	3.890	0.259	259.387	1.484	3.806	0.253	253.778	1.413	3.618	0.241	241.203
0.631	1.087	2.751	0.183	183.404	1.463	3.750	0.250	250.059	1.078	2.726	0.181	181.751
0.316	0.714	1.760	0.117	117.339	0.994	2.503	0.166	166.873	0.889	2.225	0.148	148.394

0.158	0.440	1.033	0.068	68.927	0.558	1.346	0.089	89.768	0.58	1.403	0.093	93.547
0.079	0.237	0.492	0.032	32.855	0.306	0.676	0.045	45.076	0.341	0.769	0.051	51.275
	Conc: 6.25µg/ml											
	Trial 1				**Trial 2**				**Trial 3**			
	Absorbance at 405nm	**Amt of Product (mmol)**	**Velocity (mmol/min)**	**Velocity (µmol/min)**	**Absorbance at 405nm**	**Amt of Product (mmol)**	**Velocity (mmol/min)**	**Velocity (µmol/min)**	**Absorbance at 405nm**	**Amt of Product (mmol)**	**Velocity (mmol/min)**	**Velocity (µmol/min)**
1.263	2.126	5.512	0.367	367.487	2.021	5.232	0.348	348.831	2.277	5.912	0.394	394.172
0.631	1.536	3.943	0.262	262.929	1.497	3.839	0.255	255.962	1.824	4.709	0.313	313.939
0.316	1.001	2.524	0.168	168.290	1.004	2.531	0.168	168.762	1.258	3.205	0.213	213.691
0.158	0.516	1.235	0.082	82.388	0.593	1.438	0.095	95.908	0.686	1.684	0.112	112.321
0.079	0.290	0.634	0.042	42.301	0.325	0.727	0.048	48.500	0.342	0.772	0.051	51.511

Table 20: Velocity calculations for 4FS

Conc of substrate(mM)	**Conc: 50µg/ml**											
	Trial 1				**Trial 2**				**Trial 3**			
	Absorbance at 405nm	**Amt of Product (mmol)**	**Velocity (mmol/min)**	**Velocity (µmol/min)**	**Absorbance at 405nm**	**Amt of Product (mmol)**	**Velocity (mmol/min)**	**Velocity (µmol/min)**	**Absorbance at 405nm**	**Amt of Product (mmol)**	**Velocity (mmol/min)**	**Velocity (µmol/min)**
1.263	0.389	0.897	0.059	59.835	0.363	0.827	0.055	55.171	0.384	0.882	0.058	58.832
0.631	0.284	0.617	0.041	41.179	0.273	0.589	0.039	39.290	0.305	0.673	0.044	44.879
0.316	0.256	0.544	0.036	36.279	0.242	0.505	0.033	33.681	0.253	0.535	0.035	35.688
0.158	0.23	0.474	0.031	31.615	0.212	0.425	0.028	28.368	0.206	0.410	0.027	27.364
0.079	0.151	0.264	0.017	17.623	0.093	0.109	0.007	7.291	0.121	0.184	0.012	12.309
	Conc: 25µg/ml											
	Trial 1				**Trial 2**				**Trial 3**			
	Absorbance at 405nm	**Amt of Product (mmol)**	**Velocity (mmol/min)**	**Velocity (µmol/min)**	**Absorbance at 405nm**	**Amt of Product (mmol)**	**Velocity (mmol/min)**	**Velocity (µmol/min)**	**Absorbance at 405nm**	**Amt of Product (mmol)**	**Velocity (mmol/min)**	**Velocity (µmol/min)**
1.263	0.895	2.240	0.149	149.397	0.996	2.510	0.167	167.345	0.936	2.349	0.156	156.600
0.631	0.768	1.904	0.126	126.963	0.735	1.816	0.121	121.118	0.687	1.689	0.112	112.616
0.316	0.518	1.239	0.082	82.624	0.491	1.168	0.077	77.901	0.473	1.1207	0.074	74.713

0.158	0.329	0.738	0.049	49.208	0.319	0.710	0.047	47.378	0.309	0.683	0.045	45.548
0.079	0.209	0.420	0.028	28.013	0.224	0.457	0.030	30.493	0.213	0.429	0.028	28.604
	Conc: 12.5µg/ml											
	Trial 1				**Trial 2**				**Trial 3**			
	Absorbance at 405nm	**Amt of Product (mmol)**	**Velocity (mmol/min)**	**Velocity (µmol/min)**	**Absorbance at 405nm**	**Amt of Product (mmol)**	**Velocity (mmol/min)**	**Velocity (µmol/min)**	**Absorbance at 405nm**	**Amt of Product (mmol)**	**Velocity (mmol/min)**	**Velocity (µmol/min)**
1.263	1.671	4.304	0.286	286.958	2.213	5.742	0.382	382.837	2.552	6.644	0.442	442.939
0.631	1.201	3.054	0.203	203.654	1.521	3.904	0.260	260.272	1.709	4.402	0.293	293.511
0.316	0.777	1.928	0.128	128.557	1.005	2.532	0.168	168.821	1.204	3.061	0.204	204.067
0.158	0.498	1.186	0.079	79.082	0.589	1.428	0.095	95.200	0.688	1.691	0.112	112.793
0.079	0.290	0.634	0.042	42.301	0.317	0.704	0.046	46.965	0.356	0.808	0.053	53.872
	Conc: 6.25µg/ml											
	Trial 1				**Trial 2**				**Trial 3**			
	Absorbance at 405nm	**Amt of Product (mmol)**	**Velocity (mmol/min)**	**Velocity (µmol/min)**	**Absorbance at 405nm**	**Amt of Product (mmol)**	**Velocity (mmol/min)**	**Velocity (µmol/min)**	**Absorbance at 405nm**	**Amt of Product (mmol)**	**Velocity (mmol/min)**	**Velocity (µmol/min)**
1.263	2.128	5.517	0.367	367.841	2.184	5.664	0.377	377.642	2.573	6.698	0.446	446.599
0.631	1.517	3.879	0.258	258.619	1.695	4.366	0.291	291.091	1.880	4.857	0.323	323.857
0.316	0.929	2.333	0.155	155.537	1.181	3.001	0.200	200.112	1.175	2.984	0.198	198.990
0.158	0.557	1.344	0.089	89.650	0.651	1.592	0.106	106.181	0.68	1.669	0.111	111.317
0.079	0.305	0.6734	0.044	44.899	0.337	0.758	0.050	50.566	0.33	0.739	0.049	49.326

Table 21: Velocity calculations for 2FS

Conc of substrate(mM)	**Conc: 50µg/ml**											
	Trial 1				**Trial 2**				**Trial 3**			
	Absorbance at 405nm	**Amt of Product (mmol)**	**Velocity (mmol/min)**	**Velocity (µmol/min)**	**Absorbance at 405nm**	**Amt of Product (mmol)**	**Velocity (mmol/min)**	**Velocity (µmol/min)**	**Absorbance at 405nm**	**Amt of Product (mmol)**	**Velocity (mmol/min)**	**Velocity (µmol/min)**
1.263	1.540	3.954	0.263	263.638	1.542	3.958	0.263	263.933	1.546	3.969	0.264	264.622

0.631	1.124	2.851	0.190	190.075	1.125	2.852	0.190	190.134	1.132	2.870	0.191	191.394
0.316	0.726	1.792	0.119	119.524	0.924	2.318	0.154	154.593	0.869	2.170	0.144	144.714
0.158	0.437	1.025	0.068	68.396	0.503	1.200	0.080	80.027	0.490	1.166	0.077	77.744
0.079	0.226	0.463	0.030	30.906	0.262	0.558	0.037	37.2239	0.254	0.538	0.035	35.885
	Conc: 25µg/ml											
	Trial 1				**Trial 2**				**Trial 3**			
	Absorbance at 405nm	**Amt of Product (mmol)**	**Velocity (mmol/min)**	**Velocity (µmol/min)**	**Absorbance at 405nm**	**Amt of Product (mmol)**	**Velocity (mmol/min)**	**Velocity (µmol/min)**	**Absorbance at 405nm**	**Amt of Product (mmol)**	**Velocity (mmol/min)**	**Velocity (µmol/min)**
1.263	1.790	4.620	0.308	308.035	1.718	4.426	0.295	295.105	1.744	4.497	0.299	299.828
0.631	1.321	3.374	0.224	224.967	1.346	3.438	0.229	229.218	1.306	3.332	0.222	222.133
0.316	0.896	2.243	0.149	149.574	0.834	2.079	0.138	138.652	0.823	2.049	0.136	136.645
0.158	0.522	1.251	0.083	83.451	0.613	1.492	0.099	99.509	0.545	1.310	0.087	87.347
0.079	0.290	0.634	0.042	42.301	0.326	0.729	0.048	48.618	0.306	0.675	0.045	45.017
	Conc: 12.5µg/ml											
	Trial 1				**Trial 2**				**Trial 3**			
	Absorbance at 405nm	**Amt of Product (mmol)**	**Velocity (mmol/min)**	**Velocity (µmol/min)**	**Absorbance at 405nm**	**Amt of Product (mmol)**	**Velocity (mmol/min)**	**Velocity (µmol/min)**	**Absorbance at 405nm**	**Amt of Product (mmol)**	**Velocity (mmol/min)**	**Velocity (µmol/min)**
1.263	1.806	4.663	0.310	310.869	2.085	5.401	0.360	360.107	2.526	6.575	0.438	438.333
0.631	1.325	3.385	0.225	225.676	1.567	4.026	0.268	268.420	1.849	4.774	0.318	318.307
0.316	0.888	2.223	0.148	148.217	0.984	2.476	0.165	165.102	1.222	3.108	0.207	207.255
0.158	0.479	1.136	0.075	75.776	0.625	1.522	0.101	101.517	0.64	1.562	0.104	104.174
0.079	0.287	0.627	0.041	41.829	0.291	0.636	0.042	42.419	0.405	0.938	0.062	62.551
	Conc: 6.25µg/ml											
	Trial 1				**Trial 2**				**Trial 3**			
	Absorbance at 405nm	**Amt of Product (mmol)**	**Velocity (mmol/min)**	**Velocity (µmol/min)**	**Absorbance at 405nm**	**Amt of Product (mmol)**	**Velocity (mmol/min)**	**Velocity (µmol/min)**	**Absorbance at 405nm**	**Amt of Product (mmol)**	**Velocity (mmol/min)**	**Velocity (µmol/min)**
1.263	2.237	5.806	0.387	387.088	2.392	6.218	0.414	414.541	2.590	6.743	0.449	449.551
0.631	1.528	3.924	0.261	261.630	1.728	4.454	0.296	296.935	1.932	4.995	0.333	333.008
0.316	1.070	2.707	0.180	180.511	1.224	3.115	0.207	207.669	1.209	3.075	0.205	205.012
0.158	0.389	0.898	0.059	59.894	0.680	1.669	0.111	111.317	0.620	1.510	0.100	100.690
0.079	0.447	1.051	0.070	70.108	0.369	0.843	0.056	56.234	0.332	0.746	0.049	49.740

Table 22: Velocity calculations for 4CiI

Conc of substrate(mM)	Conc: 50µg/ml											
	Trial 1				Trial 2				Trial 3			
	Absorbance at 405nm	Amt of Product (mmol)	Velocity (mmol/min)	Velocity (µmol/min)	Absorbance at 405nm	Amt of Product (mmol)	Velocity (mmol/min)	Velocity (µmol/min)	Absorbance at 405nm	Amt of Product (mmol)	Velocity (mmol/min)	Velocity (µmol/min)
1.263	0.288	0.630	0.042	42.006	0.297	0.653	0.044	43.541	0.286	0.623	0.042	41.554
0.631	0.202	0.401	0.027	26.715	0.268	0.575	0.038	38.346	0.225	0.462	0.031	30.789
0.316	0.169	0.314	0.021	20.929	0.213	0.430	0.029	28.663	0.173	0.322	0.021	21.480
0.158	0.124	0.193	0.013	12.841	0.182	0.347	0.023	23.114	0.148	0.257	0.017	17.111
0.079	0.107	0.147	0.010	9.830	0.114	0.165	0.011	11.011	0.102	0.134	0.009	8.925
	Conc: 25µg/ml											
	Trial 1				Trial 2				Trial 3			
	Absorbance at 405nm	Amt of Product (mmol)	Velocity (mmol/min)	Velocity (µmol/min)	Absorbance at 405nm	Amt of Product (mmol)	Velocity (mmol/min)	Velocity (µmol/min)	Absorbance at 405nm	Amt of Product (mmol)	Velocity (mmol/min)	Velocity (µmol/min)
1.263	0.731	1.806	0.120	120.410	0.714	1.759	0.117	117.281	0.730	1.803	0.120	120.174
0.631	0.649	1.589	0.106	105.945	0.631	1.540	0.103	102.698	0.654	1.601	0.107	106.713
0.316	0.441	1.037	0.069	69.105	0.431	1.009	0.067	67.275	0.427	0.998	0.067	66.507
0.158	0.291	0.637	0.042	42.478	0.315	0.699	0.047	46.611	0.340	0.766	0.051	51.098
0.079	0.156	0.279	0.019	18.627	0.220	0.447	0.030	29.785	0.243	0.510	0.034	33.977
	Conc: 12.5µg/ml											
	Trial 1				Trial 2				Trial 3			
	Absorbance at 405nm	Amt of Product (mmol)	Velocity (mmol/min)	Velocity (µmol/min)	Absorbance at 405nm	Amt of Product (mmol)	Velocity (mmol/min)	Velocity (µmol/min)	Absorbance at 405nm	Amt of Product (mmol)	Velocity (mmol/min)	Velocity (µmol/min)
1.263	1.402	3.588	0.239	239.196	1.816	4.688	0.313	312.522	1.795	4.632	0.309	308.803
0.631	0.714	1.761	0.117	117.399	1.381	3.531	0.235	235.417	1.773	4.574	0.305	304.965
0.316	0.795	1.977	0.132	131.804	0.688	1.691	0.113	112.735	1.124	2.849	0.190	189.958
0.158	0.399	0.924	0.062	61.607	0.397	0.917	0.061	61.135	0.561	1.354	0.090	90.241
0.079	0.234	0.485	0.032	32.324	0.277	0.599	0.040	39.940	0.327	0.733	0.049	48.855
	Conc: 6.25µg/ml											

	Trial 1				Trial 2				Trial 3			
	Absorbance at 405nm	Amt of Product (mmol)	Velocity (mmol/min)	Velocity (µmol/min)	Absorbance at 405nm	Amt of Product (mmol)	Velocity (mmol/min)	Velocity (µmol/min)	Absorbance at 405nm	Amt of Product (mmol)	Velocity (mmol/min)	Velocity (µmol/min)
1.263	2.001	5.180	0.345	345.348	2.243	5.823	0.388	388.210	2.278	5.916	0.394	394.409
0.631	1.478	3.790	0.253	252.657	1.686	4.342	0.289	289.497	1.491	3.825	0.255	255.018
0.316	0.944	2.373	0.158	158.195	1.102	2.792	0.186	186.120	1.123	2.847	0.190	189.780
0.158	0.499	1.190	0.079	79.319	0.658	1.610	0.107	107.362	0.607	1.475	0.098	98.329
0.079	0.277	0.600	0.040	39.999	0.350	0.792	0.053	52.810	0.312	0.691	0.046	46.080

Table 23: Velocity calculations for Acarbose

Conc of substrate(mM)	Conc: 50µg/ml											
	Trial 1				Trial 2				Trial 3			
	Absorbance at 405nm	Amt of Product (mmol)	Velocity (mmol/min)	Velocity (µmol/min)	Absorbance at 405nm	Amt of Product (mmol)	Velocity (mmol/min)	Velocity (µmol/min)	Absorbance at 405nm	Amt of Product (mmol)	Velocity (mmol/min)	Velocity (µmol/min)
1.263	1.691	4.356	0.290	290.383	1.663	4.281	0.285	285.423	1.819	4.696	0.313	313.053
0.631	1.043	2.634	0.176	175.611	1.147	2.910	0.194	194.031	1.153	2.926	0.195	195.094
0.316	0.616	1.501	0.100	100.041	0.615	1.496	0.100	99.746	0.604	1.468	0.098	97.857
0.158	0.335	0.753	0.050	50.213	0.328	0.735	0.049	48.973	0.313	0.696	0.046	46.375
0.079	0.208	0.415	0.028	27.660	0.158	0.283	0.019	18.863	0.141	0.238	0.016	15.852
	Conc: 25µg/ml											
	Trial 1				Trial 2				Trial 3			
	Absorbance at 405nm	Amt of Product (mmol)	Velocity (mmol/min)	Velocity (µmol/min)	Absorbance at 405nm	Amt of Product (mmol)	Velocity (mmol/min)	Velocity (µmol/min)	Absorbance at 405nm	Amt of Product (mmol)	Velocity (mmol/min)	Velocity (µmol/min)
1.263	1.874	4.843	0.323	322.854	2.046	5.299	0.353	353.259	1.598	4.110	0.274	273.970
0.631	1.132	2.870	0.191	191.315	1.170	2.972	0.198	198.105	1.117	2.832	0.189	188.777

0.316	0.619	1.508	0.101	100.514	0.621	1.514	0.101	100.927	0.572	1.382	0.092	92.130
0.158	0.339	0.764	0.051	50.921	0.329	0.738	0.049	49.209	0.298	0.655	0.044	43.659
0.079	0.220	0.448	0.030	29.844	0.171	0.317	0.021	21.165	0.160	0.289	0.019	19.276
	Conc: 12.5µg/ml											
	Trial 1				**Trial 2**				**Trial 3**			
	Absorbance at 405nm	**Amt of Product (mmol)**	**Velocity (mmol/min)**	**Velocity (µmol/min)**	**Absorbance at 405nm**	**Amt of Product (mmol)**	**Velocity (mmol/min)**	**Velocity (µmol/min)**	**Absorbance at 405nm**	**Amt of Product (mmol)**	**Velocity (mmol/min)**	**Velocity (µmol/min)**
1.263	2.576	6.706	0.447	447.072	2.406	6.254	0.417	416.962	2.416	6.281	0.419	418.733
0.631	1.905	4.924	0.328	328.286	2.085	5.402	0.360	360.107	1.468	3.764	0.251	250.945
0.316	1.162	2.950	0.197	196.688	1.122	2.845	0.190	189.662	1.171	2.975	0.198	198.341
0.158	0.705	1.735	0.116	115.687	0.652	1.596	0.106	106.418	0.561	1.354	0.090	90.300
0.079	0.397	0.917	0.061	61.135	0.325	0.727	0.048	48.441	0.320	0.713	0.048	47.556
	Conc: 6.25µg/ml											
	Trial 1				**Trial 2**				**Trial 3**			
	Absorbance at 405nm	**Amt of Product (mmol)**	**Velocity (mmol/min)**	**Velocity (µmol/min)**	**Absorbance at 405nm**	**Amt of Product (mmol)**	**Velocity (mmol/min)**	**Velocity (µmol/min)**	**Absorbance at 405nm**	**Amt of Product (mmol)**	**Velocity (mmol/min)**	**Velocity (µmol/min)**
1.263	2.459	6.397	0.426	426.467	2.402	6.244	0.416	416.253	2.288	5.942	0.396	396.121
0.631	1.724	4.443	0.296	296.168	1.692	4.358	0.291	290.560	1.765	4.552	0.303	303.489
0.316	1.162	2.951	0.197	196.747	1.156	2.935	0.196	195.684	0.984	2.478	0.165	165.220
0.158	0.672	1.649	0.110	109.901	0.663	1.625	0.108	108.307	0.629	1.534	0.102	102.285
0.079	0.368	0.841	0.056	56.057	0.366	0.835	0.056	55.644	0.331	0.742	0.049	49.445

Table 24: Velocity calculations for enzyme without inhibitor

Conc of substrate(mM)	No inhibitor											
	Trial 1				Trial 2				Trial 3			
	Absorbance at 405nm	Amt of Product (mmol)	Velocity (mmol/min)	Velocity (µmol/min)	Absorbance at 405nm	Amt of Product (mmol)	Velocity (mmol/min)	Velocity (µmol/min)	Absorbance at 405nm	Amt of Product (mmol)	Velocity (mmol/min)	Velocity (µmol/min)
1.263	2.601	6.773	0.452	451.565	2.669	6.953	0.464	463.544	2.858	7.456	0.497	497.078
0.631	1.794	4.631	0.309	308.750	1.920	4.965	0.331	331.001	1.809	4.668	0.311	311.223
0.316	1.182	3.004	0.200	200.236	1.251	3.187	0.212	212.451	0.908	2.276	0.152	151.759
0.158	0.672	1.649	0.110	109.966	0.682	1.676	0.112	111.731	0.509	1.216	0.081	81.090
0.079	0.357	0.813	0.054	54.233	0.353	0.801	0.053	53.401	0.291	0.635	0.042	42.360

4.3.2 α-amylase kinetics

Table 26: Velocity calculations for 4FI

Conc of substrate(mM)	Conc: 50µg/ml											
	Trial 1				Trial 2				Trial 3			
	Absorbance at 540nm	Amt of Product (mmol)	Velocity (mmol/min)	Velocity (µmol/min)	Absorbance at 540nm	Amt of Product (mmol)	Velocity (mmol/min)	Velocity (µmol/min)	Absorbance at 540nm	Amt of Product (mmol)	Velocity (mmol/min)	Velocity (µmol/min)
8.4259	0.189	0.0007	0.0001	0.138	0.159	0.0006	0.0001	0.116	0.180	0.0006	0.0001	0.131
25.275	0.312	0.0011	0.0002	0.227	0.339	0.0012	0.0002	0.246	0.362	0.0013	0.0003	0.263
42.135	0.413	0.0014	0.0003	0.300	0.304	0.0011	0.0002	0.221	0.413	0.0014	0.0003	0.300
58.987	0.560	0.0019	0.0004	0.407	0.350	0.0012	0.0003	0.254	0.495	0.0017	0.0004	0.359
75.844	0.547	0.0019	0.0004	0.397	0.469	0.0016	0.0003	0.341	0.547	0.0019	0.0004	0.397
	Conc: 25µg/ml											
	Trial 1				**Trial 2**				**Trial 3**			
	Absorbance at 540nm	**Amt of Product (mmol)**	**Velocity (mmol/min)**	**Velocity (µmol/min)**	**Absorbance at 540nm**	**Amt of Product (mmol)**	**Velocity (mmol/min)**	**Velocity (µmol/min)**	**Absorbance at 540nm**	**Amt of Product (mmol)**	**Velocity (mmol/min)**	**Velocity (µmol/min)**
8.4259	0.184	0.0006	0.0001	0.134	0.165	0.0006	0.0001	0.120	0.169	0.0006	0.0001	0.123
25.275	0.439	0.0015	0.0003	0.319	0.459	0.0016	0.0003	0.333	0.479	0.0017	0.0003	0.348
42.135	0.584	0.0020	0.0004	0.424	0.576	0.0020	0.0004	0.418	0.593	0.0020	0.0004	0.430
58.987	0.697	0.0024	0.0005	0.506	0.646	0.0022	0.0005	0.469	0.685	0.0024	0.0005	0.497
75.844	0.812	0.0028	0.0006	0.589	0.771	0.0027	0.0006	0.559	0.754	0.0026	0.0005	0.547
	Conc: 12.5µg/ml											
	Trial 1				**Trial 2**				**Trial 3**			
	Absorbance at 540nm	**Amt of Product (mmol)**	**Velocity (mmol/min)**	**Velocity (µmol/min)**	**Absorbance at 540nm**	**Amt of Product (mmol)**	**Velocity (mmol/min)**	**Velocity (µmol/min)**	**Absorbance at 540nm**	**Amt of Product (mmol)**	**Velocity (mmol/min)**	**Velocity (µmol/min)**
8.4259	0.199	0.0007	0.0001	0.145	0.191	0.0007	0.0001	0.139	0.206	0.0007	0.0002	0.150
25.275	0.480	0.0017	0.0003	0.349	0.466	0.0016	0.0003	0.338	0.480	0.0017	0.0003	0.349
42.135	0.709	0.0024	0.0005	0.514	0.650	0.0022	0.0005	0.472	0.639	0.0022	0.0005	0.464
58.987	0.723	0.0025	0.0005	0.525	0.703	0.0024	0.0005	0.510	0.666	0.0023	0.0005	0.483
75.844	0.847	0.0029	0.0006	0.614	0.819	0.0028	0.0006	0.594	0.828	0.0029	0.0006	0.601

	Conc: 6.25µg/ml											
	Trial 1				Trial 2				Trial 3			
	Absorbance at 540nm	Amt of Product (mmol)	Velocity (mmol/min)	Velocity (µmol/min)	Absorbance at 540nm	Amt of Product (mmol)	Velocity (mmol/min)	Velocity (µmol/min)	Absorbance at 540nm	Amt of Product (mmol)	Velocity (mmol/min)	Velocity (µmol/min)
8.4259	0.254	0.0009	0.0002	0.185	0.229	0.0008	0.0002	0.167	0.221	0.0008	0.0002	0.161
25.275	0.340	0.0012	0.0002	0.247	0.353	0.0012	0.0003	0.257	0.334	0.0012	0.0002	0.243
42.135	0.607	0.0021	0.0004	0.441	0.596	0.0021	0.0004	0.433	0.570	0.0020	0.0004	0.414
58.987	0.674	0.0023	0.0005	0.489	0.701	0.0024	0.0005	0.509	0.747	0.0026	0.0005	0.542
75.844	0.893	0.0031	0.0006	0.648	0.898	0.0031	0.0007	0.651	0.867	0.0030	0.0006	0.629

Table 27: Velocity calculations for 4FS

Conc of substrate(mM)	Conc: 50µg/ml											
	Trial 1				Trial 2				Trial 3			
	Absorbance at 540nm	Amt of Product (mmol)	Velocity (mmol/min)	Velocity (µmol/min)	Absorbance at 540nm	Amt of Product (mmol)	Velocity (mmol/min)	Velocity (µmol/min)	Absorbance at 540nm	Amt of Product (mmol)	Velocity (mmol/min)	Velocity (µmol/min)
8.4259	0.0001	0.00003	0.028	0.027	0.0001	0.00002	0.020	0.043	0.0002	0.00003	0.032	0.0001
25.275	0.0005	0.00010	0.096	0.104	0.0004	0.00008	0.076	0.143	0.0005	0.00010	0.104	0.0005
42.135	0.0007	0.00014	0.142	0.169	0.0006	0.00012	0.123	0.213	0.0007	0.00016	0.155	0.0007
58.987	0.0007	0.00015	0.149	0.207	0.0007	0.00015	0.151	0.261	0.0009	0.00019	0.190	0.0007
75.844	0.0010	0.00022	0.220	0.264	0.0009	0.00019	0.192	0.328	0.0011	0.00024	0.238	0.0010
	Conc: 25µg/ml											
	Trial 1				Trial 2				Trial 3			
	Absorbance at 540nm	Amt of Product (mmol)	Velocity (mmol/min)	Velocity (µmol/min)	Absorbance at 540nm	Amt of Product (mmol)	Velocity (mmol/min)	Velocity (µmol/min)	Absorbance at 540nm	Amt of Product (mmol)	Velocity (mmol/min)	Velocity (µmol/min)
8.4259	0.0002	0.0000	0.038	0.049	0.0002	0.0000	0.036	0.065	0.0002	0.0000	0.048	0.0002
25.275	0.0006	0.0001	0.123	0.138	0.0005	0.0001	0.101	0.158	0.0005	0.0001	0.115	0.0006
42.135	0.0009	0.0002	0.183	0.242	0.0008	0.0002	0.176	0.246	0.0009	0.0002	0.179	0.0009
58.987	0.0011	0.0002	0.236	0.302	0.0010	0.0002	0.220	0.305	0.0011	0.0002	0.222	0.0011
75.844	0.0014	0.0003	0.298	0.384	0.0013	0.0003	0.279	0.393	0.0014	0.0003	0.286	0.0014

	Conc: 12.5µg/ml											
	Trial 1				Trial 2				Trial 3			
	Absorbance at 540nm	Amt of Product (mmol)	Velocity (mmol/min)	Velocity (µmol/min)	Absorbance at 540nm	Amt of Product (mmol)	Velocity (mmol/min)	Velocity (µmol/min)	Absorbance at 540nm	Amt of Product (mmol)	Velocity (mmol/min)	Velocity (µmol/min)
8.4259	0.0003	0.0001	0.070	0.069	0.0002	0.0001	0.051	0.082	0.0003	0.0001	0.060	0.0003
25.275	0.0006	0.0001	0.135	0.164	0.0006	0.0001	0.120	0.179	0.0006	0.0001	0.131	0.0006
42.135	0.0011	0.0002	0.231	0.246	0.0009	0.0002	0.179	0.241	0.0008	0.0002	0.175	0.0011
58.987	0.0012	0.0003	0.259	0.265	0.0009	0.0002	0.193	0.297	0.0010	0.0002	0.216	0.0012
75.844	0.0013	0.0003	0.281	0.343	0.0012	0.0002	0.249	0.349	0.0012	0.0003	0.254	0.0013
	Conc: 6.25µg/ml											
	Trial 1				Trial 2				Trial 3			
	Absorbance at 540nm	Amt of Product (mmol)	Velocity (mmol/min)	Velocity (µmol/min)	Absorbance at 540nm	Amt of Product (mmol)	Velocity (mmol/min)	Velocity (µmol/min)	Absorbance at 540nm	Amt of Product (mmol)	Velocity (mmol/min)	Velocity (µmol/min)
8.4259	0.0007	0.0001	0.137	0.174	0.0006	0.0001	0.127	0.165	0.0006	0.0001	0.120	0.0007
25.275	0.0010	0.0002	0.213	0.264	0.0009	0.0002	0.192	0.268	0.0009	0.0002	0.195	0.0010
42.135	0.0014	0.0003	0.284	0.340	0.0012	0.0002	0.247	0.326	0.0011	0.0002	0.237	0.0014
58.987	0.0016	0.0003	0.330	0.401	0.0014	0.0003	0.291	0.389	0.0013	0.0003	0.283	0.0016
75.844	0.0018	0.0004	0.378	0.507	0.0018	0.0004	0.368	0.490	0.0017	0.0004	0.356	0.0018

Table 28: Velocity calculations for 2FS

Conc of substrate(mM)	Conc: 50µg/ml											
	Trial 1				Trial 2				Trial 3			
	Absorbance at 540nm	Amt of Product (mmol)	Velocity (mmol/min)	Velocity (µmol/min)	Absorbance at 540nm	Amt of Product (mmol)	Velocity (mmol/min)	Velocity (µmol/min)	Absorbance at 540nm	Amt of Product (mmol)	Velocity (mmol/min)	Velocity (µmol/min)
8.4259	0.180	0.0006	0.0001	0.131	0.107	0.0004	0.0001	0.078	0.166	0.0006	0.0001	0.121
25.275	0.424	0.0015	0.0003	0.308	0.389	0.0013	0.0003	0.283	0.321	0.0011	0.0002	0.233
42.135	0.584	0.0020	0.0004	0.424	0.440	0.0015	0.0003	0.320	0.449	0.0016	0.0003	0.326

58.987	0.553	0.0019	0.0004	0.401	0.555	0.0019	0.0004	0.403	0.597	0.0021	0.0004	0.433
75.844	0.624	0.0022	0.0005	0.453	0.633	0.0022	0.0005	0.459	0.627	0.0022	0.0005	0.455
	Conc: 25µg/ml											
	Trial 1				**Trial 2**				**Trial 3**			
	Absorbance at 540nm	**Amt of Product (mmol)**	**Velocity (mmol/min)**	**Velocity (µmol/min)**	**Absorbance at 540nm**	**Amt of Product (mmol)**	**Velocity (mmol/min)**	**Velocity (µmol/min)**	**Absorbance at 540nm**	**Amt of Product (mmol)**	**Velocity (mmol/min)**	**Velocity (µmol/min)**
8.4259	0.124	0.0004	0.0001	0.091	0.197	0.0007	0.0001	0.144	0.199	0.0007	0.0001	0.145
25.275	0.446	0.0015	0.0003	0.324	0.470	0.0016	0.0003	0.341	0.477	0.0016	0.0003	0.346
42.135	0.533	0.0018	0.0004	0.387	0.525	0.0018	0.0004	0.381	0.537	0.0019	0.0004	0.390
58.987	0.596	0.0021	0.0004	0.433	0.556	0.0019	0.0004	0.404	0.539	0.0019	0.0004	0.391
75.844	0.688	0.0024	0.0005	0.499	0.626	0.0022	0.0005	0.454	0.695	0.0024	0.0005	0.504
	Conc: 12.5µg/ml											
	Trial 1				**Trial 2**				**Trial 3**			
	Absorbance at 540nm	**Amt of Product (mmol)**	**Velocity (mmol/min)**	**Velocity (µmol/min)**	**Absorbance at 540nm**	**Amt of Product (mmol)**	**Velocity (mmol/min)**	**Velocity (µmol/min)**	**Absorbance at 540nm**	**Amt of Product (mmol)**	**Velocity (mmol/min)**	**Velocity (µmol/min)**
8.4259	0.170	0.0006	0.0001	0.124	0.197	0.0007	0.0001	0.144	0.204	0.0007	0.0001	0.149
25.275	0.487	0.0017	0.0004	0.354	0.464	0.0016	0.0003	0.337	0.429	0.0015	0.0003	0.312
42.135	0.582	0.0020	0.0004	0.422	0.564	0.0019	0.0004	0.409	0.510	0.0018	0.0004	0.370
58.987	0.616	0.0021	0.0004	0.447	0.687	0.0024	0.0005	0.499	0.688	0.0024	0.0005	0.499
75.844	0.729	0.0025	0.0005	0.529	0.794	0.0027	0.0006	0.576	0.788	0.0027	0.0006	0.572
	Conc: 6.25µg/ml											
	Trial 1				**Trial 2**				**Trial 3**			
	Absorbance at 540nm	**Amt of Product (mmol)**	**Velocity (mmol/min)**	**Velocity (µmol/min)**	**Absorbance at 540nm**	**Amt of Product (mmol)**	**Velocity (mmol/min)**	**Velocity (µmol/min)**	**Absorbance at 540nm**	**Amt of Product (mmol)**	**Velocity (mmol/min)**	**Velocity (µmol/min)**
8.4259	0.272	0.0009	0.0002	0.198	0.276	0.0010	0.0002	0.201	0.263	0.0009	0.0002	0.191
25.275	0.484	0.0017	0.0004	0.351	0.478	0.0017	0.0003	0.347	0.443	0.0015	0.0003	0.322
42.135	0.578	0.0020	0.0004	0.420	0.579	0.0020	0.0004	0.420	0.550	0.0019	0.0004	0.399
58.987	0.742	0.0026	0.0005	0.538	0.749	0.0026	0.0005	0.543	0.795	0.0027	0.0006	0.577
75.844	0.894	0.0031	0.0006	0.648	0.870	0.0030	0.0006	0.631	0.871	0.0030	0.0006	0.632

Table 29: Velocity calculations for 4CiI

Conc of substrate(mM)	Conc: 50µg/ml											
	Trial 1				Trial 2				Trial 3			
	Absorbance at 540nm	Amt of Product (mmol)	Velocity (mmol/min)	Velocity (µmol/min)	Absorbance at 540nm	Amt of Product (mmol)	Velocity (mmol/min)	Velocity (µmol/min)	Absorbance at 540nm	Amt of Product (mmol)	Velocity (mmol/min)	Velocity (µmol/min)
8.4259	0.103	0.0004	0.0001	0.075	0.085	0.0003	0.0001	0.062	0.058	0.0002	0.0000	0.043
25.275	0.257	0.0009	0.0002	0.187	0.198	0.0007	0.0001	0.144	0.246	0.0009	0.0002	0.179
42.135	0.277	0.0010	0.0002	0.202	0.273	0.0009	0.0002	0.199	0.271	0.0009	0.0002	0.197
58.987	0.327	0.0011	0.0002	0.238	0.328	0.0011	0.0002	0.238	0.288	0.0010	0.0002	0.209
75.844	0.329	0.0011	0.0002	0.239	0.371	0.0013	0.0003	0.270	0.346	0.0012	0.0003	0.252
	Conc: 25µg/ml											
	Trial 1				**Trial 2**				**Trial 3**			
	Absorbance at 540nm	**Amt of Product (mmol)**	**Velocity (mmol/min)**	**Velocity (µmol/min)**	**Absorbance at 540nm**	**Amt of Product (mmol)**	**Velocity (mmol/min)**	**Velocity (µmol/min)**	**Absorbance at 540nm**	**Amt of Product (mmol)**	**Velocity (mmol/min)**	**Velocity (µmol/min)**
8.4259	0.132	0.0005	0.0001	0.096	0.138	0.0005	0.0001	0.101	0.122	0.0004	0.0001	0.089
25.275	0.231	0.0008	0.0002	0.168	0.297	0.0010	0.0002	0.216	0.239	0.0008	0.0002	0.174
42.135	0.367	0.0013	0.0003	0.267	0.395	0.0014	0.0003	0.287	0.389	0.0013	0.0003	0.283
58.987	0.412	0.0014	0.0003	0.299	0.434	0.0015	0.0003	0.315	0.428	0.0015	0.0003	0.311
75.844	0.492	0.0017	0.0004	0.357	0.495	0.0017	0.0004	0.359	0.447	0.0015	0.0003	0.325
	Conc: 12.5µg/ml											
	Trial 1				**Trial 2**				**Trial 3**			
	Absorbance at 540nm	**Amt of Product (mmol)**	**Velocity (mmol/min)**	**Velocity (µmol/min)**	**Absorbance at 540nm**	**Amt of Product (mmol)**	**Velocity (mmol/min)**	**Velocity (µmol/min)**	**Absorbance at 540nm**	**Amt of Product (mmol)**	**Velocity (mmol/min)**	**Velocity (µmol/min)**
8.4259	0.260	0.0009	0.0002	0.189	0.289	0.0010	0.0002	0.210	0.193	0.0007	0.0001	0.141
25.275	0.243	0.0008	0.0002	0.177	0.251	0.0009	0.0002	0.183	0.262	0.0009	0.0002	0.191
42.135	0.404	0.0014	0.0003	0.294	0.424	0.0015	0.0003	0.308	0.421	0.0015	0.0003	0.306
58.987	0.466	0.0016	0.0003	0.338	0.451	0.0016	0.0003	0.328	0.491	0.0017	0.0004	0.357
75.844	0.550	0.0019	0.0004	0.399	0.556	0.0019	0.0004	0.404	0.530	0.0018	0.0004	0.385
	Conc: 6.25µg/ml											
	Trial 1				**Trial 2**				**Trial 3**			

	Absorbance at 540nm	Amt of Product (mmol)	Velocity (mmol/min)	Velocity (µmol/min)	Absorbance at 540nm	Amt of Product (mmol)	Velocity (mmol/min)	Velocity (µmol/min)	Absorbance at 540nm	Amt of Product (mmol)	Velocity (mmol/min)	Velocity (µmol/min)
8.4259	0.248	0.0009	0.0002	0.181	0.233	0.0008	0.0002	0.170	0.232	0.0008	0.0002	0.169
25.275	0.281	0.0010	0.0002	0.204	0.346	0.0012	0.0003	0.252	0.235	0.0008	0.0002	0.171
42.135	0.494	0.0017	0.0004	0.359	0.404	0.0014	0.0003	0.294	0.498	0.0017	0.0004	0.362
58.987	0.557	0.0019	0.0004	0.404	0.578	0.0020	0.0004	0.420	0.567	0.0020	0.0004	0.412
75.844	0.691	0.0024	0.0005	0.501	0.692	0.0024	0.0005	0.502	0.695	0.0024	0.0005	0.504

Table 30: Velocity calculations for Acarbose

Conc of substrate(mM)	Conc: 50µg/ml											
	Trial 1				Trial 2				Trial 3			
	Absorbance at 540nm	Amt of Product (mmol)	Velocity (mmol/min)	Velocity (µmol/min)	Absorbance at 540nm	Amt of Product (mmol)	Velocity (mmol/min)	Velocity (µmol/min)	Absorbance at 540nm	Amt of Product (mmol)	Velocity (mmol/min)	Velocity (µmol/min)
8.4259	0.001	0.00001	0.00000	0.002	0.000	0.00000	0.00000	0.001	0.001	0.00001	0.00000	0.002
25.275	0.003	0.00001	0.00000	0.003	0.005	0.00002	0.00000	0.004	0.003	0.00001	0.00000	0.003
42.135	0.006	0.00002	0.00001	0.005	0.006	0.00002	0.00001	0.005	0.008	0.00003	0.00001	0.007
58.987	0.009	0.00004	0.00001	0.007	0.008	0.00003	0.00001	0.007	0.012	0.00005	0.00001	0.010
75.844	0.012	0.00005	0.00001	0.010	0.014	0.00005	0.00001	0.011	0.013	0.00005	0.00001	0.010

	Conc: 25µg/ml											
	Trial 1				Trial 2				Trial 3			
	Absorbance at 540nm	Amt of Product (mmol)	Velocity (mmol/min)	Velocity (µmol/min)	Absorbance at 540nm	Amt of Product (mmol)	Velocity (mmol/min)	Velocity (µmol/min)	Absorbance at 540nm	Amt of Product (mmol)	Velocity (mmol/min)	Velocity (µmol/min)
8.4259	0.002	0.00001	0.00000	0.002	0.002	0.00001	0.00000	0.002	0.002	0.00001	0.00000	0.002
25.275	0.006	0.00002	0.00001	0.005	0.007	0.00003	0.00001	0.006	0.006	0.00002	0.00001	0.005
42.135	0.008	0.00003	0.00001	0.007	0.009	0.00004	0.00001	0.007	0.011	0.00004	0.00001	0.009
58.987	0.010	0.00004	0.00001	0.008	0.010	0.00004	0.00001	0.008	0.013	0.00005	0.00001	0.010
75.844	0.011	0.00004	0.00001	0.009	0.012	0.00005	0.00001	0.010	0.015	0.00006	0.00001	0.012
	Conc: 12.5µg/ml											
	Trial 1				Trial 2				Trial 3			
	Absorbance at 540nm	Amt of Product (mmol)	Velocity (mmol/min)	Velocity (µmol/min)	Absorbance at 540nm	Amt of Product (mmol)	Velocity (mmol/min)	Velocity (µmol/min)	Absorbance at 540nm	Amt of Product (mmol)	Velocity (mmol/min)	Velocity (µmol/min)
8.4259	0.003	0.00001	0.00000	0.003	0.005	0.00002	0.00000	0.004	0.005	0.00002	0.00000	0.004
25.275	0.011	0.00004	0.00001	0.009	0.015	0.00006	0.00001	0.012	0.011	0.00004	0.00001	0.009
42.135	0.026	0.00009	0.00002	0.020	0.023	0.00008	0.00002	0.018	0.027	0.00010	0.00002	0.020
58.987	0.039	0.00014	0.00003	0.029	0.036	0.00013	0.00003	0.027	0.036	0.00013	0.00003	0.027
75.844	0.049	0.00017	0.00004	0.036	0.051	0.00018	0.00004	0.038	0.049	0.00017	0.00004	0.036
	Conc: 6.25µg/ml											
	Trial 1				Trial 2				Trial 3			
	Absorbance at 540nm	Amt of Product (mmol)	Velocity (mmol/min)	Velocity (µmol/min)	Absorbance at 540nm	Amt of Product (mmol)	Velocity (mmol/min)	Velocity (µmol/min)	Absorbance at 540nm	Amt of Product (mmol)	Velocity (mmol/min)	Velocity (µmol/min)
8.4259	0.009	0.00004	0.00001	0.007	0.010	0.00004	0.00001	0.008	0.009	0.00004	0.00001	0.007
25.275	0.020	0.00007	0.00002	0.015	0.024	0.00009	0.00002	0.018	0.020	0.00007	0.00002	0.015
42.135	0.035	0.00012	0.00003	0.026	0.038	0.00014	0.00003	0.028	0.039	0.00014	0.00003	0.029
58.987	0.050	0.00018	0.00004	0.037	0.066	0.00023	0.00005	0.049	0.066	0.00023	0.00005	0.049
75.844	0.108	0.00038	0.00008	0.079	0.082	0.00029	0.00006	0.060	0.113	0.00039	0.00008	0.083

Table 31: Velocity calculations for enzyme without inhibitor

Conc of substrate(mM)	No inhibitor											
	Trial 1				Trial 2				Trial 3			
	Absorbance at 540nm	Amt of Product (mmol)	Velocity (mmol/min)	Velocity (µmol/min)	Absorbance at 540nm	Amt of Product (mmol)	Velocity (mmol/min)	Velocity (µmol/min)	Absorbance at 540nm	Amt of Product (mmol)	Velocity (mmol/min)	Velocity (µmol/min)
8.4259	0.173	0.0006	0.0001	0.126	0.186	0.0006	0.0001	0.136	0.179	0.0006	0.0001	0.131
25.275	0.499	0.0017	0.0004	0.362	0.495	0.0017	0.0004	0.359	0.452	0.0016	0.0003	0.328
42.135	0.691	0.0024	0.0005	0.501	0.666	0.0023	0.0005	0.483	0.696	0.0024	0.0005	0.505
58.987	0.925	0.0032	0.0007	0.671	0.807	0.0028	0.0006	0.585	0.840	0.0029	0.0006	0.609
75.844	1.081	0.0037	0.0008	0.784	1.015	0.0035	0.0007	0.736	1.000	0.0035	0.0007	0.725

Chapter 5. Evaluation of anti-diabetic activity of lead compound, 4FI in *in vivo* mouse model

5.1 Introduction

Diabetes is becoming increasingly prevalent across the globe and there is an urgent need to discover new therapies to treat it. In order to understand the pathogenesis, the genetic and environmental risk factors for T2D, appropriate animal models are indispensable. Although genetic predisposition is a determinant factor in development of type 2 diabetes, age, obesity and cardiovascular diseases also play an important role in disease development. Thus, there is a very complex interaction between the genetic factors and environmental factors and this is poorly understood in humans. For obvious reasons, research of diabetes in humans is limited by ethical considerations. Therefore, in order to better understand the etiology of the disease and the metabolic pathways involved in type 2 diabetes, and to investigate new treatments, animal models are used in research. Use of these models makes it possible for experimentation which is not possible on humans. Each different model can help investigate one of many genetic, endocrine, metabolic mechanisms in the development of T2D in humans.[91–93]

Diabetic animal models can be either spontaneously derived, induced by diet or nutrition, chemically induced, surgically induced or induced by means of genetic manipulation (transgenic/knock out models).[92] In models of T2D, the diabetes manifests due to either pancreatic beta cell destruction or insulin resistance being the predominant cause. Even though the beta cell arrangement within the pancreatic islet in mice is not similar to humans, they still remain the most used models as they display several pathophysiological conditions observed in humans with T2D.[93] Other rodent models used in the study of diabetes are rats (Zucker diabetic fatty rat, Goto-Katazaki rat), spiny mice (*A. cahirinus*) and Desert Gerbil (*P. obesus).* The development of diabetes in these animals can be due to mutations on leptin receptors, impaired β-cell proliferation, over-nutrition and muscle insulin resistance respectively. There are feline models (domestic cat), swine models and primate models used in diabetes research as well, although they are less common. Rodent models are the most commonly used because of their small size ensuring ease in handling, short breeding times, ease of availability, knowledge of the genome and the relative ease of physiological and

invasive tests makes them very economical animal models. The use of mouse models provides the opportunity to study the onset and development of diabetes as they show several characteristics similar to human T2D.[93] Several hallmark signs of human T2D like polyuria, polyphagia, polydipsia and lethargy can be observed in the mouse models.[92]

Diabetes mellitus is a progressive disorder; in effect, loss of insulin secreting capacity starts years before disease diagnosis and the relative risk for complications progressively increases over time. Testing of new therapies would take years to accomplish and as such human trials for such extended periods is not feasible. Therefore, appropriate animal models to study pathogenesis and evaluate therapeutics are essential. Although no single model is an accurate representation of human T2D, a suitable model can be chosen depending on the metabolic or other disease pathway targeted.[93] The following section gives a brief introduction on the types of mouse models that are used in the study of diabetes.

5.1.1 Mouse models

5.1.1.1 Spontaneous diabetic models

In this model, diabetes develops spontaneously because of genetic factors and it resembles human T2D. This model involves selecting for hyperglycemic mice after generations of inbreeding in the laboratory.[91] Variability is small and therefore a small sample size is enough. However, since it is highly inbred, diabetes develops due to genetic factors rather than other factors. Also, these are quite expensive and have limited availability. Examples of this model are ob/ob mouse, db/db mouse, Zucker fatty rat. Diabetes is inherited as a result of autosomal recessive mutation on chromosome 6 which encodes for the protein leptin. This mutation leads to diminished binding of insulin to receptors. Leptin is involved in signaling satiety to the brain. Therefore, mutation of the gene alters the feeding pattern of mice and makes them obese due to a lack of the satiety factor. The db/db mouse on the other hand lacks insulin receptors due to an autosomal recessive mutation on chromosome 4. As a result, there is oversecretion of insulin with the mice displaying hypoinsulinemia, hyperglycemia by three to four months of age.[92]

5.1.1.2 Diet/nutrition induced diabetic models

In this model, diabetes develops due to over-nutrition similar to that observed in humans. The rodents need to be fed with fatty diet for a long period before they develop diabetes. This is not a suitable model to study drugs that affect circulating glucose levels since this model does not display overt hyperglycemia. C57/BL 6J mouse, sand rat and spiny mouse are the most widely used animals for this model. T2D model using C57/BL J6 can be obtained by simply feeding the mice on high fat diet to the originally non obese non diabetic mice.[92] These mice exhibit marked hyperglycemia and the model represents development of diabetes as a combination of both genetic and environmental risk factors.

5.1.1.3 Surgically induced diabetic models

Here, diabetes is surgically induced by the complete or partial surgical removal of the pancreas. This avoids the cytotoxic effects produced by chemical diabetogens. This procedure can be technically challenging and may cause various other complications. The mortality rate is quite high for this model.[91,92]

5.1.1.4 Transgenic or knockout diabetic models

Genetic manipulation can produce mice in which a certain gene has been knocked out or mutated. This can help study the role of a particular gene or gene products and the mechanisms involved in diabetes. In case of gene targeting, a single gene is disrupted in the embryonic stem cells producing knockout mice whereas in transgenic animals, a modified gene is incorporated into the zygote.[91] Transgenic animals apart from giving information on gene regulation and pathogenesis, can also help in aiding discovery of new targets for the treatment of diabetes. However, it is an expensive procedure that requires sophisticated technical skills to perform and constant screening.

5.1.1.5 Chemically induced diabetic models

Treatment with cytotoxic agents like Streptozotocin (STZ) and Alloxan causes selective loss of pancreatic beta cells and gives rise to chemically induced diabetes, type 1. However, these models are used in the study of anti-hyperglycemic agents even in case of type 2 diabetes where the object of study is to measure hyperglycemia only. Relative mortality in

these animals is relatively low and they are cheaper and easy to maintain. This model helps elucidate the role of environmental factors that cause diabetes by means of pancreatic beta cell destruction. Alloxan was the first cytotoxic agent used to induce diabetes when it was discovered to cause pancreatic beta cell necrosis in rabbits.[92] Alloxan is a uric acid derivative which is unstable in water or at neutral pH but is stable at pH 3. It also has a relatively shorter half-life of less than one minute, therefore an intravenous route is preferred. Animals treated with Alloxan display signs of uncontrolled diabetes and have severe hyperglycemia, polyuria, polydipsia, polyphagia and other neurological, cardiological and retinal complications. Mortality as a result of Alloxan treatment is quite high and the reversal of hyperglycemia can occur in very early stages. As a result of the several disadvantages of Alloxan, STZ is now the most preferred chemical agent for induction of diabetes. STZ is a glucosamine derivative of nitrosurea, a broad-spectrum antibiotic derived from *Streptomyces achromogenes*. It is a strong alkylating agent and causes breaks in DNA strands along with impairing glucose transport and glucokinase function.[91] Its diabetogenic activity on dogs and rats was first reported in 1963 by Rakieten and collegaues.[92] STZ is preferred over Alloxan as its half-life is relatively longer (15 minutes) and the associated incidences of mortality are fewer. STZ treated models are preferred to test drug candidates that display antihyperglycemic, insulinomimetics or insolinotropic properties. They display hyperglycemia due to loss of insulin producing beta pancreatic cells rather than insulin resistance. Diabetes induced by this method is not very stable and can sometimes be reversed due to regeneration of beta cells. Therefore, it may not be very suitable for long term experiments. The main disadvantage of this model is that the variability is very high and hence the sample size needs to be bigger.[92]

For the present study, of the available PSEs, **4FI** was chosen to be tested in vivo as it displayed a higher selectivity towards α-glucosidase than α-amylase. As already discussed in the chapters preceding, this selectivity is desirable in order to reduce the GI side effects that accompany AGIs. The SAR studies indicate that PSE **4FI** being tetra substituted feruloyl PSE (with free aromatic 'OH' group) and having the diisopropylidene group combines all the desired attributes. Of the models described above, the STZ model was selected because it is relatively easy to induce diabetes and maintain the mice besides being cost-effective. It is routinely used in the initial testing of AGIs. As the drug being studied

is anti-hyperglycemic and is to control postprandial hyperglycemia, this model is well suited to the testing of the AGI, PSE **4FI**.

5.2 Methods

5.2.1 Formulation of capsules containing the drug, 4FI

Enteric coated capsules of Acarbose and the test drug, PSE **4FI** (Fig. 62) were prepared according to the method proposed by Wu and co-workers.[94] Hard gelatin capsules (purchased from Torpac Inc.) were filled with either Acarbose or 4FI at a dose of 3mg/capsule. The capsules were then immersed in HP55 solution (made in methylene chloride and acetone (4:1 v/v) (40mg/L)). The capsules were then air dried at room temperature. The procedure was repeated three times after which the capsules were kept in a desiccator for further use.

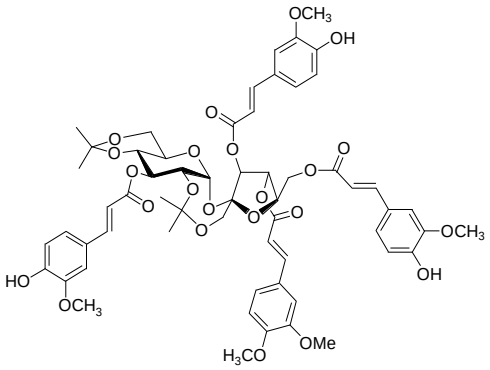

4FI (48)

Figure 62: Test drug **4FI**.

5.2.2 Testing of enteric coating

The HP55 coated capsules were dispersed in 5ml of simulated gastric fluid (SGF; pH 1.2) and simulated intestinal fluid (SIF; pH 6.8) in order to test the enteric coating. The recipes for the two fluids and the procedure was as detailed in the USP standard. SGF was prepared by dissolving 2g of sodium chloride and 3.2g of purified pepsin (from porcine stomach) in 7.0ml of HCl which was later diluted with DI H_2O to make up the volume to 1000ml. SIF was prepared by first dissolving 6.8g of monobasic potassium phosphate in 250ml of DI

H_2O to which 77ml of 0.2N NaOH and 500ml of DI H_2O was added. Next, 10g of pancreatin was added to the mix and the net volume made up to 1000ml with DI H_2O. The pH of the SIF was adjusted to 6.8 using either 0.2N NaOH or 0.2N HCl. The capsules were stirred in 5ml of SGF for half an hour with shaking at 100rpm at 37°C. Then, the fluid was extracted with ethyl acetate, the ethyl acetate layer was dried and was analyzed by ^{1}H NMR to test if there was any leakage of the drug PSE **4FI** from the capsule. Next, the capsule was rinsed with DI water and the capsule immersed in 5ml of SIF and shaken at the same conditions for two hours. Extraction and ^{1}H NMR of the dried extract was done to test for the presence of the drug this time.

5.2.3 Experimental animals

Male mice strain C57BL/6J were used for these trials. All animals were housed individually in a light-(12 h on/12 h off) and temperature- controlled room with pelleted food and water available ad libitum. They were split into three groups, PSE, Acarbose, and untreated control. After an adjustment period of 1 week, they were injected with STZ for induction of diabetes. STZ was administered at a dose of 200mg/kg, 150mg/kg and 50mg/kg respectively, in three independent trials. All procedures were approved by IACUC (protocol number 140905).

5.2.4 STZ injection

Diabetes was induced in mice by intraperitoneal STZ injection.[95] Briefly,0.1M fresh citrate buffer pH 4.5 was made by dissolving 1.05g citric acid monohydrate (MW 192g/mol) and 1.48g of sodium citrate tribasic dihydrate (MW 294.1g/mol) in DI water and was stored in ice cold conditions. The buffer was then filter sterilized. STZ was prepared by dissolving it in the freshly prepared citrate buffer (0.1M, pH 4.5) just prior to injection as STZ degrades rapidly once dissolved. For high dose treatment, the dosage used was 150-200mg/kg. High dose treatment involved a single injection which was followed by blood glucose and weight monitoring for 4 days. Mice treated with high dose STZ were fed 10% sucrose water instead of regular water for the first three days to prevent hypoglycemia. For low dose STZ, the mice were injected with 50mg/kg dose for 5 consecutive days.[96] Mice displaying polyuria,

weight loss and those having fasting blood glucose greater than 12mM (250mg/dL) were considered to be diabetic and were used for further experiments.

5.2.5 In vivo study for hypoglycemic effects of PSE

The procedure for monitoring post-prandial blood glucose levels following oral administration of starch was a modified version of that used by Park and colleagues.[97] The mice were allowed to acclimatize for 3 days. The STZ treated mice were divided into 3 groups, Acarbose group, PSE group and untreated control group. The mice were fasted for 8 hours but were given free access to water. Following this, the mice were given oral starch load followed by the drug in one of two ways:

a. Drug in capsule: The mice were administered the capsules containing Acarbose or PSE (10mg/kg body weight) by oral gavage. After 15 minutes, the blood glucose at 'time 0' was measured and the mice were fed orally soluble starch solution (2g/kg body weight). The blood glucose was measured at 15, 30, 60, 90 and 120-minute time intervals.

b. Drug co-administered with starch: The mice were given Acarbose or PSE **4FI** (10mg/kg body weight) mixed with the oral starch load instead of in capsules. The blood glucose was measured at 'time 0' before administration and following the co-administration of starch and the drug, blood glucose was measured at 15, 30, 60, 90 and 120-minute time intervals.

5.2.6 Statistical analysis

Statistical analysis was performed using Graphpad Prism software. The values represented in the graphs are mean ± standard error. The data set was evaluated by two-way analysis of variance followed by Tukey's post hoc test with the statistical significance set at $p<0.05$.

5.3 Results and discussion

5.3.1 Formulation of capsules containing the drug, PSE 4FI

To test the ability of PSE **4FI** to mitigate the rise in systemic blood glucose levels, **4FI** was orally administered to mice either before or together with starch. However, through the oral route, **4FI** will be exposed to the acidic environment of the stomach. The PSE **4FI** is unstable in an acidic environment due to the presence of ester bonds. Ester groups are hydrolyzed in the presence of acids. The ester bonds in drugs are easily cleaved in the acidic environment of the stomach by hydrolytic enzymes.[98] To prevent this, usually, a prodrug formulation or an enteric coating is employed. To ensure the integrity of the PSE **4FI** in the stomach, HP55 was chosen as a suitable enteric coating to coat the hard gelatin capsules containing the PSE. The integrity of the HP55 coating was observed using optical microscopy. Under the microscope, the uncoated capsule was observed to be dense and opaque while the coating was seen as a thin layer surrounding it. All of the capsules were inspected to ensure the integrity of the coating before use. The following figure shows a section of the capsule where the two halves envelop each other (highlighted in Fig. 63), before and after the coating.

Figure 63: (A) Capsule before HP55 coating **(B)** Capsule after HP55 coating as observed under optical microscope.

5.3.2 Testing of enteric coating

After coating the **4FI** containing gelatin capsules with HP55, the integrity of the coating was tested in SGF followed by the dissolution in SIF. The HP55 coated capsules were shaken in SGF for 30 minutes at the end of which the capsules were observed to be intact

with no disintegration. HP55 is a pH sensitive coating which swells up in low, acidic pH but dissolves at a pH greater than 5.5. The SGF was nevertheless extracted with ethyl acetate and the dried extract was subjected to NMR and was found to contain no peaks pertaining to the drug 4FI. On shaking the capsules in the SIF, it was observed that after 15 minutes, the capsules slowly started to disintegrate and disintegrated fully by 25 minutes. The SIF was then extracted with ethyl acetate, the ethyl acetate extract dried and was assessed by NMR. The ^{1}H NMR analysis revealed the presence of the drug 4FI intact and without disintegration as evidenced by the same peaks in the aromatic region (Fig.64 (B)) when compared to the reference (Fig.64 (A)). However, there are additional peaks seen which are due to the other components in the SIF extracted into the ethyl acetate layer as well. It was thus established that the enteric coating protects the drug at acidic pH and releases the drug in its original form in basic conditions of the intestine which is the site of action for the drug. The ^{1}H NMR spectra compared to the reference is given below.

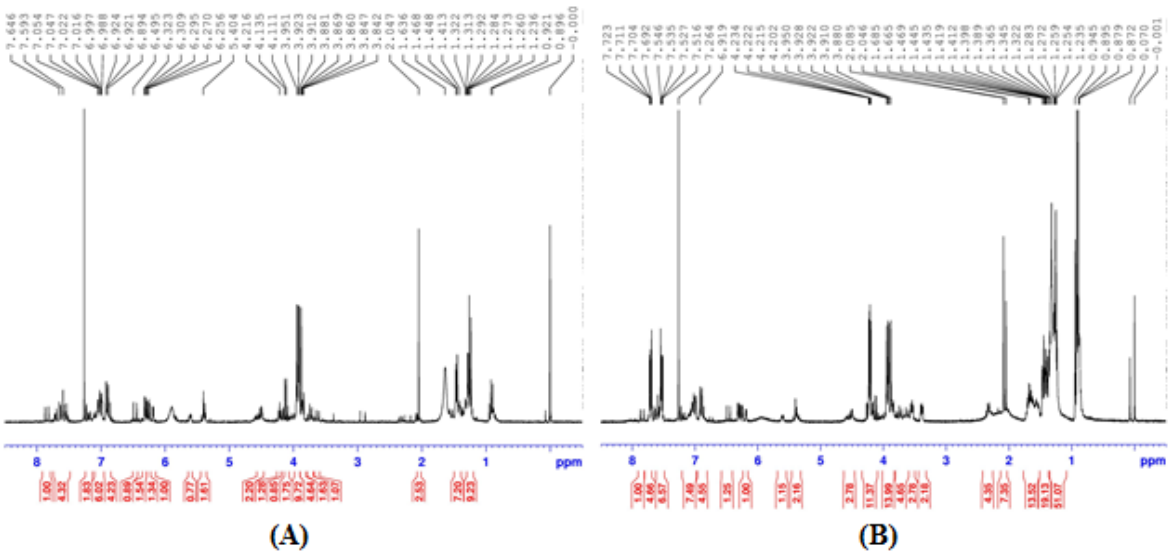

Figure 64: ^{1}H NMR for 4FI (A) pure drug (B) after stirring for 2.5 hrs in SIF.

5.3.3 In vivo study for hypoglycemic effects of PSE, 4FI

5.3.3.1 Trial 1: Diabetes induced with high dose STZ (200mg/kg body weight).

This trial was performed with a small sample size of 15 mice. After injection of STZ, mice were monitored for a week and blood glucose measurements were made every alternate

day. The blood glucose after an 8-hour fast is shown in table 33. It was noted that many of the mice showed signs of morbid diabetes over time and had a very high blood glucose level, greater than 33mM. By day 8, out of the 15 mice treated with STZ only 9 survived. Also, during monitoring, it was observed that the blood glucose levels were very erratic. This coupled with that fact that the mortality rate for high dose STZ treated mice was very high (loss of 50% mice within 3 weeks of STZ treatment) led to the conclusion that this model was not suited for further experimentation.

Table 33: Blood glucose (mM) on Day 4 after STZ injection

Animal #	Cage 1	Cage 2	Cage 3
1	32.2	25.4	High*
2	6.3	19.0	25.6
3	High*	28.1	High*
4	9.8	33.0	24.4
5	27.0	26.9	25.9

***High= outside the measuring range of the glucometer

5.3.3.2 Trial 2: Diabetes induced with high dose STZ (150mg/kg body weight)

A slightly lower dose of STZ (150mg/kg) was used. Once again, 15 mice were treated with STZ at a dose of 150mg/kg body weight. On day 5, out of the 15 mice treated with STZ, 13 survived. The remaining mice were regrouped into three cages of 4 animals each. The three cages were untreated, treated with Acarbose and with PSE respectively. The gastric emptying time in fasted mice is reported to be 2±1 minutes ($T_{1/2}$).[99] The disintegration testing of the enteric coating of the capsule took between 15-25 minutes when examined in vitro in simulated intestinal fluid. Hence, the drug was administered in the capsule fifteen minutes prior to administration of starch orally. Figure 65 shows the change in the blood glucose level after the oral starch load in all three treatment groups (table 34 section 5.5).

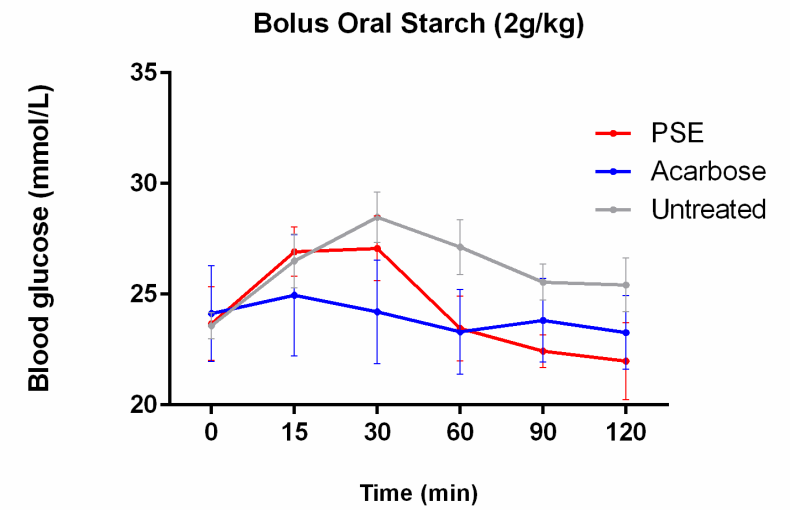

Figure 65: Blood glucose response after bolus oral starch (2g/kg). Acarbose and PSE were administered in enteric coated capsule (n=4).

From figure 65, it can be observed that the response to the PSE as well as Acarbose was erratic and the standard error was very high. Statistical analysis showed that treatment with Acarbose and PSE was not significantly different from the control group. Hence, the experiment was repeated once again with three animals in each group, the results for which are summarized in figure 66 given below (table 35 section 5.5):

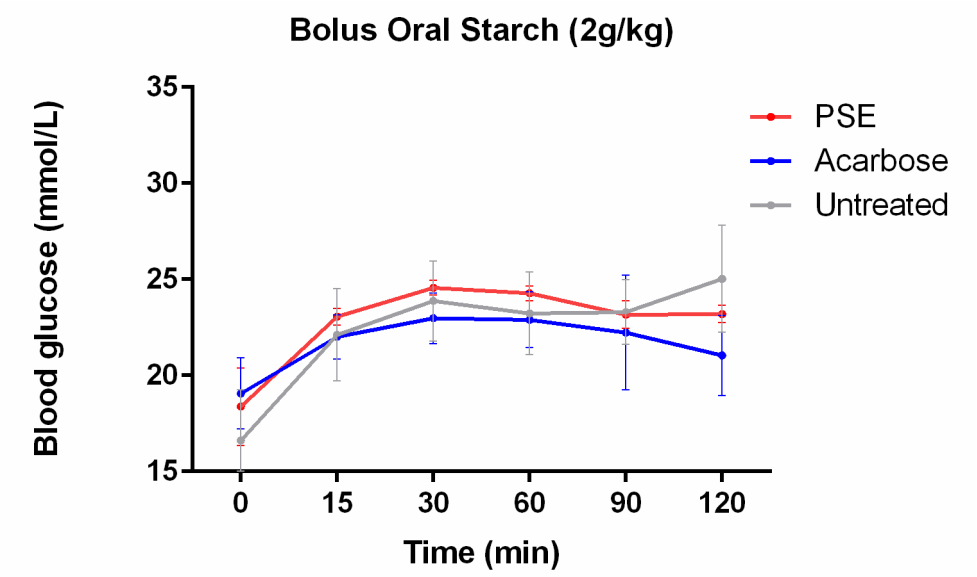

Figure 66: Blood glucose response after bolus oral starch (2g/kg). Acarbose and PSE were administered in enteric coated capsule (n=3).

Once again, it was seen that (figure 66) the blood glucose response after administration of both Acarbose and PSE was similar to that of the untreated group and was not significant. Since even the positive control, Acarbose failed to elicit a significant response on blood glucose control, it was hypothesized that the drug release from the capsules was not efficient. A study conducted by McConnell and co-workers reports the mean intestinal pH in mice to be much lower than that in man with values of pH <5.2 in the former and >7.0 in the latter.[100] This suggests that the enteric coated capsule may not be effective in a mouse model since it requires a pH >5.5 for disintegration in order to release the drugs. Another trial was conducted, this time by co-administering the drugs, both Acarbose and PSE along with the starch load. The results for the same are summarized in figure 67 below (table 36, section 5.5).

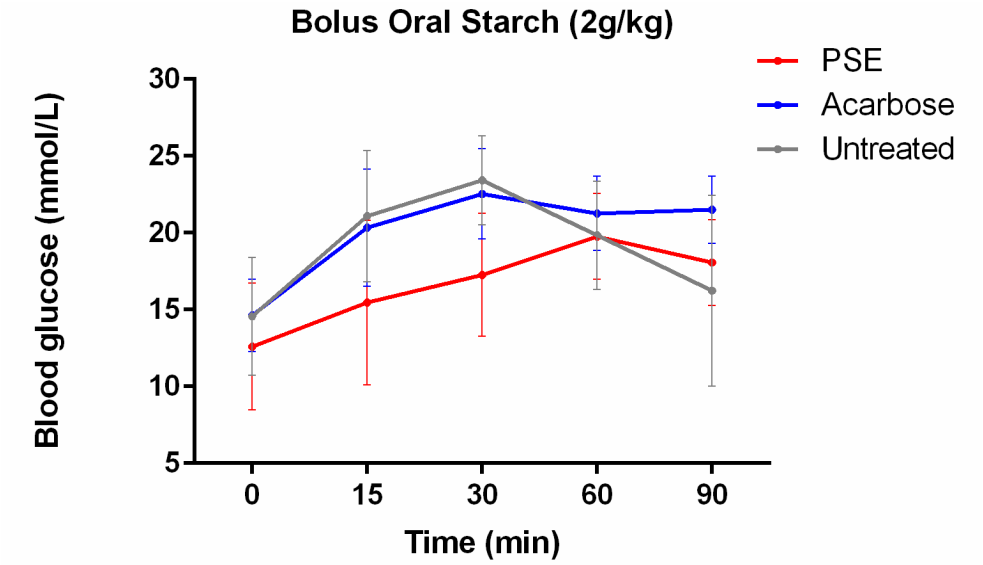

Figure 67: Blood glucose response after bolus oral starch (2g/kg). Acarbose and PSE were co-administered with starch (n=3).

From figure 67, once again it was seen that neither Acarbose nor PSE were able to show any significant difference in controlling the rise in post-prandial glucose. However, the blood glucose levels in the untreated group remained the highest of the three groups. Once again, the positive control, Acarbose did not show significant results. An interesting thing that was noted was that the absence of enteric coated capsule made no difference to the response indicating that enteric coating was not necessary. This can be attributed to the fact

that the pH in the stomach of mice is about 3.0 in the fed state and 4.0 in the fasted state, significantly higher than human stomach pH which is around 1.7 in the fasted state.[100] Therefore, in comparison, in mice, the stomach conditions are less acidic which may be why the drugs do not fare worse without the enteric coating. As the enteric coating was tested on simulated gastric and intestinal fluids for humans (which is the standard protocol), it may be an inaccurate model when extrapolated to mice. It was hypothesized that the sample size selected was too small and the starting blood glucose of each animal was too varied to draw effective conclusions. Therefore, the next trial was done with a bigger sample size.

5.3.3.3 Trial 3: Diabetes induced with low dose STZ (50mg/kg body weight)

A low dose STZ dose of 50mg/kg body weight was chosen to ensure a high survival rate. Low dose STZ treated mice show mild diabetes. The experiments above were repeated this time with a much bigger sample size of n=14. Once again, the drugs were co-administered with starch and without the use of capsules and blood glucose monitored post administration of starch. The change in the blood glucose levels after co-administration of starch with Acarbose and PSE along with the untreated group are detailed in the supplementary data (tables 37-39, section 5.5). The tables are summarized in a graph below (Fig. 68).

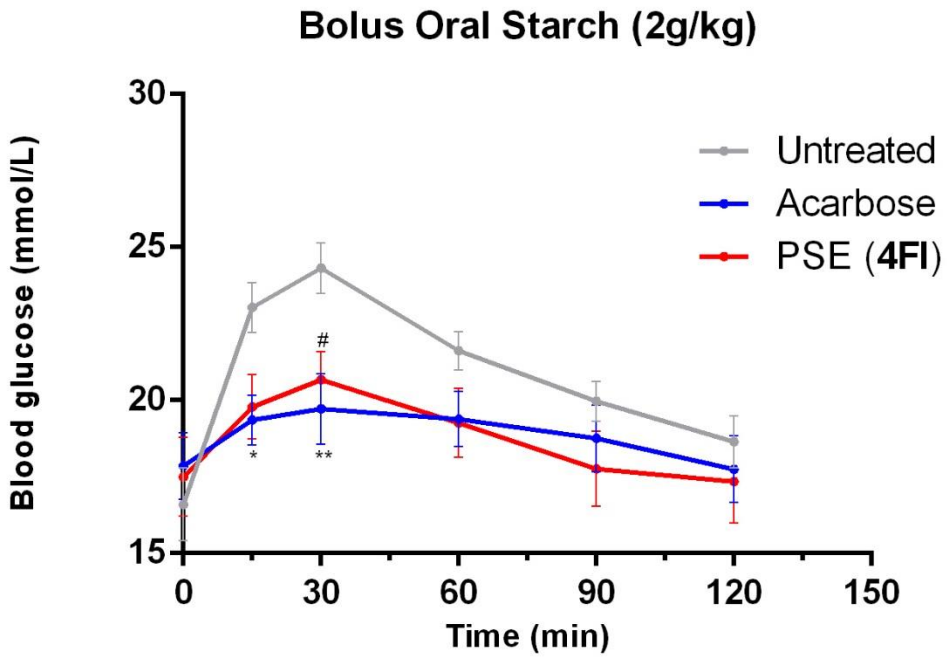

Figure 68: Blood glucose response after bolus oral starch (2g/kg). Acarbose and PSE were co-administered with starch (n=14). (*: statistical significance for comparison of untreated with Acarbose group; #: statistical significance for comparison of untreated with PSE group).

Figure 68 represents the collective data from Tables 37-39 (section 5.5). It can be seen that both Acarbose and PSE help control the rise in blood glucose levels following starch administration. In all three cases, untreated, Acarbose and PSE, blood glucose levels rise from t=0 min (point of starch administration) and peak at t=30 minutes following which the blood glucose levels start to decline slowly. Statistical tests on the data show that Acarbose treated group shows significant decrease in blood glucose levels as compared to the untreated group at both 15 and 30 minutes after starch load. However, PSE shows a statistically significant decrease at only 30 mins. From the results thus far, it can be concluded that PSE is just as effective as Acarbose at controlling post-prandial blood glucose at 30 mins after administration of complex carbohydrate (starch) orally. The general

trend as seen from Figure 68, points to the conclusion that the new PSE drug, 4FI does work as an AGI, though its efficacy needs to be tested further.

5.4 Summary

In chapters 2, 3 and 4, the SAR studies for the PSEs was developed. The in vitro, in silico and enzyme kinetic studies together gave a picture of the relationship of the functional groups and structure to the biological activity, the site of ligand (PSE) binding to the enzymes, the interactions holding it in place and finally the type of inhibition. In this chapter, one lead drug, **4FI** was selected in order to test its ability to mitigate PPHG *in vivo*. Formulation using enteric coated hard gelatin capsules was found to be ineffective for drug release. Administration of the drug, as is, without formulation along with starch was seen to reduce the increase in blood glucose levels following oral starch tolerance test in low dose STZ treated mice. **4FI** was seen to be just as effective as Acarbose and was seen to reduce the surge in blood glucose levels after a starch load when compared to the untreated diabetic group. However, further evaluation is necessary.

Further work to improve PSE as an oral drug for diabetes will firstly address the solubility of the PSE. One cannot be sure that all of the drug that is dosed reaches the target site and is available as it was observed that the drug is not water soluble. Another concern is the integrity of the drug in the stomach as well as the intestinal fluid because the pH conditions in mice is quite different than in humans. This study combined with the SAR studies thus far, will lead to the development of a better PSE drug that is more soluble and has the right type and number of substituents that will enhance the activity while maintaining the desired selectivity. The future scope of this study is to develop new PSE(s) based on this and progress to testing in spontaneous diabetic models as well testing of other metabolic parameters concerning diabetes.

5.5 Supplementary data

Table 34: Blood glucose measurements (mM) after starch load (2g/kg) on day 5 after STZ administration (150mg/kg). PSE and Acarbose administered in capsule.

Untreated						
Animal #	**0'**	**15'**	**30'**	**60'**	**90'**	**120'**
1	25	29.3	30.5	30.8	26.8	26.6
2	23.9	23.5	26.5	25.8	26.3	23.5
3	23.2	26	26.5	25.4	25.9	28.3
4	22.2	27.2	30.4	26.5	23.2	23.3
Acarbose treated						
Animal #	**0'**	**15'**	**30'**	**60'**	**90'**	**120'**
1	27.5	29.9	26.5	25.7	24.2	26.1
2	18.0	17.1	17.2	17.6	18.4	18.5
3	24.1	26.0	26.2	24.9	25.8	24.0
4	26.9	26.8	26.9	25.0	26.9	24.5
PSE treated						
Animal #	**0'**	**15'**	**30'**	**60'**	**90'**	**120'**
1	23.2	26.4	26.7	23.2	23.4	23.6
2	27.5	29.0	29.4	26.2	23.6	22.1
3	24.5	28.3	29.1	24.9	22.3	25.1
4	19.5	24.0	23.1	19.5	20.4	17.1

Table 35: Blood glucose measurements(mM) after starch load (2g/kg) on day 10 after STZ administration (150mg/kg). PSE and Acarbose administered in capsule.

Untreated						
Animal #	**0'**	**15'**	**30'**	**60'**	**90'**	**120'**
1	18.0	24.5	22.0	21.6	21.0	22.1
2	20.3	24.5	28.0	27.5	26.6	30.6
3	11.5	17.3	21.6	20.6	22.3	22.4
Acarbose treated						
Animal #	**0'**	**15'**	**30'**	**60'**	**90'**	**120'**
1	22.7	24.3	25.1	25.8	26.5	20.9
2	17.9	20.8	20.6	21.3	16.5	17.5
3	16.6	20.9	23.2	21.6	23.7	24.7
PSE treated						
Animal #	**0'**	**15'**	**30'**	**60'**	**90'**	**120'**
1	17.1	23.1	23.9	24.9	24.6	23.2
2	15.7	22.3	24.6	23.6	22.6	24.0
3	22.3	23.8	25.2	24.3	22.3	22.4

Table 36: Blood glucose measurements after starch load (2g/kg). STZ dose-150mg/kg. Starch was co-administered with drug without capsules.

Blood glucose (mmol/L)	**Untreated**				
#	**0'**	**15'**	**30'**	**60'**	**90'**
1	20.9	27.7	27.9	20.6	13.5
2	7.7	13.1	18.0	13.4	7.1
3	15.1	22.5	24.4	25.5	28.1
Acarbose treated					
#	**0'**	**15'**	**30'**	**60'**	**90'**
1	14.0	20.4	21.4	19.8	21.1
2	19.0	26.9	28.1	26.0	25.5
3	10.9	13.7	18.1	18.0	17.9
PSE treated					
#	**0'**	**15'**	**30'**	**60'**	**90'**
1	7.5	8.5	11.7	15.1	14.7
2	9.5	11.9	15.1	19.4	15.9
3	20.8	26.0	25.0	24.8	23.6

Table 37: Blood glucose measurements after starch load in untreated control group, n=14, STZ dose = 50mg/kg.

Untreated														
Time (Min)	**Animal number**													
	#1	**#2**	**#3**	**#4**	**#5**	**#6**	**#7**	**#8**	**#9**	**#10**	**#11**	**#12**	**#13**	**#14**
0	11.3	13.2	10.9	16.5	15.3	14.3	20.8	20.8	12.1	26.1	19.9	20.9	15.1	15.1
15	20.7	20.3	21.1	21.0	25.2	20.6	27.4	26.5	25.4	25.0	22.8	27.7	19.9	18.8
30	22.1	20.8	21.0	22.5	25.8	24.1	29.9	29.2	23.1	27.3	21.3	27.9	22.6	22.8
60	18.8	19.8	23.8	19.0	22.4	22.1	25.6	20.5	19.9	24.6	19.1	20.6	25.0	21.4
90	17.2	15.9	20.6	19.9	23.7	19.1	21.5	20.7	17.9	23.5	18.9	15.0	18.7	22.0
120	15.3	16.4	16.0	19.6	19.6	18.8	25.2	21.0	17.4	21.6	16.6	13.5	17.3	22.7

Table 38: Blood glucose measurements after starch load in Acarbose group, n = 14, STZ dose = 50mg/kg. Starch was co-administered with Acarbose without capsules.

Acarbose														
Time (Min)	**Animal number**													
	#1	**#2**	**#3**	**#4**	**#5**	**#6**	**#7**	**#8**	**#9**	**#10**	**#11**	**#12**	**#13**	**#14**
0	14.0	21.3	18.1	14.0	17.7	14.3	16.1	22.6	15.4	14.2	25.4	21.8	22.1	12.9
15	16.7	24.4	19.4	14.0	20.8	17.8	18.9	18.9	16.4	18.9	21.5	20.6	25.2	17.4
30	14.0	25.7	19.5	14.5	23.5	18.1	18.6	19.0	16.3	17.4	23.9	24.5	26.3	14.7
60	18.6	24.4	20.6	15.4	23.1	18.3	18.0	19.0	15.3	18.6	22.6	22.2	22.3	13.0
90	20.1	24.4	19.9	15.4	23.6	17.1	17.5	19.5	13.5	14.8	24.4	19.8	21.2	11.3
120	17.0	23.8	19.1	13.8	21.9	14.7	16.4	19.1	12.0	14.2	24.7	17.4	21.5	12.9

Table 39: Blood glucose measurements after starch load in PSE (**4FI**) group, n = 14, STZ dose = 50mg/kg. Starch was co-administered with **4FI** without capsules.

Acarbose														
Time (Min)	**Animal number**													
	#1	**#2**	**#3**	**#4**	**#5**	**#6**	**#7**	**#8**	**#9**	**#10**	**#11**	**#12**	**#13**	**#14**
0	17.0	21.8	18.9	15.0	18.1	15.2	14.8	11.3	25.2	24.5	15.8	12.4	17.0	21.8
15	23.4	22.9	22.8	16.4	21.8	17.3	18.3	12.4	23.5	23.1	18.8	16.7	23.4	22.9
30	20.0	25.3	24.6	18.0	21.1	20.5	20.5	14.2	23.0	23.2	20.6	17.0	20.0	25.3
60	20.2	24.3	20.5	15.6	22.8	17.1	19.2	11.7	22.8	23.8	18.3	14.8	20.2	24.3
90	18.6	18.4	25.0	17.0	20.8	15.2	17.4	10.5	20.1	23.3	13.0	13.8	18.6	18.4
120	18.4	21.0	23.8	16.6	20.6	15.7	17.5	7.5	17.3	23.4	13.7	12.6	18.4	21.0

Chapter 6. SAR studies: Synthesis and modification of PSEs

Thus far, we have seen the SAR of PSEs develop in relation to its anti-diabetic activity. The in vitro inhibition of the enzymes α-glucosidase and α-amylase were dealt with in chapter 2 followed by in silico binding studies in order to correlate the effect of the structure on the binding modes. Following this, the type of inhibition was established and then the in vivo effect of lead drug PSE **4FI** was studied in STZ diabetic model.

One of the objectives of this project is to establish the SAR of the PSEs by correlating it to its anti-diabetic activity in order to synthesize superior AGI drugs. This chapter focuses on furthering the SAR study by synthesizing new PSEs as well as modification of some PSEs already available from the compound library (chapter 2). Synthesis and modification of PSEs was done in order to study the effects of certain key structural features, the alkenyl C=C in the phenylpropanoid substituent, aromaticity and finally the effect of the methoxy and the 'OH' groups on the aromatic ring. Following the synthesis, the in vitro enzyme inhibition of the PSEs was once again assessed to establish the SAR and conclusions drawn to guide the synthesis of the ideal anti-diabetic PSE drug candidate in the future.

6.1 Hydrogenation of the alkenyl C=C of the phenylpropanoid substituent in PSEs

Hydrogenation reaction using ammonium formate was employed to hydrogenate the alkenyl C=C bonds in the phenylpropanoid substituents of the PSEs. Reduction using ammonium formate and Pd/C catalyst as described by Paryzek and colleagues was used with some modifications.[101] Four PSEs were chosen to study the effect of saturation, **4CiI, 2CiIP, 2CoIP** and **3FI**. These PSEs were chosen as they represent different type and number of phenylpropanoid substituents and therefore would represent a comprehensive test sample.

6.1.1 Hydrogenation of 4CiI (**54**)

4CiI (**54**) was hydrogenated with ammonium formate in MeOH and EtOAc mixture (10:1) (scheme 2). On completion, the reaction mixture was subjected to purification by column chromatography to give an off-white solid with mp 39-41°C. FT-IR analysis of the compound showed the absence of the characteristic peaks for alkenyl C=C stretch in the region between 1620-1680cm^{-1} confirming the reduction of the alkenyl C=C bond in the

phenylpropanoid chain. HR-ESI-MS of the compound showed a molecular ion *m/z* value of 951.4147 corresponding to $[M+H]^+$ and supporting the molecular formula $C_{54}H_{63}O_{15}$ (*m/z* calcd for $C_{54}H_{63}O_{15}$ $[M+H]^+$: 951.4167). Comparison of ^1H NMR with the starting material showed the disappearance of the peaks corresponding to the trans-double bonds at δ 6.43, 6.45, 6.46, 6.63, 7.63-7.65, and 7.96.[32] Instead, there was a new signal at δ 2.61-2.84 and 2.90-3.11 for 16 protons corresponding to the now aliphatic chain of the phenylpropanoid moiety. The ^{13}C NMR showed four signals corresponding to the ester carbonyl at δ 171.67, 171.91, 172.25 and 172.40. On comparing the ^{13}C NMR with the reference for starting material **54**, it was observed that the carbon signals corresponding to the eight CH=CH carbons at δ 116-188 and δ 144-147 were found to be absent.[32] There were eight new carbon signals corresponding to CH_2-CH_2 carbons at δ 30-36. All of the above data confirmed the off-white solid to be the desired product **59**.

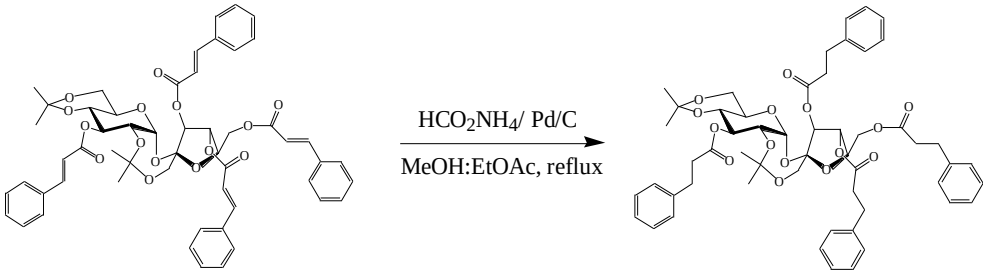

4CiI (54) **59** (85%)

Scheme 2: Hydrogenation of **4CiI (54)**

6.1.2 Hydrogenation of 2CiIP (55)

2CiIP (**55**) was hydrogenated with ammonium formate in MeOH and EtOAc mixture (10:1) (scheme 3). On completion, the reaction mix was subjected to purification by column chromatography to give an off-white solid with mp 35-38°C. FT-IR analysis of the compound showed the absence of the characteristic peaks for akenyl C=C stretch in the region between 1620-1680cm^{-1} confirming the reduction of the alkenyl C=C in the phenylpropanoid chain. HR-ESI-MS of the compound showed a molecular ion *m/z* value of 771.3200 corresponding to $[M+H]^+$ and supporting the molecular formula $C_{40}H_{51}O_{15}$ (*m/z* calcd for $C_{40}H_{51}O_{15}$ $[M+H]^+$: 771.3228). Comparison of ^1H NMR with the starting material showed the disappearance of the peaks corresponding to the trans-double bonds at δ 6.48,

6.54, 7.71 and 7.82.[32] Instead, there was a new signal at δ 2.51-2.83 integrating for 8 protons corresponding to the now aliphatic chain of the phenylpropanoid moiety. The ^{13}C NMR showed four signals corresponding to carbonyl carbons at δ 169.76, 169.93, 172.28 and 172.38. On comparing the ^{13}C NMR with the reference for starting material **55**, it was observed that the carbon signals corresponding to the four CH=CH carbons at δ 116-188 and δ 144-147 were found to be absent.[32] There were four new carbon signals corresponding to CH_2-CH_2 carbons at δ 29-36. All of the above data confirmed the off-white solid to be the desired product **60** which was obtained in 81% yield.

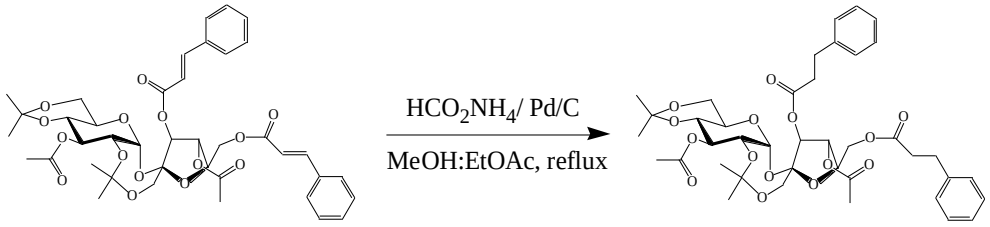

2CiIP (55) **60** (81%)

Scheme 3: Hydrogenation of **2CiIP (55)**

6.1.3 Hydrogenation of 2CoIP (49)

Hydrogenation of **2CoIP** (**49**) was done with ammonium formate in MeOH and EtOAc mixture (10:1) (scheme 4). On completion, the reaction mix was subjected to purification by column chromatography to give a white solid with mp 69-72°C. FT-IR analysis of the compound showed the absence of the characteristic peaks for akenyl C=C stretch in the region between 1620-1680cm^{-1} confirming the reduction of the alkenyl C=C in the phenylpropanoid chain. HR-ESI-MS of the compound showed a molecular ion *m/z* value of 803.3129 corresponding to $[M+H]^+$ and supporting the molecular formula $C_{40}H_{51}O_{17}$ (*m/z* calcd for $C_{40}H_{51}O_{17}$ $[M+H]^+$: 803.3126). Comparison of ^1H NMR with the starting material showed the disappearance of the peaks corresponding to the trans-double bonds at δ 6.43, 6.49, 7.73 and 7.79.[32] Instead, there was a new signal at δ 2.51-2.83 for 8 protons corresponding to the now aliphatic chain of the phenylpropanoid moiety. The ^{13}C NMR showed four signals corresponding to carbonyl carbons at δ 169.48, 169.99, 172.98 and 172.31. On comparing the ^{13}C NMR with the reference for starting material **49**, it was observed that the carbon signals corresponding to the four CH=CH carbons at δ 116-188

and δ 144-147 were found to be absent.[32] There were four new carbon signals corresponding to CH_2-CH_2 carbons at δ 29-31. All of the above data confirmed the white solid to be the desired product **61** which was obtained in 80% yield.

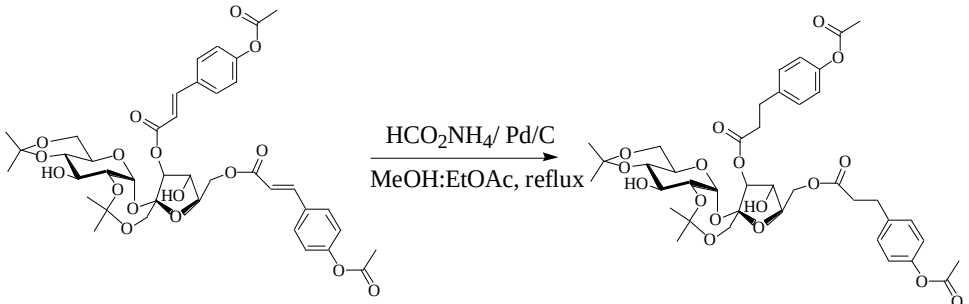

2CoIP (49) **61** (80%)

Scheme 4: Hydrogenation of **2CoIP (49)**

6.1.4 Hydrogenation of 3FI (47)

The tri feruloyl PSE **3FI** (**47**) was hydrogenated with ammonium formate in MeOH and EtOAc mixture (10:1) (scheme 5). On completion, the reaction mix was subjected to purification by column chromatography to give a white solid with mp 68-71°C. FT-IR analysis of the compound showed the absence of the characteristic peaks for alkenyl C=C stretch in the region between 1620-1680cm^{-1} confirming the reduction of the alkenyl C=C bond in the phenylpropanoid chain. HR-ESI-MS of the compound showed a molecular ion *m/z* value of 957.3729 corresponding to $[M+H]^+$ and supporting the molecular formula $C_{48}H_{61}O_{20}$ (*m/z* calcd for $C_{48}H_{61}O_{20}$ $[M+H]^+$: 957.3756). Comparison of ^1H NMR with the starting material showed the disappearance of the peaks corresponding to the trans-double bonds at δ 6.2-6.3, 7.5-7.7.[33] Instead, there was a new signal at δ 2.77-2.87 for 12 protons corresponding to the now aliphatic chain of the phenylpropanoid moiety. The ^{13}C NMR showed three signals corresponding to the ester carbon at δ 171-173. On comparing the ^{13}C NMR with the reference for starting material **47**, it was observed that there were six new carbon signals corresponding to CH_2-CH_2 carbons at δ 30-48.[33] All of the above data confirmed the white solid to be the desired product **62** which was obtained in 97% yield.

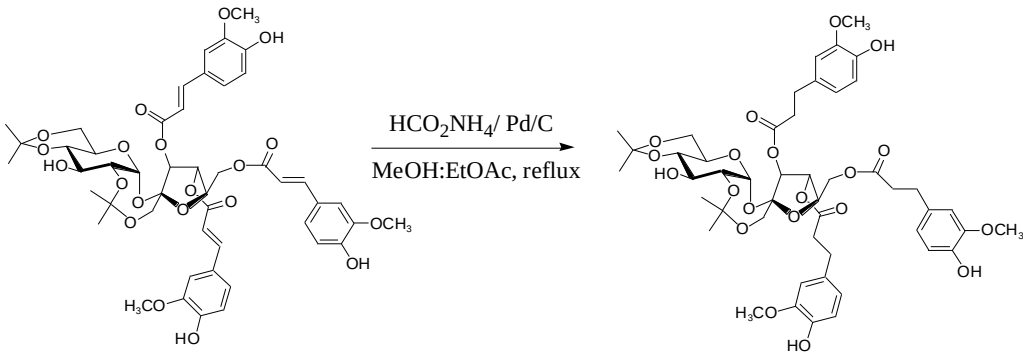

3FI (47) **62** (97%)

Scheme 5: Hydrogenation of **3FI (47)**

In conclusion, the alkenyl C=C bonds in all of the four PSEs were successfully reduced and the reaction yielded the products in excellent yields using the method described above.

6.2 Synthesis of 2,1′:4,6-Di-*O*-isopropylidene sucrose (Diacetonide)

Diacetonide **64** was synthesized using the same procedure as described by Panda and colleagues (scheme 6).[32] TLC analysis of the reaction mixture upon completion revealed the presence of two spots corresponding to 2,1′:4,6-Di-*O*-isopropylidene sucrose **64** and 4,6-Mono-*O*-isopropylidene sucrose **65**. Upon purification, compounds **64** and **65** were obtained in 49% and 14% yields respectively. ^{1}H NMR (refer appendix section 8.5) for **64** revealed the characteristic peak at δ 6.26 (refer appendix) corresponding to the anomeric proton which was in accordance with literature.[32]

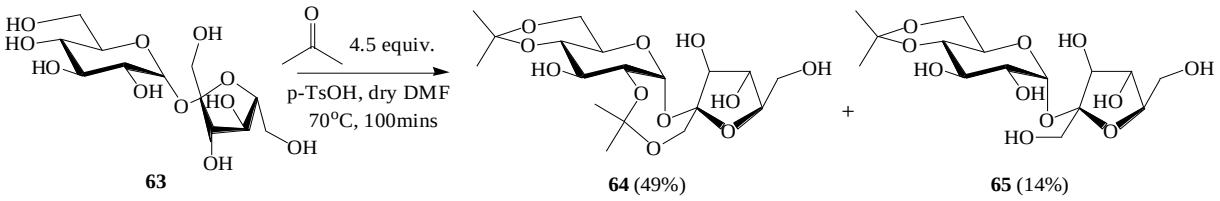

63 **64** (49%) + **65** (14%)

Scheme 6: Synthesis of 2,1′:4,6-Di-*O*-isopropylidene sucrose

6.3 Synthesis of 3,3′,4′,6′-Tetra-cyclohexanepropanoyl-2,1′:4,6-di-isopropylidene sucrose (**68**)

6.3.1 Synthesis of 3-cyclohexanepropionic acid (67)

Cinnamic acid was hydrogenated (H_2, Pd/C) using a modified procedure of that used by Anderson and coworkers according to scheme 7.[102] After 3 days of reaction, the reaction mix was filtered and evaporated under reduced pressure which upon purification by column chromatography yielded compound **67** in 68%yield. The ^{1}H NMR of **67** (refer appendix section 8.6) corresponded with literature for 3-cyclohexanepropionic acid[103] characterized by the absence of peaks in the aromatic region (δ = 6 to 8 ppm) and the shifting of the peaks in the region between 0.6-2.3ppm (refer appendix).

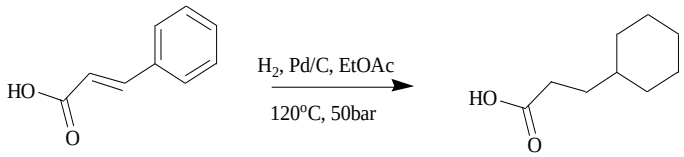

66 **67** (68%)

Scheme 7: Synthesis of 3-cyclohexanepropionic acid (**67**)

6.3.2 Synthesis of 3,3′,4′,6′-Tetra-cyclohexanepropanoyl-2,1′:4,6-di-isopropylidene sucrose (**68**)

Reaction of compound **67** with diacetonide **64** using the Steglich esterification method gave a white solid upon purification by column chromatography with mp 36-39°C (scheme 8). The high resolution ESI-MS showed a molecular ion *m/z* value of 975.6015 corresponding to $[M+H]^+$ thus supporting the molecular formula $C_{54}H_{87}O_{15}$ (*m/z* calcd. for $C_{54}H_{87}O_{15}$: 975.6045). FT-IR analysis of the white solid revealed sharp peaks at 1450, 2847 and 2930cm^{-1} corresponding to the absorption bands characteristic to cyclohexane rings. The ^{1}H NMR of the solid showed the presence of 72 protons in the region 0.78-2.38ppm which correspond to protons from the diisopropylidene rings and the four cyclohexanepropionoyl moieties (12+60 protons respectively). This indicated the presence of four cyclohexanepropionoyl substituents. A comparison of the ^{1}H NMR to that of 3-

cyclohexanepropionic acid (refer appendix section 8.6 and 8.7) confirmed the presence of four substituents as the proton numbers are clearly observed to be quadrupled. The proton signals from the sucrose moiety were present in the region 3.44-5.97 with a characteristic doublet from the anomeric proton at δ 5.97. The ^{13}C NMR showed signals corresponding to the ester carbon at δ 171-173. All of the above data confirmed the white solid to be compound **68** which was obtained in 20% yield.

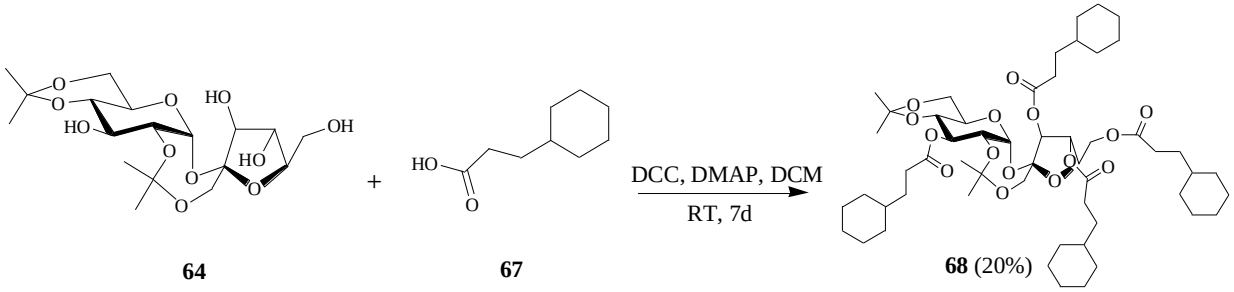

64 **67** **68** (20%)

Scheme 8: Synthesis of 3,3′,4′,6′-Tetra-cyclohexanepropanoyl-2,1′:4,6-di-isopropylidene sucrose (**68**)

6.4 Synthesis of sinapoyl PSEs

6.4.1 Synthesis of 4-acetoxysinapic acid (70)

4-acetoxy sinapic acid was synthesized by reacting sinapic acid with acetic anhydride in one of two methods, in pyridine or NaoH and H_2O (scheme 9 and 10). On completion of the reaction, a white solid precipitated out which was confirmed to be 4-acetoxysinapic acid **70** on comparison of the ^1H NMR (refer appendix section 8.8) that showed a peak at δ = 2.342ppm (s, 3H) corresponding to the -$COCH_3$ group on the phenyl ring with reported values in literature.[104]

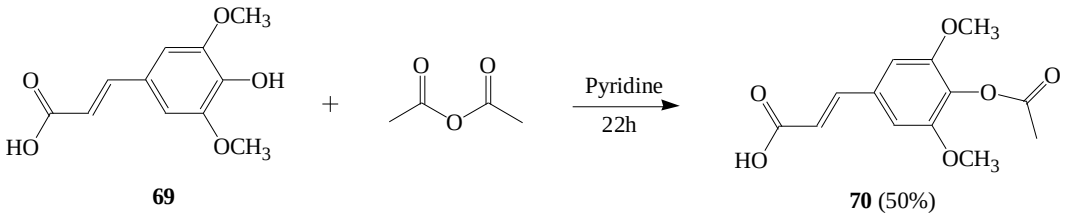

69 **70** (50%)

Scheme 9: Synthesis of 4-acetoxysinapic acid using pyridine (**70**)

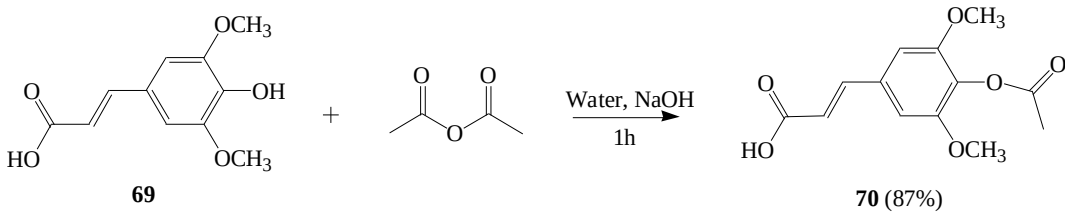

Scheme 10: Synthesis of 4-acetoxysinapic acid using NaOH and H_2O (**70**)

Of the two methods above, the latter utilizing water and NaOH was deemed more suitable for synthesis of compound **70** as it gave a much higher yield of 87% with a shorter reaction time as well as utilizing 'green' reactants as opposed to pyridine.

6.4.2 Synthesis of 3,3′,4′,6′-Tetra-*O*-acetylsinapoyl-2,1′:4,6-di-isopropylidene sucrose 72 (4SIP)

Steglich esterification method was also employed in the synthesis of **4SIP.** Diacetonide **64** was reacted with 4-acetoxysinapic acid **70** (scheme 11). TLC analysis showed the completion of reaction in 3 days. The reaction mixture upon purification by column chromatography gave a white solid with mp 162-165°C. ^{1}H NMR analysis revealed the presence of 16 protons (δ = 6.23-6.36 (m, 4H), 6.47-6.52 (m, 1H), 6.69 (s, 3H), 6.76-6.88 (m, 1H), 6.88 (s, 1H), 7.42-7.64 (m, 4H), 7.78-7.84 (m, 1H)) corresponding to four sinapoyl groups confirming a tetra substituted product. The presence of the acetoxy protection of the aromatic 'OH' was confirmed by the presence of a peak at δ 2.27 corresponding to 12 protons. A multiplet corresponding to 24 protons from the methoxy groups on the sinapoyl moiety was observed in the region 7.42-7.64ppm. High resolution ESI-MS that showed a molecular ion *m/z* value of 1415.4609 corresponding to $[M+H]^+$ thus supporting the molecular formula $C_{70}H_{79}O_{31}$ (*m/z* calcd. for $C_{70}H_{79}O_{31}$: 1415.4609). FT-IR analysis showed characteristic signal for trans-double bond at 1635 cm^{-1}, the acetyl carbonyl at 1767cm^{-1} and the ester carbonyl group at 1719cm^{-1} which were found to be similar to the values reported for **4FIP** (tetraferuloyl PSE-chapter 2).[33] The ^{13}C NMR showed signals corresponding to the *trans*-double bond at δ 116-118 and 145-147 which is similar to the values reported for **4FIP**. Similarly, ^{13}C NMR signals at δ 165-166 indicate the present of ester groups while that at δ 168 reveal the presence of signals from the acetoxy group. The signals corresponding to the $(CH_3)_2C$ carbons in the diisopropylidene group in the ^{13}C NMR

were observed at δ 19.0, 23.90, 25.44, 28.85 which was similar to that reported for **4FIP.** All of the above data confirmed the white solid obtained to be the desired product **4SIP** (**71**) which was obtained in 57% yield.

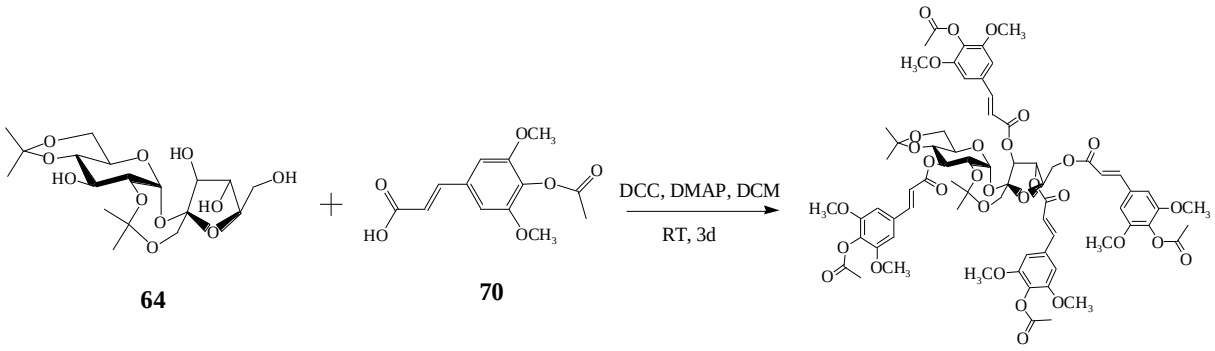

64 **70** **4SIP (71)** (57%)

Scheme 11: Synthesis of 3,3′,4′,6′-Tetra-*O*-acetylsinapoyl-2,1′:4,6-di-isopropylidene sucrose **4SIP (71)** by Steglich esterification method

6.4.3 Acetal deprotection of 4SIP (71) to get 3,3′,4′,6′-Tetra-*O*-acetylsinapoyl sucrose, 4SSP (72)

Deacetylation of **4SIP** (**71**) to remove the diisopropylidene group was done by reacting it with aqueous acetic acid (scheme 12).[105] The reaction mixture was then subjected to column chromatography to isolate a white solid with mp 147-150°C. ^{1}H NMR analysis of the solid revealed the absence of the characteristic peaks corresponding to the diisopropylidene group seen in **4SIP** (δ: diisopropylidene ring: 1.12, 1.21 (2xs, 3H), 1.37-1.40 (m, 3H), 1.58 (s, 6H)) (section 6.4.2). This confirmed the successful removal of the diisopropylidene group. The 16 protons corresponding to the aromatic ring and the *trans*-double bond were observed in the region of 6.44-7.74ppm. Similarly, the presence of acetoxy protecting group and the methoxy groups on the sinapoyl moiety were observed at δ 2.25-2.27 (s, 12H, -$COCH_3$) and 3.75-3.78 (m, 24H, -OCH_3) respectively. FT-IR analysis showed characteristic signal for trans-double bond at 1636 cm^{-1}, the acetyl carbonyl at 1762cm^{-1} and the ester carbonyl group at 1714cm^{-1}. The absence of signals corresponding to the $(CH_3)_2C$ carbons in the diisopropylidene group in the ^{13}C NMR 19.0, 23.90, 25.44, 28.85 in case of **4SIP** indicate the successful removal of the group. High resolution ESI-MS that showed a molecular ion *m/z* value of 1335.3976 corresponding to $[M+H]^+$ thus supporting the

molecular formula $C_{64}H_{71}O_{31}$ (*m/z* calcd. for $C_{64}H_{71}O_{31}$: 1335.3979). Thus, it was concluded that the white solid was product **72** (**4SSP**) obtained in 72% yield.

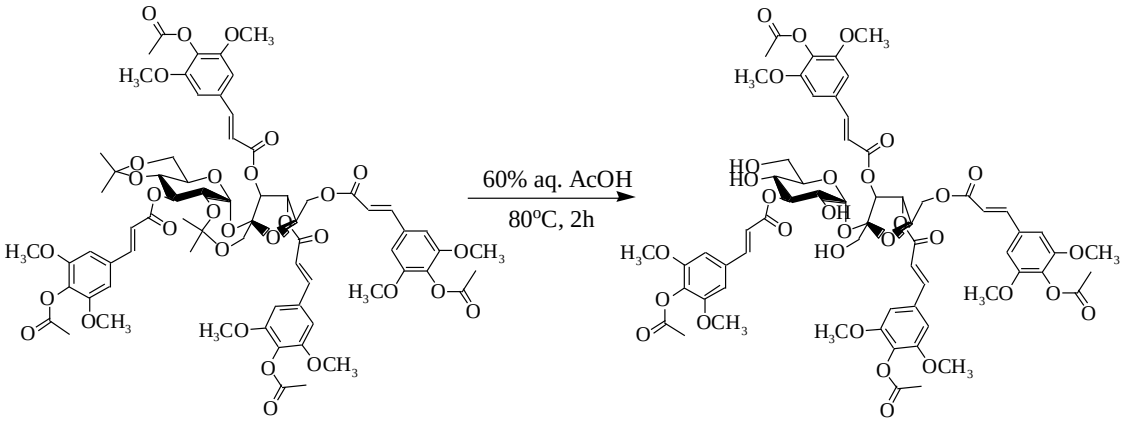

4SIP (71) **4SSP (72)** (72%)

Scheme 12: Synthesis of 3,3′,4′,6′-Tetra-*O*-acetylsinapoyl sucrose**, 4SSP** (**72**)

6.4.4 Deacetylation of 4SIP (71) to get 3,3′,4′,6′-Tetra-*O*-sinapoyl-2,1′:4,6-di-isopropylidene sucrose 4SI (73)

4SIP (**71**) was reacted with piperidine in 95% EtOH (20ml) to remove the acetoxy group protecting the aromatic 'OH' of the sinapoyl substituent (scheme 13).[105] On reaction completion, a yellow solid was isolated with mp 145-148°C. Absence of peaks corresponding to the -$COCH_3$ group in ^{1}H NMR (on comparison with **4SIP**) in the region 2.2-2.4ppm confirmed the successful deprotection of the aromatic 'OH' group. The signals corresponding to the diisopropylidene and the aromatic -OCH_3 group were found at: diisopropylidene ring δ:1.23-1.25 (m, 6H), 1.43-1.46 (m, 6H); and at δ:3.85-3.90 (m, 24H, -OCH_3). High resolution ESI-MS that showed a molecular ion *m/z* value of 1247.4164 corresponding to $[M+H]^+$ thus supporting the molecular formula $C_{62}H_{71}O_{27}$ (*m/z* calcd. for $C_{62}H_{71}O_{27}$: 1247.4183). FT-IR analysis showed the disappearance of the signal corresponding to acetyl ester carbonyl group at 1767cm^{-1}. The signal for trans-double bond at 1630 cm^{-1} and the ester carbonyl group at 1712cm^{-1} was observed by FT-IR analysis. The carbon signals corresponding to the acetyl moiety observed in case of **4SIP** (δ 20.44 168.43, 168.54) were found to be absent in the ^{13}C NMR thus confirming the successful removal of the acetyl groups. Thus, the yellow solid was assigned to be compound **73** (**4SI**).

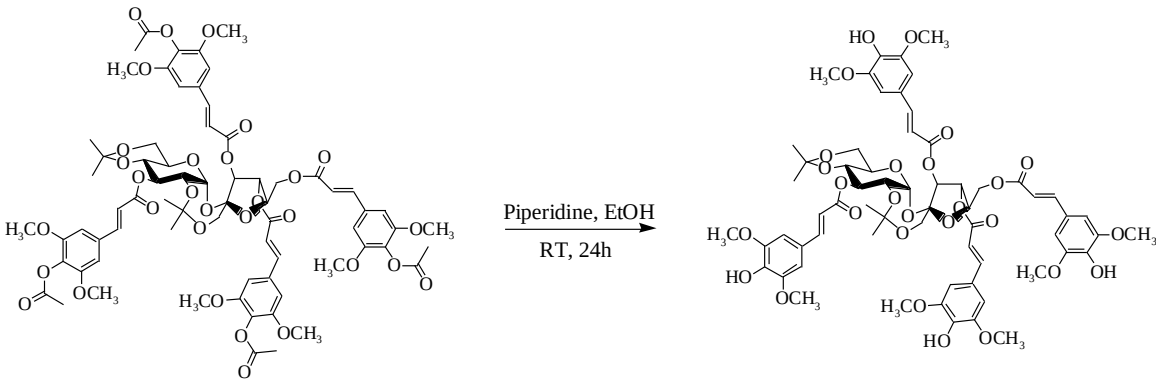

4SIP (71)

4SI (73) (54%)

Scheme 13: Synthesis of 3,3′,4′,6′-Tetra-*O*-sinapoyl-2,1′:4,6-di-isopropylidene sucrose **4SI** (**73**)

6.4.5 Deacetylation of 4SSP (72) to get 3,3′,4′,6′-Tetra-*O*-sinapoyl sucrose 4SS (74)

4SSP (**72**) was reacted with piperidine in 95% EtOH (20ml) to remove the acetoxy group protecting the aromatic 'OH' of the sinapoyl substituent (scheme 14).[105] On reaction completion, a yellow solid was isolated with mp 127-130°C. Successful removal of the protecting group (-$COCH_3$) was confirmed by comparison of ^{1}H NMR of **4SSP** and **4SS** where the characteristic signal at δ: 2.25-2.27 (s, 12H, -$COCH_3$) was absent. The peaks for the -OCH_3 were observed at δ: 3.80-3.91(m, 24H) and the region between 6-8ppm revealed the presence of 16H corresponding to the sinapoyl group. High resolution ESI-MS that showed a molecular ion *m/z* value of 1167.3557 corresponding to $[M+H]^+$ thus supporting the molecular formula $C_{56}H_{63}O_{27}$ (*m/z* calcd. for $C_{56}H_{63}O_{27}$: 1167.3557). FT-IR analysis showed the disappearance of the signal corresponding to acetyl ester carbonyl group at 1762cm^{-1}. The signal for trans-double bond at 1629 cm^{-1} and the ester carbonyl group at 1707cm^{-1} was observed by FT-IR analysis. ^{13}C NMR showed the absence of peaks at δ 165.70, 166.59, 166.85 (seen in **4SSP**) that correspond to the acetyl carbons. Therefore, the new product was assigned to be **4SS** (**74**).

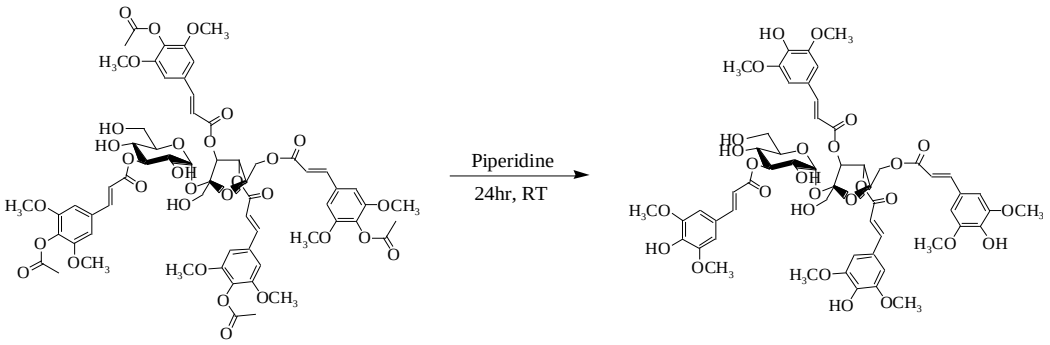

4SSP (72) **4SS (74)** (74%)

Scheme 14: Synthesis of 3,3′,4′,6′-Tetra-*O*-sinapoyl sucrose **4SS** (**74**)

6.5 α-glucosidase and α-amylase inhibition of newly synthesized PSEs

The PSEs in the previous sections were synthesized in order to enhance the SAR study by correlating specific structural features or functional groups to the inhibition of α-glucosidase and α-amylase. The newly synthesized PSEs contain the following modifications:

a. Reduction of the alkenyl C=C in the phenylpropanoid substituent (compounds **59-62**)
b. Reduction of the phenyl ring (compound **68**)
c. Tetra sinapoyl substituted PSEs with and without the diisopropylidene group as well as with and without protected aromatic 'OH' group.

Each of these PSEs were tested according to the same inhibition method as described in chapter 2. Table 40 shows the percentage inhibition values of the hydrogenated compounds **59-62**. Each of these is compared against the respective parent compound (non-hydrogenated) in order to show the effect of double bonds.

From table 40, it can be seen that hydrogenation of alkenyl C=C bond in case of all four compounds **59-62** greatly reduces both α-glucosidase and α-amylase inhibition (table 40, entries 1-4). The same compounds when compared to their non-hydrogenated counterparts exhibit a marked reduction in the activity leading to the conclusion that the C=C of the phenylpropanoid chain is essential to inhibition activity. The most significant reduction can be seen in the case of hydrogenation of **4CiI** which cause a ten-fold decrease in α-glucosidase inhibition (table 40, entry 1). However, in case of α-amylase, there is a two-

fold decrease for **4CiI** indicating that hydrogenation has a greater effect with respect to the former enzyme. This reduction in activity was similar whether the PSE was feruloyl, coumaroyl or cinnamoyl and whatever the number of substituents. In case of the fully hydrogenated counterpart of **4CiI,** compound **68,** once again there was a marked decrease in the α-glucosidase inhibition with only 10% inhibition (table 40, entry 68). However, it was interesting to note that for **68,** the inhibition of α-amylase is decreased even further when compared to the compound where only the C=C bond is hydrogenated (compound **59**). These results show conclusively that the presence of the alkenyl C=C bond as well as the aromatic ring is essential to the activity of the PSEs.

Table 40: α-glucosidase and α-amylase inhibition of PSEs with alkenyl C=C bond hydrogenation

% α-Glucosidase inhibition of hydrogenated compounds compared to the parent compounds				
Entry	**Hydrogenated Compound (50µg/ml)**	**% α-Glucosidase Inhibition**	**Parent Compound (50µg/ml)**	**% α-Glucosidase Inhibition**
1	**59**	7±3	**4CiI**	77±5
2	**60**	NSA*	**2CiIP**	46±3
3	**61**	7±3	**2CoIP**	29±7
4	**62**	14±4	**3FI**	39±4
5	**68**	10±6	**4CiI**	77±5
6	**Acarbose**	35±3	**Acarbose**	31±2
% α-Amylase inhibition of hydrogenated compounds compared to the parent compounds				
Entry	**Hydrogenated Compound (50µg/ml)**	**% α-Amylase Inhibition**	**Parent Compound (50µg/ml)**	**% α-Amylase Inhibition**
7	**59**	50±10	**4CiI**	98±2
8	**60**	7±4	**2CiIP**	14±4
9	**61**	6±9	**2CoIP**	12±10
10	**62**	NSA*	**3FI**	12±9
11	**68**	33±12	**4CiI**	98±2
12	**Acarbose**	100±2	**Acarbose**	95±1

**Compounds with less than 5% enzyme inhibition are considered to have No Significant Activity (NSA).*

The next group of compounds that were studied were the newly synthesized sinapoyl substituted PSEs. Four new tetra substituted sinapoyl PSEs were synthesized as it was already established in chapter 2 that PSEs with four phenylpropanoid substituents were

most active. The enzyme inhibition study values are given below in table 41 and are compared with their feruloyl counterparts to show the differences.

Table 41: α-glucosidase and α-amylase inhibition of sinapoyl PSEs compared with feruloyl PSEs

% α-Glucosidase inhibition of sinapoyl PSEs compared with feruloyl PSEs				
Entry	**Sinapoyl PSEs (50µg/ml)**	**% α-Glucosidase Inhibition**	**Feruloyl PSEs (50µg/ml)**	**% α-Glucosidase Inhibition**
1	**4SIP**	43±3	**4FIP**	46±4
2	**4SI**	34±14	**4FI**	90±8
3	**4SSP**	8±4	**4FSP**	35±10
4	**4SS**	21±8	**4FS**	98±4
5	**Acarbose**	35±3	**Acarbose**	31±2
% α-Amylase inhibition of sinapoyl PSEs compared with feruloyl PSEs				
Entry	**Compound (50µg/ml)**	**% α-Amylase Inhibition**	**Feruloyl PSEs (50µg/ml)**	**% α-Amylase Inhibition**
6	**4SIP**	NSA*	**4FIP**	13±3
7	**4SI**	NSA*	**4FI**	54±4
8	**4SSP**	NSA*	**4FSP**	13±4
9	**4SS**	NSA*	**4FS**	98±1
10	**Acarbose**	100±2	**Acarbose**	95±1

**Compounds with less than 5% enzyme inhibition are considered to have No Significant Activity (NSA).*

From the α-glucosidase and α-amylase inhibition values presented in table 41, it becomes clear that sinapoyl substituent greatly reduces the potency of the PSEs especially evidenced in case of **4SI** and **4SS. 4SIP** is an anomaly here and shows a similar inhibition value as compared to **4FIP**. Where their feruloyl counterparts exhibit almost complete inhibition of α-glucosidase, the sinapoyl PSEs show between 20 and 30% inhibition (table 41, entries 1 and 4). In case of α-amylase, all of the sinapoyl PSEs showed no significant activity. The difference between the sinapic and ferulic acid substituents groups is the presence of an additional methoxy group on the aromatic ring in sinapoyl substituent (Fig. 69). From the results above, it is clear that the presence of more than one methoxy group reduces the efficacy of the PSEs and the sinapoyl group is not an ideal substituent.

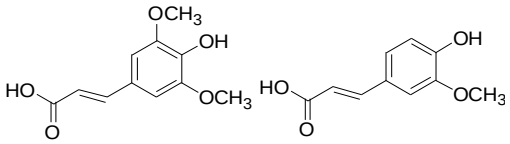

Figure 69: Sinapic and ferulic acid.

In order to complete the SAR study regarding the type of substituent, the following section is included which was obtained with permission through private communication from Ms. Ong Li Lin who is a PhD student at the same lab in SCBE, NTU (as yet unpublished). The following work includes five other PSE compounds that were synthesized and tested for their α-glucosidase and α-amylase inhibitory activities under collaboration. These results are simply included to form a complete picture regarding the SAR between the structure of PSE with its anti-diabetic activity. The first two compounds, **75** and **76** are tetra substituted PSEs with the aromatic ring having two and three methoxy groups respectively along with the diisopropylidene group. **77** is compound **76** without the diisopropylidene group. The final two compounds, **78** and **79** are tetra substituted PSEs substituted with caffeic acid with and without the diisopropylidene group respectively. These were included for the specific reason that the former three have only methoxy substituents on the aromatic ring whereas the latter two have only aromatic 'OH' groups. The structures of these compounds are illustrated in Fig. 70 and their enzyme inhibition values are in table 42.

Table 42: α-glucosidase and α-amylase inhibition of PSEs

Entry	**Compound (50µg/ml)**	**% α-Glucosidase Inhibition**
1	**75**	25±18
2	**76**	15±8
3	**77**	NSA*
4	**78**	99±3
5	**79**	99±2
6	**Acarbose**	35±3
Entry	**Compound (50µg/ml)**	**% α-Amylase Inhibition**
7	**75**	NSA*
8	**76**	NSA*
9	**77**	9±5
10	**78**	NSA*
11	**79**	29±7
12	**Acarbose**	100±2

**Compounds with less than 5% enzyme inhibition are considered to have No Significant Activity (NSA).*

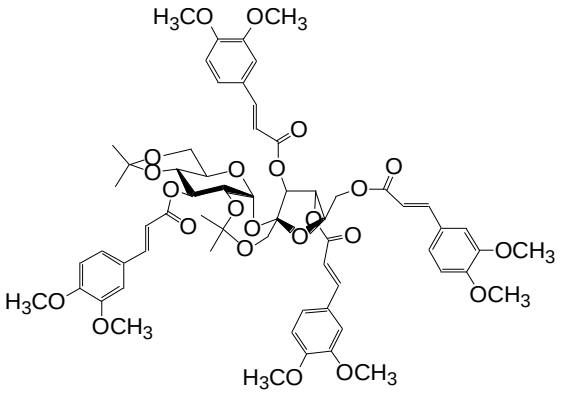

75

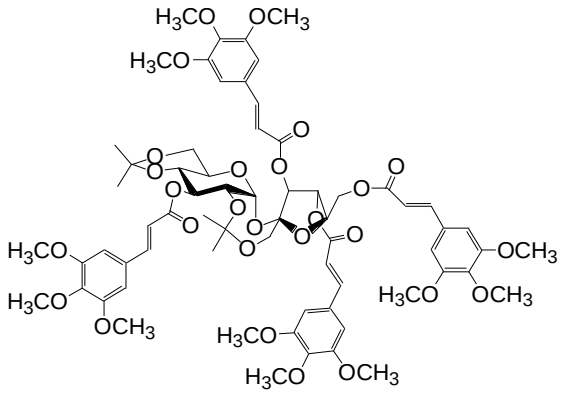

76

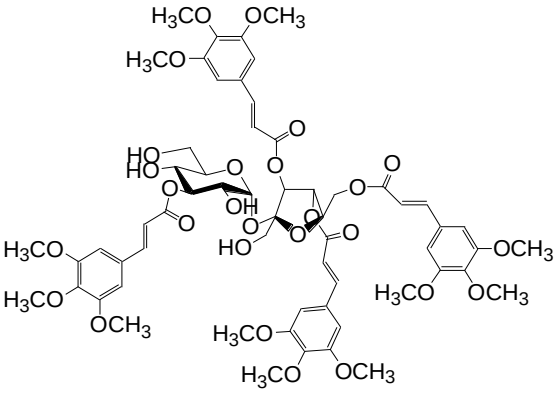

77

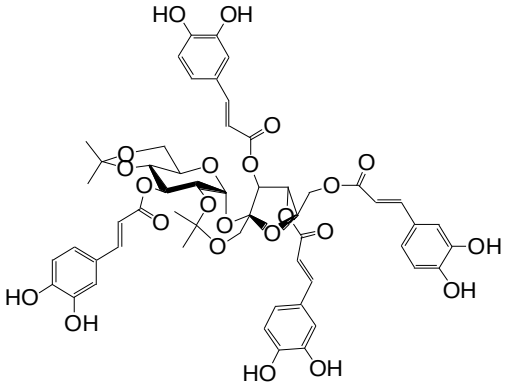

78

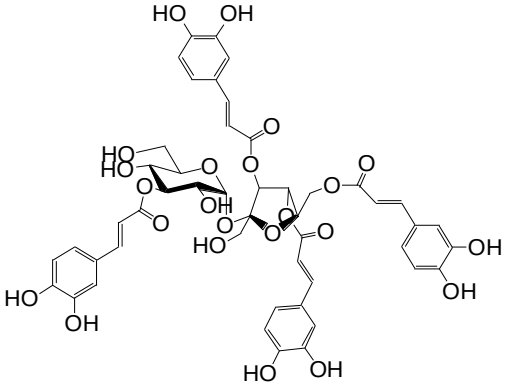

79

Figure 70: Structures of new PSEs.

A careful inspection of table 42 shows that as was the case with sinapoyl PSEs, PSEs with an excess of methoxy substituents on the phenyl ring show very little α-glucosidase inhibition (table 42, entries 1-2) and no significant α-amylase inhibition. In case of compounds **75-77** there is no aromatic 'OH' group and they are seen to fare worse than the sinapoyl PSEs. The absence of the diisopropylidene group in compound **77** reduces the α-

glucosidase inhibition to almost nil, however, this cannot be stated conclusively as the inhibition value for **76** is already very low at 15%. In case of the caffeoyl PSEs, **78** and **79**, a very interesting trend can be observed. Both these PSEs have two aromatic 'OH' groups and no methoxy groups. It can be seen from table 42 that both these compounds exhibit almost complete inhibition of α-glucosidase (table 42, entries 4 and 5). Compound **78** exhibits no inhibition of α-amylase whereas **79** which does not have the diisopropylidene group exhibits an inhibition of 29% (table 42, entries 10 and 11). This trend is similar to that observed in feruloyl PSEs where the presence of the diisopropylidene group in tetraferuloyl PSE **4FI** reduced its capacity to inhibit α-amylase. From the above study, it can be observed that the selectivity between α-glucosidase and α-amylase is greatly affected by the type of phenylpropanoid substituent. Whereas the methoxy group reduces inhibition of both the enzymes, the aromatic 'OH' group drives selectivity in favour of α-glucosidase.

6.6 Summary

In the chapters leading up to the current one, we have seen the SAR for PSEs as AGIs develop. The in vitro, in silico, in vivo and enzyme kinetic studies led to the conclusion that tetra substituted PSEs were the most active. Although both feruloyl and cinnamoyl PSEs had high efficacy, the tetraferuloyl PSE, **4FI** that has the diisopropylidene group was thought to be the best as it was found to be more selective to the enzyme α-glucosidase than α-amylase which is hypothesized to greatly diminish the GI side-effects accompanying AGIs. However, the solubility of the PSEs is limited due to the presence of the phenyl rings. Also, the effect of certain other structural features on the activity was still unclear. Thus, in this chapter the synthesis and modification of PSEs was undertaken in order to establish the effect of the alkenyl C=C in the phenylpropanoid substituent, the effect of the presence of cyclohexyl as opposed to the phenyl ring and finally the effect of the presence of methoxy and 'OH' groups on the phenyl rings. For this purpose, new PSEs were synthesized while five were acquired. Synthesis was successfully established using Steglich esterification. Four PSEs with the alkenyl C=C bond hydrogenated and one with complete hydrogenation of the phenyl rings as well were synthesized. Apart from this, four tetrasinapoyl PSEs were synthesized. On testing of these compounds along with the ones obtained externally, it was found that hydrogenation has an adverse effect on the potency. Hydrogenated compounds inhibit both the enzymes to a much lesser degree. Similarly, compounds with sinapic acid

substituents display a loss in activity which is attributed to the presence of more than one methoxy substituent on the phenyl ring. For sinapoyl PSEs there is mild inhibition of α-glucosidase and no significant inhibition of α-amylase. Towards the end, the effect of PSEs with two and three methoxy substituents on the phenyl ring were also tested and had similar results as compared to sinapoyl PSEs. Finally, caffeoyl PSEs (having two aromatic 'OH' groups) were tested and it was observed that for these, there is near complete inhibition of α-glucosidase and little to no inhibition of α-amylase. Therefore, combining the results thus far, it can be concluded that the presence of 'OH' groups on the phenyl ring is essential to activity along with four substituents on sucrose and the diisopropylidene group. The presence of methoxy groups generally lowers activity, however in case of the feruloyl PSEs there is an exception with the presence of one 'OH' and one methoxy group each.

From the SAR studies in this thesis regarding PSEs as AGIs, the following conclusions are drawn regarding the ideal PSE:

- A tetra substituted PSE with the fourth phenylpropanoid substituent at position 3 on the sucrose ring is essential for high enzyme inhibition of both α-glucosidase and α-amylase.
- The presence of the diisopropylidene ring reduces the inhibition of α-amylase as compared to α-glucosidase which is desirable to reduce the GI side-effects.
- The alkenyl C=C is important to the activity of the PSEs.
- The aromaticity of the PSEs plays an important role in its potency.
- The aromatic 'OH' is a key structural feature that influences the potency.
- Presence of only methoxy substituents on the aromatic ring is detrimental to the potency of the PSEs as AGIs. However, the presence of one methoxy and one 'OH' group in ferulic acid is an exception as seen with PSE **4FI**.
- The presence of only 'OH' groups on the aromatic ring drives selectivity completely in favour of α-glucosidase.
- **4FI** and **79** (tetra caffeoyl PSE) are the most promising candidates for development into lead drug(s). The former faces challenges with solubility while the latter needs to be tested in vivo to verify if negligible inhibition of α-amylase is desirable.

Chapter 7. Future work

7.1 Solubility of PSEs

We aim to develop optimum PSEs as AGI lead drug candidates that are potent, non-systemic and highly selective towards α-glucosidase inhibition. In order to ensure effective oral delivery of PSEs, it is essential that they are soluble. Therefore, our primary goal is to enhance the solubility of the PSEs. The various co-solvents or polymers that would be tested for formulation are those that are approved for use both in animal models as well as for humans. Keeping these in mind, formulation of the PSEs will be tested using the following excipients.

a. *PEG-300*. Using a maximum limit of 60% PEG-300 in water, solubility of the PSEs will be tested in solutions of PEG-300: water of varying percentage. In each case, the maximum solubility will be tested.[106,107]
b. *DMSO*: DMSO at concentrations below 10% is an allowed excipient in drug formulation. Therefore, similar to PEG-300, the solubility of the PSEs in DMSO: water solutions will be tested.[106,107]
c. *Edible oils:* Edible oils like peanut oil, corn oil are used routinely in order to formulate poorly soluble drugs. These edible oils will be tested as suitable solvents for the formulation of PSEs.[106,107]
d. *Cyclodextrins*: Complexation of drugs with cyclodextrins enhances the solubility as the drug molecule is encapsulated into the core. To do this, the drug (PSE) and cyclodextrins will be dissolved separately in a common solvent at the same molar ratio and then mixed and stirred. The solution will then be evaporated to recover the cyclodextrin-drug complex.[106,107]

7.2 SAR studies- Ester linkage vs ether

To study the importance of the ester bond to the anti-diabetic activity of PSEs, the effect of the modification of PSEs by substituting the ester linkage of the phenylpropanoid substituent to ether linkage will be tested. This modification can be done by either direct reduction of ester linkage to ether linkage (Scheme 15a)[108] or by Williamson ether synthesis between diacetonide derivative and 3-phenylpropanol derivative (Scheme 15b).

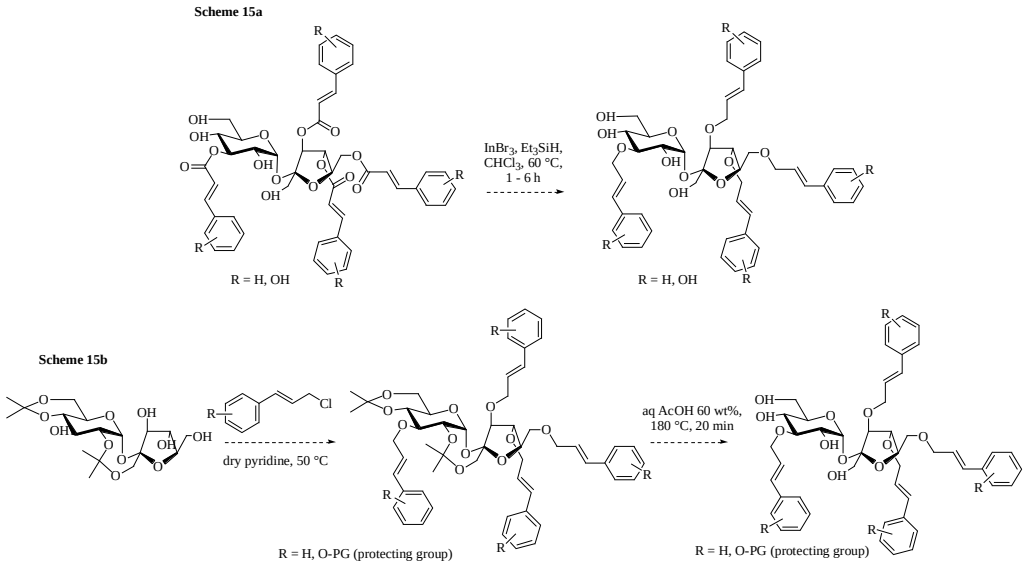

Scheme 15: Synthesis of modified PSE with ether linkages check scheme diagram

7.3 Evaluation of the antidiabetic potential of PSEs in Type 2 diabetic mouse model (T2DM)

Leptin-deficient (ob/ob) mice will be the prototypic genetically-modified T2DM used for this purpose. The mice are hyperphagic and exhibit increased glucose intolerance from 4 weeks of age. At 4 weeks of age, the variation in weight in ob/ob mice is minimal. These mice will then be morbidly obese by 8 weeks of age.[93] For this set of experiments, ob/ob mice will be separately housed from 4 weeks of age (following genotyping). We aim to place the PSEs, Acarbose and vehicle in the drinking water of these mice from 4 weeks of age right up to 8 weeks of age. During these 4 weeks, we will determine change in weight gain, plasma insulin levels periodically and we will perform an IPGTT once a week throughout the 4-week treatment period. We expect the weight gain to be significantly less in the PSE and Acarbose group and anticipate the glucose excursion will be lower in the PSE group as compared to Acarbose group. After the treatment, the mice will be culled and we will harvest the liver, soleus muscle, white epididymal fat and pancreas for evaluation of insulin-responsive genes by real-time PCR, immunoblotting and immunofluorescence staining (specifically for islets containing insulin in the pancreas). The HbA1C levels in mice treated with the PSEs over a period of time will be measured. Caco-2 permeability assay will be evaluated to ensure that the drugs are non-systemic. We will also conduct studies to determine the metabolites in blood (if any) and analyze stool samples.

Chapter 8. Experimental

General

All commercial materials used in this project were obtained from Sigma-Aldrich, Merck, Alfa Aesar, Acros and Fisher Scientific, and were used as received unless otherwise indicated. Analytical thin layer chromatography (TLC) was performed using Merck 60 F254 pre-coated silica gel plate (0.2 mm thickness) and visualized using UV radiation (254 nm), $KMnO_4$ or *p*-anisaldehyde staining solution. Column chromatography for purification of the compounds was performed using Merck silica gel 60 (230-400 mesh). FT-IR spectra were recorded using a Perkin-Elmer FTIR system Spectrum BS spectrometer. Melting points were tested by Buchi Melting Point-B450 apparatus. High resolution mass spectra were recorded using Waters Q-tof Premier mass spectrometer. HPLC was performed on Agilent 1100 using C18 column (Kromasil 100-3.5C18). ^{1}H NMR spectra were recorded at 300 MHz using a Bruker Avance DPX 300 machine. ^{1}H NMR multiplicities were assigned as singlet (s), doublet (d), doublet of doublet (dd), and multiplet (m). ^{13}C NMR spectra were recorded at 75.47 MHz using a Bruker 156 Avance DPX 300 machine. Unless stated, all the experiments were run in CDCl3 solvent with the TMS as internal reference.

7.1 Reduction of alkenyl C=C

General procedure

To a solution of the desired PSE in a MeOH and EtOAc mixture (10:1, ml per mmol), ammonium formate (5eq.) and 20% (by weight) of the catalyst Pd/C was added. The solution was refluxed for 2 days whereby the progress of the reduction of the alkenyl C=C was monitored by TLC. The solution was then cooled, filtered and the solvent evaporated under reduced pressure. The residue was then dissolved in $CHCl_3$ (20ml) to precipitate excess ammonium formate, then once again filtered and evaporated. The product was purified by column chromatography using hexane:EtOAc gradient.

7.1.1 3,3′,4′,6′-Tetra-*3*-phenyl-propanoyl-2,1′:4,6-di-*o*-isopropylidene sucrose 59

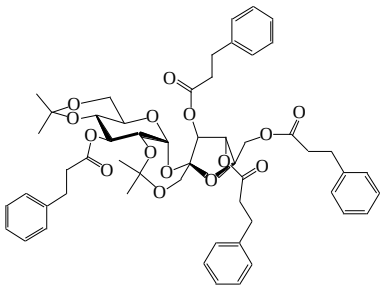

59

Following the general procedure, the reduction of **4CiI** (**54**) (100mg, 0.106mmol) using ammonium formate (5eq.) and Pd/C (20 wt%) gave the product **59** as an off-white solid**,** yield 85% (85mg, 0.089mmo l) after 2 days of reaction. Analytical data for **59**: R_f = 0.72 (2:1 EtOAc:hexane). mp 39-41°C. FTIR (KBr) ν_{max}: 2957, 1757, 1594, 1501, 1460, 1392, 956, 864, 756, 703, 690 cm^{-1}. ^1H NMR (300MHz, $CDCl_3$) δ: diisopropylidene ring: 1.38-1.44 (m, 12H); aliphatic chain: 2.61-2.84 (m, 8H), 2.90-3.11(m, 8H); sucrose unit: 3.46 (d, *J* = 12.3Hz, 1H), 3.65-3.82 (m, 2H), 3.75-3.90 (m, 2H), 3.92 (dd, *J* = 5.1, 10.2Hz, 1H), 4.05 (d, *J* = 12.6Hz, 1H), 4.19-4.38 (m, 3H), 5.06-5.26 (m, 3H), 6.06 (d, *J* = 3.6Hz, 1H); phenyl rings: 7.16-7.31 (m, 20H). ^{13}C NMR (75.48MHz, $CDCl_3$) δ: 19.0, 23.90, 25.50, 29.10, 30.6, 30.75, 30.78, 31.1, 35.35, 35.53, 35.54, 35.85, 62.1, 64.34, 64.89, 66.1, 70.60, 71.45, 71.78, 76.7, 77.45, 77.53, 79.9, 91.51, 99.68, 101.4, 104.6, 126.18, 126.24, 126.26, 126.47, 128.22, 128.28, 128.34, 128.45, 128.47, 128.49, 128.51, 128.61, 139.90, 140.27, 140.55, 140.67, 171.67, 171.91, 172.25, 172.40. HRMS (ESI-positive mode): *m/z* calcd. for $C_{54}H_{63}O_{15}$ 951.4167; found 951.4147 $[M+H]^+$.

7.1.2 3,4′-di-*o*-acetyl-3′,6′-di-*3*-phenyl-propanoyl-2,1′:4,6-2,1′:4,6-di-*o*-isopropylidene sucrose 60

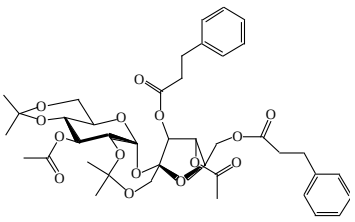

60

Following the general procedure, hydrogenation of **55** (100mg, 0.133mmol) for 2 days using ammonium formate (0.665mmol) and Pd/C (20 wt%) provided compound **60** as an off-white solid (82mg, 0.108mmol) in 81% yield after 2 days of reaction. Analytical data for **60**: R_f = 0.729 (4:1 EtOAc:hexane). mp 35-38°C. FTIR (KBr) ν_{max}: 3450, 3060, 2934, 1758, 1608, 1599, 1461, 1384, 1269, 1084, 757, 704 cm^{-1}. ^1H NMR (300MHz, $CDCl_3$) δ: diisopropylidene ring: 1.18-1.34 (m, 12H); 1.97, 2.08 (2xs, 6H, -$COCH_3$); aliphatic chain: 2.52-2.59 (m, 2H), 2.71-2.87 (m, 4H), 2.96-3.02 (m, 2H); sucrose unit: 3.36-3.43 (m, 4H), 3.56-3.60 (m, 2H), 3.73-3.80 (m, 2H), 3.82-3.95 (m, 1H), 3.95-4.16 (m, 2H), 4.12-4.35 (m, 3H), 5.04 (d, *J* = 5.4 Hz, 1H), 5.16-5.17 (m, 2H), 6.00 (d, *J* = 5.4 Hz, 1H); phenyl ring: 7.09-7.18 (m, 10H).

^{13}C NMR (75.48MHz, $CDCl_3$) δ: 19.0, 20.73, 20.93, 22.70, 23.8, 25.4, 29.38, 29.68, 29.72, 32.0, 35.38, 35.54, 62.1, 64.35, 64.94, 66.1, 70.5, 71.44, 71.80, 76.6, 77.5, 91.5, 99.7, 101.4, 104.6, 126.15, 126.20, 128.29, 128.42, 128.47, 140.23, 140.51, 169.76, 169.93, 172.28, 172.38; HRMS (ESI-positive mode): *m/z* calcd. for $C_{40}H_{51}O_{15}$ 771.3228; found 771.3200 $[M+H]^+$.

7.1.3 3′,6′-di-*3*-acetoxyphenyl-propanoyl-2,1′:4,6-di-*o*-isopropylidene sucrose 61

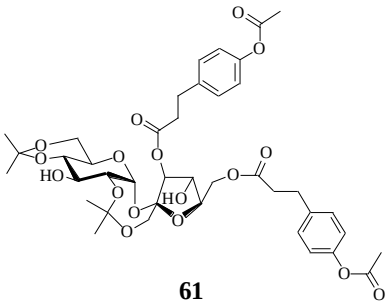

61

Following the general procedure, reduction of **2CoIP** (**49**) (75mg, 0.093mmol) using ammonium formate (5 eq.) and Pd/C (20 wt%) and purification using column chromatography (EtOAc: hexane gradient) gave product **61** as a white solid in 80% yield (60mg, 0.074mmol) after 2 days of reaction. Analytical data for **61**: R_f = 0.62 (9:1 EtOAc:MeOH). mp 69-72°C. FTIR (KBr) ν_{max}: 3457, 2974, 1744, 1597, 1509, 1457, 1368, 1259, 1047, 935, 737, 664 cm^{-1}. ^{1}H NMR (300MHz, $CDCl_3$) δ: diisopropylidene ring: 1.18-1.43 (m, 12H); 1.98 (d, *J* = 3Hz, 2H, -R-OH); 2.20 (d, *J* = 3.6Hz, 6H, $-COCH_3$); aliphatic chain: 2.51-2.83(m, 8H); sucrose unit: 3.73-3.80 (m, 8H), 3.90-3.91 (m, 1H), 4.08-4.13 (m, 1H), 4.25-4.28 (m, 1H), 4.94-5.01 (m, 1H), 5.16-5.19 (m, 1H), 5.92 (d, *J* = 2.4Hz, 1H); phenyl ring: 6.56-6.89 (m, 8H). ^{13}C NMR (75.48MHz, $CDCl_3$) δ: 19.10, 20.70, 22.7, 25.3, 29.12, 29.37, 29.70, 30.44, 30.58, 30.65, 55.83, 55.85, 55.88, 55.98, 64.3, 73.0, 76.6, 79.20, 91.2, 99.79, 99.82, 101.70, 101.72, 122.63, 122.76, 131.9, 138.07, 138.14, 138.24, 138.89, 138.93, 139.50, 150.87, 150.93, 169.48, 169.99, 172.98, 172.31. HRMS (ESI-positive mode): *m/z* calcd. for $C_{40}H_{51}O_{17}$ 803.3126; found 803.3129 $[M+H]^+$.

7.1.4 3′,4′,6′-Tri-3-(4-Hydroxy-3-methoxy-phenyl)-propanoyl-2,1′:4,6-di-isopropylidene sucrose 62

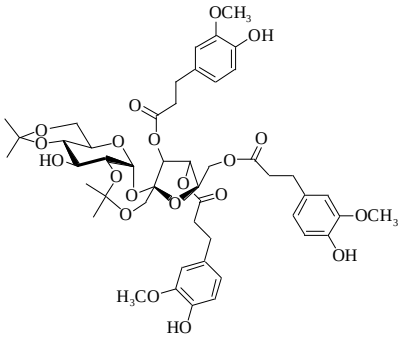

62

Following the general procedure, the reduction of **3FI** (**47**) (100mg, 0.105mmol) using ammonium formate (5 eq.) and Pd/C (20 wt%) and purification using column chromatography (EtOAc: hexane gradient) afforded product **62** as a white solid in 97% yield (98mg, 0.102mmol) after 2 days of reaction. Analytical data for **62**: R_f = 0.23 (2:1 EtOAc:hexane). mp 68-71°C FTIR (KBr) ν_{max}: 3455, 2936, 1739, 1600, 1518, 1447, 1373, 1268, 1149, 1061, 1033, 939, 851 cm^{-1}. ^1H NMR (300MHz, $CDCl_3$) δ: diisopropylidene ring: 1.18-1.43 (m, 12H); aliphatic chain: 2.77-2.87 (m, 12H); sucrose unit: 3.45-3.65 (m, 6H) 4.03-4.16 (m, 4H), 4.236-4.255 (m, 1H), 4.95 (d, *J* = 5.4Hz, 1H), 5.15-5.18 (m, 1H), 5.92 (d, *J* = 2.1Hz, 1H); 3.72-3.80 (m, 9H, -OCH3); phenyl ring: 6.59-6.76 (m, 9H). ^{13}C NMR (75.48MHz, $CDCl_3$) δ: 19.10, 24.40, 25.40, 29.70, 30.50, 35.72, 35.85, 35.90, 42.60, 47.50, 53.40, 55.89, 55.98, 60.4, 62.0, 63.8, 64.8, 66.1, 70.20, 72.8, 73.7, 76.6, 77.10, 79.70, 91.30, 99.82, 99.94, 101.7, 104.40, 110.90, 110.99, 111.0, 114.35, 114.44, 114.56, 120.77, 120.82, 120.86, 131.76, 131.93, 132.4, 144.00, 144.06, 144.18, 146.44, 146.51, 146.56, 171.99, 172.14, 172.48. HRMS (ESI-positive mode): *m/z* calcd. for $C_{48}H_{61}O_{20}$ 957.3756; found 957.3729 $[M+H]^+$.

7.2 2,1′:4,6-Di-*O*-isopropylidene sucrose (Diacetonide)

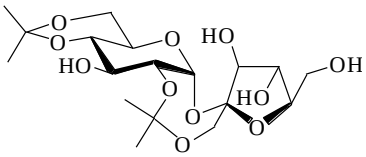

64

Diacetonide **64** was synthesized using the same procedure as described by Panda and colleagues. Briefly, sucrose (65g, 190.1mmol) was dissolved in dry DMF (700ml). To this, Drierite (366g) was added and the resulting mixture was stirred under nitrogen at 70^0C for 30 minutes. 2-Methoxypropene (86ml, 898.1mmol) was then added to the mix followed by catalyst pTsOH (82mg) and the resulting mix was allowed to be stirred at the same conditions for 100 minutes. Finally, NEt_3 (7ml) was added to quench the reaction. The reaction mix was filtered under vacuum to remove the drierite and the solvent was evaporated to dryness under low pressure. The resulting yellow slurry

was suspended in water (652ml) while stirring followed by the sequential addition of AcOH (1.7ml) and Na_2CO_3 (16.3g). Once again, the mixture was evaporated to dryness and the residue was dissolved in EtOAc (403ml). The solution was dried over anhydrous $MgSO_4$, filtered and EtOAc solution recovered. TLC analysis revealed the presence of two spots corresponding to 2,1′:4,6-Di-*O*-isopropylidene sucrose **64** and 4,6-Mono-*O*-isopropylidene sucrose **65**. Upon purification, compounds **64** and **65** were obtained in 49% and 14% yields respectively. Comparison of ^{1}H NMR with literature values confirmed product **64**.[32]

7.3 3-cylcohexanepropionic acid 67

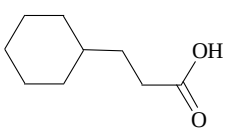

67

Cinnamic acid **66** (500mg, 3.37mmol) was dissolved in 200ml of EtOAc and the solution was transferred to a hydrogen reactor. To this, 50% Pd/C was added and high pressure hydrogenation was carried out at 50bar pressure and 120°C. After 3 days of reaction, the reaction mix was filtered and evaporated under reduced pressure which upon purification by column chromatography (hexane:EtOAc gradient) yielded compound **67** (3-cylcohexanepropionic acid) as a pale yellow liquid in 68% yield (360mg, 2.30mmol).). The ^{1}H NMR of **67** corresponded with literature for 3-cyclohexanepropionic acid.[103]

7.4 3,3′,4′,6′-Tetra-cyclohexanepropanoyl-2,1′:4,6-di-isopropylidene sucrose 68

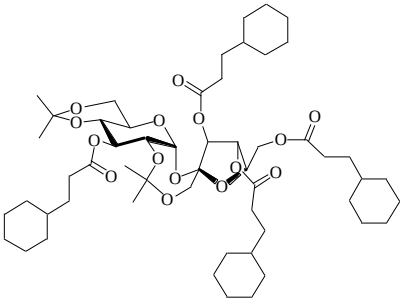

68

Compound **67** was reacted with diacetonide **64** (194mg, 0.45mmol) in DCM (20 ml). To this, DMAP (0.046mmol) was added followed by DCC (475mg, 2.30mmol). The reaction was left to stir for 7 days at room temperature. The reaction was monitored by TLC and upon completion was filtered to remove the byproduct, dicyclourea and the filtrate was evaporated and subjected to purification by column chromatography (hexane:EtOAc gradient). The column purification yielded the desired product **68** as a white solid in 20% yield (92mg, 0.094mmol). Analytical data for **68**: R_f = 0.39 (2:1 hexane:EtOAc). mp 36-39°C. FTIR (KBr) ν_{max}: 3494, 2930, 2847, 1744, 1450, 1375, 935, 851, 720, 651 cm^{-1}. ^{1}H NMR (300MHz, $CDCl_3$) δ: diisopropylidene ring, cyclohexane ring, aliphatic chain: 0.785-0.868 (m, 9H), 1.108-1.299 (m, 17H), 1.39 (s, 5H),

1.41-1.45 (m, 16H), 1.47-1.49 (m, 2H), 1.52-1.63 (m, 19H), 2.20-2.28 (m, 5H), 2.33-2.38 (m, 3H); sucrose unit: 3.44-3.57 (m, 2H) 3.60-3.74 (m, 4H), 3.85-3.90 (m, 1H), 3.95-4.06 (m, 1H), 4.12-4.23 (m, 2H), 4.26-4.28 (m, 1H), 5.01 (d, *J* = 5.1Hz, 1H), 5.20-5.23 (m, 1H), 5.97 (d, *J* = 3.6Hz, 1H); ^{13}C NMR (75.48MHz, $CDCl_3$) δ: 19.10, 24.10, 25.40, 26.17, 26.23, 26.46, 26.52, 29.08, 29.69, 31.56, 31.63, 31.66, 32.10, 32.13, 32.28, 32.86, 32.90, 32.96, 37.10, 37.14, 37.23, 62.0, 63.8, 64.70, 66.20, 70.30, 72.80, 73.80, 76.60, 77.04, 77.25, 77.47, 79.90, 91.20, 99.80, 101.70, 104.5, 128.6, 173.08, 173.35, 173.61. HRMS (ESI-positive mode): *m/z* calcd. for $C_{54}H_{87}O_{15}$ 975.6045; found 975.6015 $[M+H]^+$.

7.5 *p*-acetoxy-sinapic acid 70

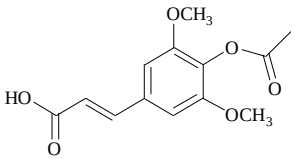

70

Method 1: Using Ac_2O in Pyridine

Sinapic acid **69** (4.5g, 20mmol) was dissolved in Pyridine (10ml) to which acetic anhydride (7 ml) was slowly added (scheme 8). The reaction was stirred for 22 hours at room temperature and finally quenched with 95% EtOH (33ml). The resulting solution was evaporated to remove the solvent and pyridine was removed by co-distillation with toluene. The precipitate was redissolved in 95% EtOH and pure crystals of 4-acetoxysinapic acid **70** (3.23g, 12.13mmol) were obtained in 50% yield (refer appendix for ^{1}H NMR). The ^{1}H NMR of **70** corresponded with literature for *p*-acetoxysinapic acid.[104]

Method 2: Using H_2O and NaOH

Sinapic acid **69** (20g, 89mmol) was dissolved in water (200ml) in a round bottom flask. The whole setup was placed in an ice bath. To this, solid NaOH (9.2g, 0.23mol) was added slowly with stirring. After all of it dissolved, Ac_2O (17ml, 0.178mol) was added drop wise and the reaction left to stir for 1 hour .[109] Visible precipitate of 4-acetoxysinapic acid was observed. The reaction mixture was filtered and the precipitate redissolved in and crystallised from EtOAc to give 4-acetoxysinapic acid **70** (20.62g, 77.16mmol) in 87% yield. The ^{1}H NMR of **70** corresponded with literature for *p*-acetoxysinapic acid.[104]

7.6 3,3′,4′,6′-Tetra-*O*-acetylsinapoyl-2,1′:4,6-di-isopropylidene sucrose 4SIP (71)

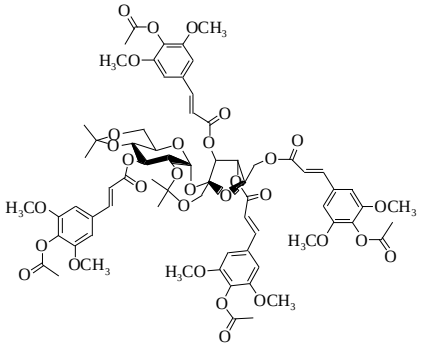

4SIP (71)

Diacetonide **64** (0.1g, 0.23mmol) was dissolved in DCM (5 ml) to which DMAP (2 mg) was added followed by DCC (0.237g, 1.15mmol). Finally, *p*-acetoxysinapic acid **70** (0.34g, 1.27mmol) was added. The reaction was left to stir for 3 days and monitored with TLC in 2:1 EtOAc:Hex. The reaction mixture was filtered to remove the byproduct, dicyclourea and the filtrate was evaporated and subjected to purification by column chromatography (hexane:EtOAc gradient). The desired product **4SIP** was obtained as a white solid in 57% yield (0.19g,0.13mmol). Analytical data for **71**: R_f = 0.71 (2:1 EtOAc:hexane). mp 162-165°C. FTIR (KBr) ν_{max}: 3610, 2992, 2933, 2844, 1767, 1719, 1635, 1596, 1506, 1464, 1418, 1368, 1343, 1323, 1198, 1131, 1008, 940, 901, 825, 645, 586 cm^{-1}. ^1H NMR (300MHz, $CDCl_3$) δ: diisopropylidene ring: 1.12, 1.21 (2xs, 3H), 1.37-1.40 (m, 3H), 1.58 (s, 6H); 2.27 (s, 12H, -$COCH_3$); 3.75-3.78 (m, 24H, -OCH_3); sucrose unit: 3.54-3.69 (m, 4H), 3.84-3.94 (m, 2H), 4.13-4.17 (m, 1H), 4.37-4.55 (m, 3H), 5.23-5.39 (m, 2H), 5.52 (s, 1H), 6.13(s, 1H); phenyl ring and alkenyl -HC=CH-: 6.23-6.36 (m, 4H), 6.47-6.52 (m, 1H), 6.69 (s, 3H), 6.76-6.88 (m, 1H), 6.88 (s, 1H), 7.42-7.64 (m, 4H), 7.78-7.84 (m, 1H). ^{13}C NMR (75.48MHz, $CDCl_3$) δ: 19.0, 20.40, 23.90, 25.40, 26.28, 26.35, 28.80, 30.50, 56.18, 56.23, 56.25, 62.10, 64.40, 65.1, 66.1, 70.90, 71.52, 71.88, 76.60, 80.20, 92.0, 99.70, 101.59, 101.78, 104.68, 104.82, 104.97, 105.21, 105.50, 111.40, 116.68, 116.87, 117.0, 118.02, 118.18, 130.39, 130.43, 130.60, 130.77, 130.88, 132.14, 132.26, 132.56, 132.64, 132.68, 132.82, 144.66, 144.85, 146.2, 147.1, 152.31, 152.41, 152.43, 152.48, 165.70, 165.93, 166.27, 166.80, 168.43, 168.54. HRMS (ESI-positive mode): *m/z* calcd. for $C_{70}H_{79}O_{31}$ 1415.4605; found 1415.4609 $[M+H]^+$.

7.7 3,3′,4′,6′-Tetra-*O*-acetylsinapoyl sucrose 4SSP (72)

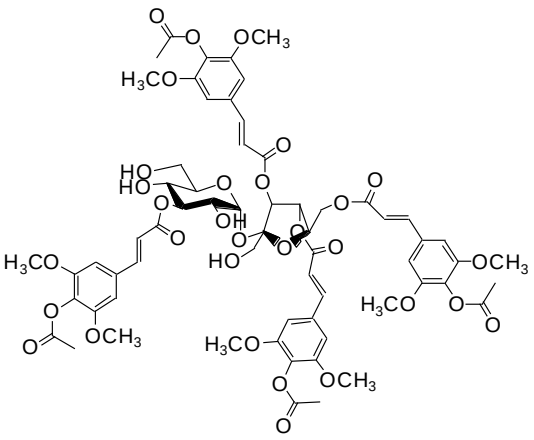

4SSP (72)

4SIP (**71**) (0.8g, 0.565mmol) was dissolved in 60% aqueous acetic acid (50.9 ml). The reaction was stirred for 2 hours at 80°C and later worked up by co-distillation with toluene, to remove acetic acid. The procedure was repeated three times. The reaction mixture was then subjected to column chromatography with a gradient of hexane and EtOAc to give the desired product **4SSP** (**72**) as a white solid in 72% yield (0.545g). Analytical data for **72**: R_f = 0.85 (EtOAc); mp 147-150°C; FTIR (KBr) ν_{max}: 3473, 2936, 2839, 1762, 1714, 1636, 1600, 1502, 1462, 1418, 1367, 1344, 1325, 1273, 1201, 1128, 1042, 1006, 903, 823, 643, 586, 519 cm^{-1}; ^1H NMR (300MHz, $CDCl_3$) δ: 2.25-2.27 (s, 12H, -$COCH_3$); 3.75-3.78 (m, 24H, -OCH_3); sucrose unit: 3.54-3.69 (m, 4H), 3.84-3.94 (m, 2H), 4.44-4.61 (m, 3H), 5.02-5.08 (m, 1H), 5.48-5.53 (m, 2H), 5.61-5.65 (m, 1H), 6.30(d, *J* = 2.1Hz, 1H); phenyl ring and alkenyl -HC=CH-: 6.33-6.38 (m, 2H), 6.47-6.53 (m, 1H), 6.66-6.70 (m, 6H), 6.82 (s, 2H), 7.48 (d, *J* = 15.3Hz, 1H), 7.54-7.63 (m, 2H), 7.74 (d, *J* = 16.2Hz, 1H). ^{13}C NMR (75.48MHz, $CDCl_3$) δ: 20.40, 22.70, 29.30, 29.76, 56.21, 56.25, 56.27, 59.20, 61.80, 69.80, 70.60, 71.60, 73.60, 75.10, 76.60, 78.20, 79.90, 92.50, 104.85, 104.88, 105.39, 105.52, 116.60, 117.30, 130.63, 130.65, 130.68, 130.81, 132.10, 132.29, 132.36, 132.40, 145.80, 146.10, 146.65, 147.7, 152.38, 152.46, 165.70, 166.69, 166.85, 168.40, 268.60. HRMS (ESI-positive mode): *m/z* calcd. for $C_{64}H_{71}O_{31}$ 1335.3979; found 1335.3976 $[M+H]^+$.

7.8 3,3′,4′,6′-Tetra-*O*-sinapoyl-2,1′:4,6-di-isopropylidene sucrose 4SI (73)

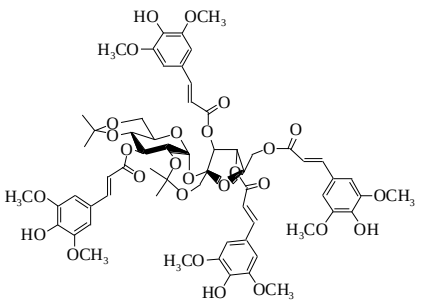

4SI (73)

4SIP (**71**) (0.5g, 0.353mmol) was dissolved in 95% EtOH (20ml). To this, piperidine (210µl, 2.118mmol) was slowly added. The reaction was allowed to stir overnight. The colour of the reaction mixture was observed to change to fluorescent yellow towards the end. Finally, to quench the reaction, AcOH (162µl) was added and pure product, **4SI** (**73**) was isolated as a yellow solid in 54% yield (238mg, 0.19mmol). Analytical data for **73**: R_f = 0.36 (4:1 EtOAc:hexane). mp 145-148°C; FTIR (KBr) ν_{max}: 3419, 2995, 2936, 2839, 1712, 1630, 1600, 1512, 1453, 1426, 1373, 1340, 1285, 1254, 1216, 1147, 1109, 940, 855, 823 cm^{-1}. ; ^1H NMR (300MHz, $CDCl_3$) δ: diisopropylidene ring:1.23-1.25 (m, 6H), 1.43-1.46 (m, 6H); 3.85-3.90 (m, 24H, -OCH_3); sucrose unit: 3.63-3.80 (m, 6H), 4.01-4.22 (m, 3H), 4.56-4.63 (m, 2H), 5.41-5.49 (m, 1H), 5.63-5.65 (m, 1H), 6.20(d, *J* = 4.8Hz, 1H); phenyl ring and alkenyl -HC=CH-: 6.26-6.36 (m, 3H), 6.49 (d, *J* = 16.5Hz, 1H), 6.71-6.82 (m, 6H), 6.96 (s, 2H), 7.53-7.65 (m, 3H), 7.85 (d, *J* = 16.5Hz, 1H). ^{13}C NMR (75.48MHz, $CDCl_3$) δ: 18.30, 23.20, 24.70, 27.60, 28.20, 29.0, 44.60, 50.10, 55.57, 55.61, 55.64, 55.66, 61.4, 63.50, 64.40, 65.30, 70.13, 70.90, 71.20, 75.90, 76.32, 76.52, 76.74, 79.20, 90.90, 98.90, 100.80, 104.13, 104.34, 104.37, 105.20, 113.68, 113.72, 114.75, 114.96, 124.78, 124.81, 125.11, 125.18, 136.38, 136.45, 136.55, 136.74, 136.78, 144.41, 144.64, 145.8, 146.39, 146.45, 146.51, 146.79, 165.32, 165.58, 165.89. HRMS (ESI-positive mode): *m/z* calcd. for $C_{62}H_{71}O_{27}$ 1247.4183; found 1247.4164 $[M+H]^+$

7.9 3,3′,4′,6′-Tetra-*O*-sinapoyl sucrose 4SS (74)

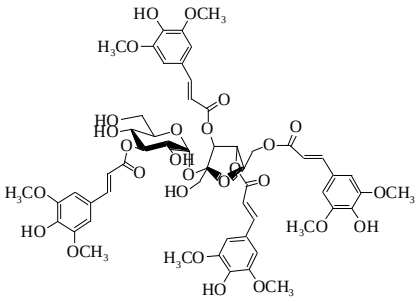

4SS (74)

4SSP (**72**) (0.6g, 0.47mmol) was dissolved in 95% EtOH (25ml). To this, piperidine (328µl, 3.318mmol) was slowly added. The reaction was allowed to stir overnight. The colour of the reaction mixture was observed to change to fluorescent yellow towards the end. Finally, AcOH (217µl) was added to quench the reaction. Compound **4SS** (**74**) was isolated as a yellow solid in 74% yield (0.4g, 0.342mmol). Analytical data for **74**: R_f = 0.77 (9:1 EtOAc:MeOH); mp 127-130°C; FTIR (KBr) ν_{max}: 3399, 2936, 2839, 1707, 1629, 1599, 1510, 1456, 1426, 1377, 1337, 1283, 1247, 1218, 1150, 1110, 1039, 989, 824, 595 cm^{-1}; ^1H NMR (300MHz, MeOD) δ: 3.80-3.91 (m, 24H, -OCH_3); sucrose unit: 4.09-4.28 (m, 3H), 4.47-4.63 (m, 4H), 5.35-5.57 (m, 2H), 5.58-5.64 (m, 1H), 5.64-5.80 (m, 2H), 5.82-5.88 (m, 1H), 6.29-6.36(m, 1H); phenyl ring and alkenyl -HC=CH- δ: 6.36-6.40 (m, 4H), 6.73-6.79 (m, 2H), 6.83-6.91 (m, 5H), 6.95-6.98 (m, 1H), 7.51-7.61 (m, 3H), 7.67-7.75 (m, 1H). ^{13}C NMR (75.48MHz, MeOD) δ: 28.50, 51.50, 56.87, 56.95, 57.0, 62.3, 64.50, 65.70, 69.30, 71.70, 74.26, 74.80, 76.90, 77.10, 93.70, 105.90, 106.12, 106.90, 107.15, 107.43, 114.80, 115.24, 115.35, 115.48, 115.68, 116.40, 125.80, 126.41, 126.49, 126.56, 126.60, 126.71, 126.81, 139.54, 139.69, 139.76, 147.15, 147.26, 147.60, 147.75, 148.60, 149.37, 149.44, 149.49, 168.00, 168.21, 168.73, 168.81, 168.84, 172.20, 172.80. HRMS (ESI-positive mode): *m/z* calcd. for $C_{56}H_{63}O_{27}$ 1167.3557; found 1167.3524 $[M+H]^+$.

APPENDIX

8.1 59 ^{1}H NMR

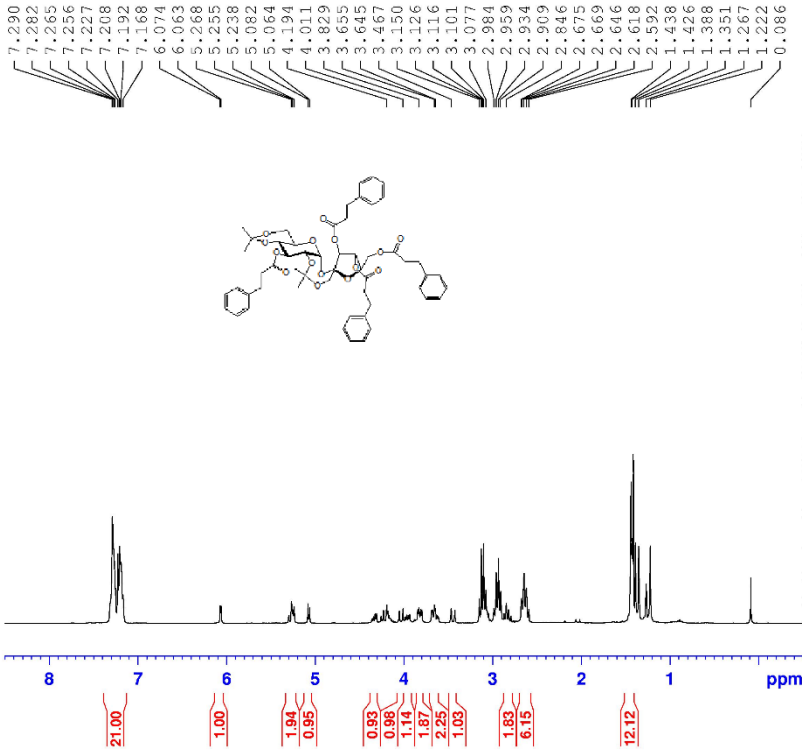

59 ^{13}C NMR

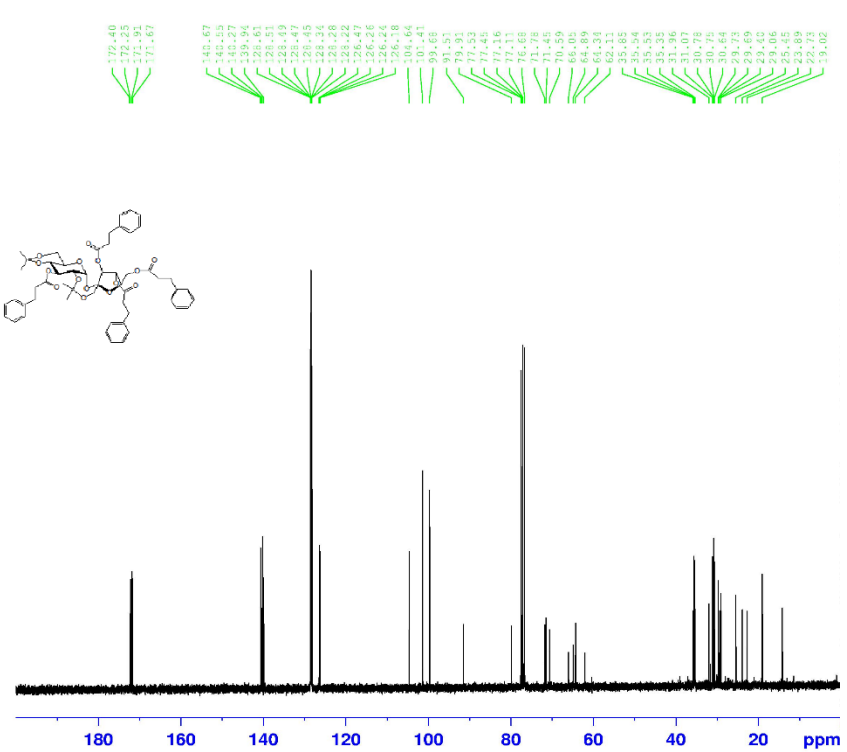

8.2 **60 ^{1}H NMR** **60 ^{13}C NMR**

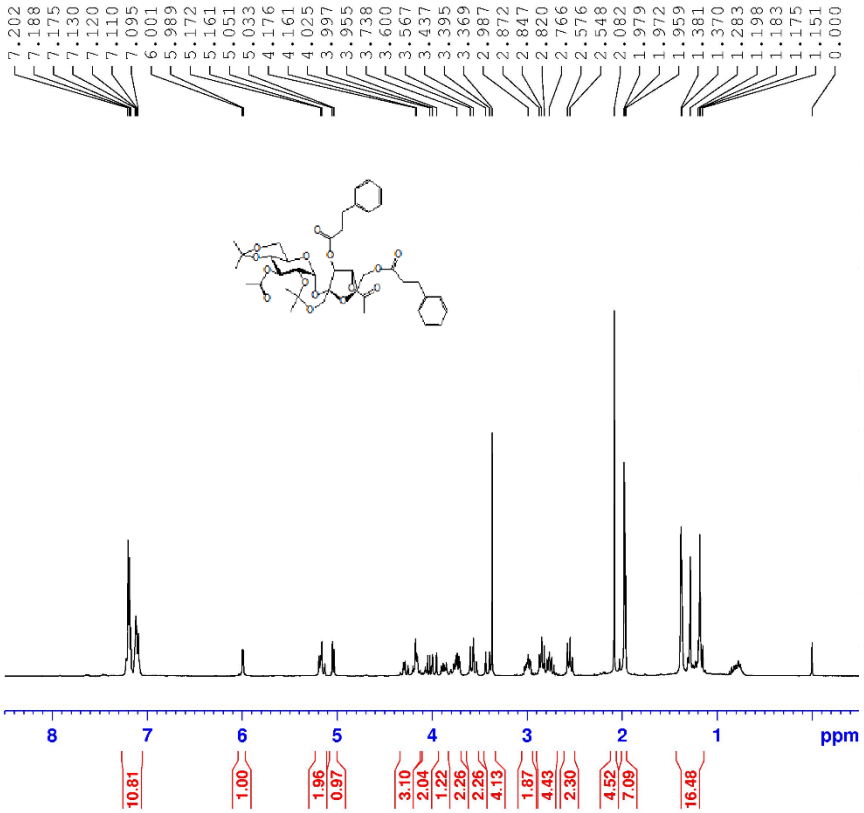

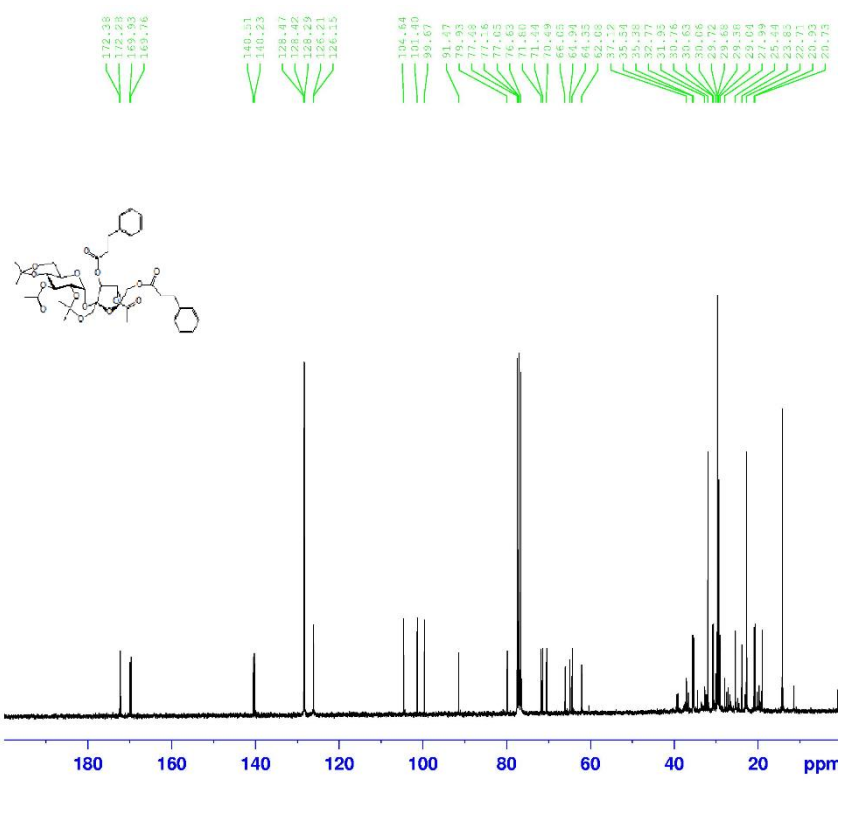

8.3 **61 ^{1}H NMR** **61 ^{13}C NMR**

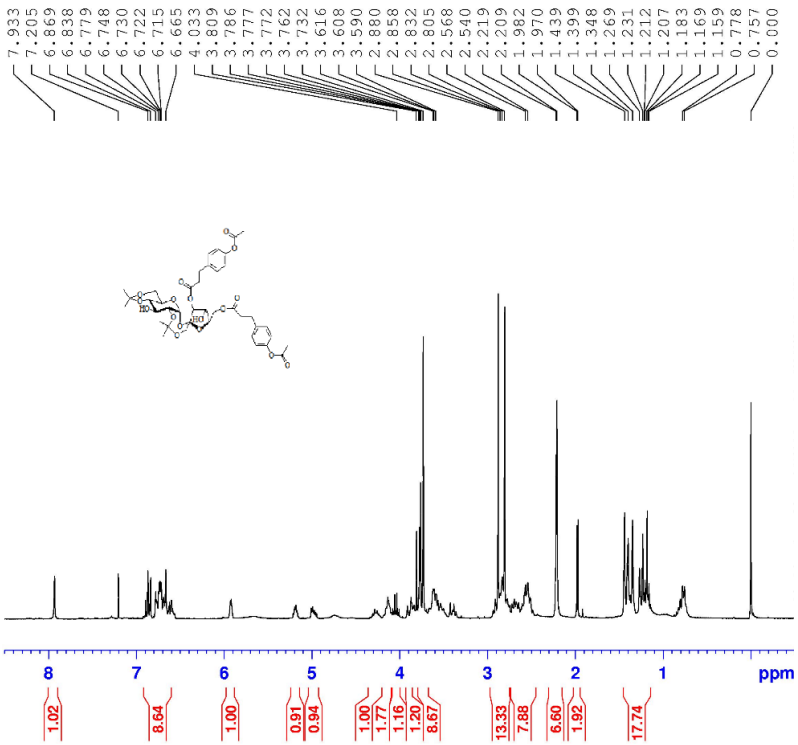

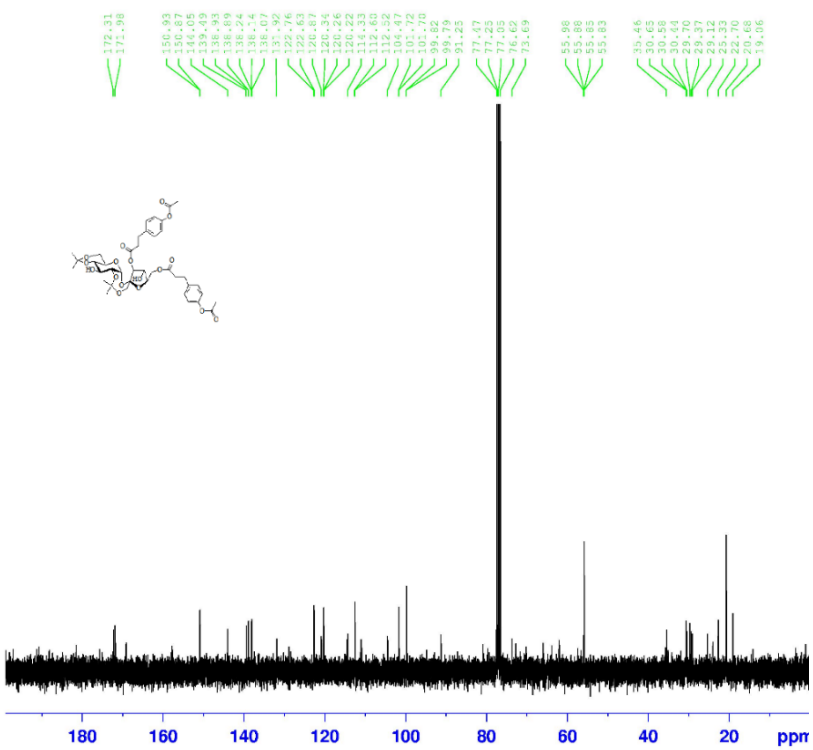

8.4 **62 ^{1}H NMR**

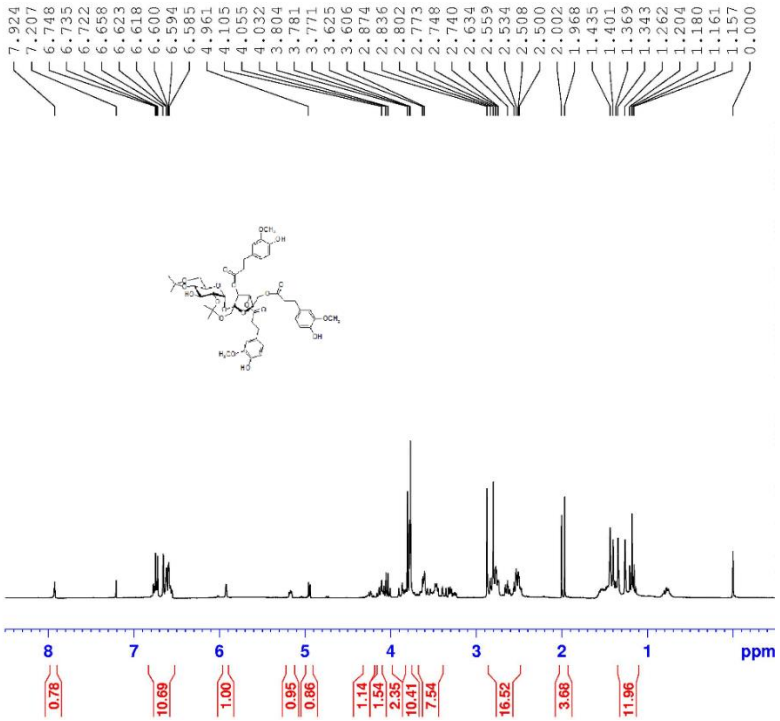

62 ^{13}C NMR

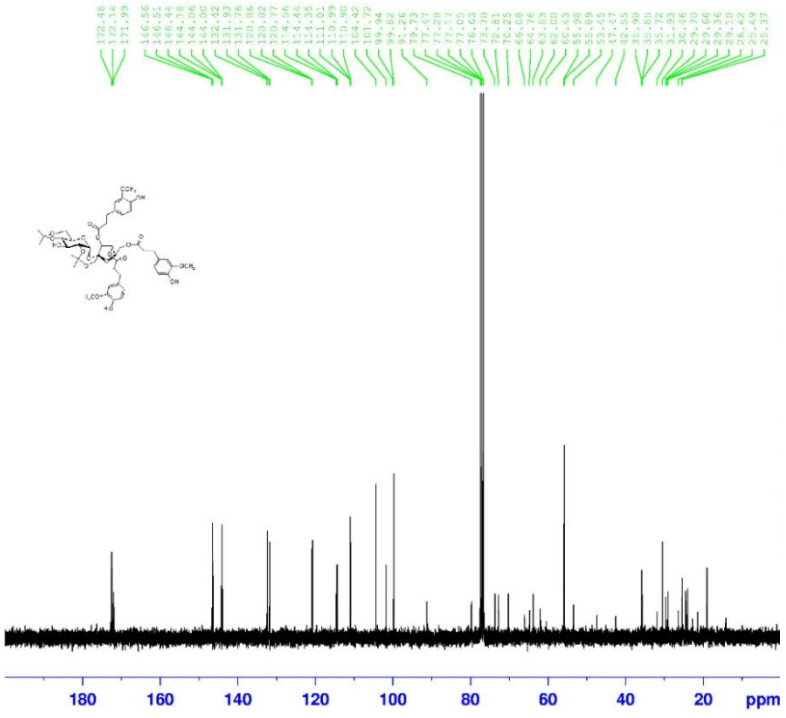

8.5 **64 ^{1}H NMR**

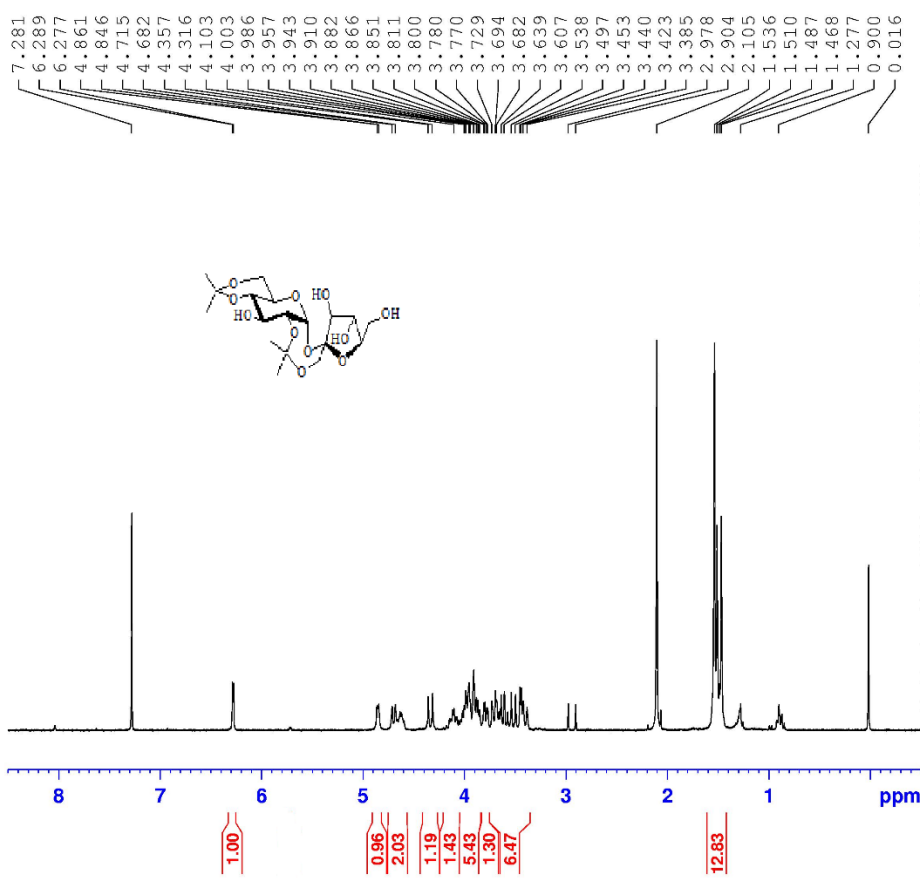

8.6 **67 ^{1}H NMR**

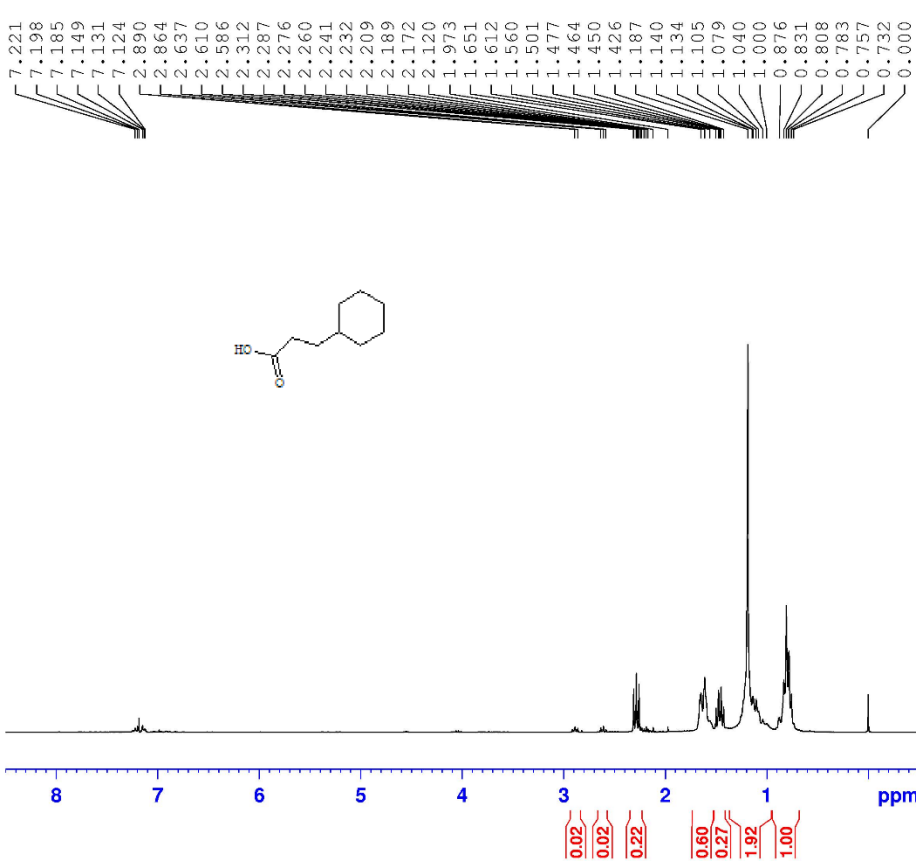

8.7 **68 ^{1}H NMR** **68 ^{13}C NMR**

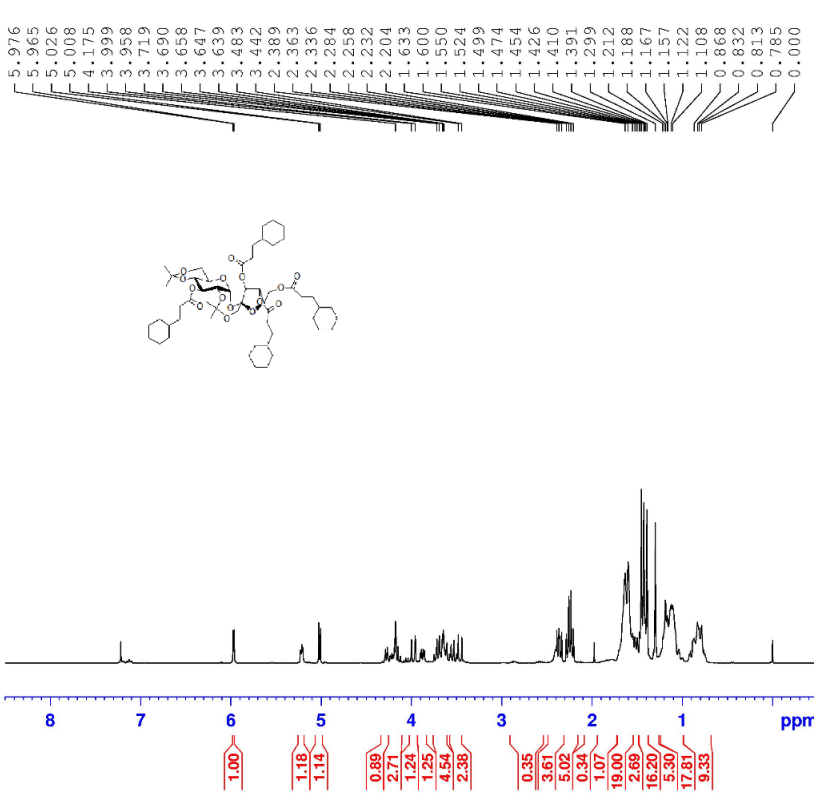

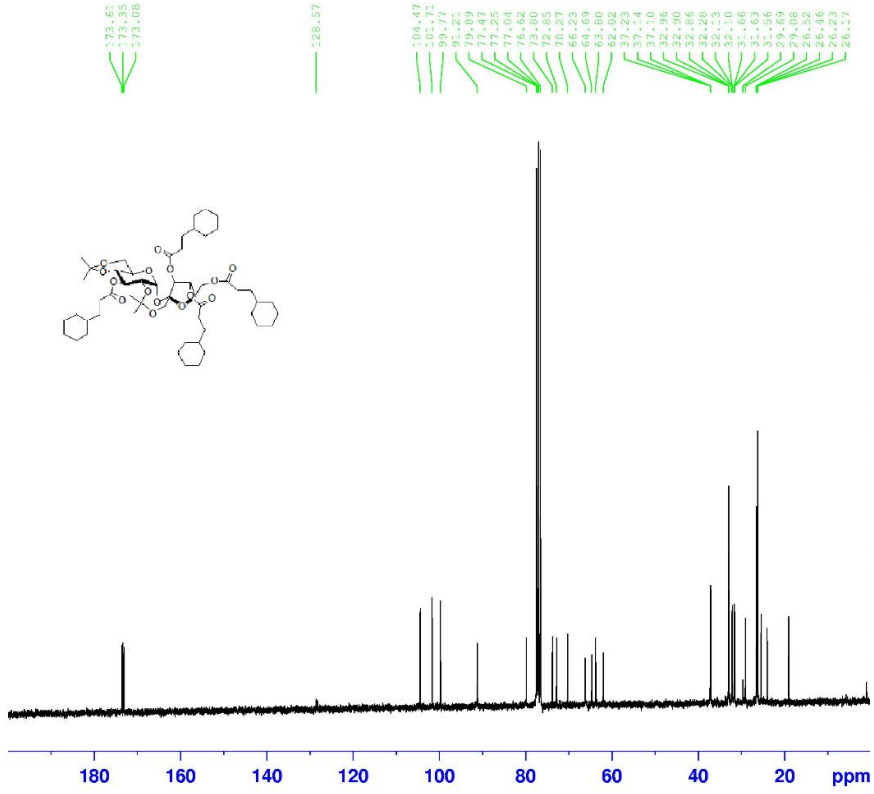

8.8 **70 ^{1}H NMR**

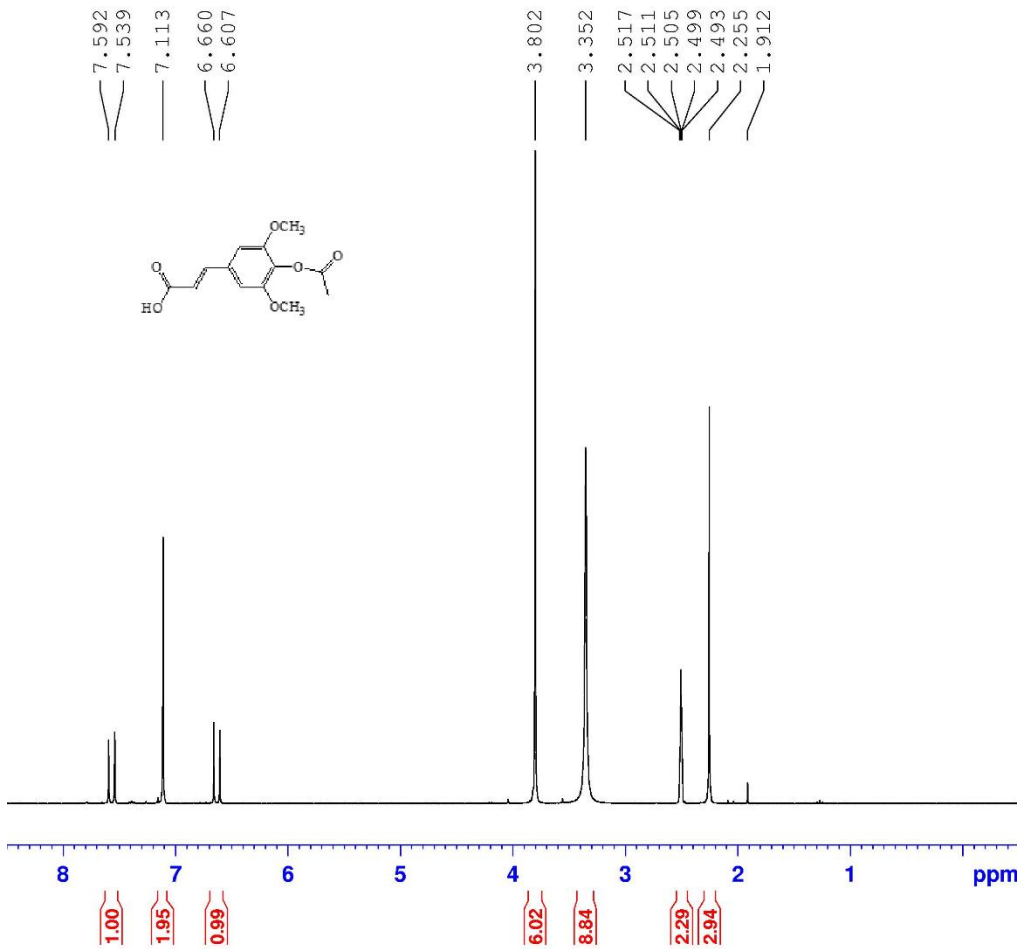
7.592
7.539
7.113
6.660
6.607
3.802
3.352
2.517
2.511
2.505
2.499
2.493
2.255
1.912
OCH3
O
HO
O
O
OCH3
8
7
6
5
4
3
2
1
ppm
1.00
1.95
0.99
6.02
8.84
2.29
2.94

8.9 **71 ^{1}H NMR**

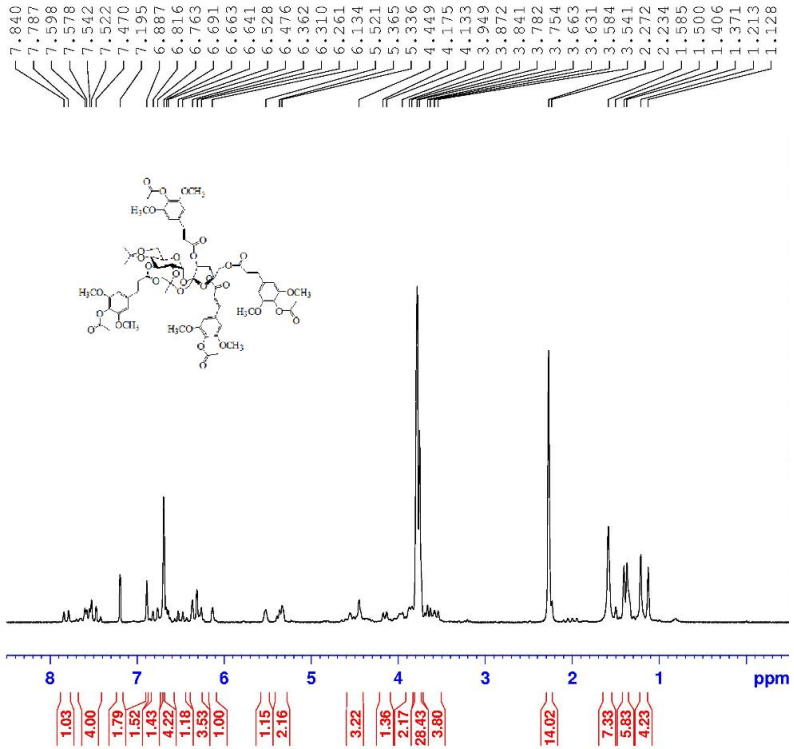

71 ^{13}C NMR

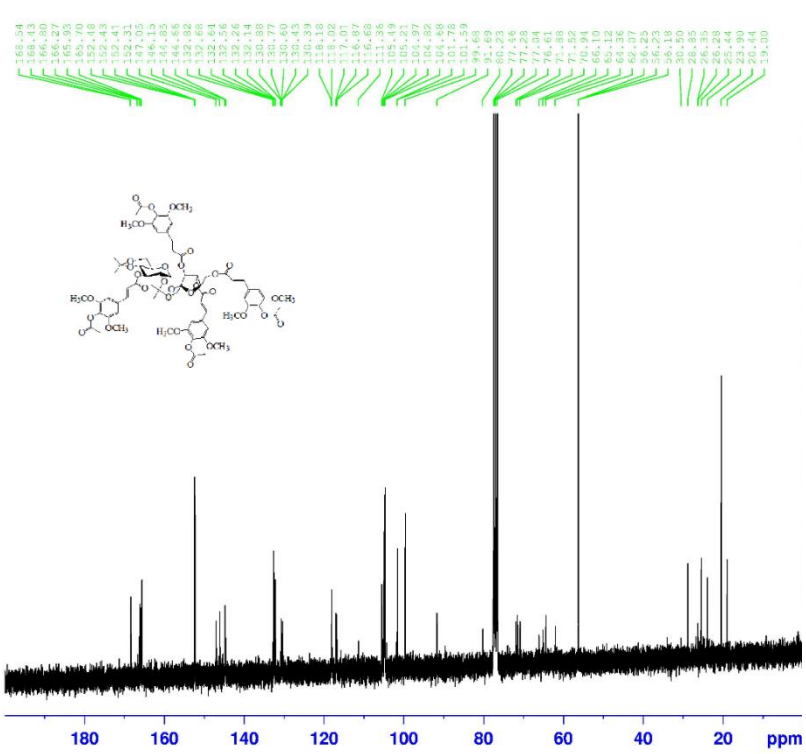

8.10 **72 ^{1}H NMR** **72 ^{13}C NMR**

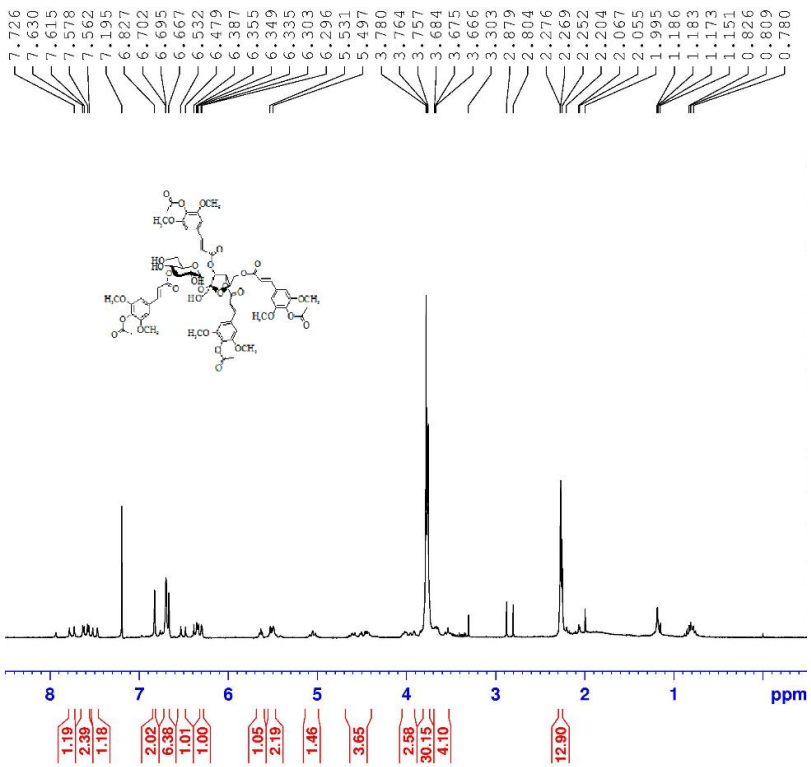

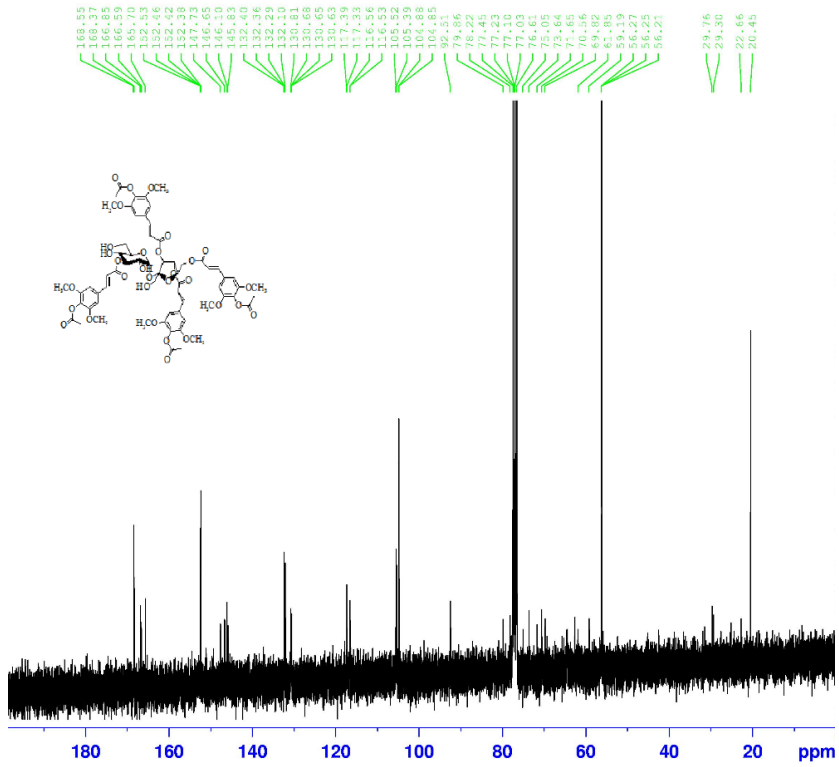

8.11 **73 ^{1}H NMR** **73 ^{13}C NMR**

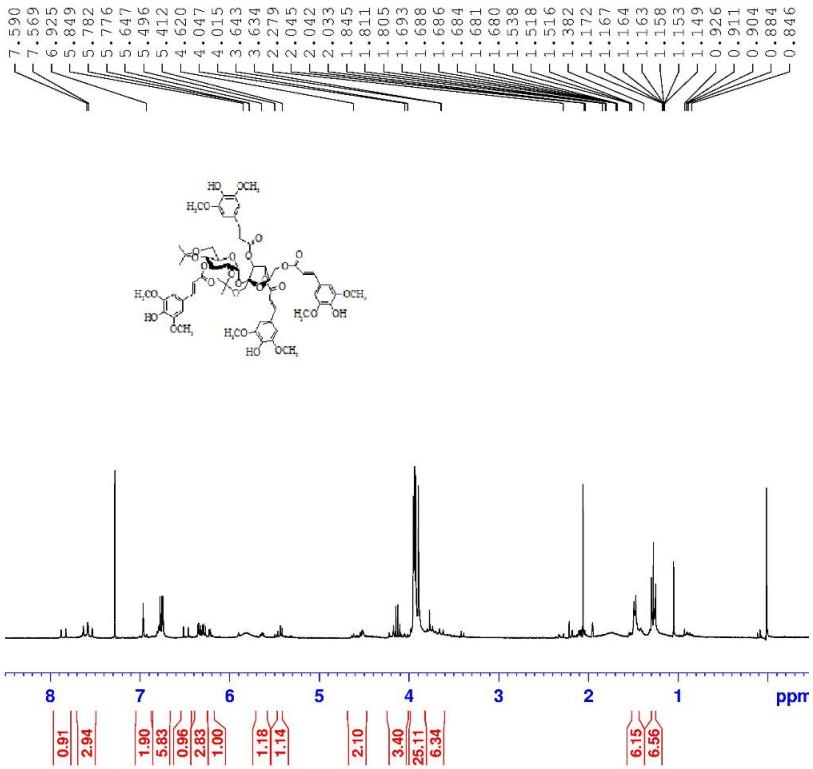

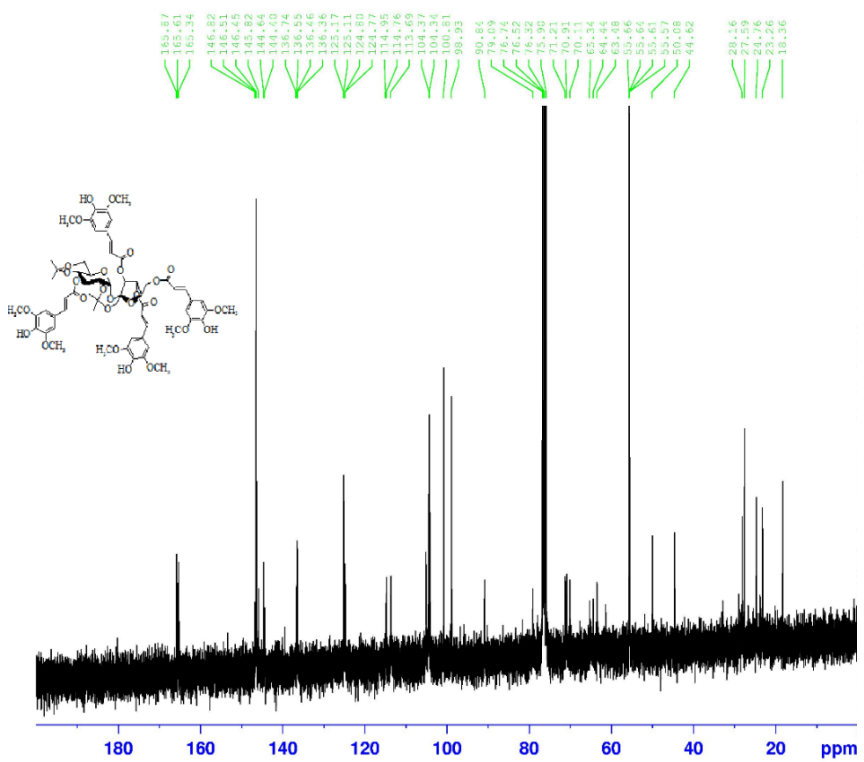

8.12 **75 ^{1}H NMR** **75 ^{13}C NMR**

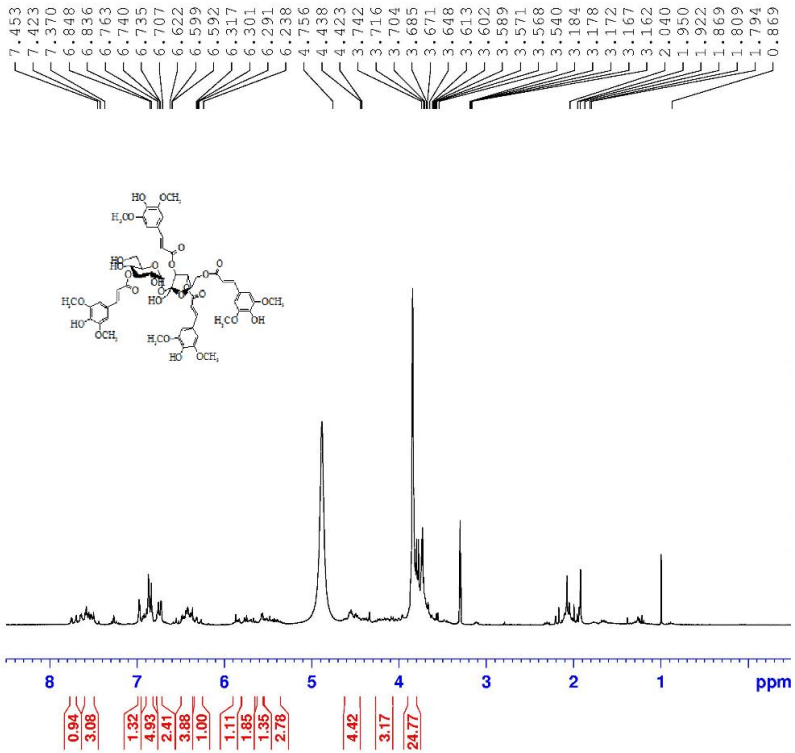

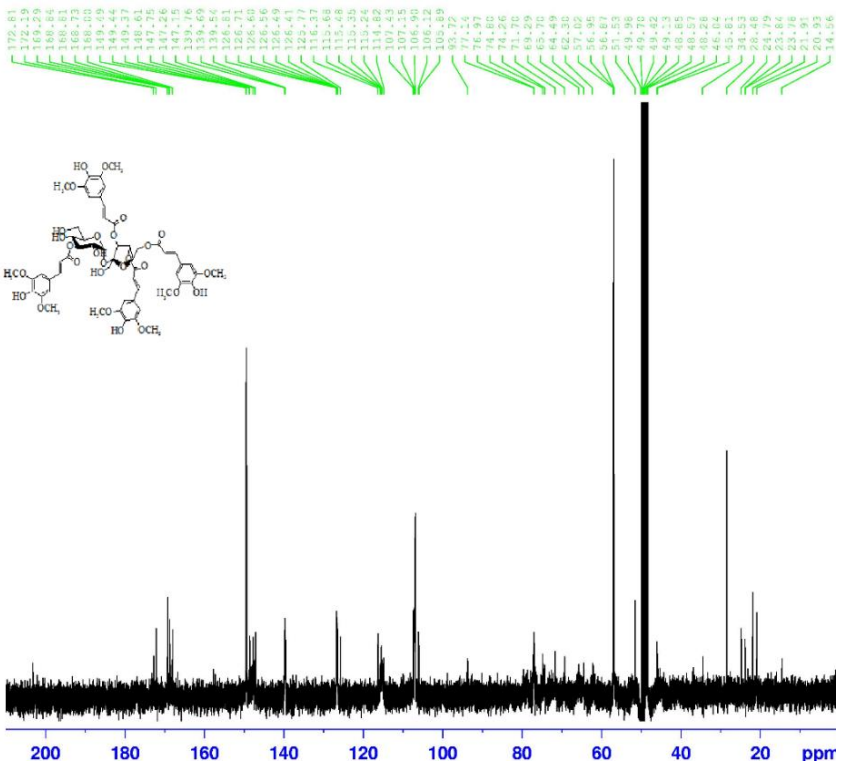

References

1. *IDF Diabetes Atlas -Seventh edition*. (2015).

2. *World Health Organisation-Fact sheet N138*.

3. All About Diabetes. at <http://www.medicalnewstoday.com/info/diabetes>

4. Akkati, S., Sam, K. G. & Tungha, G. Emergence of promising therapies in diabetes mellitus. *J. Clin. Pharmacol.* **51,** 796–804 (2011).

5. Kumar, R. V & Sinha, V. R. Newer insights into the drug delivery approaches of α-glucosidase inhibitors. *Expert Opin. Drug Deliv.* **9,** 403–16 (2012).

6. Kruger, D. F. Exploring the pharmacotherapeutic options for treating type 2 diabetes. *Diabetes Educ.* **34,** 60S–65S (2008).

7. Levetan, C. Oral antidiabetic agents in type 2 diabetes. *Curr. Med. Res. Opin.* **23,** 945–52 (2007).

8. Diabetes. at <http://www.nlm.nih.gov/medlineplus/diabetes.html>

9. Hanefeld, M. & Schaper, F. in *Pharmacother. Diabetes New Dev.* 143–152 (2007).

10. Kelley, D. E. *et al.* Efficacy and safety of acarbose in insulin-treated patients with type 2 diabetes. *Diabetes Care* **21,** 2056–61 (1998).

11. Waring, W. S. Antidiabetic drugs. *Medicine (Baltimore).* **40,** 98–99 (2012).

12. Wheeler, S. *et al.* Mortality among veterans with type 2 diabetes initiating metformin, sulfonylurea or rosiglitazone monotherapy. *Diabetologia* 1934–1943 (2013).

13. Quillen, D. M. & Kuritzky, L. Type 2 diabetes management: a comprehensive clinical review of oral medications. *Compr. Ther.* **28,** 50–61 (2002).

14. Guo, Z.-H., Huang, J., Wan, G.-S., Huo, X.-L. & Gao, H.-Y. New inhibitors of α-glucosidase in Salacia hainanensis Chun et How. *J. Nat. Med.* **67,** 844–9 (2013).

15. Miao, M. *et al.* Phytonutrients for controlling starch digestion: Evaluation of grape skin extract. *Food Chem.* **145,** 205–211 (2014).

16. Ajish, K. R. *et al.* Synthesis and biological evaluation of carbohydrate appended hydrazinocyclopentenes with potent glycation and α-glucosidase inhibition activities. *Tetrahedron Lett.* **54,** 5682–5685 (2013).

17. Phan, M. A. T., Wang, J., Tang, J., Lee, Y. Z. & Ng, K. Evaluation of α-glucosidase inhibition potential of some flavonoids from Epimedium brevicornum. *LWT - Food Sci. Technol.* **53,** 492–498 (2013).

18. Derosa, G. & Maffioli, P. α-Glucosidase inhibitors and their use in clinical practice. *Arch. Med. Sci.* **8,** 899–906 (2012).

19. Chiasson, J. L. *et al.* The efficacy of acarbose in the treatment of patients with non-insulin-dependent diabetes mellitus. A multicenter controlled clinical trial. *Ann. Intern. Med.* **121,** 928–35 (1994).

20. Lippincott Williams & Wilkins. *Diabetes Mellitus: A Fundamental and Clinical Text*. (2004).

21. Snyder, R. W. & Berns, J. S. Use of insulin and oral hypoglycemic medications in patients with diabetes mellitus and advanced kidney disease. *Semin. Dial.* **17,** 365–370 (2004).

22. Sels, J. P., Huijberts, M. S. & Wolffenbuttel, B. H. Miglitol, a new alpha-glucosidase inhibitor. *Expert Opin. Pharmacother.* **1,** 149–56 (1999).

23. Vichayanrat, A., Ploybutr, S., Tunlakit, M. & Watanakejorn, P. Efficacy and safety of voglibose in comparison with acarbose in type 2 diabetic patients. *Diabetes Res. Clin. Pract.* **55,** 99–103 (2002).

24. Kageyama, S., Nakamichi, N., Sekino, H. & Nakano, S. Comparison of the effects of acarbose and voglibose in healthy subjects. *Clin. Ther.* **19,** 720–729 (1997).

25. Panda, P. ., Appalashetti, M. . & M.A. Judeh, Z. Phenylpropanoid Sucrose Esters:

Plant-Derived Natural Products as Potential Leads for New Therapeutics. *Curr. Med. Chem.* **18,** 3234–3251 (2011).

26. Kurkin, V. A. Phenylpropanoids from medicinal plants:distribution, classification, structural analysis, and biological activity. *Chem. Nat. Compd.* **39,** 87–110 (2003).

27. Nhiem, N. X. *et al.* Phenylpropanoid glycosides from Heterosmilax erythrantha and their antioxidant activity. *Arch. Pharm. Res.* **32,** 1373–7 (2009).

28. Kiem, P. Van *et al.* New phenylpropanoid esters of sucrose from Polygonum hydropiper and their antioxidant activity. *Arch. Pharm. Res.* **31,** 1477–82 (2008).

29. Chan, H.-H., Sun, H.-D., Reddy, M. V. B. & Wu, T.-S. Potent alpha-glucosidase inhibitors from the roots of Panax japonicus C. A. Meyer var. major. *Phytochemistry* **71,** 1360–4 (2010).

30. Fan, P., Terrier, L., Hay, A.-E., Marston, A. & Hostettmann, K. Antioxidant and enzyme inhibition activities and chemical profiles of Polygonum sachalinensis F.Schmidt ex Maxim (Polygonaceae). *Fitoterapia* **81,** 124–31 (2010).

31. Wan, C., Yuan, T., Cirello, A. L. & Seeram, N. P. Antioxidant and α-glucosidase inhibitory phenolics isolated from highbush blueberry flowers. *Food Chem.* **135,** 1929–37 (2012).

32. Panda, P. *et al.* Synthesis and antitumor activity of lapathoside D and its analogs. *Eur. J. Med. Chem.* **53,** 1–12 (2012).

33. Panda, P. *et al.* Synthesis and antiproliferative activity of helonioside A, 3’,4',6'-tri-O-feruloylsucrose, lapathoside C and their analogs. *Eur. J. Med. Chem.* **58,** 418–30 (2012).

34. Suo, M., Ohta, T., Takano, F. & Jin, S. Bioactive phenylpropanoid glycosides from Tabebuia avellanedae. *Molecules* **18,** 7336–45 (2013).

35. Kumagai, H. *et al.* Antimicrobial substances from rhizomes of the giant knotweed Polygonum sachalinense against the fish pathogen Photobacterium damselae subsp.

piscicida. *Z. Naturforsch. C.* **60,** 39–44 (2005).

36. Kawai, Y. *et al.* Beta-Glucosidase inhibitory activities of phenylpropanoid glycosides, vanicoside A and B from Polygonum sachalinense rhizome. *Fitoterapia* **77,** 456–9 (2006).

37. Yuan, T., Wan, C., Liu, K. & Seeram, N. P. New maplexins F–I and phenolic glycosides from red maple (Acer rubrum) bark. *Tetrahedron* **68,** 959–964 (2012).

38. Cruz-Vega, D. *et al.* Review of pharmacological effects of Glycyrrhiza radix and its bioactive compounds. *China J. Chinese Mater. medica* **22,** 557–559 (2009).

39. Liu, T. *et al.* Inhibiting enzymatic starch digestion by the phenolic compound diboside A: A mechanistic and in silico study. *Food Res. Int.* **54,** 595–600 (2013).

40. Meyre-Silva, C. & Cechinel-Filho, V. A review of the chemical and pharmacological aspects of the genus marrubium. *Curr. Pharm. Des.* **16,** 3503–18 (2010).

41. Boudjelal, A., Henchiri, C., Siracusa, L., Sari, M. & Ruberto, G. Compositional analysis and in vivo anti-diabetic activity of wild Algerian Marrubium vulgare L. infusion. *Fitoterapia* **83,** 286–92 (2012).

42. Benalla, W., Bellahcen, S. & Bnouham, M. Antidiabetic medicinal plants as a source of alpha glucosidase inhibitors. *Curr. Diabetes Rev.* **6,** 247–54 (2010).

43. Kim, J.-S., Kwon, Y.-S., Sa, Y.-J. & Kim, M.-J. Isolation and identification of sea buckthorn (Hippophae rhamnoides) phenolics with antioxidant activity and α-glucosidase inhibitory effect. *J. Agric. Food Chem.* **59,** 138–44 (2011).

44. Mncwangi, N., Chen, W., Vermaak, I., Viljoen, A. M. & Gericke, N. Devil's Claw-a review of the ethnobotany, phytochemistry and biological activity of Harpagophytum procumbens. *J. Ethnopharmacol.* **143,** 755–71 (2012).

45. Andrade Cetto, a, Wiedenfeld, H., Revilla, M. C. & Sergio, I. a. Hypoglycemic effect of Equisetum myriochaetum aerial parts on streptozotocin diabetic rats. *J. Ethnopharmacol.* **72,** 129–33 (2000).

46. Vinholes, J. *et al.* In vitro studies to assess the antidiabetic, anti-cholinesterase and antioxidant potential of Spergularia rubra. *Food Chem.* **129,** 454–462 (2011).

47. Wan, C., Yuan, T., Cirello, A. L. & Seeram, N. P. Antioxidant and α-glucosidase inhibitory phenolics isolated from highbush blueberry flowers. *Food Chem.* **135,** 1929–37 (2012).

48. Lee, S.-S., Lin, H.-C. & Chen, C.-K. Acylated flavonol monorhamnosides, alpha-glucosidase inhibitors, from Machilus philippinensis. *Phytochemistry* **69,** 2347–53 (2008).

49. Fan, P., Terrier, L., Hay, A.-E., Marston, A. & Hostettmann, K. Antioxidant and enzyme inhibition activities and chemical profiles of Polygonum sachalinensis F.Schmidt ex Maxim (Polygonaceae). *Fitoterapia* **81,** 124–31 (2010).

50. Kumar, M., Rawat, P., Rahuja, N., Srivastava, A. K. & Maurya, R. Antihyperglycemic activity of phenylpropanoyl esters of catechol glycoside and its dimers from Dodecadenia grandiflora. *Phytochemistry* **70,** 1448–55 (2009).

51. Tanaka, T., Uehara, R., Nishida, K. & Kouno, I. Galloyl, caffeoyl and hexahydroxydiphenoyl esters of dihydrochalcone glucosides from Balanophora tobiracola. *Phytochemistry* **66,** 675–81 (2005).

52. Matsuura, H. *et al.* Isolation of α-glusosidase inhibitors from hyssop (Hyssopus officinalis). *Phytochemistry* **65,** 91–97 (2004).

53. Matsui, T. *et al.* Anti-hyperglycemic effect of diacylated anthocyanin derived from Ipomoea batatas cultivar Ayamurasaki can be achieved through the alpha-glucosidase inhibitory action. *J. Agric. Food Chem.* **50,** 7244–8 (2002).

54. Phuwapraisirisan, P., Puksasook, T., Kokpol, U. & Suwanborirux, K. Corchorusides A and B, new flavonol glycosides as α-glucosidase inhibitors from the leaves of Corchorus olitorius. *Tetrahedron Lett.* **50,** 5864–5867 (2009).

55. Liu, T. *et al.* Inhibiting enzymatic starch digestion by the phenolic compound diboside A: A mechanistic and in silico study. *Food Res. Int.* **54,** 595–600 (2013).

56. Yoshida, K., Hishida, A., Iida, O., Hosokawa, K. & Kawabata, J. Flavonol Caffeoylglycosides as alpha-Glucosidase Inhibitors from Spiraea cantoniensis Flower. *J. Agric. Food Chem.* **56,** 4367–71 (2008).

57. Hua, J., Qi, J. & Yu, B.-Y. Iridoid and phenylpropanoid glycosides from Scrophularia ningpoensis Hemsl. and their α-Glucosidase inhibitory activities. *Fitoterapia* **93,** 67–73 (2014).

58. Qiu, F., Luo, J., Yao, S., Ma, L. & Kong, L. Preparative isolation and purification of anthocyanins from purple sweet potato by high-speed counter-current chromatography. *J. Sep. Sci.* **32,** 2146–51 (2009).

59. Gund, P., Andose, J. D., Rhodes, J. B. & Smith, G. M. Three-Dimensional Molecular Modeling and Drug Design. *Science.* **208,** 1425–1431 (1980).

60. Bohacek, R. S., McMartin, C. & Guida, W. C. The art and practice of structure-based drug design: a molecular modeling perspective. *Med. Res. Rev.* **16,** 3–50 (1996).

61. Lybrand, T. P. Ligand Protein Docking and Rational Drug Design. *Curr. Opin. Struct. Biol.* **5,** 224–228 (1995).

62. Marshall, G. R. in *Clin. Pharmacol. Psychiatry Sel. Psychotr. Drug Action --- Promises or Problems?*(Dahl, S. G., Gram, L. F., Paul, S. M. & Potter, W. Z.) 3–11 (Springer Berlin Heidelberg, 1987).

63. Robinson, V. Finding alternatives : an overview of the 3Rs and the use of animals in research. *Sch. Sci. Rev.* **87,** 1–4 (2005).

64. Montagutelli, X. Animal models are essential to biological research : issues and perspectives. *Futur. Sci. OA* **1,** 4–6 (2015).

65. Rees, D. A. & Alcolado, J. C. Animal models of diabetes mellitus. *Diabet. Med.* **22,** 359–70 (2005).

66. Gerich, J. E. Clinical Significance, Pathogenesis, and Management of Postprandial Hyperglycemia. *Arch Intern Med* **163,** 1306–1316 (2003).

67. Kang, W.-Y., Song, Y.-L. & Zhang, L. α-Glucosidase inhibitory and antioxidant properties and antidiabetic activity of Hypericum ascyron L. *Med. Chem. Res.* **20,** 809–816 (2010).

68. Gilson, M. K. & Zhou, H.-X. Calculation of protein-ligand binding affinities. *Annu. Rev. Biophys. Biomol. Struct.* **36,** 21–42 (2007).

69. Sousa, F., Fernandes, P. A. & Joa, M. Protein – Ligand Docking : Current Status and Future. *Proteins Struct. Funct. Bioinforma.* **26,** 15–26 (2006).

70. Alonso, H., Bliznyuk, A. a & Gready, J. E. Combining docking and molecular dynamic simulations in drug design. *Med. Res. Rev.* **26,** 531–68 (2006).

71. Mohan, V., Gibbs, A. C., Cummings, M. D., Jaeger, E. P. & DesJarlais, R. L. Docking: successes and challenges. *Curr. Pharm. Des.* **11,** 323–33 (2005).

72. Lybrand, T. P. Ligand-protein docking and rational drug design. *Curr. Opin. Struct. Biol.* **5,** 224–8 (1995).

73. Yan, J., Zhang, G., Pan, J. & Wang, Y. α-Glucosidase inhibition by luteolin: Kinetics, interaction and molecular docking. *Int. J. Biol. Macromol.* **64,** 213–223 (2014).

74. Liu, T. *et al.* Inhibiting enzymatic starch digestion by the phenolic compound diboside A: A mechanistic and in silico study. *Food Res. Int.* **54,** 595–600 (2013).

75. Hornak, V. *et al.* Comparison of Multiple Amber Force Fields and Development of Improved Protein Backbone Parameters. *Proteins Struct. Funct. Bioinforma.* **65,** 712–725 (2006).

76. D.A. Case, T.A. Darden, T.E. Cheatham III, C.L. Simmerling, J. Wang, R.E. Duke, R. Luo, K.M. Merz, D.A. Pearlman, M. Crowley, R.C. Walker, W. Zhang, B. Wang, S. Hayik, A. Roitberg, G. Seabra, K.F. Wong, F. Paesani, X. Wu, S. Brozell, V. Tsui, H. Gohlke, L, P. A. K. *Amber 9*. (2006).

77. Ryckaert, J.-P., Ciccotti, G. & Berendsen, H. J. C. Numerical integration of the

Cartesian Equations of Motion of a System with Constraints: Molecular Dynamics of n-Alkanes. *J. Comput. Phys.* **23,** 327–341 (1977).

78. Naı, M. *et al.* Solvated Interaction Energy (SIE) for Scoring Protein - Ligand Binding Affinities . 1 . Exploring the Parameter Space. *J. Chem. Inf. Model* **47,** 122–133 (2007).

79. Cui, Q. *et al.* Molecular Dynamics — Solvated Interaction Energy Studies of Protein – Protein Interactions : The MP1 – p14 Scaffolding Complex. *J. Mol. Biol.* **379,** 787–802 (2008).

80. Holt, A. in *Cell Neurobiol. Tech.* **33,** 131–194 (Humana Press, 1999).

81. Lineweaver, H. & Burk, D. The determination of enzyme dissociation constants. *J. Am. Chem. Soc.* **56,** 658–666 (1934).

82. Burlingham, B. T. & Widlanski, T. S. An Intuitive Look at the Relationship of Ki and IC50: A More General Use for the Dixon Plot. *J. Chem. Educ.* **80,** 214 (2003).

83. Whiteley, C. G. Enzyme Kinetics: Partial and Complete Competitive Inhibition. *Biochem. Educ.* **4412,** 144–146 (1997).

84. Whiteley, C. . Enzyme kinetics: partial and complete uncompetitive inhibition. *Biochem. Educ.* **28,** 144–147 (2000).

85. Cornish-Bowden, A. A simple graphical method for determining the inhibition constants of mixed, uncompetitive and non-competitive inhibitors. *Biochem. J.* **137,** 143–4 (1974).

86. Mahomoodally, M. F. & Muthoora, D. D. Kinetic of inhibition of carbohydrate-hydrolysing enzymes, antioxidant activity and polyphenolic content of Phyllanthus amarus Schum. & Thonn. (Phyllanthaceae). *J. Herb. Med.* **4,** 208–223 (2014).

87. Senger, M. R. *et al.* Kinetics Studies on the Inhibition Mechanism of Pancreatic α-Amylase by Glycoconjugated 1H-1,2,3-Triazoles: A New Class of Inhibitors with Hypoglycemiant Activity. *ChemBioChem* **13,** 1584–1593 (2012).

88. Jung, H. A. *et al.* Kinetics and molecular docking studies of an anti-diabetic complication inhibitor fucosterol from edible brown algae Eisenia bicyclis and Ecklonia stolonifera. *Chem. Biol. Interact.* **206,** 55–62 (2013).

89. Dhital, S., Gidley, M. J. & Warren, F. J. Inhibition of α-amylase activity by cellulose: Kinetic analysis and nutritional implications. *Carbohydr. Polym.* **123,** 305–12 (2015).

90. Kim, M.-J. *et al.* Comparative Study of the Inhibition of α-Glucosidase, α-Amylase, and Cyclomaltodextrin Glucanosyltransferase by Acarbose, Isoacarbose, and Acarviosine–Glucose. *Arch. Biochem. Biophys.* **371,** 277–283 (1999).

91. Rees, D. a & Alcolado, J. C. Animal models of diabetes mellitus. *Diabet. Med.* **22,** 359–70 (2005).

92. Srinivasan, K. & Ramarao, P. Animal models in type 2 diabetes research: an overview. *Indian J. Med. Res.* **125,** 451–472 (2007).

93. Cefalu, W. T. Animal models of type 2 diabetes: clinical presentation and pathophysiological relevance to the human condition. *ILAR J.* **47,** 186–198 (2006).

94. Wu, Z. M. *et al.* HP55-coated capsule containing PLGA/RS nanoparticles for oral delivery of insulin. *Int. J. Pharm.* **425,** 1–8 (2012).

95. Wu, K. K. & Huan, Y. Streptozotocin-induced diabetic models in mice and rats. *Curr. Protoc. Pharmacol.* 1–14 (2008).

96. Brosius, F. Low-Dose Streptozotocin Induction Protocol (Mouse) Summary : Reagents and Materials : Reagent Preparation : *Protocol* 4–6 (2003).

97. Park, M. H., Ju, J. W., Park, M. J. & Han, J. S. Daidzein inhibits carbohydrate digestive enzymes in vitro and alleviates postprandial hyperglycemia in diabetic mice. *Eur. J. Pharmacol.* **712,** 48–52 (2013).

98. Snape, T. J., Astles, A. M. & Davies, J. Understanding the chemical basis of drug stability and degradation. *Pharm. J.* **285,** 416 (2010).

99. Roda, a., Mezzanotte, L., Aldini, R., Michelini, E. & Cevenini, L. A new gastric-emptying mouse model based on in vivo non-invasive bioluminescence imaging. *Neurogastroenterol. Motil.* **22,** 21–23 (2010).

100. McConnell, E. L., Basit, A. W. & Murdan, S. Measurements of rat and mouse gastrointestinal pH, fluid and lymphoid tissue, and implications for in-vivo experiments. *J. Pharm. Pharmacol.* **60,** 63–70 (2008).

101. Paryzek, Z., Koenig, H. & Tabaczka, B. Ammonium Formate/Palladium on Carbon: A Versatile System for Catalytic Hydrogen Transfer Reductions of Carbon-Carbon Double Bonds. *Synthesis (Stuttg).* 2023–2026 (2003).

102. Anderson, J. A. *et al.* Aqueous phase hydrogenation of substituted phenyls over carbon nanofibre and activated carbon supported Pd. *J. Catal.* **270,** 9–15 (2010).

103. Porter, N. A. *et al.* Origins of stereoselectivity in radical additions: reactions of alkenes and radicals bearing oxazolidine and thiazolidine amide groups. *J. Am. Chem. Soc.* **114,** 7664–7676 (1992).

104. Allais, F., Martinet, S. & Ducrot, P. H. Straightforward total synthesis of 2-O-feruloyl-L-malate, 2-O-sinapoyl-L-malate and 2-O-5-hydroxyferuloyl-L-malate. *Synthesis (Stuttg).* 3571–3578 (2009).

105. Panda, P., Appalashetti, M. & Judeh, Z. M. A. Phenylpropanoid Sucrose Esters: Plant-Derived Natural Products as Potential Leads for New Therapeutics. *Curr. Med. Chem.* **18,** 3234–3251 (2011).

106. Gad, S., Cassidy, C., Aubert, N., Spainhour, B. & Robbe, H. Nonclinical Vehicle Use in Studies by Multiple Routes in Multiple Species. *Int. J. Toxicol.* **25,** 499–521 (2006).

107. Neervannan, S. Preclinical formulations for discovery and toxicology: physicochemical challenges. *Expert Opin. Drug Metab. Toxicol.* **2,** 715–31 (2006).

108. Sakai, N., Moriya, T. & Konakahara, T. An Efficient One-Pot Synthesis of Unsymmetrical Ethers : A Directly Reductive Deoxygenation of Esters Using an

InBr 3 / Et 3 SiH Catalytic System. *J. Org. Chem.* **72,** 5920–5922 (2007).

109. Hosoda, A., Nomura, E., Mizuno, K. & Taniguchi, H. Preparation of a (±)-1,6-di-O-feruloyl-myo-inositol derivative: An efficient method for introduction of ferulic acid to 1,6-vicinal hydroxyl groups of myo-inositol. *J. Org. Chem.* **66,** 7199–7201 (2001).